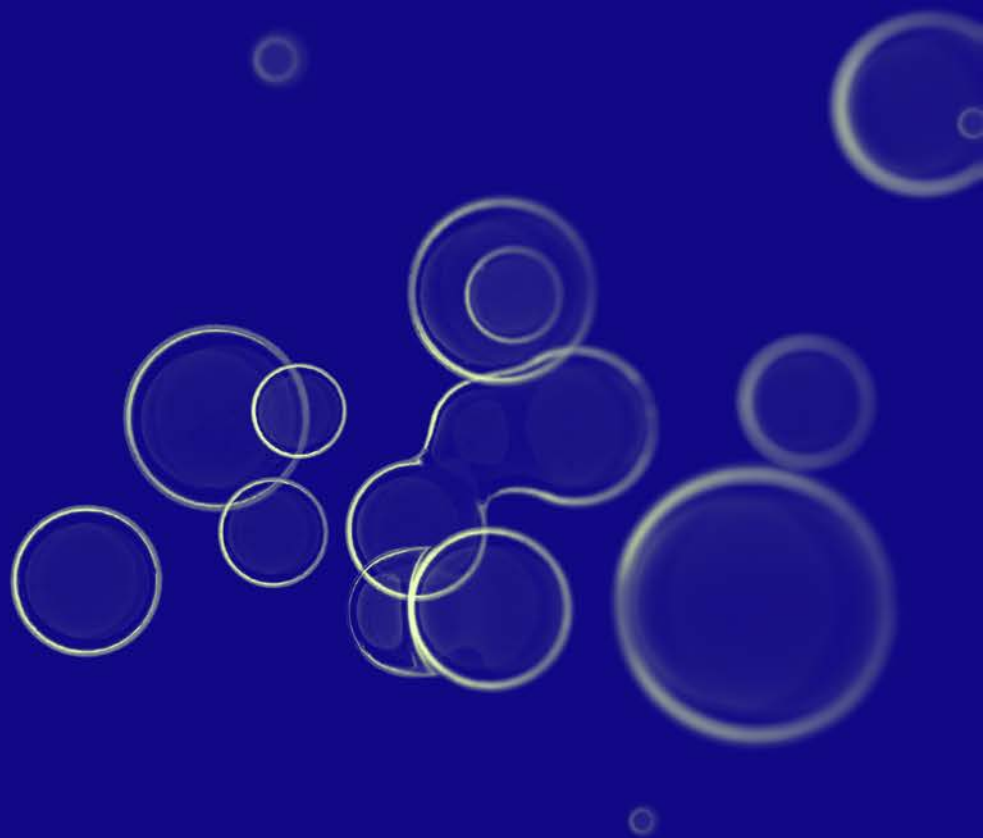


Modelling of isoprene distribution and cycling in the ocean

Pablo Rodríguez-Ros



UNIVERSITAT POLITÈCNICA
DE CATALUNYA
BARCELONATECH



Institut
de Ciències
del Mar



Modelling of isoprene distribution and cycling in the ocean

International PhD degree in Marine Sciences

Memòria per optar al títol de Doctor en Ciències del Mar del Departament d'Enginyeria Civil i Ambiental per la Universitat Politècnica de Catalunya (UPC), sota la direcció del Dr. Rafel Simó (ICM-CSIC) i del Dr. Sergio Vallina (IEO-Gijón).

Institut de Ciències del Mar (ICM)
Spanish National Research Council (CSIC)

Universitat Politècnica de Catalunya (UPC)

Pablo Rodríguez-Ros

Rafel Simó (Advisor)
Sergio Vallina (Co-advisor)

June 16, 2020

The author was supported by a "la Caixa" Foundation PhD fellowship (2015-2019), and a Fulbright grant (2019-2020) from the Spanish Fulbright Commission and the Spanish Ministry of Foreign Affairs. The research work presented in this thesis was funded by the projects PEGASO (CTM2012–37615) and BIOGAPS (CTM2016–81008–R), supported by the Spanish Ministry of Economy and Competitiveness (MINECO), and the Antarctic Circumnavigation Expedition (ACE), carried out under the auspices of the Swiss Polar Institute and supported by funding from the ACE Foundation and Ferring Pharmaceuticals. The studies were carried out at the following research institutions:

- **Institut de Ciències del Mar de Barcelona** (ICM-CSIC; Barcelona, Spain). Grant: "la Caixa" Foundation (2015-2019).
- **TAKUVIK** joint laboratory University Laval (Québec, Canada) and the Centre National de la Recherche Scientifique (CNRS - France). Grant: "la Caixa" Foundation (2015-2019).
- **Swiss Federal Institute of Technology in Zurich** (ETH Zürich). Grant: Fellowship for International Mobility of Researches (Universitat Politècnica Catalunya - BarcelonaT-ech, UPC - "la Caixa"). Editions of 2017 and 2018.
- **Instituto Mediterráneo de Estudios Avanzados** (CSIC-UIB; Mallorca, Spain). Grant: "la Caixa" Foundation (2015-2019).
- **Scripps Institution of Oceanography** (University of California San Diego). Grant: Fulbright Fellowship (2019-2020).



Abstract

Modelling of isoprene distribution and cycling in the ocean

Isoprene (C_5H_8) is the most widely emitted biogenic volatile organic carbon (BVOC). It is produced in the biosphere both on land and in the ocean, and in the atmosphere it acts as a precursor of secondary organic aerosols. Isoprene has an eminently biological origin in phytoplankton; but its agents, production and recycling mechanisms, including photochemistry, are very poorly known. There still are large discrepancies in the estimations of global oceanic emission of isoprene (0.1 - 11.6 Tg C yr⁻¹). Despite lower marine emissions than terrestrial ones, they play a key role in cloud formation and brightness in remote regions of the oceans. Due to the unfeasibility of getting synoptic measurements of isoprene emissions over the global ocean, they need to be calculated with numerical models that use variables that can be measured using remote sensing data from satellites or generated through ecosystem models. To achieve the capacity to predict the distribution and emission of isoprene in the surface ocean in time and space, in this thesis computational tools for the statistical treatment of data and for the diagnosis/prognosis were used. Thus, different approaches to predict and study isoprene in surface waters, including statistical modeling, biogeochemical-ecological modeling, and remote sensing retrieval were tested. Despite most of the focus of this PhD thesis is focused on the Southern Ocean (SO) waters, the patterns of isoprene cycling at the global scale were also assessed.

Regarding the SO, isoprene concentration levels are driven by phytoplankton abundance over environmental or physical descriptors. Simple statistical models based on chlorophyll-a were developed showing different slopes and intercepts above and below a sea surface temperature threshold of 3.4°C. The strong relationship between isoprene and photoprotective pigments brought new evidence to the potential role of marine isoprene as a photoprotective response in phytoplankton. Isoprene concentration levels were retrieved for SO waters using remote sensing algorithm based on chlorophyll-a and sea surface temperature products from MODIS-Aqua. The highest values of isoprene concentration and emissions peak in summer season, in coastal areas of Antarctica, in blooming areas close to islands, and around latitudes of 40°S. The results suggested a total emission value of 0.063 Tg C yr⁻¹, which supports the range of previous bottom-up estimates. We estimated new values of isoprene production and degradation rates from Lagrangian experiments during the PEGASO cruise. These rates together with others previously published in the literature and estimated in laboratory conditions, were implemented on the ROMS-BEC model, a regional ecological model for the SO which includes 3 Phytoplankton Functional Groups (PFT's): diatoms, coccolitophores and a group of small mixed phytoplankton. Diatoms dominated the isoprene production in SO waters and a value of total emission of isoprene of 0.071 Tg C yr⁻¹ was calculated, agreeing with the values from remote sensing retrieval of isoprene concentration and bottom-up estimates.

As to the global ocean, isoprene production rates were implemented in DARWNI-MITgcm model, which includes 35 PFT's that are grouped in 6 groups: diatoms, coccolitophores, mixotrophic dinoflagellates, prokaryotes, diazotrophs, and pico-eukaryotes. According to the model outputs,

diatoms were the most important PFT in terms of isoprene production at the global scale, being specially relevant in surface waters of the SO. Finally, the turnover of isoprene in the surface ocean was studied from incubation experiments performed in different oceanic regions. Production of isoprene normalized to chlorophyll-a levels increased with temperature until 23°C, and drastically decreased in warmer waters. Biological degradation rate constants were dependent on chlorophyll-a concentration and were generally similar or faster than ventilation rate constants, and much faster than vertical mixing. Overall, the results suggest that isoprene cycling in the surface ocean is faster than previously thought, with turnover times in the range 1-16 days.

Resumen

Modelización de la distribución y el ciclo del isopreno en el océano

El isopreno (C_5H_8) es el carbono orgánico volátil biogénico (BVOC, por sus siglas en inglés) más ampliamente emitido. Se produce en la biosfera tanto en tierra como en el océano, y en la atmósfera actúa como precursor de aerosoles orgánicos secundarios. El isopreno tiene un origen eminentemente biológico en el fitoplancton pero sus agentes, mecanismos de producción y reciclado, incluida la fotoquímica, son muy poco conocidos. Todavía hay grandes discrepancias en las estimaciones de la emisión oceánica global de isopreno (0.1 - 11.6 Tg C año⁻¹). A pesar de que las emisiones marinas son más bajas que las terrestres, juegan un papel clave en la formación y brillo de las nubes en regiones remotas de los océanos. Debido a la inviabilidad de obtener mediciones sinópticas de las emisiones de isopreno sobre el océano global, deben calcularse con modelos numéricos que utilicen variables que se puedan medir utilizando datos de detección remota de satélites o generados a través de modelos de ecosistemas. Para poder predecir la distribución y emisión de isopreno en el océano superficial en el tiempo y el espacio, en esta tesis se han utilizado herramientas computacionales para el tratamiento estadístico de datos y para el diagnóstico/pronóstico. Por lo tanto, se han probado diferentes enfoques para predecir y estudiar el isopreno en aguas superficiales, incluidos el modelado estadístico, el modelado biogeoquímico-ecológico y la detección remota. A pesar de que la mayor parte del enfoque de esta tesis doctoral se centra en las aguas del Océano Austral (OA), también se han evaluado los patrones del ciclo del isopreno a escala global.

Con respecto al OA, los niveles de concentración de isopreno son controlados por la abundancia de fitoplancton sobre los descriptores ambientales o físicos. Se han desarrollado modelos estadísticos simples basados en clorofila-a que muestran diferentes pendientes e intersecciones por encima y por debajo de un umbral de temperatura de la superficie del mar de 3.4 °C. La fuerte relación entre el isopreno y los pigmentos fotoprotectores ha aportado nuevas pruebas del papel potencial del isopreno marino como respuesta fotoprotectora en el fitoplancton. Los niveles de concentración de isopreno se han recuperado para las aguas del OA utilizando un nuevo algoritmo de detección remota basado en productos de clorofila-a y la temperatura de la superficie del mar de MODIS-Aqua. Los valores de concentración de isopreno y emisiones alcanzan su punto máximo en la temporada de verano en las zonas costeras de la Antártida, en las zonas productivas ("blooms") cercanas a las islas y alrededor de los 40 °S. Los resultados sugieren un valor de emisión total de 0.063 Tg C año⁻¹, que respalda el rango de estimaciones anteriores del tipo "bottom-up". Se han estimado nuevos valores de producción de isopreno y tasas de degradación a partir de experimentos lagrangianos durante la campaña PEGASO. Estas tasas, junto con otras publicadas anteriormente en la literatura y estimadas en condiciones de laboratorio, se han implementado en el modelo ROMS-BEC, un modelo ecológico regional para el OA que incluye 3 Grupos Funcionales de Fitoplancton (PFT, por sus siglas en inglés): diatomeas, coccolitóforos y un grupo de fitoplancton pequeño mixto. Se ha encontrado que las diatomeas dominan la producción de isopreno en las aguas del OA y se ha calculado un valor de emisión total de isopreno de 0.071 Tg C año⁻¹, que se encuentra en el rango de los valores estimados mediante detección remota de la concentración de

isopreno y estos de estimas "bottom-up".

En cuanto al océano global, las tasas de producción de isopreno se han implementado en el modelo DARWNI-MITgcm, que incluye 35 PFT que se agrupan en 6 grupos: diatomeas, coccolitóforos, dinoflagelados mixotrofos, procariotas, diazotrofos y pico-eucariotas. Según los resultados del modelo, las diatomeas son el PFT más importante en términos de producción de isopreno a escala mundial, siendo especialmente relevantes en las aguas superficiales del OA. Finalmente, se ha estudiado el recambio de isopreno en la superficie del océano a partir de experimentos de incubación realizados en diferentes regiones oceánicas. Se ha encontrado que la producción de isopreno normalizado a clorofila-a aumenta con la temperatura hasta 23 °C y disminuye drásticamente en aguas más cálidas. Las constantes de la tasa de degradación biológica dependen de la concentración de clorofila-a y generalmente son similares o más rápidas que las constantes de la tasa de ventilación, y mucho más rápidas que la mezcla vertical. En general, los resultados sugieren que el reciclado del isopreno en la superficie del océano es más rápido de lo que se pensaba anteriormente, con tiempos de reciclado en el rango de 1-16 días.

A Lúcia Ribot,
"coautora en la sombra" de esta tesis y autora principal de los mejores años de mi vida.

A mis padres,
por creer en la educación como pilar irrenunciable, sobre todo en la mía,
pese a que no lo puse precisamente fácil.

La vida no es un ensayo, aunque tratemos muchas cosas; no es un cuento; aunque inventemos muchas cosas; no es un poema, aunque soñemos muchas cosas. El ensayo del cuento del poema de la vida es un movimiento perpetuo; eso es, un movimiento perpetuo.

Movimiento Perpetuo – Augusto Monterroso

Vamos partido a partido.

Diego Pablo Simeone

Contents

Introduction	33
Marine microorganisms, trace gases and aerosols in the context of global change	35
The cycling of volatiles in the ocean	37
Isoprene in the Earth's biosphere	39
Isoprene on land	39
Isoprene in the ocean	41
Distribution of isoprene across the oceans	42
Production and degradation of marine isoprene	43
Modelling of marine isoprene distribution and cycling	44
Ph.D Thesis objectives	47
1 Distribution and drivers of marine isoprene concentration across the Southern Ocean	55
Pablo Rodríguez-Ros, Pau Cortés, Charlotte Mary Robinson, Sdena Nunes, Christel Hassler, Sarah-Jeanne Royer, Marta Estrada, M. Montserrat Sala, Rafel Simó	
1.1 Introduction	59
1.2 Materials and Methods	60
1.2.1 The PEGASO, TransPEGASO and ACE cruises	60
1.2.2 Isoprene concentration measurements	60
1.2.3 Biological, physical and environmental variables	61
1.2.4 Other data sources in the Southern Ocean	62
1.2.5 Statistical analysis and model development	64
1.3 Results and Discussion	65

1.3.1	General patterns of isoprene surface concentration in the Southern Ocean	65
1.3.2	Drivers of isoprene concentration in the Southern Ocean	66
1.3.3	The predictive capacity of chlorophyll-a and sea surface temperature to isoprene concentration in the Southern Ocean	71
1.4	Appendix	76
2	Remote sensing retrieval of isoprene concentrations in the Southern Ocean	83
	Pablo Rodríguez-Ros, Martí Galí, Pau Cortés, Charlotte Mary Robinson, David Antoine, Charel Wohl, MingXi Yang, Rafel Simó	
2.1	Introduction	87
2.2	In situ measurements	88
2.3	Remote sensing matchups	89
2.4	ISOREMS: a new remote sensing-based model to predict isoprene concentrations in the Southern Ocean	90
2.5	Validation of ISOREMS	92
2.6	ISOREMS implementation to compute isoprene concentrations and emission fluxes	92
2.7	ISOREMS-derived isoprene concentrations and emission in the Southern Ocean	93
2.8	Caveats of ISOREMS and future research	95
2.8.1	Lack of observations in a complex ocean	95
2.8.2	Uncertainties about potential sources of atmospheric isoprene from the Southern Ocean	96
2.9	Closing remarks	96
2.10	Appendix	98
3	Ecological modelling of marine isoprene in the Southern Ocean	109
	Pablo Rodríguez-Ros, Cara Nissen, Pau Cortés, Nicolas Gruber, Sergio Vallina, Meike Vogt, Rafel Simó	
3.1	Introduction	113
3.2	Methods	115
3.2.1	Sampling and physical measurements	115
3.2.2	Lagrangian studies during PEGASO	115
3.2.3	Phytoplankton pigments and taxonomy	116

3.2.4	Isoprene concentration	117
3.3	Isoprene cycling processes from Lagrangian series	117
3.3.1	The isoprene budget in the surface mixed layer	117
3.3.2	Bacterial degradation and chemical oxidation rates	117
3.3.3	Air-sea exchange fluxes and rates	118
3.3.4	Vertical mixing fluxes and rates	119
3.3.5	PFT-specific production rates	119
3.4	An ecosystem model for isoprene concentration and emission in the Southern Ocean	122
3.4.1	Description of the ROMS-BEC model and setup	122
3.4.2	An isoprene module for ROMS-BEC	122
3.4.3	BASELINE simulation and model experiments	123
3.4.4	Model evaluation	128
3.4.5	Sensitivity experiments	131
3.5	Discussion	133
3.5.1	Sources and sinks of isoprene	133
3.5.2	The role of community structure in the production of isoprene	134
3.5.3	Limitations within the model	134
3.5.4	Paucity of in situ measurements and experiments	135
3.5.5	The annual emission of isoprene from the SO	136
3.6	Conclusions	136
3.7	Appendix	139
4	Global ecological modelling of marine isoprene production	157
	Pablo Rodríguez-Ros, Andrew Barton, Sergio Vallina, Stephanie Dutkiewicz, Oliver Jahn, Rafel Simó	
4.1	Introduction	161
4.2	Methods	162
4.2.1	DARWIN model setup	162
4.2.2	Isoprene production in DARWIN	162

4.2.3	Baseline simulation and experiments	163
4.2.4	Sensitivity experiments	164
4.2.5	Data of isoprene concentration	164
4.3	Results and Discussion	164
4.3.1	Assessment of published isoprene production rates	164
4.3.2	Seasonality and spatial distribution of isoprene production in the global ocean	166
4.3.3	Which PFT dominates isoprene production in each oceanic region?	170
4.3.4	Sensitivity analysis	173
4.3.5	Isoprene production and concentration in the global ocean	173
4.3.6	Uncertainties related to isoprene production	177
4.4	Appendix	179
5	Isoprene turnover in the surface ocean	195
	Rafel Simó, Pau Cortés, Pablo Rodríguez-Ros, Marta Masdeu	
5.1	Introduction	199
5.2	Methods	200
5.2.1	Sampling and physical measurements	200
5.2.2	Incubations	202
5.2.3	Isoprene concentration	202
5.2.4	Isoprene ventilation rate constant	203
5.2.5	Isoprene vertical mixing rate constant	203
5.2.6	Chlorophyll <i>a</i> concentration	204
5.2.7	Bacterial abundance	204
5.3	Results and Discussion	204
5.3.1	Isoprene loss rate: variability and drivers	204
5.3.2	Comparison of isoprene sinks	207
5.3.3	Isoprene production	207
5.3.4	Revising the magnitude and players of the marine isoprene cycle	208

Discussion	215
Drivers and modelling of isoprene distribution in the Southern Ocean	217
Combining laboratory and Lagrangian studies in the Southern Ocean	220
Shedding light on isoprene production	220
New insights on the turnover of isoprene in the surface global ocean	222
Emission of isoprene: bottom-up or top-down estimates?	223
Concluding considerations about modelling of marine isoprene	225
Future perspectives	227
Conclusions	229
Acknowledgements	243
Curriculum vitae	247

List of Figures

1	SOLAS Research Theme 4: Interconnections between aerosols, clouds, and marine ecosystems. The Surface Ocean – Lower Atmosphere Study (SOLAS) project is an international research initiative aiming to understand the key biogeochemical-physical interactions and feedbacks between the ocean and atmosphere.	36
2	Cycling of volatiles in the ocean. Extracted from Carpenter et al. (2012).	38
3	Isoprene budget and cycling on Earth. Extracted from Murrell et al. (2020).	40
4	Isoprene emissions from land and atmospheric reactions. Source: T.S. Dibble, State University of New York.	41
5	Biogenic emissions from land plants, including isoprene, and their roles as SOA precursors. Source: Pöhlker et al. (2012).	42
1.1	Dataset of measurements compiled in this work: (a) research cruises, (b) isoprene surface concentration, (c) chlorophyll-a concentration, and (d) sea surface temperature. A summary of the data shown in this figure can be found in Table 3.3.	64
1.2	Isoprene (a and c) and chlorophyll-a (b and d) concentrations in surface waters (0 to 10 meters depth) of the Southern Ocean (> 40°S) along with sea surface temperature and latitude gradients for all cruises compiled in this work (Figure 4.8, Table 3.3). Blue lines show the trend of the full dataset, while red lines represent the trend when excluding PEGASO cruise data. Notation for latitude in (a) and (b) is decimal degrees.	67
1.3	Principal Components Analysis (PCA) results for PEGASO and ACE. Abbreviations can be found in Table 1.1. PEGASO cruise: North of the South Orkney Islands (NSO), Southeast of the South Orkney Islands (SSO), Northwest of South Georgia Island (NSG), and West of Anvers Island (WA). ACE cruise: Cape Town - Hobart (Leg 1), Hobart - Punta Arenas (Leg 2), and Punta Arenas - Cape Town (Leg 3).	70
1.4	Comparison of different isoprene statistical models based on CHLA-FLUO and SST with measurements of isoprene concentration (Table 3.3). a: Comparison of our model (Figure 1.7a and b). b: Comparison of the (Ooki et al., 2015) model. c: Comparison of the (Hackenberg et al., 2017) model. d: Comparison of our model predictions with the measurements used in its development.	72

1.5	Comparison of the relationship between isoprene and chlorophyll-a concentrations on the cruises examined in this work (Table 3.3).	74
1.6	Scatterplot of misfit (residuals) among observed and predicted isoprene concentration values from PEGASO and ACE cruises versus chlorophyll-a levels (Fluorometric: a and b; and HPLC: c and d).	77
1.7	(a) and (b) Isoprene model based on CHLA-FLUO with the shifting regime based on a SST threshold of 3.4°C. (c) and (d) Isoprene model based on CHLA-HPLC with the shifting regime based on a SST threshold of 3.4°C. (e) CHLA-HPLC vs CHLA-FLUO. For these plots only data from TransPEGASO, PEGASO and ACE cruises were used (Figure 4.8, Table 3.3). RMSE = Root Mean Square Error (see equation 1.2).	78
2.1	(a) Surface ocean isoprene concentrations from the six cruises. Note the log scale. (b) Cruise tracks. More information in Table 3.3	89
2.2	Scatter plot of ISOREMS predictions vs. observations of isoprene concentrations.	91
2.3	Monthly climatology of $ISO_{ISOREMS}$ concentration in the Southern Ocean.	94
2.4	(a) Climatological seasonality of $ISO_{ISOREMS}$ concentrations in the entire Southern Ocean (red) and integrated by latitudinal bands (40 to 70°S). (b) Boxplot of annual mean concentrations of isoprene grouped by latitude. (c) Climatological accumulated emissions of $ISO_{ISOREMS}$ through the year. (d) Boxplot of annual mean isoprene emission fluxes grouped by latitude. In the boxplots (b and d), the horizontal black line inside the boxes is the median, the upper and lower limits of the boxes are, respectively, 75th and 25th percentiles; and the horizontal bars represent the upper and lower whiskers (largest values within 1.5 times interquartile range above 75th percentile and below 25th percentile).	95
2.5	Number of isoprene concentration measurements over the diel cycle of solar times. Solar times were calculated from GMT time and longitude using the <i>solAR</i> package on R.	99
2.6	Redundancy analysis (RDA) (Legendre and Legendre, 2012) of isoprene concentration and remote sensing variables using <i>vegan</i> package on R. After checking the non-normality distribution of our variables using Shapiro-Wilk's test, data were log-transformed. See Table 2.2 for abbreviations.	100
2.7	Misfit (residuals) of ISOREMS-predictions vs. each of the potential predictive variables tested (ISO, CHL, SST, PIC, PAR, POC, ZEU, MLD; Table 2.2). Last panel: Misfit of ISOREMS-predictions vs. observed isoprene concentrations.	101
2.8	(a) Scatter-plot of the coefficients of CHL and SST and the intercepts of the multiple linear regressions of random-sampling (80%) simulations (see text for details). (b) Histograms of the validation statistics (r^2 , RMSE, relative RMSE, BIAS, percent BIAS, and MAPE) randomly generated by the above simulations on 20% of the data. Number of simulations = 10,000.	102
2.9	Monthly climatology of $ISO_{ISOREMS}$ emission fluxes in the Southern Ocean. Blank spaces are pixels where either satellite CHL or wind speed are lacking.	103

3.1	Location of the three blooms during the PEGASO Cruise (pink circles) and track (blue line): North of the South Orkney Islands= NSO , Southeast of the South Orkney Islands = SSO and Northwest of South Georgia = NSG	116
3.2	Phytoplankton community composition based on CHEMTAX-HPLC analyses (Nunes et al., 2019a) for the three blooms during the PEGASO cruise (See Figure 3.1: North of the South Orkney Islands= NSO , Southeast of the South Orkney Islands = SSO and Northwest of South Georgia = NSG).	120
3.3	Overview of the mean isoprene surface (0–10 m) concentration (a), chlorophyll-a biomass (c) and isoprene emission (e) patterns in ROMS-BEC from the BASELINE run (Table 4.2). Boxplots representing the latitudinal distribution of the year integration of isoprene surface concentration (b), total chlorophyll-a biomass (d) and emission of isoprene (f). In the boxplots only values within percentile 5% and 95% are shown.	126
3.4	Changes in annual mean isoprene concentration (0-10), as percent difference, among all experiments (a : In situ - Direct; b : In situ - Light; c : Laboratory) (Table 4.2) for all latitudes higher than 40°S, and 10° latitudinal bands (40-50°S, 50-60°S, 60-70°S). BASELINE run is taken as reference (white color in a, b and c). d : Sensitivity Analysis results of BASELINE simulation to changing parameter by ±50% (Table 3.4). The state variable selected to that aim was isoprene concentration. Black bars indicate that an increase of the parameter causes an increase of the state variable, while grey bars indicate that an increase of the parameter causes a decrease of the variable state.	128
3.5	Global estimates (light blue) vs estimates from this work (blue). Dash lines in the results from this work represents the maximum and minimum values of isoprene emission from our experiments. The estimates from published works included in this graphs are bottom-up approaches.	129
3.6	a : Validation data set of isoprene concentration for the cruises compiled in Table 3.3 plotted together with the monthly average of isoprene surface concentration for the months of December, January, February and March (BASELINE run, Table 4.2). b : Latitudinal distribution of monthly averaged isoprene surface (0-10 m) concentrations for the months of concentration December, January, February and March and number of observations in our data set (Table 3.3). c : Boxplot of latitudinal values of observations and BASELINE run for the climatological period November - March, and latitudes higher than 40°S. d : Scatterplot of observations of isoprene concentration and model results from BASELINE run (Table 4.2).	132
3.7	a : Comparison of the relative contribution (%) of each PFT to chlorophyll-a and to isoprene production. b : Time series of isoprene production (logarithm of 10) per PFT throughout the climatological months. Data used for A and B is BASELINE (Table 4.2).	133
3.8	Monthly climatologies of isoprene concentration (pM) for the BASELINE run (Table 4.2).	139
3.9	Monthly climatologies of flux of isoprene ($\text{mmol m}^{-2} \text{d}^{-1}$) for the BASELINE run (Table 4.2).	139
3.10	Monthly climatologies of total chlorophyll-a concentration ($\mu\text{g L}^{-1}$)for the ROMS-BEC configuration used in this work.	139
3.11	Time series of monthly integrated isoprene concentration (left) and flux (right) in the Southern Ocean (>40°S) from ROMS-BEC runs. Note that the results of applying the statistical models from Ooki et al. (2015) (blue) and Hackenberg et al. (2017) are not shown.	140

3.12	Validation of isoprene concentration results from our simulations (Table 4.2) with observations of isoprene concentration from the cruises compiled in 3.3. RMSE = Root Mean Squared Error.	141
3.13	Relative contribution of every oceanic basin: Atlantic, Indian and Pacific Ocean (limits are defined according to NODC-NOAA: https://www.nodc.noaa.gov/woce/woce_v3/wocedata_1/woce-uot/summary/bound.htm) when latitude was below 40 °S (3.13). The marine emission of isoprene is proportional to the size of each ocean basin. Thus, for our BASELINE run, the Pacific Ocean is the main emitter (12.15 Mg C y ⁻¹) followed by the Indian Ocean (11.37 Mg C y ⁻¹) and the Atlantic Ocean (7.58 Mg C y ⁻¹).	142
3.14	Hovmoller diagram of isoprene emission in the Southern Ocean (>40°S) from the BASELINE simulation.	143
3.15	Hovmoller diagram of the vertical distribution of isoprene concentration in the Southern Ocean from the BASELINE simulation.	144
3.16	Hovmoller diagram of the vertical distribution of isoprene production in the Southern Ocean from the BASELINE simulation.	145
3.17	Hovmoller diagram of the vertical distribution of isoprene biological + chemical degradation (k_{LOSS} , see Section 3.4) in the Southern Ocean from the BASELINE simulation.	146
3.18	Hovmoller diagram of the vertical distribution of diatom biomass in the Southern Ocean from the BASELINE simulation.	147
3.19	Hovmoller diagram of the vertical distribution of diazotroph biomass in the Southern Ocean from the BASELINE simulation.	148
3.20	Hovmoller diagram of the vertical distribution of coccolithophore biomass in the Southern Ocean from the BASELINE simulation.	149
3.21	Hovmoller diagram of the vertical distribution of small phytoplankton biomass in the Southern Ocean from the BASELINE simulation.	150
3.22	Hovmoller diagram of the vertical distribution of total chlorophyll-a biomass in the Southern Ocean from the BASELINE simulation.	151
4.1	Isoprene production rates normalized by chlorophyll-a from lab experiments by taxon (a), by species (c), and a combination of both (c). Isoprene production rates vs (d) temperature in the cultures, and vs (e) light conditions in the cultures. (e) Isoprene production rates per cell vs cell volume. The values used for this Figure can be found in Table 4.4.	166
4.2	Seasonality of isoprene production in the surface global ocean (0-20 m) for each PFT (BASELINE simulation, Table 4.2).	167
4.3	Total surface isoprene production (0-20 meters depth) along the full climatological year for all PFTs (TOP) and each of them individually (BASELINE simulation, Table 4.2).	168
4.4	Hovmoller diagrams of the vertical distribution of isoprene production integrated along the full climatological year for all PFTs (TOP) and each of them individually (BASELINE simulation, Table 4.2).	169

4.5	Dominance of isoprene production (top) and chlorophyll-a levels (bottom) of each PFT implemented in DARWIN for January and July (BASELINE simulation, Table 4.2).	171
4.6	Results of the experiments described in Table 4.2. for the global ocean and each of its ocean basins (A : Global Ocean, B : Atlantic, C : Indian, and D : Pacific). The right column shows the annual integrated total production of isoprene per latitudinal bands. The left column depicts the DARWIN-predicted dominant PFT in terms of isoprene production in the first 20 meters of the water column during the climatological year.	172
4.7	Results from the Sensitivity Analysis for our BASELINE simulation. The target variable to measure the effects of varying each parameters by -50% or +50% is the integrated production of isoprene per year in surface waters (0-20 meters).	173
4.8	Global data-set of isoprene published measurements from cruises compiled in Table 4.3. (a) measurement locations and values. (b) Latitudinal distribution of isoprene concentrations. . . .	175
4.9	(a) Comparison of measurements of isoprene concentration (Table 4.3) with (a) isoprene production rates from the BASELINE simulation of DARWIN, (b) climatological chlorophyll-a concentration from DARWIN, (c) and sea surface temperature.	176
4.10	Monthly climatology (January and July) of total isoprene production (BASELINE simulation, Table 4.2).	180
4.11	Monthly climatology (January and July) of minor PFT's dominating isoprene production in the Global Ocean (BASELINE simulation, Table 4.2).	181
4.12	Dominance of isoprene production and relative contribution to chlorophyll-a levels of all PFT's in the global surface ocean. This figure shows the results for the climatological months of January and July.	182
4.13	Simplification of a marine ecosystem model showing its main parameters. Source: Banas (2011).185	
4.14	Environmental niches along three gradients: temperature (SST), dissolved inorganic nitrogen (DIC) and photosynthetically active radiation (PAR). Source: Pedro Cermeño (Institute of Marine Sciences - CSIC).	185
5.1	Geographical distribution of the experiments. Location of the sampling and incubation sites, coloured for isoprene concentration.	200
5.2	Isoprene processes and their main drivers. a. Rate constant of isoprene loss in dark incubations (k_{loss} , considered to be microbial and chemical consumption) vs. chlorophyll-a concentration. The linear regression equation is $k_{loss} = 0.10 \cdot [chl_a] + 0.05$ ($R^2=0.96$, $p=10^{-7}$, $n=11$). Error bars represent the experimentally-determined standard error of k_{loss} . The colour scale of the circles indicates bacterial abundances. b. Specific (chl_a - normalised) rate of isoprene production vs seawater temperature (SST) across the sample series. The dashed line is the general smoothed trend. The blue line is the exponential adjustment at $SST < 23^\circ C$: $isoprene\ sp.prod. = 2.04 \cdot e^{(0.13 \cdot SST)} + 0.71$ ($R^2=0.85$, $p=10^{-3}$, $n=8$).	205

5.3	Steady state cycling processes of isoprene in the surface ocean, according to oceanic productivity. Process rates averaged from the seven oligotrophic sites with $[chl a] < 0.5 \text{ mg m}^{-3}$ (blue arrows) and from the four productive sites with $[chl a] > 0.5 \text{ mg m}^{-3}$ (green arrows). The width of the arrows is proportional to the magnitude of the process rate. Note the change in the relative magnitude of the sinks.	209
5.4	Contribution of our cruises to the global dataset of isoprene concentrations.	219
5.5	Estimates of isoprene emission from the Southern Ocean, calculated in Chapters 2 and 3 of this thesis, in comparison with global bottom-up estimates from previous works (Brüggemann et al., 2018).	224

List of Tables

1.1	Variables from PEGASO and ACE cruises used in this study. Data were log10-transformed after checking their non-normality using the Shapiro–Wilk’s test. Temperature was transformed to Kelvin degrees to avoid negative values. The last columns show the statistics of the logarithmic regression of isoprene with all independent variables (r^2 : explained variance (in bold when p-value < 0.05); p-value: levels of significance; n = sample size.). * Effective quantum efficiency of ϕ_{PSII} photochemistry. "n. d." = non dimensional.	63
1.2	Statistics of the relationships between isoprene and chlorophyll-a and sea surface temperature. Data used for these analyses were sampled in surface waters of the Southern Ocean (>40°S) during TransPEGASO, PEGASO and ACE cruises (Table 3.3). Abbreviations can be found in Table 1.1. *RMSE = Root Mean Square Error (see equation 1.2).	71
1.3	Surface isoprene concentration measurements (0 – 10 meters depth) in the Southern Ocean (>40°S) along the research cruises used for model comparisons (Figure 4.8): PEGASO, TransPEGASO, ACE Expedition, AMT22, AMT23, KH-09-5, and ANDREXII. For more details, see Rodríguez-Ros et al. (2020b).	76
2.1	Surface (0 – 10 m) isoprene concentration measurements (pM) in the SO (>40°S) used for ISOREMS model development. *GC-MS: Gas Chromatography-Mass Spectrometry. **PTR-MS: Proton Transfer Reaction - Mass Spectrometry.	98
2.2	Variables used in this work and their sources.	98
3.1	Parameters used to estimate the isoprene production rates of each PFT (diatoms, coccolithophores and small mixed phytoplankton) calculated from <i>in situ</i> data in three different blooms studied in the PEGASO cruise (See Figure 3.1: North of the South Orkney Islands = NSO , Southeast of the South Orkney Islands = SSO and Northwest of South Georgia = NSG). *Mean of k_{LOSS} in the PEGASO cruise experiments = 0.29 d ⁻¹	121
3.2	Overview of model parameters used in BASELINE simulation and model experiments. Annual means of isoprene concentration (0-10 m), and integrated annual flux values in surface waters are shown for latitudes > 40°S.	124
3.3	Surface isoprene concentration (0 – 10 m, pM) in the SO (>40°S) along the research cruises represented in Figure 3.6 A: PEGASO, TransPEGASO, ACE Expedition, AMT23, AMT22, KH-09-5 and ANDREXII.	129

3.4	Overview of sensitivity experiments (as described in Section 4.2.4) for BASELINE simulation (Table 4.2).	131
3.5	Global estimates of isoprene emissions for the global ocean in comparison with our results for the Southern Ocean. A more complete version of global estimates of isoprene emission can be found in (Brüggemann et al., 2018).	137
4.1	Overview of the PFT's implemented in the configuration of the DARWIN model used in this work (Dutkiewicz et al., 2019; Kuhn et al., 2019)	162
4.2	Overview of model experiments using DARWIN model.	163
4.3	Isoprene concentration measurements compiled for this work.	165
4.4	Compilation of isoprene production rates (normalized by chlorophyll-a biomass or number of cells) by different species estimated in laboratory experiments and their culture conditions. References: Milne et al. (1995); Shaw et al. (2003); Bonsang et al. (2010); Colomb et al. (2009); Arnold et al. (2009); Exton et al. (2013). * Rates from Meskhidze et al. (2015) included in this table are the average of Tables 2 and 3 in (Meskhidze et al., 2015).	179
4.5	Ecosystem model state-variables.	189
4.6	Ecosystem model terms.	189
4.7	Ecosystem model parameters.	190
5.1	Sample characteristics and estimates of isoprene process rates. Sample location on map of Figure 5.1, sea surface temperature (SST, which was the temperature of the incubation), chlorophyll-a concentration (chl _a), concentration of heterotrophic prokaryotes (mostly bacteria), isoprene concentration, rate constants for isoprene loss (k_{loss} , biological and chemical) and ventilation (k_{vent}), total turnover time (τ), and specific or chl _a -normalized production rate.	201
5.2	Location of the experimental sites, sampling depth, and physical variables. SSS: sea surface salinity; SST: sea surface temperature; Z_{ML} : mixed layer depth; U_{10} 24h: wind speed at 10 m above sea surface, averaged over 24 hours. ^a : Estimated from a monthly climatology (Holte et al., 2017).	201
5.3	Measured biological variables and isoprene process rate constants. chl _a : chlorophyll a concentration; BA: bacterial (prokaryotic heterotroph) abundance; HNA-BA: high nucleic acid containing bacterial abundance; k_{loss} : rate constant of isoprene loss in incubations (microbial degradation + chemical oxidation); k_{vent} : rate constant of isoprene ventilation to the atmosphere; k_{mix} : rate constant of isoprene vertical mixing by turbulent diffusion at the bottom of the mixed layer (negative means import into the surface mixed layer); k_{prod} : rate constant of isoprene production, assuming 24-h steady state for the isoprene concentration. ^a : Taken from the global integral suggested by the model of Conte et al. (2020).	206

5.4	Summary of isoprene production rates ($\rho_{\text{CHLA}}^{\text{PFT}}$) estimates per PFTs in this thesis: Chapter 3 (DARWIN-MITgsm) and Chapter 4 (ROMS-BEC). ^a : Estimated in Lagrangian experiments during PEGASO. ^b : Estimated using Booge et al. (2016). ^c : Estimated in Lagrangian experiments during PEGASO using the light factors from Booge et al. (2018) or Gantt et al. (2009). ^d : Estimated using Booge et al. (2016) and Meskhidze et al. (2015).	222
-----	---	-----



Introduction

Introduction

In considering the study of physical phenomena, not merely in its bearings on the material wants of life, but in its general influence on the intellectual advancement of mankind, we find its noblest and most important result to be a knowledge of the chain of connection, by which all natural forces are linked together, and made mutually dependent upon each other; and it is the perception of these relations that exalts our views and ennobles our enjoyments.

Cosmos – Alexander von Humboldt

Marine microorganisms, trace gases and aerosols in the context of global change

At the global scale, atmospheric particles have the ability to strongly influence the formation and the optical properties of clouds; affecting the planetary energy balance (Andreae and Rosenfeld, 2008). However, the behaviour of these particles, named aerosols, as cloud seeders is still one of the biggest sources of uncertainty in global warming projections to the future (Hu et al., 2013; Stocker et al., 2013). The climate implications of aerosol-cloud processes are still very difficult to predict, in part due to incomplete knowledge about sources of aerosols. Trace gases, when oxidized in the lower atmosphere, are involved in these effects by forming new aerosols and making them grow to cloud-active sizes, namely **cloud condensation nuclei (CCN)**. The impact of human activities since the industrial revolution has been pointed out as a possible agent that has modified CCN numbers, distribution and behaviour. On this line, (Carslaw et al., 2013) suggested that the CCN concentrations in the pre-industrial era were similar to those in the present pristine oceanic regions. Thus, the study of these remote areas will allow defining a baseline atmosphere and better assessing anthropogenic impacts on CCN numbers and cloud formation processes and, therefore, on the **global climate**.

In the marine atmosphere, where cloud formation processes are highly susceptible to aerosol emissions, an important proportion of particle formation occurs through the oxidation of **trace gases** exhaled from sea (O'Dowd et al., 2002b), many of them produced by the **marine biota** (Carpenter et al., 2012) (Figure 1). Marine microorganisms are widespread in the global ocean, where they play several roles in biogeochemical processes between the ocean and the atmosphere, being trace gas production one of the most important ones for atmospheric processes. However, the global assessment of trace gas production by marine biota is a challenge due to two main issues: (1) the distribution and species richness of microorganisms differs from one place to another, being its global contribution to ocean-atmosphere processes extremely difficult to quantify (Carpenter et al., 2012); and (2) the emission of trace gases differs from one microbial taxon to another (Exton et al., 2013; Meskhidze et al., 2015; Booge et al., 2016). Coupling current and future knowledge about aerosol precursor production mechanisms within the marine ecosystem with atmospheric models is the only way to achieve a synoptic assessment of the impact of marine biota on climate.

The **CLAW hypothesis** (Charlson et al., 1987) was proposed in the late '80s by a group of researchers who gave the first letter of their names to create the acronym CLAW: **C**harlson, **L**ovelock, **A**ndreae, and **W**arren. This hypothesis was built upon the Gaia hypothesis, previously developed by Lovelock (Lovelock and Margulis, 1974; Lovelock, 1979), which suggested that planet Earth has developed the ability to regulate the chemical composition of its components, the surface pH, and possibly the climate. It must be highlighted that, although the Gaia hypothesis is nowadays considered an intuitive theory difficult to be proven, it has demonstrated its potential as a trigger for a new holistic view of the Earth system, strongly influencing the current biogeochemical and environmental sciences in many different aspects (Lovelock, 2003). Thus, as a case of the Gaia hypothesis, the CLAW hypothesis suggests that marine phytoplankton is able to regulate climate at the regional and even global scales through the emission of cloud-forming volatile sulfur. Specifically,

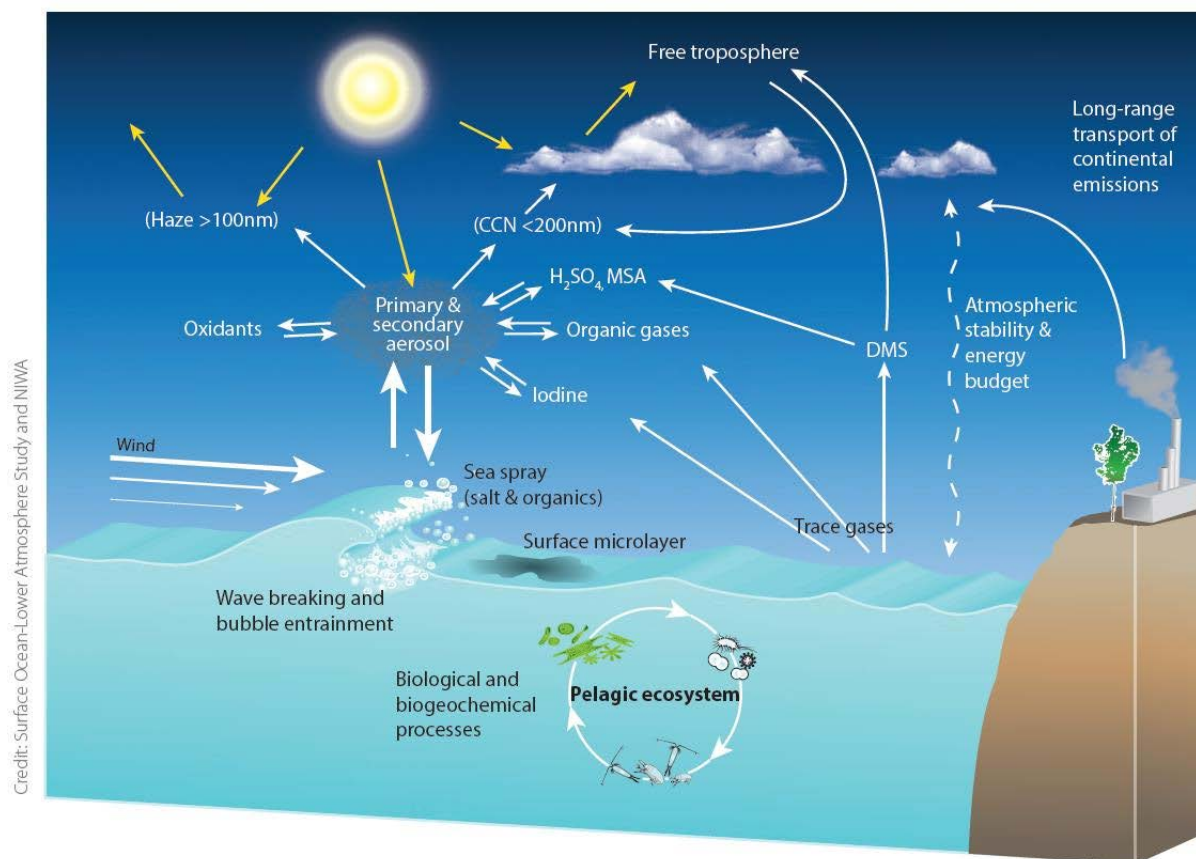


Figure 1: SOLAS Research Theme 4: Interconnections between aerosols, clouds, and marine ecosystems. The Surface Ocean – Lower Atmosphere Study (SOLAS) project is an international research initiative aiming to understand the key biogeochemical-physical interactions and feedbacks between the ocean and atmosphere.

the hypothesis suggests that marine phytoplankton is able to produce and release DMS (dimethyl sulfide, $(\text{CH}_3)_2\text{S}$), which, when leaving the ocean to the atmosphere, oxidizes to non-volatile acids that eventually become particles. These particles are known as **secondary aerosols (SA)**, in contrast with primary aerosols like salt crystals risen with sea spray by wind friction (O'Dowd et al., 2002a). If SA grow large enough, eventually become cloud condensation nuclei (CCN) upon which water droplets condense. The number of CCN influences cloud droplet concentration and cloud brightness, which is relevant for the albedo of the Earth. Increases in cloud albedo reduce the amount of solar radiation reaching the ocean surface and, therefore, lower phytoplankton activity and UV-related stress, causing lowered DMS production. In other words, CLAW proposes that more DMS production causes higher cloud albedo, lower light and temperature in the ocean and, consequently, lower DMS and lower albedo, and so on and so forth in a negative feedback loop by which phytoplankton help regulate the climate. Although DMS is the key component of CLAW and has been the most studied marine trace gas up to date (Lana et al., 2011; Carpenter et al., 2012), there are other volatiles that participate in aerosol formation and may play a similar atmospheric role, in what can be regarded as an extended version of CLAW: isoprene (C_5H_8) (Meskhidze and Nenes, 2006; Dani and Loreto, 2017), methylamines (Van Neste et al., 1987; Gibb et al., 1999; Airs and Archer, 2010), and iodomethanes (CH_3I , CH_2I_2 , CH_2ClI) (Richter and Wallace, 2004; Archer et al.,

2007; Carpenter et al., 2013). Still other compounds, such as bromomethanes (CHBr_3 , CH_2Br_2) (Saiz-Lopez and von Glasow, 2012; Carpenter et al., 2012; Ziska et al., 2013), are also emitted by the ocean and, despite not being involved in aerosol formation, they affect ozone concentrations and the oxidative capacity of the atmosphere.

Due to the impossibility of measuring emissions of trace gases in a synoptic way over the global ocean, using numerical models is vital to assess and monitor the aforementioned processes. In recent years, there have been very significant advances in **numerical modelling of the microbial-ocean-atmosphere processes**, including aerosols formation and behaviour. This requires the use of predictor variables that can be measured using remote sensing data from satellites or generated through ecosystem models. However, any numerical model aimed to be realistic requires a good knowledge of the processes upon which it is created. Consequently, a close interaction between modelling and experimental approaches is required to achieve the necessary predictive capacity to study these processes and mechanisms.

Nowadays, under a **global change scenario**, there is a need to understand the hidden phenomena in nature that trigger positive and/or negative feedbacks within Earth's subsystems (biosphere, atmosphere, geosphere, and hydrosphere). This requires disentangling the most relevant components that dominate local processes that are able to influence global scale processes. Anthropogenic climate change will be, if not the most, one of the most important challenges for humankind during the present XXI century. In this context, improving the current knowledge related to climate change science is essential to properly assess its risks for present and future society. During the past decades, climate change has forced the international scientific community to join forces from different areas of Earth Sciences (oceanography, meteorology, etc.) in order to shed light on this global challenge. As part of it, the study of the processes that regulate the global biogeochemical cycles within the ocean-atmosphere system is a keystone for the comprehension, assessment and early detection of risks associated with global climate change.

The cycling of volatiles in the ocean

In order to study air-sea exchanges of trace gases, there is the need to gather the available theoretical and experimental knowledge of the relevant biogeochemical processes that drive their concentrations and fluxes. There are different **mechanisms of production and degradation of trace gases in the ocean** (Carpenter et al., 2012), the most important ones being closely linked to the biological activity of marine organisms (from bacteria to macroalgae and corals) and the photochemical processes in the surface ocean (Figure 2).

If we are to parameterize these processes and develop tools ranging from statistical models to complex ecosystem models, we must be able to mathematically describe all production and consumption terms of a specific volatile in the ocean. Thus, at any time (t) and depth (z), the volatile compound concentration [VOL] will be the net result of production and consumption pro-

cesses (equation 1):

$$[\text{VOL}]_{z,t+\Delta t} = [\text{VOL}]_{z,t} + (\text{GP}_{z,t} - \text{BC}_{z,t} - \text{P}_{z,t} - \text{V}_{z,t} - \text{T}_{z,t})\Delta t \quad (1)$$

Where GP = gross volatile production; BC = bacterial volatile consumption; P = volatile photochemistry; T = volatile ventilation; T = volatile displacement by vertical turbulent diffusivity. Volatile photochemistry (P) can be represented as the balance between photochemical loss (PC) and production processes (PP) (equation 2):

$$[\text{VOL}]_{z,t+\Delta t} = [\text{VOL}]_{z,t} + (\text{GP}_{z,t} + \text{PP}_{z,t} - \text{BC}_{z,t} - \text{PC}_{z,t} - \text{V}_{z,t} - \text{T}_{z,t})\Delta t \quad (2)$$

For the calculation of volatile photochemistry, PP (equation 4) and PC (equation 5), total surface irradiance ($E_{d,o,t}$) (equation 3) and the underwater light extinction coefficients K_d can be combined to obtain the amount of radiation available at each t and z ($E_{d,z,t}$):

$$E_{d,z,t} = E_{d,o,t} * e^{-K_d * z} \quad (3)$$

$$\text{PP}_{z,t} = [\text{VOL}]_{z,t} * K_{p_{\max}} * (E_{d,z,t}/E_{d,o,\max}) \quad (4)$$

$$\text{PC}_{z,t} = [\text{VOL}]_{z,t} * K_{c_{\max}} * (E_{d,z,t}/E_{d,o,\max}) \quad (5)$$

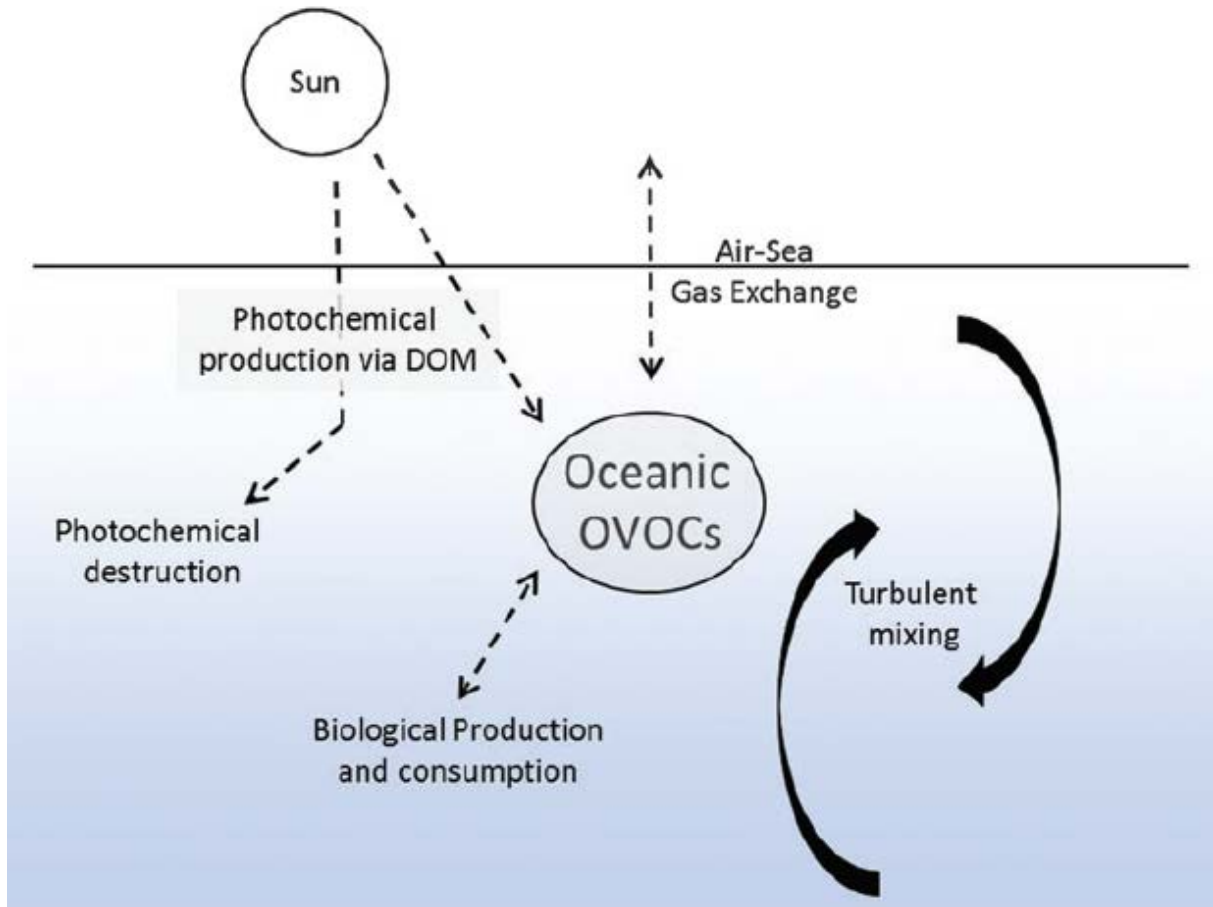


Figure 2: Cycling of volatiles in the ocean. Extracted from Carpenter et al. (2012).

Where K_{\max} = photochemical rate constant at the water surface, and $Ed_{,o,\max}$ = maximum irradiance at the water surface. Both parameters, K_{\max} and $Ed_{,o,\max}$, depend on the involved environmental variables for PP (equation 4) and PC (equation 5) of each different volatile, such as for example $[CDOM]$, $[DOM]$, $[OH^-]$, $[I^-]$ or $[O_3]_{air}$.

Ventilation applies only to the very upper water layer, from where its effects are “redistributed” by turbulent diffusion. Emission or ventilation fluxes (V) can be obtained as described in equation 6, where $[VOL]$ is volatile concentration in sea water, $[VOL]_a$ is the volatile concentration in the air, $k_{c_w,VOL}$ ($cm\ h^{-1}$) is the transfer or piston velocity, and H is the dimensionless gas-over-liquid form of the Henry’s law constant for the specific volatile (equation 6):

$$V = k_{c_w,VOL} * ([VOL] - [VOL]_a * H) \quad (6)$$

However, when a volatile is largely supersaturated in the surface ocean and its atmospheric lifetime is short, $[VOL]_a$ can be taken as ≈ 0 . Therefore, V can be estimated as the product of $k_{c_w,VOL}$ and $[VOL_w]$ (equation 7):

$$V = k_{c_w,VOL} * [VOL] \quad (7)$$

$[VOL]$ transport can be calculated from vertical turbulent diffusivity (K_z) previously diagnosed with a 1D water column model and vertical $[VOL]$ gradient as described in equation (equation 8).

$$T = K_z * d[VOL]/dz \quad (8)$$

In conclusion, by estimating the values of all the processes described above, it is possible to quantify the concentration of a trace gas in seawater from the balance between its production and degradation rates and/or values. Despite this formulation may look simple, the cycling of traces gases varies not only depending on the different volatile but also across every ocean in terms of horizontal space, depth and seasonality. Consequently, prior to attempting to model the cycling of a specific trace gas, achieving the maximum quantity of knowledge about the parameters in all the equations described above is needed. Unfortunately, for many trace gases, there is still a **lack of experimental data** of its cycling process, in many cases even a lack of concentration measurements, which makes understanding its distribution and cycling across the oceans a formidable challenge. Consequently, more experimental studies of cycling processes, conducted in laboratory and field conditions, are essential to improve the basic knowledge to be implemented in numerical models of ocean-atmosphere exchanges.

Isoprene in the Earth’s biosphere

Isoprene on land

Isoprene (C_5H_8), or 2-methyl-1,3-butadiene, is a volatile (boiling point of $34^\circ C$) non-methane hydrocarbon (NMHC) included in the group of biogenic volatile organic compounds (BVOC). Isoprene is produced in the biosphere both on land and in the ocean, being **the most widely emitted BVOC to the atmosphere** and the second most abundant natural hydrocarbon, after methane

(CH₄) (Guenther et al., 2006; Müller et al., 2008; Arneth et al., 2008) (Figure 4). Figure 3 (extracted from (Murrell et al., 2020)) sketches the cycle of isoprene on Earth. Globally, **its main source is photosynthetic vegetation**, mostly trees and shrubs, (Zimmerman et al., 1988; Sharkey and Yeh, 2001), whose emission ranges from 413 Tg C yr⁻¹ (Müller et al., 2008) to 500 Tg C yr⁻¹ (Guenther et al., 1995), representing approximately 90% of global isoprene emissions (Sharkey et al., 2008). Furthermore, isoprene plays several roles in vegetation communities like forests, where it can account for up to 80% of all hydrocarbons released (Lamb et al., 1987), protecting plants from reactive oxygen species (ROS) and heat stress (Sharkey et al., 2008; Zeinali et al., 2016). If we include crops in the budget of isoprene production by plants, the total emission amounts 530 Tg C yr⁻¹ (Murrell et al., 2020). Apart from plants, its production has also been detected for bacteria, algae, protists, fungi, and animals. Regarding its sinks, atmospheric reactions and bacterial communities in terrestrial soils are the most relevant loss pathways of emitted isoprene (Cleveland and Yavitt, 1998; El Khawand et al., 2016). All in all, as shown in Figure 3, the net contribution to the isoprene budget of many sources and sinks, such as anthropogenic activities, humans themselves, animal livestock, freshwater ecosystems, fens, or biomes like tundra, is still unknown.

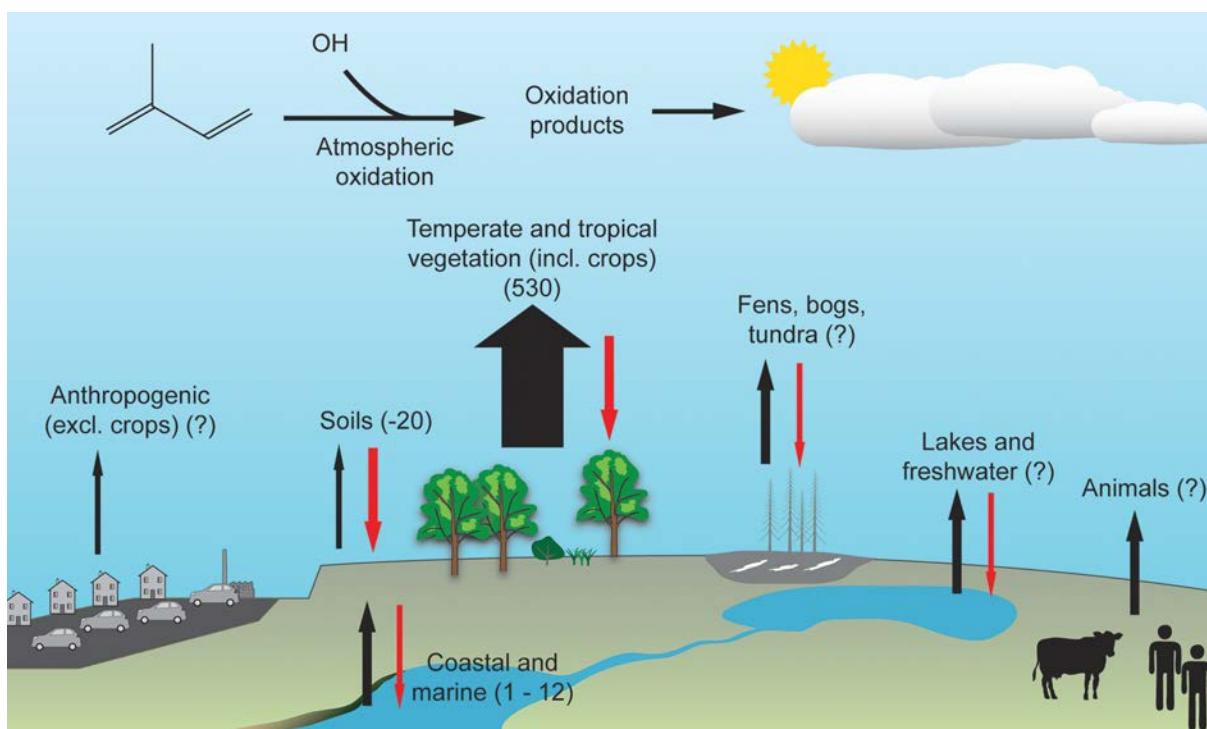


Figure 3: Isoprene budget and cycling on Earth. Extracted from Murrell et al. (2020).

When emitted to the atmosphere, its **high reactivity and short life-time** make this compound relevant for the climate (Pacifico et al., 2009). Overall, isoprene has several impacts on the atmosphere (Figures 4 and 5), from increasing the levels of tropospheric ozone (O₃) through reaction with NO (Sharkey et al., 2008; Pacifico et al., 2009), to the formation of secondary organic aerosols, which can impact human health (Heal et al., 2012) but also absorb and scatter solar radiation and participate in cloud formation processes (Carslaw et al., 2013). Moreover, isoprene, together with CH₄, contributes to atmospheric CO₂ through oxidation processes (Stocker et al., 2013).

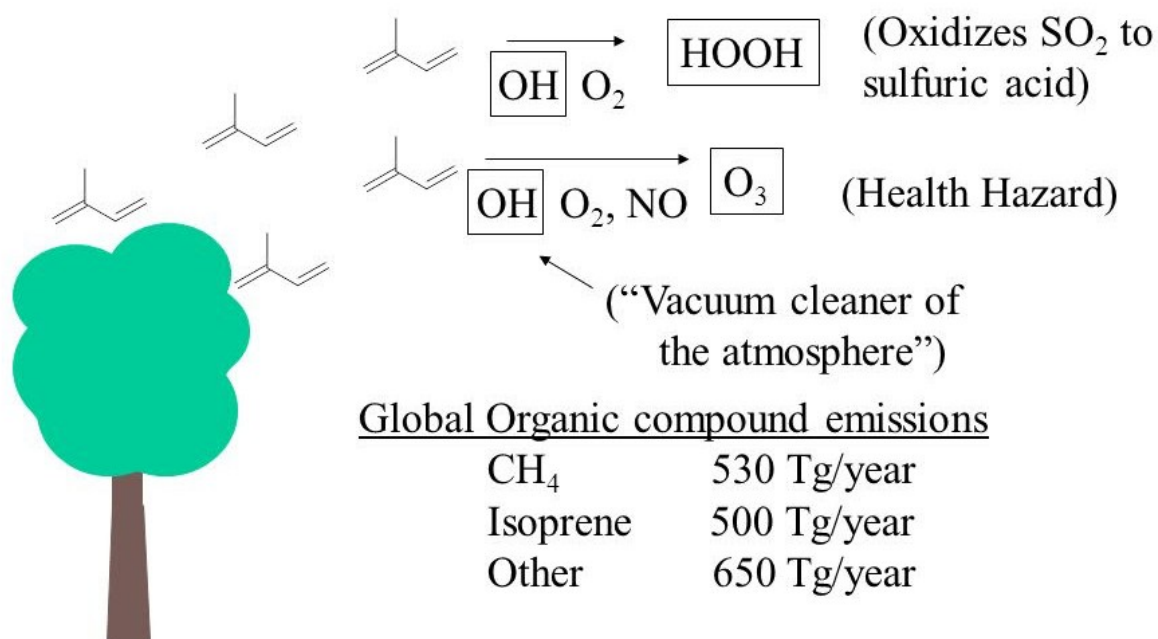


Figure 4: Isoprene emissions from land and atmospheric reactions. Source: T.S. Dibble, State University of New York.

Isoprene in the ocean

At sea, isoprene was first described by Bonsang et al. (1992), who quantified a global marine emission of 0.1 Tg C yr⁻¹, four orders of magnitude lower than terrestrial emissions (Guenther et al., 1995). However, there still are large discrepancies in the **bottom-up or top-down estimations** of global oceanic emission (Brüggemann et al., 2018). Recent estimates range from ≈ 1 Tg C yr⁻¹ (Palmer and Shaw, 2005; Gantt et al., 2009) to 11.6 Tg C yr⁻¹ (Luo and Yu, 2010). Consequently, despite isoprene was detected in marine waters decades ago, we are still far from possessing enough knowledge to be able to assess the direct or indirect effects that this trace gas can trigger in the local atmosphere or the global climate. Most of the inaccuracies in quantifying global marine isoprene emissions are due to the lack of knowledge of its production and degradation processes (Booge et al., 2018), magnitude and spatial distribution (Oooki et al., 2015; Hackenberg et al., 2017), and its relationship with environmental parameters and phytoplankton speciation (Carpenter et al., 2012; Exton et al., 2013). Despite marine isoprene emissions are much lower than terrestrial emissions, in the remote oceans far from continental influence ocean-leaving isoprene impacts in local remote marine boundary layer (MBL) chemistry and represents a **major source of secondary organic aerosols (SOA)** (Claeys et al., 2004; Kroll et al., 2006; Liao et al., 2007; Gantt et al., 2009; Luo and Yu, 2010) (Figure 1). Consequently, isoprene-derived SOA will serve as cloud condensation nuclei (CCN) and result in reduced radiative forcing over the oceans (Carslaw et al., 2010). It has been estimated that **isoprene may trigger climate cooling by contributing 5-25 percent of global of natural SOA** (Claeys et al., 2004), and this contribution is expected to be even higher in remote oceanic regions like the Southern Ocean (Meskhidze and Nenes, 2006).

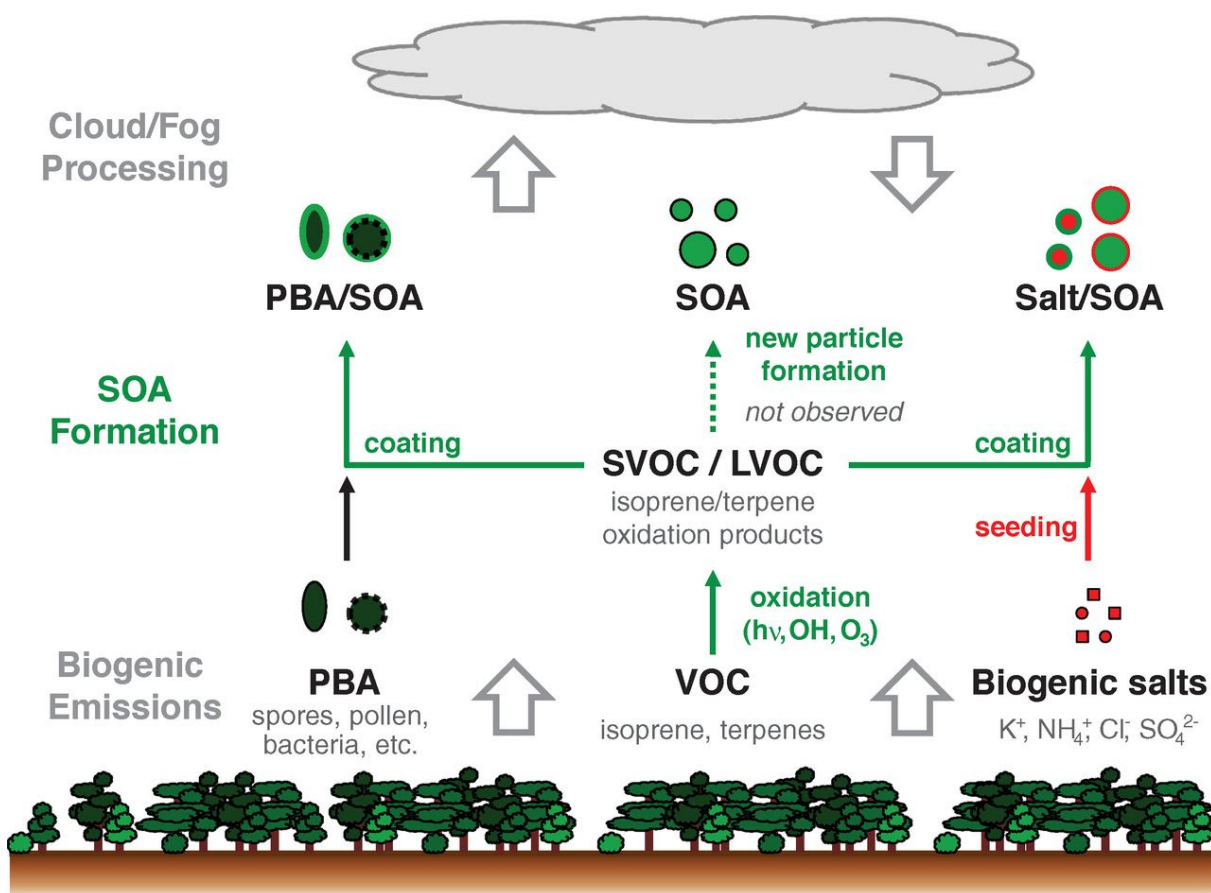


Figure 5: Biogenic emissions from land plants, including isoprene, and their roles as SOA precursors. Source: Pöhlker et al. (2012).

Distribution of isoprene across the oceans

Isoprene is **produced by phytoplankton**, which has been repeatedly confirmed in the field since three decades ago (Bonsang et al., 1992; Milne et al., 1995; Broadgate et al., 1997; Baker et al., 2000; Matsunaga et al., 2002; Shaw et al., 2003; Wingenter et al., 2004; Kurihara et al., 2010; Kameyama et al., 2010; Kurihara et al., 2012; Tran et al., 2013; Kameyama et al., 2014; Zindler et al., 2014; Ooki et al., 2015; Hackenberg et al., 2017). Due to this close relationship with phytoplankton, hot-spots of isoprene concentration have been found in **biologically enriched areas**, such as coastal areas or phytoplankton blooms, specially in **spring and summer** seasons (Liakakou et al., 2007; Zindler et al., 2014; Ooki et al., 2015; Booge et al., 2016; Hackenberg et al., 2017; Wohl et al., 2020). Not surprisingly, high levels of isoprene concentration have also been measured in experiments of iron fertilization performed in the Southern Ocean (Wingenter et al., 2004; Moore, 2006). Some areas of the ocean are still greatly under-sampled, such as the Pacific Ocean (see compilation in Conte et al. (2020)). Overall, isoprene concentration values in the surface ocean typically **range from 1 to 100 pM**, with some exceptions that can reach up to 200 pM (Tran et al., 2013; Kameyama et al., 2010). Regarding its vertical distribution, isoprene typically follows chlorophyll-a concentrations and primary production (Hackenberg et al., 2017; Booge et al., 2018; Conte et al., 2020), which suggest again its strong dependency on phytoplankton. Nevertheless, the number of

field studies addressing these questions in remote oceanic areas is still quite small. This is the case for the Southern Ocean, a region where isoprene distribution and cycling have been poorly studied (Meskhidze and Nenes, 2006; Kameyama et al., 2010; Ooki et al., 2015; Hackenberg et al., 2017), despite of its remoteness and the occurrence of spots of strong biological productivity during the austral summer.

Production and degradation of marine isoprene

Isoprene production has been confirmed for **microalgae** (Moore et al., 1994; Milne et al., 1995; McKay et al., 1996; Shaw et al., 2003; Exton et al., 2013; Liakakou et al., 2007; Bonsang et al., 2010; Meskhidze et al., 2015, in total 124 isoprene production rates), **macroalgae** (Broadgate et al., 2004), and **microbial communities** (Fall and Copley, 2000). In some of these works, isoprene production rates by the different phytoplankton species have been normalized by chlorophyll-a and, less frequently, cell size. The exploration of the estimated production rates per chlorophyll-a reveals remarkable differences of up to 2 orders of magnitude even between strains of the same species. These differences are likely due to differences in the culture conditions, such as light and temperature, as well as during the maintenance of cell stocks (Booge et al., 2016). On this line, only Meskhidze et al. (2015) have tested the effects of physiological stress conditions triggered by changes in water temperature and light irradiance over different marine microalgae species and found that physiological acclimation may trigger enhanced production of isoprene and also monoterpenes. These discrepancies hamper the use of these isoprene production rates to estimate global isoprene emissions, although some studies like Dani et al. (2017) attempted to do so based on the rates derived from two cultured diatoms. Furthermore, an additional isoprene source has recently been suggested to occur by interfacial photoproduction in the sea-surface microlayer from organic surfactants (McKay et al., 1996; Ciuraru et al., 2015a; Fu et al., 2015; Brüggemann et al., 2018).

Regarding the main loss processes of marine isoprene, these are believed to be **bacterial degradation and flux to the atmosphere** (Palmer and Shaw, 2005; Kameyama et al., 2014; Booge et al., 2018), over chemical oxidation by reactive oxygen species (ROS) (Riemer et al., 2000; Palmer and Shaw, 2005; Zinser, 2018), and vertical mixing. However, the quantification of biological degradation is still a pendant issue to solve the cycling of marine isoprene. On the one hand, Shaw et al. (2003) suggested that bacterial degradation must be very small, almost negligible. On the other hand, Alvarez et al. (2009) showed that isoprene consumption by bacteria did not exhibit first-order dependency on isoprene concentration in samples from temperate and tropical marine ecosystems. All in all, up to date no experiment of isoprene degradation has been performed in open ocean waters in natural conditions, including isoprene concentrations. Recently, Booge et al. (2018) supported the idea already stated in previous modelling studies (Palmer and Shaw, 2005; Arnold et al., 2009) that biological degradation by bacteria can not be avoided when budgeting isoprene production and its eventual emission to the atmosphere. In any case, isoprene occurs dissolved in seawater and is susceptible to be consumed by marine bacteria, likely in a similar way to that found for soil bacteria and fresh water sediments (Gray et al., 2015; Srivastva et al., 2017; McGenity et al., 2018).

Modelling of marine isoprene distribution and cycling

As described previously, if we are to achieve a complete comprehension of the cycling of any marine volatile like isoprene, we need to understand and quantify all of the processes involved. To do that, experimental studies conducted in laboratory and field conditions are essential. Ultimately, the outcomes of these experiments will allow constructing models to understand the distribution and cycling of isoprene at different spatial and temporal scales. The use of models can help to identify which are the processes and mechanisms that are still unclear and not properly quantified. Furthermore, models make it possible to assess the sensitivity of the full cycle to changes in one or more of its processes. Altogether, the **combination of experiments and models** is the way to go to evaluate the behavior of volatiles in the ocean whose theoretical and experimental knowledge is still limited, which is the case of isoprene.

Up to date, several modelling and remote sensing studies of global marine isoprene concentration and emission have been performed. These have been deeply discussed in Booge et al. (2016) and Brüggemann et al. (2018). Since isoprene is related to marine primary production, different relationships have been proposed between isoprene concentration levels and environmental variables such as chlorophyll-a and other phytoplankton pigments, temperature, and light irradiance. Ooki et al. (2015) proposed a set of **statistical models** to predict isoprene concentration based on its relationships with chlorophyll-a in different sea surface temperature regimes. In a similar way, Hackenberg et al. (2017) explored the relationship between isoprene concentration and chlorophyll-a, primary production and photoprotective pigments. Although these two works used the biggest datasets available, which covered a broad latitudinal gradient, they still lacked measurements in some important regions like the Southern Ocean. Ooki et al. (2015) provided a diagnostic equation for polar waters, merging the measurements from the Arctic and the Southern Oceans as though they were totally comparable in the phytoplankton sources. Hackenberg et al. (2017) proposed a based diagnostic model for isoprene concentration specific for sea surface temperatures below 20°C. This temperature threshold greatly exceeds the temperatures of polar and sub-polar waters.

As stated previously in this section, the attempts to quantify the total **emission of isoprene** have provided different estimates with large uncertainties in terms of magnitude still unsolved. Overall, there have been two main conceptual frameworks to tackle this questions: (1) **bottom-up estimates**: based on extrapolation of observations and/or modelling of marine concentrations of isoprene (0.1 – 1.2 Tg C yr⁻¹); and (2) **top-down estimates**: estimating marine emissions needed to account for the atmospheric isoprene concentration in the marine boundary layer (MBL) (1.5 – 11.6 Tg C yr⁻¹). Among the bottom-up approaches, Palmer and Shaw (2005) used MODIS satellite chlorophyll observations and a steady-state water column model; they assumed that air-sea exchange is the dominant isoprene sink in the surface ocean, followed by bacterial losses. Arnold et al. (2009) retrieved global distribution of phytoplankton functional types from remote sensing data, which were combined with phytoplankton-specific isoprene rates (based on phytoplankton functional types, PFT's) to estimate isoprene concentration and emission. Gantt et al. (2009) also used PFT's but related the production of isoprene to photosynthetically active radiation (PAR) irradiance along with chlorophyll-a levels. Booge et al. (2018) also provided a global map of oceanic concentrations

and emissions of isoprene, based on remote sensing estimates of PFT. Moreover, they largely discussed the limitations of bottom-up approaches and the use of a simple statistical model to study isoprene cycling at the global scale. As to top-down studies, Arnold et al. (2009), Luo and Yu (2010) and Hu et al. (2013) calculated the highest global emissions (up to 11.6 Tg C yr⁻¹), the most distant from bottom-up estimates. These discrepancies have been suggested to be due to the poor knowledge of the marine isoprene cycle processes, which are not properly described and quantified. For example, the aforementioned photochemical production or bacterial degradation. Very recently, Conte et al. (2020) have studied the global cycling of isoprene by using the PISCES ecological model (coupled to the physical model NEMO), which contains 2 phytoplankton functional groups (PFT) with two different production rates associated based on the estimates compiled in Booge et al. (2016) and Meskhidze et al. (2015). Furthermore, they have also tested the effects of the inclusion of the surface microlayer production (using the isoprene production factors provided by Brüggemann et al. (2018)) and of implementing the degradation rate as either a constant value or linked to chlorophyll-a levels. Overall, their results agree more with bottom-up than with top-down estimates.

All in all, these works attempting to model isoprene distribution and cycling have highlighted that there still is a **paucity of relevant observations and experiments in the field**. This has implications for the development of simple statistical models which rely on the extrapolation of the relationships found between isoprene concentration and environmental descriptors to the global scale. The same applies to all the production and loss terms belonging to the marine cycle of isoprene, which are far from being constrained, making their correct implementation in complex ecological models still quite inaccurate.

Ph.D Thesis objectives

In this PhD Thesis, we investigated and modelled the regional (Southern Ocean) and global cycling of marine isoprene, focusing on its distribution, turnover and emission. To do that, we used computational tools for the statistical treatment of data and for the diagnosis and prognosis through the approximations described in the following objectives. Specifically, we combined different modelling approaches, from remote sensing to biogeochemical modelling, gathering published and new experimental and field-work data. By using this set of models, this work has shed light on the main inconsistencies and uncertainties of the conceptual and experimental knowledge of marine isoprene cycling that challenge its modelling. It also pointed out which are the main processes that must be investigated in future experiments in laboratory and fieldwork settings to achieve a global comprehension of the distribution and emission of marine isoprene.

1. Compilation of existing data of isoprene concentration, production and degradation; and estimation of new ones

What is the spatial and temporal distribution of isoprene concentration in the surface ocean?

Understanding isoprene cycling in the ocean requires a data-set of isoprene measurements as well as physical and biological descriptors. In this PhD thesis we gathered in a common data set the measurements of isoprene concentration published in previous works and new data from our research projects. This PhD thesis was developed in parallel to another PhD thesis with an experimental focus: that of Pau Cortés, PhD candidate, who was in charge of all the analytical procedures and measurements of isoprene during our cruises. The data set resulting from the compilation has a global coverage with an special focus on Southern Ocean waters. With more than 1400 observations, this is the biggest data set up to date, not only in terms of isoprene distribution but also in its associated variables: chlorophyll-a and sea surface temperature. We used these compiled values of isoprene concentration and ancillary variables to study the distribution of isoprene concentration in Southern Ocean (**Chapters 1 and 2**), and to validate model results (**Chapters 3 and 4**).

At what rates is isoprene produced by marine phytoplankton, and degraded by bacteria and chemical reagents?

To constrain the isoprene cycling process, we compiled estimates of production and degradation of isoprene from different works and calculated new values based on our own experimental results. We estimated isoprene production rates by different PFT's at the Lagrangian occupations during the PEGASO cruise, by solving the full cycle of isoprene in each studied water mass, which constitutes a novel approach. We took advantage of dark incubation experiments performed in different locations of the surface ocean to estimate new values of isoprene degradation rates. These estimates of isoprene production and loss rates were used in **Chapter 3** to model the cycling of isoprene in the Southern Ocean, in **Chapter 4** to assess the global production of isoprene in the surface ocean, and in **Chapter 5** to study the turnover of isoprene across different oceanic regions.

Through combining laboratory and field estimates of isoprene cycling, we aimed to disentangle not only how fast is isoprene produced and consumed in the oceans, but also to point which were the main gaps of knowledge to be solved in future experimental works.

2. Exploration of statistical relationships with in situ and remote sensed environmental and biological variables in the Southern Ocean

Which are the main drivers and distribution of isoprene concentration in the Southern Ocean?

To pave the way towards developing diagnostic parameterizations for isoprene concentration in the surface waters of the Southern Ocean (SO), we used data of environmental variables acquired simultaneously to isoprene measurements described in Objective 1. In **Chapter 1**, we studied which were the main drivers of isoprene concentration in contrasting surface waters of the SO among environmental, physical, and biological variables. We explored the potential relationships between those parameters and isoprene levels which hold potential for the development of simple statistical models.

Is it possible to retrieve isoprene concentrations in the Southern Ocean using remotely-sensed variables?

Remote sensing algorithms are vital to obtain synoptic assessments of the distribution of trace gases in the surface ocean at the regional and global scales. These type of models incorporate variables easily extracted from satellite data and global databases, such as chlorophyll, temperature and mixing layer depth. In **Chapter 2**, we matched-up our own in situ measurements with remotely sensed variables obtained from MODIS Aqua products. We explored the relationship of isoprene concentration levels and the remotely-sensed variables to develop a remote sensing algorithm to estimate isoprene concentrations in the Southern Ocean. A model of this type can be considered as a first step towards the development of future models to retrieve isoprene concentration from remote sensing images at the regional and global scales.

3. Ecological modelling of marine isoprene cycling in the surface ocean: from the Southern Ocean to the Global Ocean

Which are the most relevant phytoplankton groups for isoprene production at the regional (Southern Ocean) and global scales?

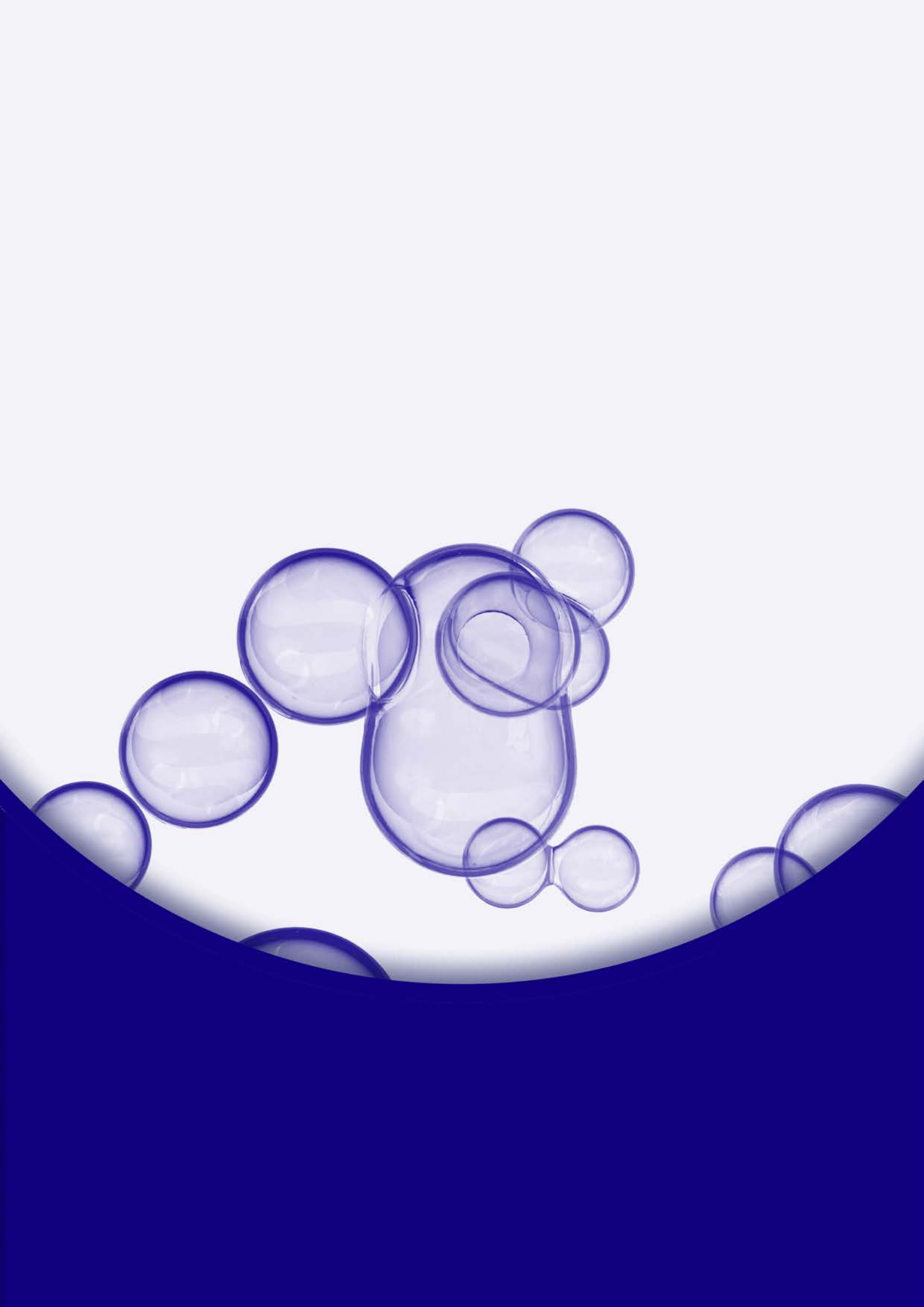
Ecological-biogeochemical models are a useful tool to study trace gas cycling and emission in the oceans. We studied (1) marine isoprene production, degradation, and emission at the regional scale (Southern Ocean), and (2) isoprene production at a global scale. To that aim, we took advantage of two different ecological models: ROMS-BEC for the Southern Ocean in **Chapter 3** (ETH Zurich), and DARWIN-MITgcm for the Global Ocean in **Chapter 4** (Massachusetts Institute of Technology). In both approaches, we used all new and published values of cycling process rate parameters (e.g. production and degradation terms from Objective 2) and implemented them,

and used the measurements of isoprene concentration (from Objective 1) to validate the results. In **Chapter 3**, we used the ROMS-BEC model to explore the concentration and emission patterns from the Southern Ocean. Moreover, we compared the results of using different estimates of isoprene production and consumption rates derived from laboratory and field work (PEGASO cruise) to assess the predictive capacity of each approach. In **Chapter 4**, we addressed isoprene production patterns at the global scale using DARWIN-MITgcm. We gathered a data set of up to 124 lab-derived isoprene production rates and used the model to assess the key phytoplankton taxa that dominate the production of isoprene in each oceanic region. Overall, we assessed the potential of ecological-biogeochemical models as a complementary tool to remote sensing algorithms and statistical models to predict and understand the regional and global cycling of marine isoprene.

4. Shedding light on the turnover of isoprene in the global surface ocean

How fast is isoprene cycling in the surface ocean?

Although some processes of isoprene cycling in the surface ocean have been discussed in previous works, their focus has been limited to the concentrations, production and emission to the atmosphere. The degradation pathways of isoprene in the ocean are still far from being properly constrained because no measurements exist. In **Chapter 5**, we used data from field measurements and incubation experiments in different regions across the oceans to understand how fast is isoprene produced, degraded, ventilated and mixed in the surface ocean. Moreover, we pursued the parameterization of the resulting values with descriptor variables such as chlorophyll-a and/or temperature, which is essential for their application in numerical models. We quantified the relative importance of the microbial and chemical losses with respect to the other sinks. Furthermore, we quantified the chlorophyll-a normalized production of isoprene in the same experiments and explored its relationship with sea surface temperature. With this approach, we also contributed to the debate of which is the most appropriate method to estimate isoprene production levels: (1) using simple statistical relationships with total chlorophyll-a levels and other environmental descriptors (as pursued in Objective 2), or (2) through a PFT-based ecological modelling approach (Objective).



Chapter 1

Distribution and drivers of marine isoprene concentration across the Southern Ocean

Chapter 1

Distribution and drivers of marine isoprene concentration across the Southern Ocean

Pablo Rodríguez-Ros¹, Pau Cortés¹, Charlotte Mary Robinson², Sdena Nunes¹, Christel Hassler^{3,4}, Sarah-Jeanne Royer⁵, Marta Estrada¹, M. Montserrat Sala¹, Rafel Simó¹

1. Institut de Ciències del Mar. Passeig Marítim de la Barceloneta, 37-49, 08003 Barcelona, Spain
2. Remote Sensing and Satellite Research Group, School of Earth and Planetary Sciences, Curtin University, 6102 Perth, Australia
3. Department F.-A. Forel for Environmental and Aquatic Sciences, Earth and Environmental Sciences, University of Geneva, CH-1211 Geneva, Switzerland
4. Swiss Polar Institute, Ecole Polytechnique Fédérale de Lausanne, 1015 Lausanne, Switzerland
5. Scripps Institution of Oceanography, San Diego, CA 92093, USA

This chapter is published as:

Rodríguez-Ros, P., Cortés, P., Robinson, C.M., Nunes, S., Hassler, C., Royer, S.-J., Estrada, M., Sala, M.M., & Simó, R. (2020). *Distribution and Drivers of Marine Isoprene Concentration across the Southern Ocean*. *Atmosphere*, 11(6), 556. DOI: <https://doi.org/10.3390/atmos11060556>

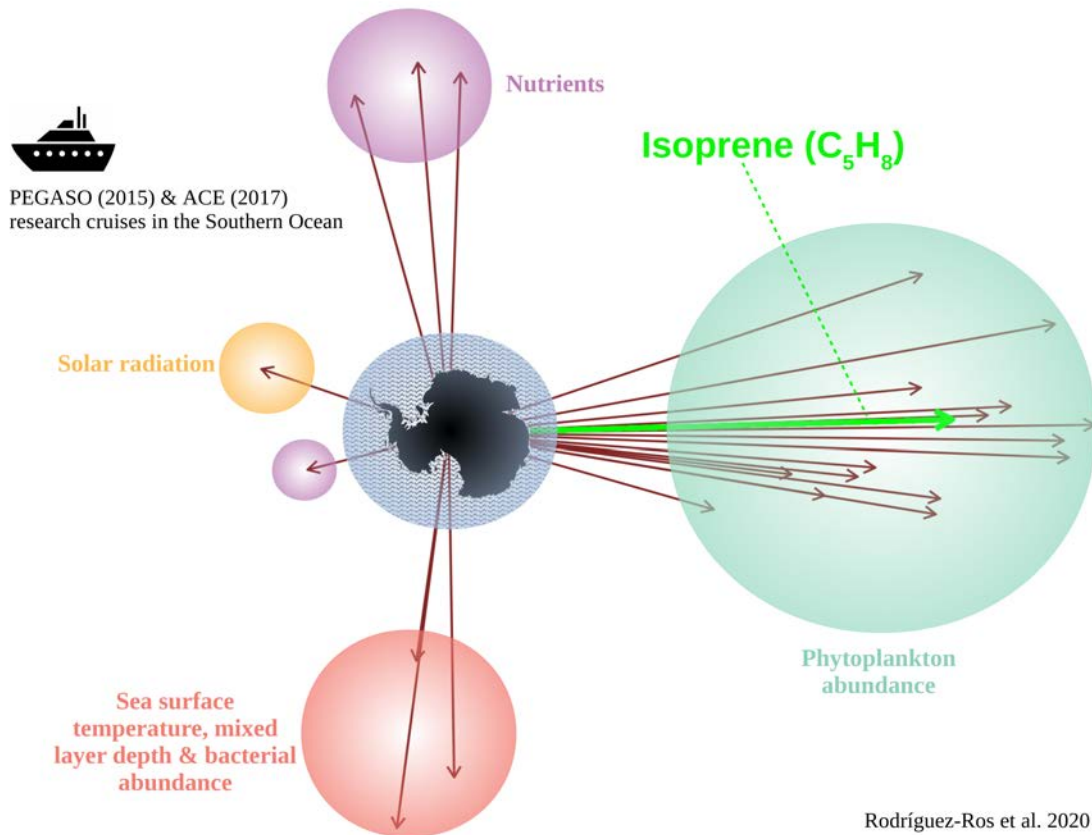
Difficulties are just things to overcome, after all.

Ernest Henry Shackleton

Abstract

Isoprene is a biogenic trace gas produced by terrestrial vegetation and marine phytoplankton. In the remote oceans, where secondary aerosols are mostly biogenic, marine isoprene emissions affect atmospheric chemistry and influence cloud formation and brightness. Here, we present the first compilation of new and published measurements of isoprene concentrations in the Southern Ocean and explore their distribution patterns. Surface ocean isoprene concentrations in November through April span 1 to 94 pM. A band of higher concentrations is observed around a latitude of $\approx 40^{\circ}\text{S}$ and a surface sea temperature of 15°C . High isoprene also occurs in high productivity waters near islands and continental coasts. We use concurrent measurements of physical, chemical, and biological variables to explore the main potential drivers of isoprene concentration by means of paired regressions and multivariate analysis. Isoprene is best explained by phytoplankton-related variables like the concentrations of chlorophyll-a, photoprotective pigments and particulate organic matter, photosynthetic efficiency (influenced by iron availability), and the chlorophyll-a shares of most phytoplankton groups, and not by macronutrients or bacterial abundance. A simple statistical model based on chlorophyll-a concentration and a sea surface temperature discontinuity accounts for half of the variance of isoprene concentrations in surface waters of the Southern Ocean.

Graphical abstract of Chapter 1



1.1 Introduction

Isoprene is a marine trace gas whose production in oceanic surface waters is associated with the photosynthetic activity of phytoplankton Carpenter et al. (2012); Shaw et al. (2003); Exton et al. (2013). When released to the atmosphere, isoprene acts as a precursor of secondary organic aerosols with the potential capability to influence cloud formation and brightness (Meskhidze and Nenes, 2006; Arnold et al., 2009). In remote regions of the planet, like the Southern Ocean, isoprene may control secondary aerosol formation together with other trace gases such as DMS (Meskhidze and Nenes, 2006; Vallina et al., 2007; Dani and Loreto, 2017). Despite its importance, there is a large discrepancy between current estimates of isoprene emission from the global ocean, which range from ~ 1 (Shaw et al., 2003) to 12 Tg C yr^{-1} (Luo and Yu, 2010). This discrepancy has been suggested to be due to a hitherto overlooked source of isoprene in the ocean, as the knowledge of its cycling processes is still rather poor (Booge et al., 2018; Alvarez et al., 2009). The existence of significant photochemical production in the surface microlayer has been suggested from lab-based experiments (Ciuraru et al., 2015a), but not confirmed in the field (Brüggemann et al., 2018). Better constraining global emission estimates is quite a challenging task due to scarcity of measurements and experiments performed in the field to better understand isoprene distribution, dynamics, cycling rates, and drivers (Booge et al., 2018).

Due to the close association of isoprene with photosynthesis and biological production, there have been several attempts to develop predictive tools for isoprene concentrations in the surface ocean. Most of them are based on simple statistical relationships with collocated measurements of potential predictors such as chlorophyll-a concentration, sea surface temperature, and light (Ooki et al., 2015; Booge et al., 2016; Hackenberg et al., 2017). Other attempts to simulate either isoprene concentration or emission patterns have involved remotely sensed satellite products, chiefly chlorophyll-a and sea surface temperature, in combination with simple numerical models of isoprene production and loss rates (Palmer and Shaw, 2005; Arnold et al., 2009; Luo and Yu, 2010). The later generation of these models have parameterized production not from total chlorophyll-a but from the pigment shares of phytoplankton functional types (PFT) estimated from satellite ocean colour, and the application of PFT-specific isoprene production rates determined in laboratory experiments with monocultures (Booge et al., 2016; Dani et al., 2017).

Only a few regional studies of the drivers of isoprene production exist, which found significant paired or multiple relationships to sea surface temperature, chlorophyll-a, photoprotective pigments, light, nutrients, and/or primary production (Zindler et al., 2014; Ooki et al., 2015; Booge et al., 2016; Hackenberg et al., 2017; Booge et al., 2018). In the Southern Ocean in particular, despite its remoteness from continental sources, and therefore the pristine oceanic origin of its aerosols, only a few reports of isoprene measurements exist (Ooki et al., 2015; Kameyama et al., 2010; Hackenberg et al., 2017; Wohl et al., 2020). In this work, we present new data of isoprene concentrations and accompanying physical and biological variables from three cruises in the Southern Ocean (below 40°S), which altogether provide an unprecedented coverage of sub-regions and contrasting environmental conditions. Our goals are (a) to identify which areas of the Southern Ocean are most relevant in terms of isoprene concentration, (b) to detect the main biological and abiotic drivers of

isoprene concentration distribution across contrasting environmental conditions, and (c) to identify which of these variables can be used as statistical predictors of isoprene concentration.

1.2 Materials and Methods

1.2.1 The PEGASO, TransPEGASO and ACE cruises

The PEGASO cruise took place on board the R/V *Hesperides* in the Atlantic sector of the Southern Ocean from 2 January to 11 February 2015 (Dall’Osto et al., 2017; Nunes et al., 2019a; Zamanillo et al., 2019a). Four locations were studied in Langrangian occupation: north of the South Orkney Islands (NSO), southeast of the South Orkney Islands (SSO), northwest of South Georgia Island (NSG), and west of Anvers Island (WA). In each location, surface waters were sampled over several days by using either the uppermost (≈ 4 m) bottle of the rosette on SBE911+ Conductivity, Temperature, and Depth (CTD) casts, which recorded temperature and salinity, or the ship’s underway pumping system, which had the water intake located 5 m below sea level. In the latter case, seawater temperature and salinity were recorded continuously via the flow-through thermosalinograph SBE21 SeaCAT (Sea Bird Scientific, Bellevue, WA, USA). The TransPEGASO cruise crossed the Atlantic Ocean from North to South on the R/V *Hesperides*, between 20 October and 21 November 2014. Surface seawater was sampled twice a day (early morning and early afternoon) using the same underway pumping system intake as above. Here, we only consider the measurements conducted south of 40° S, i.e., on the Southwestern Atlantic shelf. The Antarctic Circumnavigation Expedition (ACE) completed the full circumnavigation of the Southern Ocean in December 2016–March 2017 on the R/V *Akademik Treshnikov*. The cruise was divided into three legs: Leg 1 from Cape Town (South Africa) to Hobart (Tasmania), Leg 2 from Hobart to Punta Arenas (Chile), and Leg 3 from Punta Arenas to Cape Town. Seawater samples were collected every 6 h most of the days, using either the underway pumping system (4 m depth) or CTD casts (Henry et al., 2020).

1.2.2 Isoprene concentration measurements

Isoprene was measured along with other volatile compounds on a gas chromatography–mass spectrometry system (5975-T LTM GC/MS, Agilent Technologies). Aliquots of 25 mL were drawn from the glass bottle with a glass syringe with a teflon tube, and filtered through a 25 mm glass fibre filter while introduced into a purge and trap system (Stratum, Tekmar Teledyne). Volatiles were stripped by bubbling with 40 mL min^{-1} of ultrapure He for 12 min, trapped on solid adsorbent at room temperature, and thermally desorbed (250°C) into the GC. Isoprene, monitored as m/z 67 in selected ion monitoring mode, had a retention time of 2.4 min in the LTM DB-VRX chromatographic column held at 35°C . The detection limit was 1 pmol L^{-1} , and the median analytical precision was 5%. On TransPEGASO and PEGASO, calibration was performed by injections of a gaseous mixture of isoprene in N_2 . On ACE, a liquid standard solution prepared in cold methanol and subsequently diluted in MilliQ water was used instead.

1.2.3 Biological, physical and environmental variables

For chlorophyll-a analyses, 250 mL (PEGASO) and 2 L (ACE) seawater samples were filtered on glass fiber filters (Whatman GF/F), which were extracted with 90% acetone at 4 °C in the dark for 24 h. The fluorescence (CHL-FLUO) of extracts was measured with a calibrated Turner Designs fluorometer (Yentsch and Menzel, 1963). No phaeopigment corrections were applied. Complete suites of phytoplankton pigments were determined by HPLC (Nunes et al., 2019a; Antoine et al., 2019). The CHEMTAX chemical taxonomy software was run on the pigment distributions to derive the contribution of microalgal groups to the total chlorophyll-a biomass (ngChla L^{-1}). Eight main pigmentary classes were quantified: Chlorophytes (CHLO), Cryptophytes (CRYP), Dinoflagellates (DINO), Diatoms (DIAT; Diatom types 1 and 2 were modelled and combined to one class for ACE), Haptophytes (HAPTO; Type 6+7), Pelagophytes (PELA), Phaeocystis (PHAEO; Haptophytes type 8), and Prasinophytes (PRA). For CHEMTAX application on PEGASO pigments, see the work in Nunes et al. (2019a). For ACE, initial pigment ratios were compiled from Rodriguez et al. (2002), Zapata et al. (2000), Cook et al. (2011), Higgins et al. (2011), and Cassar et al. (2015) and included a Cyanobacteria class. The ACE pigment samples were separated into 5 clusters according to hierarchical clustering using Ward's method in R version 3.5.0 and CHEMTAX v1.95 was then run on each cluster separately 60 times to derive optimized pigment ratio matrices for each cluster before a final 20 runs determined the final taxonomic abundances for each cluster. Pigment concentrations were also used to compute sum of Photoprotective Carotenoids (PPC: zeaxanthin, alloxanthin, diadinoxanthin, and α - and β -carotenes) and the sum of the main Light Harvesting Carotenoids (LHC: fucoxanthin, 19'-butanoyloxyfucoxanthin, 19'-hexanoyloxyfucoxanthin and peridinin), as well as the coefficient PPC:LHC (Nunes et al., 2019a; Higgins et al., 2011).

The maximum quantum efficiency of PSII photochemistry ($F_v : F_m$) was continuously measured from the underway system using Fast Repetition Rate Fluorometers (FRRF): a FASTracka (Chelsea Technologies, Surrey, UK) (Kolber et al., 1998; Royer et al., 2015) on PEGASO, and a Fluorescence Relaxation and Induction system (FIRe, Satlantic, now Sea-Bird Instruments (Ryan-Keogh and Robinson, 2020)) on ACE.

The abundance of heterotrophic prokaryotes (PHA) was obtained by flow cytometry, following standard methods after fixation with 1% paraformaldehyde plus 0.05% glutaraldehyde (Gasol and Del Giorgio, 2000), as described in Zamanillo et al. (2019a).

In PEGASO and ACE, Particulate Organic Carbon (POC) and Particulate Organic Nitrogen (PON) were determined for 1 L (PEGASO) and 2 L (ACE) water samples filtered through pre-combusted (4 h, 450 °C) GF/F glass fiber filters (Whatman) that remained frozen (-20 °C) until further processing. Then, filters were oven dried (40 °C), acidified with HCl to remove carbonates and analysed with an elemental analyser (2400 CHN, Perkin-Elmer, Waltham, MA, USA for PEGASO samples and Flash EA 1112, Thermo Finnigan, San Jose, CA, USA for ACE samples). Dry blanks (measured on pre-combusted GF/F filters) were subtracted from each sample.

Daily averaged solar radiation doses (SRD) in the mixed layer were estimated during PE-

GASO and ACE as described in (Zamanillo et al., 2019a):

$$\text{SRD} = \frac{1}{K_d(\text{PAR}) \times \text{MLD}} \times \left(1 - e^{(-K_d(\text{PAR}) \times \text{MLD})}\right) \quad (1.1)$$

where $K_d(\text{PAR})$ is the diffuse attenuation coefficient in the euphotic zone for the PAR broadband (400–700 nm) and MLD is the depth of the mixed layer. MLD was determined from CTD profiles as the depth at which density was 0.125 kg m^{-3} higher than that at 5 m.

Concentrations of the macronutrients nitrate (NITRA), nitrite (NITRI), phosphate (PHOSP), and silicate (SILIC) were measured in unfiltered water samples collected in 10 mL (PEGASO) or 15 mL (ACE) sterile polypropylene bottles and stored frozen ($-20 \text{ }^\circ\text{C}$) until application of standard segmented flow analysis with colorimetric detection (Hansen and Grasshoff, 1983; Wolters, 2002; Egan, 2008). In ACE samples, phosphate was determined manually by colorimetry (Grasshoff et al., 2009).

1.2.4 Other data sources in the Southern Ocean

We expanded our dataset with isoprene concentration, chlorophyll-a concentration, and sea surface temperature measurements from other cruises (Table 4.8): AMT23 & AMT23 (Hackenberg et al., 2017), KH-09-5 (Ooki et al., 2015; Schlitzer et al., 2018), and ANDREXII (Wohl et al., 2019, 2020). We averaged the data of AMT22 & AMT23 (Hackenberg et al., 2017) and ANDREXII (Wohl et al., 2019) to intervals of 6 h in order to make them comparable to ACE measurements and avoid their overrepresentation in the entire dataset. Isoprene concentrations from cruise KH-10-7 (Kameyama et al., 2010), the other reported cruise in the SO, were excluded from our analysis as their values were significantly higher than any other in the region, most probably due to methodological biases (Kameyama, personal communication). Overall, our dataset consists of more than 450 isoprene observations (Table 3.3, Figure 4.8a), making it the most complete ever compiled for the Southern Ocean ($>40^\circ \text{ S}$).

Table 1.1: Variables from PEGASO and ACE cruises used in this study. Data were log10-transformed after checking their non-normality using the Shapiro–Wilk’s test. Temperature was transformed to Kelvin degrees to avoid negative values. The last columns show the statistics of the logarithmic regression of isoprene with all independent variables (r^2 : explained variance (in bold when p-value < 0.05); p-value: levels of significance; n = sample size.). * Effective quantum efficiency of ϕ_{PSII} photochemistry. "n. d." = non dimensional.

<i>Dependent variable</i>	Variable	Abbreviation	Units	Statistics				
	Isoprene	ISO	pmol L ⁻¹	r^2	p-value	Intercept	Slope	n
<i>Independent variables</i>	Chlorophyll-a (Fluorometric)	CHL-FLUO	$\mu\text{g L}^{-1}$	0.34	< 0.001	1.0	0.57	173
	Chlorophyll-a (HPLC)	CHL-HPLC	$\mu\text{g L}^{-1}$	0.48	< 0.001	1.4	0.56	120
	Chlorophytes	CHLO	$\mu\text{g Chl-a L}^{-1}$	0.14	< 0.001	1.4	0.15	119
	Cryptophytes	CRYP	$\mu\text{g Chl-a L}^{-1}$	0.17	< 0.001	1.4	0.14	119
	Dinoflagellates	DINO	$\mu\text{g Chl-a L}^{-1}$	0.23	< 0.001	1.7	0.3	119
	Diatoms	DIAT	$\mu\text{g Chl-a L}^{-1}$	0.26	< 0.001	1.4	0.3	119
	Haptophytes	HAPT	$\mu\text{g Chl-a L}^{-1}$	0.17	< 0.001	1.5	0.3	118
	Pelagophyceae	PELA	$\mu\text{g Chl-a L}^{-1}$	0.17	< 0.001	1.7	0.29	119
	<i>Phaeocystis</i>	PHAEO	$\mu\text{g Chl-a L}^{-1}$	0.26	< 0.001	1.3	0.30	119
	Prasinophytes	PRA	$\mu\text{g Chl-a L}^{-1}$	0.1	< 0.001	1.5	0.21	119
	Photoprotective carotenoids	PPC	$\mu\text{g L}^{-1}$	0.45	< 0.001	1.6	0.41	120
	Light harvesting carotenoids	LHC	$\mu\text{g L}^{-1}$	0.45	< 0.001	1.5	0.62	120
	PPC : LHC	PPC:LHC	n. d.	0.16	< 0.001	1.4	0.47	120
	$F_v : F_m$ *	$F_v : F_m$	n. d.	0.31	< 0.001	2.5	1.9	103
	Prokaryotic heterotrophic abundance	PHA	Cells mL ⁻¹	0.02	> 0.05			169
	Particulate organic carbon	POC	$\mu\text{mol L}^{-1}$	0.25	< 0.001	0.02	1.07	117
	Particulate organic nitrogen	PON	$\mu\text{mol L}^{-1}$	0.34	< 0.001	0.9	1.03	117
	Nitrate	NITRA	$\mu\text{mol L}^{-1}$	0.01	> 0.05			120
	Nitrite	NITRI	$\mu\text{mol L}^{-1}$	0.05	< 0.05	0.8	-0.41	120
	Phosphate	PHOSP	$\mu\text{mol L}^{-1}$	0.001	> 0.05			120
	Silicate	SILIC	$\mu\text{mol L}^{-1}$	0.03	< 0.001	1.2	-0.13	120
	Sea surface temperature	SST	Kelvin	0.002	> 0.05			166
	Mixed layer depth	MLD	m	0.01	> 0.05			120
	Solar radiation dose	SRD	W m ⁻²	0.03	> 0.05			117

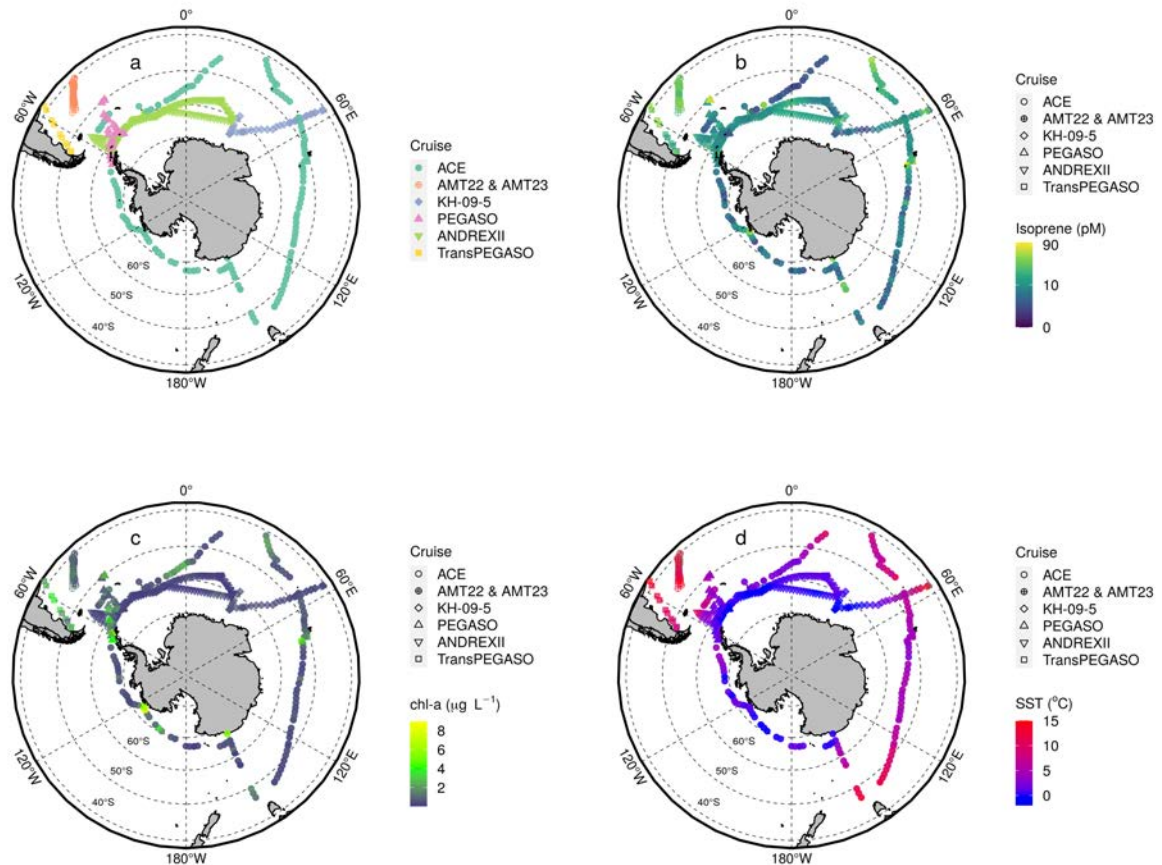


Figure 1.1: Dataset of measurements compiled in this work: (a) research cruises, (b) isoprene surface concentration, (c) chlorophyll-a concentration, and (d) sea surface temperature. A summary of the data shown in this figure can be found in Table 3.3.

1.2.5 Statistical analysis and model development

All statistical analyses were performed using *R* software implemented in the platform *R-studio* (RStudio Team, 2015). For most of the analyses *r-base* packages were used; other packages used for statistics or plotting were *ggplot2*, *ggbiblot*, *xts*, *zoo*, *reshape2*, *mapdata*, *maptools*, *mapproj*, *rgdal*, *ggthemes*, *readr*, and *viridis*.

The relationships between isoprene concentrations and collocated variables were explored with a set of statistical analyses performed on the PEGASO and ACE datasets. After checking the non-normality distribution of our variables using Shapiro–Wilk’s test, data were log-transformed. First, we performed paired regression analyses between isoprene concentrations (as dependent variable) and every biological and environmental variable available (Table 1.1). Second, we ran a Principal Components Analysis (PCA) for all measurements after centering and scaling the variables. As PCA does not accept samples with void variables, missing values during PEGASO were filled with the median of the Lagrangian site (PEGASO). In ACE, samples with void variables were entirely removed from the dataset.

We further explored the use of chlorophyll-a to develop a statistical model for predicting isoprene levels in the PEGASO and ACE datasets. We chose chlorophyll-a because (a) it showed the best correlation with isoprene of all the variables tested, (b) it was available in all the Southern Ocean cruises and, hence, could be used for cross-comparisons, and (c) it can be easily measured in future cruises or obtained from remote sensing data (Rodríguez-Ros et al., 2020b). However, in view of the limited predictive power of chlorophyll-a, previous works had combined chlorophyll-a and SST, with the latter not contributing as a predictor but as a threshold or breaking point for a shifting regime of the isoprene to chlorophyll-a regression (Ooki et al., 2015; Booge et al., 2016; Hackenberg et al., 2017). We split the TransPEGASO, PEGASO, and ACE dataset according to a SST threshold, and computed the isoprene-chlorophyll-a regressions below and above this SST. We assayed SST thresholds between 1 °C and 10 °C in 0.1 °C steps, and selected the one at which the two regressions together explained the largest variance of isoprene concentrations. We did separate analyses using the chlorophyll-a measured either fluorometrically or with HPLC (Table 1.1). To compare our regression model to the ones previously published (Booge et al., 2016; Hackenberg et al., 2017), we applied those models to the datasets from the AMT2, AMT 23, KH-09-5, and ANDREXII cruises, which were not included in the model developed in this study (Figure 4.8; Table 3.3) and compared the outcomes to the observations. The values of Root Mean Square Error (RMSE) of predicted vs. observed isoprene concentrations were used to assess the predictive capacity of each model:

$$\text{RMSE} = \sqrt{\frac{\sum_{i=1}^n (\hat{y}_i - y_i)^2}{n}} \quad (1.2)$$

where \hat{y}_i are the predicted values, y_i are the observations, and n is the sample size.

1.3 Results and Discussion

1.3.1 General patterns of isoprene surface concentration in the Southern Ocean

In Figure 4.8b, we show surface ocean isoprene concentration measurements from all cruises (see also Table 3.3). Overall, higher isoprene concentrations occurred in waters with high temperature (Figure 4.8d) and chlorophyll-a (Figure 4.8c). The highest concentrations (close to 100 pM) were measured during PEGASO in the phytoplankton bloom north of South Georgia Islands (Zamanillo et al., 2019a; Nunes et al., 2019a). In contrast, concentrations as low as 1–2 pM occurred in waters with low chlorophyll-a content during ACE and PEGASO (Figure 4.8b,c and Figure 1.2b). Concentrations of isoprene during PEGASO show the largest variability among cruises, which is due to the sampling strategy of this cruise, which aimed at blooming waters and contrasting conditions (Table 3.3). The rest of the cruises showed concentrations that rarely exceeded 50 pM (Figure 4.8b).

In the combined dataset, a hump of higher isoprene concentrations (>20 pM) is observed at water temperatures of ≈ 15 °C and a latitude 40–45° S (Figure 1.2a–d). This same pattern was already described by Ooki et al. (2015) and was attributed to the temperature range associated with phytoplankton blooms in transitional and subpolar waters, and consequently being coincident with the Subantarctic front. This latitudinal band, which covers a large area, is important for isoprene

emission, more so than coastal or near island, biologically rich sites like the South Georgia and Kerguelen blooms (Figure 1.2b,d). In most of the rest of the SO, characterized by chlorophyll-poorer waters, isoprene concentrations are low (<15 pM). Consequently, we suggest that the 40–45° S waters would be a good target for future experimental studies aiming to decipher isoprene production, cycling, and emission rates and their seasonality in the SO.

1.3.2 Drivers of isoprene concentration in the Southern Ocean

Isoprene was significantly correlated with CHL-FLUOR and CHL-HPLC ($r^2 = 0.38$ and 0.48 , respectively) across the PEGASO and ACE cruises (Table 1.1). It also correlated positively with total light-harvesting and total photoprotective carotenoids (LHC and PPC, respectively; $r^2 = 0.45$ in both cases). Positive correlation extended to all phytoplankton groups analyzed, particularly diatoms (DIAT), Phaeocystis-like haptophytes (PHAEO), and dinoflagellates (DINO) ($r^2 = 0.26$, 0.26 , and 0.23 , respectively). Among the other biological and environmental descriptors, isoprene significantly correlated with $F_v : F_m$, POC, and PON ($r^2 = 0.31$, 0.25 , and 0.34 , respectively) and showed negative but weak significant correlation with nitrite and silicate concentrations ($r^2 = 0.05$ and 0.03 , respectively).

A multivariate PCA was performed with PEGASO and ACE data to visualize combinations of variables that better explained isoprene patterns as well as the differences between the visited errorregions (Figure 1.3). PC1 + PC2 explained 57% of the total variance (Figure 1.3). Essentially, PC1 can be regarded as a “productivity” axis, contributed positively by phytoplankton-related variables and with negative weak contributions by SRD and nitrite. In contrast, PC2 represents the physico-chemical environment, with SST and MLD on one side and macronutrients on the opposite side. Note that the abundance of prokaryotic heterotrophs is strictly aligned with SST. Isoprene contributes only to PC1, and aligns positively with proxies of phytoplankton biomass (chlorophyll-a, POC, PON) and the biomass shares of most phytoplankton taxa, particularly diatoms. It also aligns positively with light-harvesting capacity (LHC) and $F_v : F_m$, which varies with phytoplankton taxonomy (Suggett et al., 2009), but is also a powerful indicator of the efficiency of photosystem II in phytoplankton (Kolber et al., 1998; Behrenfeld and Boss, 2006; Royer et al., 2015). In the overall Fe-limited Southern Ocean, spots of Fe availability, generally associated with divergence zones near islands, show increases in productivity, phytoplankton biomass and $F_v : F_m$ (Gervais et al., 2002; Holeyton et al., 2005; Morris and Sanders, 2011; Ryan-Keogh et al., 2013; Zamanillo et al., 2019a). As mentioned above, these are zones of high isoprene too. Isoprene is orthogonal to PC2, meaning that it does not contribute to the proportion of the total variance explained by this component. This confirms what the paired regressions had indicated: isoprene shows no proportionality, either positive or negative, to macronutrients, SST, MLD, or PHA. In other oceans, phytoplankton productivity is largely dictated by macronutrient availability; the SO, however, is generally macronutrient-replete but limited in micro-nutrient Fe, essential for building photosynthetic machinery (Moore et al., 2013a; Hoppe et al., 2017). Therefore, macronutrients do not contribute to the variances of phytoplankton biomass proxies and isoprene concentration. SST is also orthogonal to isoprene; previous studies had already reported that SST does not show any covariance with isoprene concentration but it rather defines regions of distinct isoprene variability (Ooki et al., 2015; Hackenberg et al., 2017).

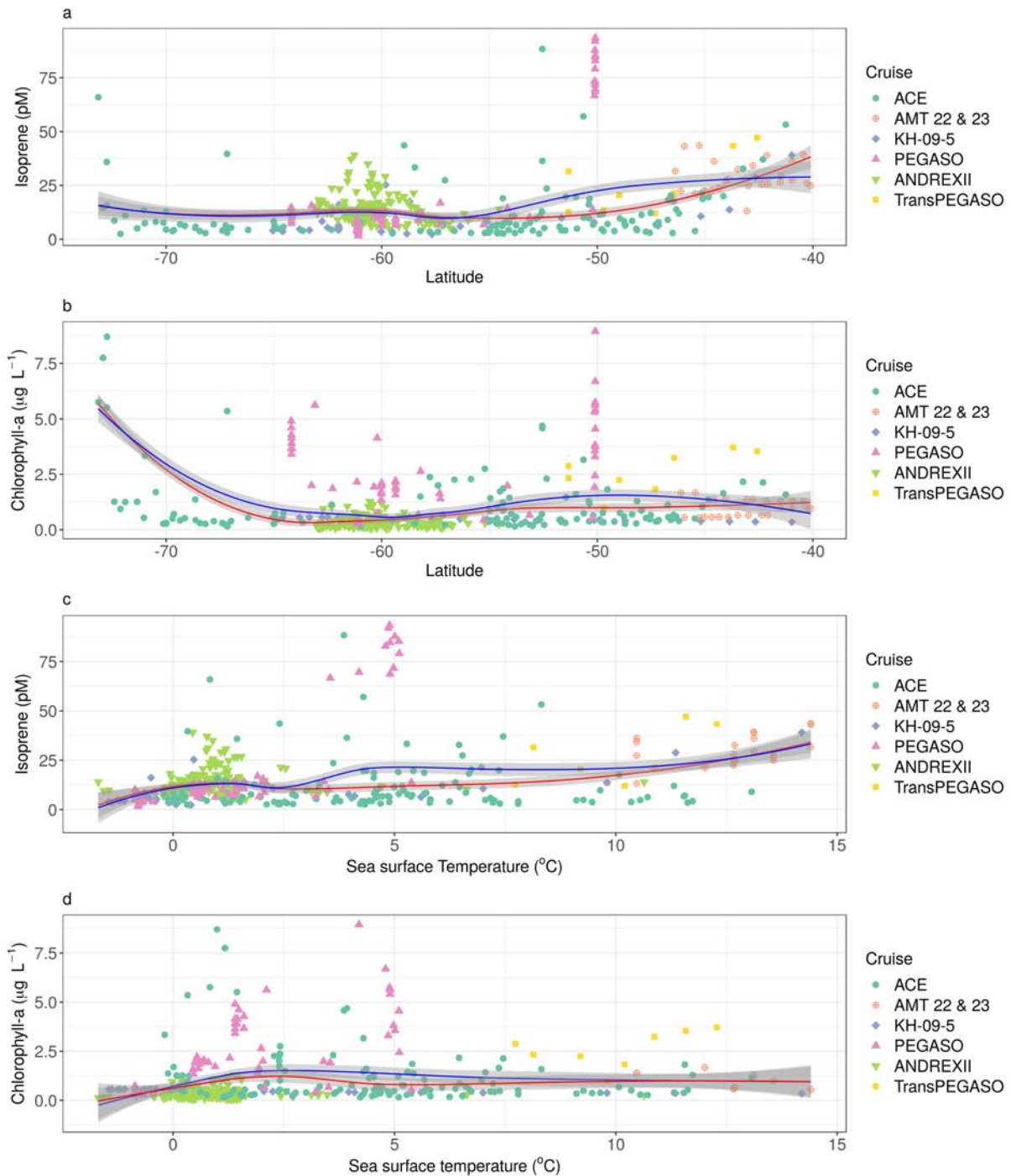


Figure 1.2: Isoprene (a and c) and chlorophyll-a (b and d) concentrations in surface waters (0 to 10 meters depth) of the Southern Ocean ($> 40^{\circ}\text{S}$) along with sea surface temperature and latitude gradients for all cruises compiled in this work (Figure 4.8, Table 3.3). Blue lines show the trend of the full dataset, while red lines represent the trend when excluding PEGASO cruise data. Notation for latitude in (a) and (b) is decimal degrees.

Regarding PHA, even though it has been demonstrated that heterotrophic prokaryotes can both produce (Fall and Copley, 2000) and consume (Alvarez et al., 2009) isoprene, their total abundance is not a significant driver of isoprene concentration. It must be noted that total prokaryotic heterotrophic abundance does not necessarily parallel prokaryotic activity, less so the activity of specific phyla potentially involved in isoprene production or consumption.

The sampling sites from PEGASO and ACE are spread over the 2D field defined by PC1 and PC2, according to the contribution of the two components to the site's total variance. PC1 splits the sampling sites between the high isoprene, chlorophyll-rich blooms of PEGASO (SG, WA, and NSO) plus a few stations near Kerguelen visited during ACE (leg 1), and the low isoprene, chlorophyll-poor waters generally encountered during ACE and in PEGASO SSO. PC2 distributed sampling sites essentially according to SST, with higher SST and lower macronutrient concentrations encountered near Hobart in the end of ACE leg 1 and the beginning of ACE leg 2, and the lowest SST, associated with high macronutrient concentrations, located near the Antarctic coasts during the two cruises.

Considering the paired regressions and the PCA, there is a clear pattern in the control mechanisms of isoprene concentration in the SO, which is largely associated with phytoplankton abundance and biological productivity (Figure 1.3). This correlation is mainly driven by the measurements from PEGASO, a cruise that purposely sampled regions of high productivity, accompanied by high isoprene concentrations. Conversely, ACE had a much less targeted cruise track, more representative of the background conditions of the SO, and the isoprene concentrations encountered were persistently low, except for a few sampling sites at lower latitudes, near the Kerguelen-Heard islands, or right at the Antarctic continental coast (Figure 4.8b).

The link of isoprene concentration to overall phytoplankton abundance has been repeatedly reported in previous works in the Southern Ocean (Wingenter et al., 2004; Meskhidze and Nenes, 2006; Moore, 2006), and is not surprising given that isoprene production has been observed and quantified in laboratory conditions for many phytoplankton species (Shaw et al., 2003; Bonsang et al., 2010; Exton et al., 2013; Meskhidze et al., 2015). Diatoms, which are common bloom formers, have been proposed as the main producers of isoprene in the global ocean (Dani et al., 2017). In this work, of the phytoplankton taxonomic indicators, diatoms (DIAT) showed the strongest correlation to isoprene concentrations. However, most phytoplankton groups were positively correlated to isoprene too, including known strong isoprene producers like dinoflagellates, haptophytes, and cryptophytes (Booge et al., 2016), but also including Phaeocystis-like haptophytes, which have not been reported to be isoprene producers (Broadgate et al., 1997). This is likely due to the tight covariation of most phytoplankton taxa throughout large sections of the cruise tracks.

Hackenberg et al. (2017) proposed a relationship between isoprene and PPC that was even better than that with chlorophyll-a for the global ocean. As PPC are indicators of photoacclimation of phytoplankton to high SRD, the tight relationship was suggestive of a photoprotective function of isoprene, or at least of isoprene being a by-product of photoprotection in phytoplankton. In land vegetation, isoprene emission as a photoprotective mechanism has been demonstrated (Sharkey and Yeh, 2001). In the ocean, however, although a connection between isoprene

and phytoplankton light stress has been speculated (Shaw et al., 2003; Gantt et al., 2009; Bonsang et al., 2010; Meskhidze et al., 2015), involvement in a photoprotective mechanism has not yet been proved (Hackenberg et al., 2017). Our observed correlation between isoprene and PPC across the Southern Ocean (Table 1.1) could support such a photoprotective role; however, a similar correlation was found with LHC, and none of the two were better than the correlation with CHL-HPLC. In the PCA, PPC were strongly aligned with all indicators of phytoplankton biomass (Figure 1.3) and, most importantly, they did not align with SRD, which had a minor and opposite-to-PPC contribution to PC1. Therefore, we believe that the variability of PPC across our Southern Oceans samples was less indicative of photoacclimation or photoprotection and essentially driven by total phytoplankton abundance. The ratio PPC/LHC normalizes photoprotective capacity with respect to the light harvesting one, hence being more appropriate to assess photoacclimation; nonetheless, isoprene concentration only weakly correlated to PPC/LHC ($r^2 = 0.16$, Table 1.1). Even though we cannot discard that isoprene may be involved in phytoplankton photoprotection mechanisms, or be a by-product of it, our results do not provide any evidence for it.

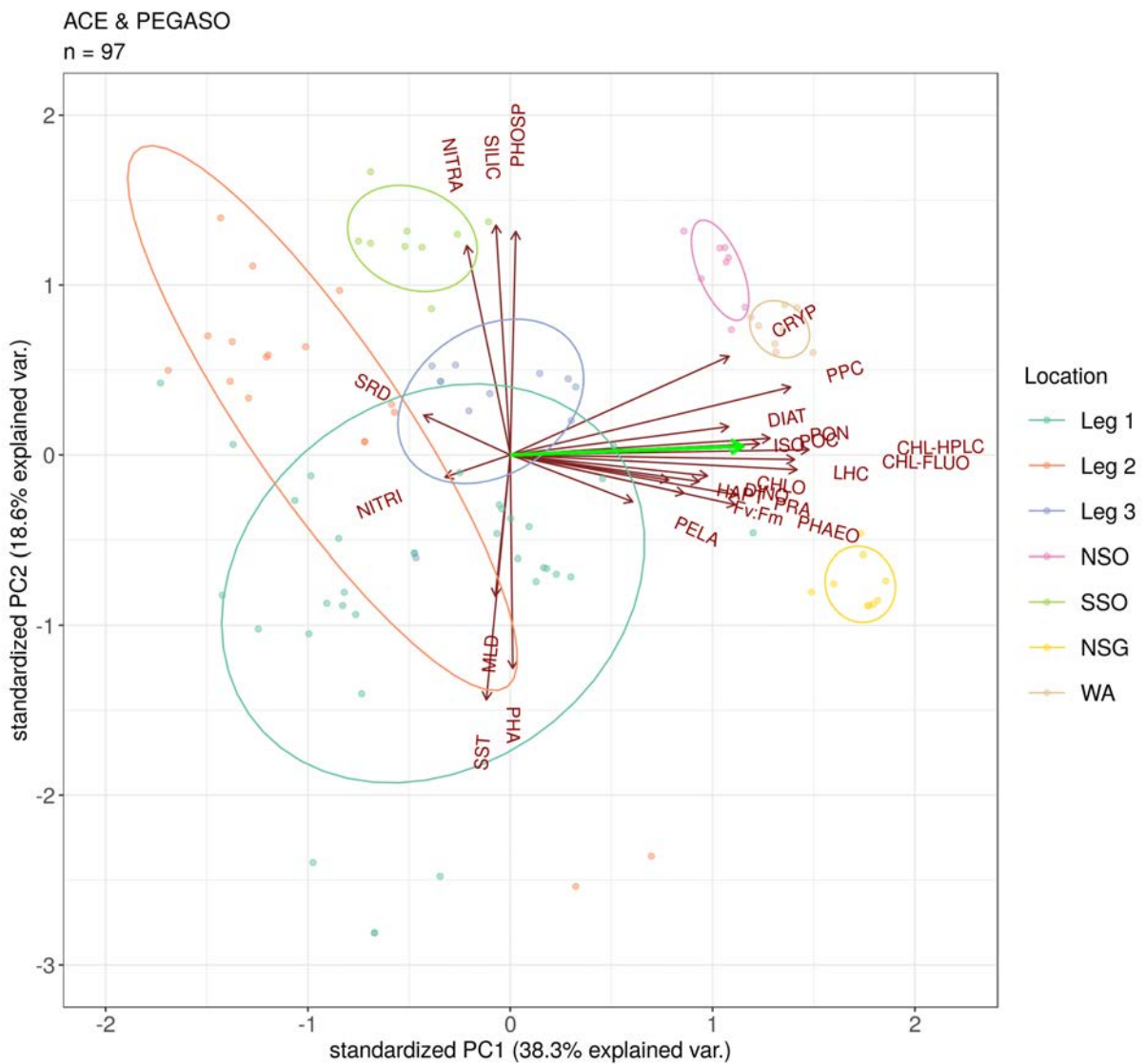


Figure 1.3: Principal Components Analysis (PCA) results for PEGASO and ACE. Abbreviations can be found in Table 1.1. PEGASO cruise: North of the South Orkney Islands (NSO), Southeast of the South Orkney Islands (SSO), Northwest of South Georgia Island (NSG), and West of Anvers Island (WA). ACE cruise: Cape Town - Hobart (Leg 1), Hobart - Punta Arenas (Leg 2), and Punta Arenas - Cape Town (Leg 3).

1.3.3 The predictive capacity of chlorophyll-a and sea surface temperature to isoprene concentration in the Southern Ocean

The ability of simple models to predict isoprene concentration in surface waters of the oceans has been widely discussed by Booge et al. (2016) and Hackenberg et al. (2017). The global dataset of isoprene concentrations in the surface ocean is still quite poor, challenging the creation of simple statistical models of global applicability. The published attempts (Ooki et al., 2015; Hackenberg et al., 2017) agree that chlorophyll-a and sea surface temperature are the best statistical predictors of isoprene concentrations, although other variables like other pigments, nutrients, or light hold potential to improve the models (Gantt et al., 2009; Booge et al., 2018; Hackenberg et al., 2017). Despite the high number of experimental approaches attempting to study the production and concentration levels of isoprene in laboratory conditions (Shaw et al., 2003; Bonsang et al., 2010; Exton et al., 2013; Booge et al., 2016), only a few publications have tried to model isoprene concentrations using field data (Broadgate et al., 1997; Kurihara et al., 2010, 2012; Ooki et al., 2015; Hackenberg et al., 2017).

Exploration of isoprene to chl-a relationships according to SST regimes, following the work in (Ooki et al., 2015; Hackenberg et al., 2017), rendered 3.4 °C as the SST break point that allowed to explain the largest portion of the isoprene concentration variance in PEGASO, ACE, and TransPEGASO (Figure 1.7a–d; Table 1.2). This break point agrees with that proposed by Ooki et al. (2015) for Arctic and Antarctic waters (3.3 °C). The fact that the resulting dual regression model is based on CHL-FLUO and SST makes it comparable to the other existing models and can be easily implemented on remote sensing measurements. Furthermore, SST and CHL-FLUO are typically sampled on oceanographic cruises, making the application of these relationships feasible to future datasets to test and improve their predictive capacity.

Table 1.2: Statistics of the relationships between isoprene and chlorophyll-a and sea surface temperature. Data used for these analyses were sampled in surface waters of the Southern Ocean (>40°S) during TransPEGASO, PEGASO and ACE cruises (Table 3.3). Abbreviations can be found in Table 1.1. *RMSE = Root Mean Square Error (see equation 1.2).

Predictor var.	SST regime	Equation	r ²	p-value	RMSE (pM)*	n
CHL-FLUO	> 3.4°C	ISO = 3.5 + 12.6 × CHL-FLUO	0.67	< 0.001	14.1	106
CHL-FLUO	< 3.4°C	ISO = 4.9 + 1.33 × CHL-FLUO	0.45	< 0.001	3.2	115
CHL-HPLC	> 3.4°C	ISO = 8.5 + 23.12 × CHL-HPLC	0.63	< 0.001	22.6	97
CHL-HPLC	< 3.4°C	ISO = 4.9 + 4.45 × CHL-HPLC	0.43	< 0.001	4.4	79

We examined the misfit between our model predictions and observations as a function of the magnitude of the predictor variables (CHL-FLUO and CHL-HPLC) (Figure 1.6). For both chlorophyll-a variables, the misfit was smaller at SST < 3.4 °C than at SST > 3.4 °C, which is due to the broader range into higher isoprene concentrations at SST > 3.4 °C. The model tended to overestimate higher isoprene concentrations as chlorophyll-a increases in both SST regimes, and underestimate lower isoprene concentrations at low chlorophyll-a concentrations.

To compare the predictive performance of our model with the other statistical models suggested to date (Ooki et al., 2015; Hackenberg et al., 2017), we applied each of the models to the measurements which were not used for their development (Figure 1.4). We only used CHL-FLUO because this is the chl-a used in the published models, and there are no CHL-HPLC data available for the rest of cruises. Our model predictions generally overestimated observations for the AMT, KH-09-05, and ADREXII cruises, and the fit was weak ($r^2 = 0.26$), but the slope was nearly 1 (Figure 1.4a). The overall fit to the data used to develop the model (developed from CHL-FLUO) was $r^2 = 0.56$ (Figure 1.4d). Conversely, the model of Ooki et al. (Ooki et al., 2015) (cruise KH-09-5) on the AMT, TransPEGASO, PEGASO, ACE, and ANDREXII data gave a slope much lower than 1, a weaker fit ($r^2 = 0.11$), and severely underestimated many isoprene measurements (Figure 1.4b). The model of Hackenberg et al. (2017) did not perform any better ($r^2 = 0.16$, slope $\ll 1$) on the data from KH-09-05, TransPEGASO, PEGASO, ACE, and ANDREXII, underestimating most of the observations (Figure 1.4c).

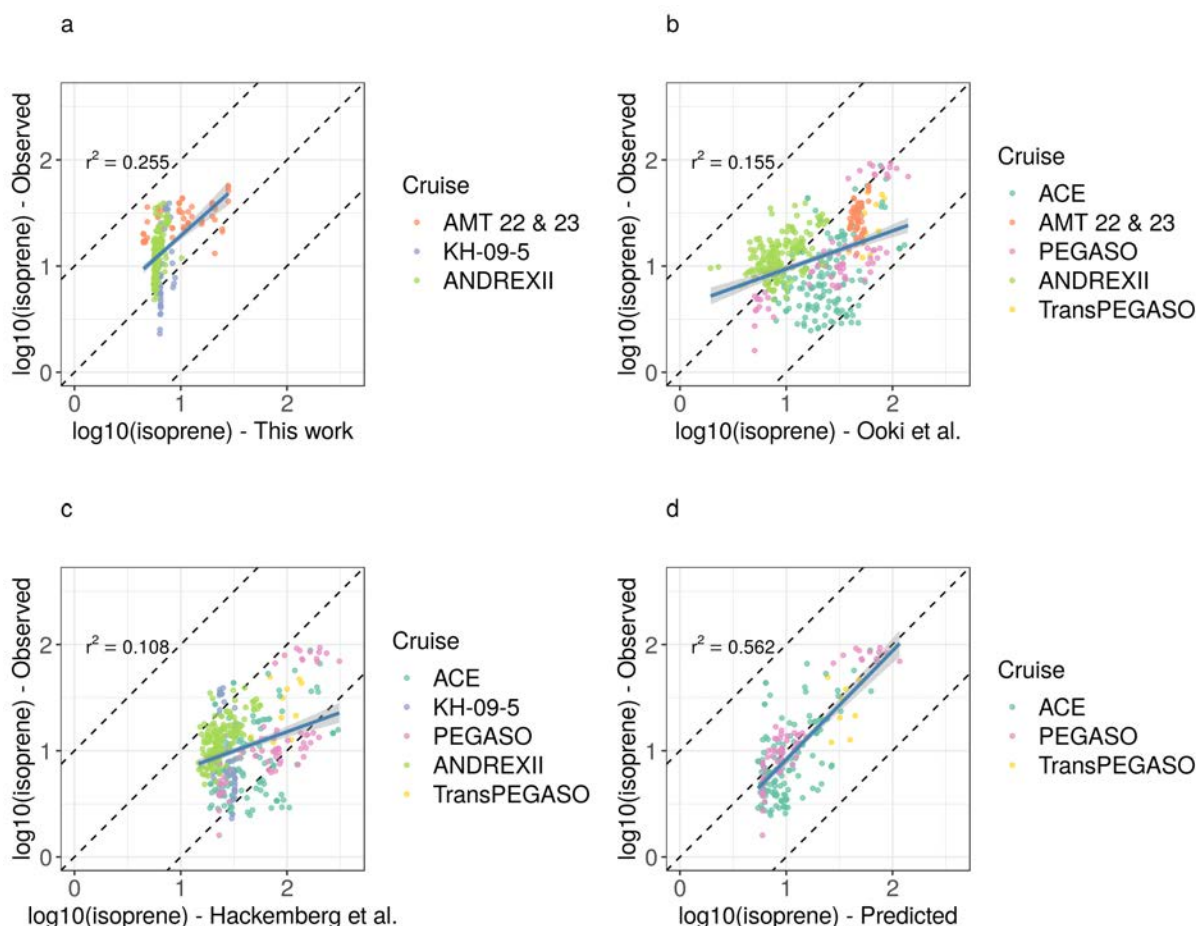


Figure 1.4: Comparison of different isoprene statistical models based on CHLA-FLUO and SST with measurements of isoprene concentration (Table 3.3). a: Comparison of our model (Figure 1.7a and b). b: Comparison of the (Ooki et al., 2015) model. c: Comparison of the (Hackenberg et al., 2017) model. d: Comparison of our model predictions with the measurements used in its development.

The cross-comparison between statistical models reveals how challenging it is to find a

simple model with good performance in an oceanic region as heterogeneous as the SO. An explanation why our model performs better than the other two models predicting isoprene concentrations from other cruises may lay in the broader geographic span and wider chlorophyll-a range (Figure 3.10) of PEGASO and ACE together. The AMT cruises (Hackenberg et al., 2017) reached a maximum southern latitude of 50° S, without making any isoprene measurements in coastal areas or island blooms. Ooki et al. (2015) pooled together Arctic and Antarctic data according to their SST despite the differences between the two regions in terms of phytoplankton taxa and environmental variables. Added to this need for a good data coverage of the SO, there is the difficulty of harmonizing the observations obtained from different cruises, methods, and operators. We compared models based on CHL-FLUO because this was available from PEGASO, TransPEGASO, ACE, KH-05-05, and the AMTs. On ANDREXII, however, chlorophyll-a concentrations were recorded with a sensor that had been calibrated against a solution prepared with pure chlorophyll-a. In the SO, Turner fluorometric measurements render CHL-FLUO concentrations that typically are more than twice the CHL-HPLC concentrations (Figure 1.7e), which can be considered close to pure chlorophyll-a. Therefore, the isoprene vs. chlorophyll-a slope of ANDREXII was higher than those of the other cruises, and it can be anticipated that, should CHL-FLUO had been available from that cruise too, our model validation would have given a better fit. Recently, Rodríguez-Ros et al. (2020b) developed a statistical model to estimate isoprene concentrations based on chlorophyll-a and sea surface temperature retrieved from satellite (MODIS Aqua) matchups to the isoprene observations. The advantage of this remote sensing approach is that it overcomes the aforementioned limitations of non-harmonized predictor data from diverse origins. Remote sensing has its own limitations, particularly in the cloudy SO, but it offers a promising alternative to studies based purely on field measurements.

In summary, our results support the idea that the complexity of the SO, with marked frontal zones and ephemeral or persistent presence of sea ice, land, and ice shelf coastlines, constitutes a challenge for ecological and biogeochemical model development of any kind (Ardyna et al., 2017), and particularly for trace gases. We have shown that, beyond an isoprene-rich band around 40° S, there is a background of low isoprene concentrations (1–2 pM) on top of which local peaks occur in shelf, polynya, and coastal waters, and island-associated blooms where phytoplankton communities are not iron-limited (Hoppe et al., 2017; Morris and Sanders, 2011; Moore et al., 2013a). Future efforts aiming to comprehensively describe isoprene distribution and cycling in the Southern Ocean should consist of a combination of the PEGASO and the ACE approaches, that is, a combination of measurements over the large low-productivity areas, across biological and physical boundaries (Ardyna et al., 2017) as well as targeting for contrasting upwelling and blooming spots at different stages of bloom development (Ardyna et al., 2019).

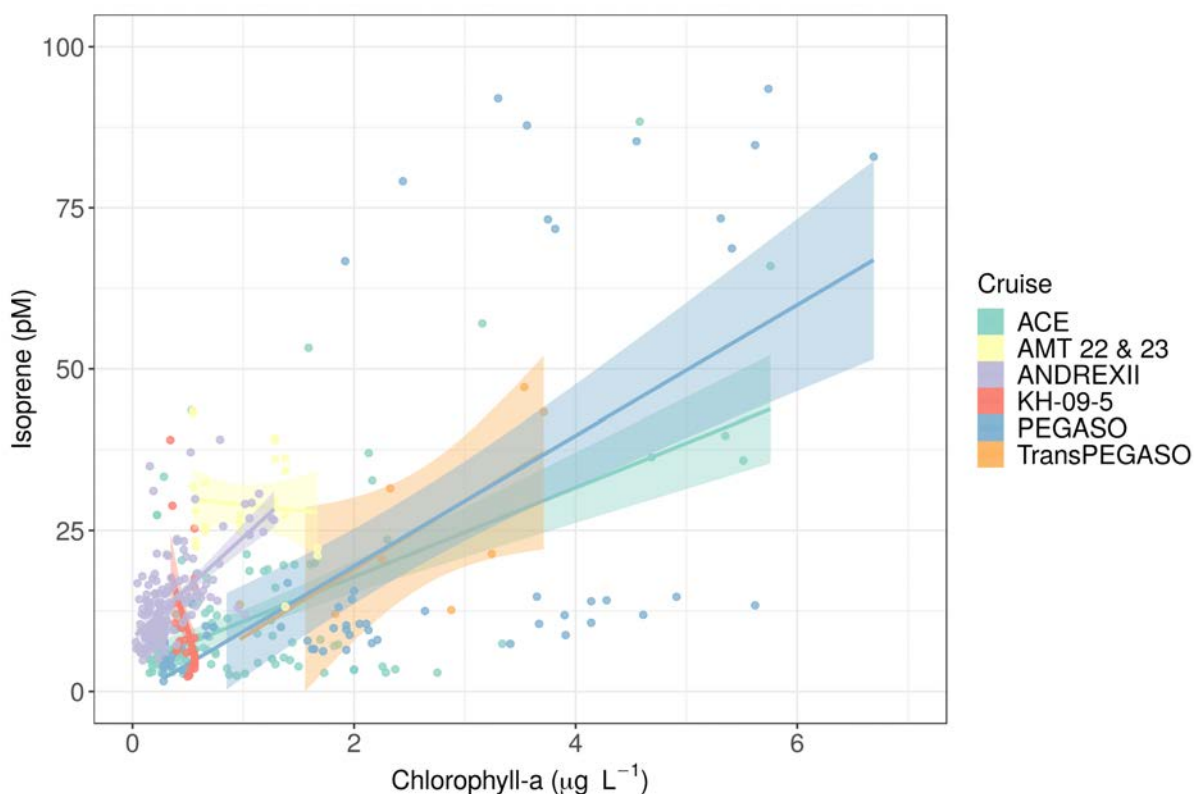


Figure 1.5: Comparison of the relationship between isoprene and chlorophyll-a concentrations on the cruises examined in this work (Table 3.3).

Funding

This research was supported by the Spanish Ministry of Economy and Competitiveness through project PEGASO (CTM2012–37615) to RS, and by the Swiss Polar Institute and Ferring Pharmaceuticals through project SORPASSO–ACE#8 to RS and project ACE#1 to David Antoine (Remote Sensing and Satellite Research Group, Curtin University) and Sandy Thomalla (Southern Ocean Carbon and Climate Observatory, Council for Scientific and Industrial Research (CSIR) and Marine Research Institute, University of Cape Town). It was also partially funded by the Australian Government through the Australian Research Council’s Discovery Projects funding scheme (project DP160103387) and South African CSIR Parliamentary Grant (SNA2011112600001). Project ACE#1 was also supported by CSIR Southern Ocean Carbon and Climate Observatory (SOCCO) programme. PRR was supported by a “la Caixa” Foundation PhD Fellowship (2015–2019).

Acknowledgements

Members of the ACE#1 research team are greatly acknowledged for providing data and technical support. PRR would like to thank Martí Galí from the Barcelona Supercomputing Centre

for his advice with the statistical analysis and data visualization. We are grateful to the British Oceanographic Data Centre (BODC). We would like to thank to Miguel Cabrera, Laura Carrillo, Encarna Borrull and Carolina Antequera (ICM-CSIC) for flow cytometry analyses, Mikhail Emelianov (ICM-CSIC) for mixed layer depth data, Nicolas Cassar and Yajuan Lin (Duke University) for sea surface temperature measurements, and Marina Zamanillo (ICM-CSIC) for computing solar radiation dose data and collecting flow cytometry samples. We also want to thank the captains, officers and crew of RV Hespérides and RV Akademik Tryoshnikov, to the ACE chief Scientist David Walton, engineers of the Marine Technology Unit (CSIC) and research colleagues for their support and help during the cruises. Data of this work can be found at the *Zenodo* repository (<https://doi.org/10.5281/zenodo.3773972>). This research is part of POLARCSIC (<https://polarcsic.es/>) activities.

1.4 Appendix

Summary of compiled cruise variables

Table 1.3: Surface isoprene concentration measurements (0 – 10 meters depth) in the Southern Ocean (>40°S) along the research cruises used for model comparisons (Figure 4.8): PEGASO, TransPEGASO, ACE Expedition, AMT22, AMT23, KH-09-5, and ANDREXII. For more details, see Rodríguez-Ros et al. (2020b).

Isoprene (pM)	Chlorophyll-a (μgL^{-1})	Sea surface temperature (°C)	Southern Ocean area	Cruise
Mean (Min – Max)	Mean (Min – Max)	Mean (Min – Max)		
10.7 (2.1 – 88.4)	1.46 (0.15 – 8.70)	4.16 (-0.18 – 13.06)	SO Circumnavigation	ACE
22.4 (1.6 – 93.5)	2.42 (0.28 – 8.95)	1.45 (-0.87 – 5.38)	SO and Weddell Sea	PEGASO
25.3 (12.0 – 49.5)	2.59 (0.97 – 3.71)	9.97 (7.73 – 12.28)	Southwestern Atlantic Self	TransPEGASO
29.0 (13.1 – 57.1)	0.97 (0.55 – 1.67)	12.68 (10.46 – 14.40)	SO + South Atlantic Ocean	AMT23 & AMT22
9.5 (2.3 – 39.0)	0.49 (0.34 – 0.56)	1.82 (-1.45 – 14.2)	SO + South Indian Ocean	KH-09-5
13.5 (4.8 – 39.1)	0.33 (0.02 – 1.27)	0.91 (-1.68 – 10.63)	SO + South Atlantic Ocean	ANDREXII

Residuals

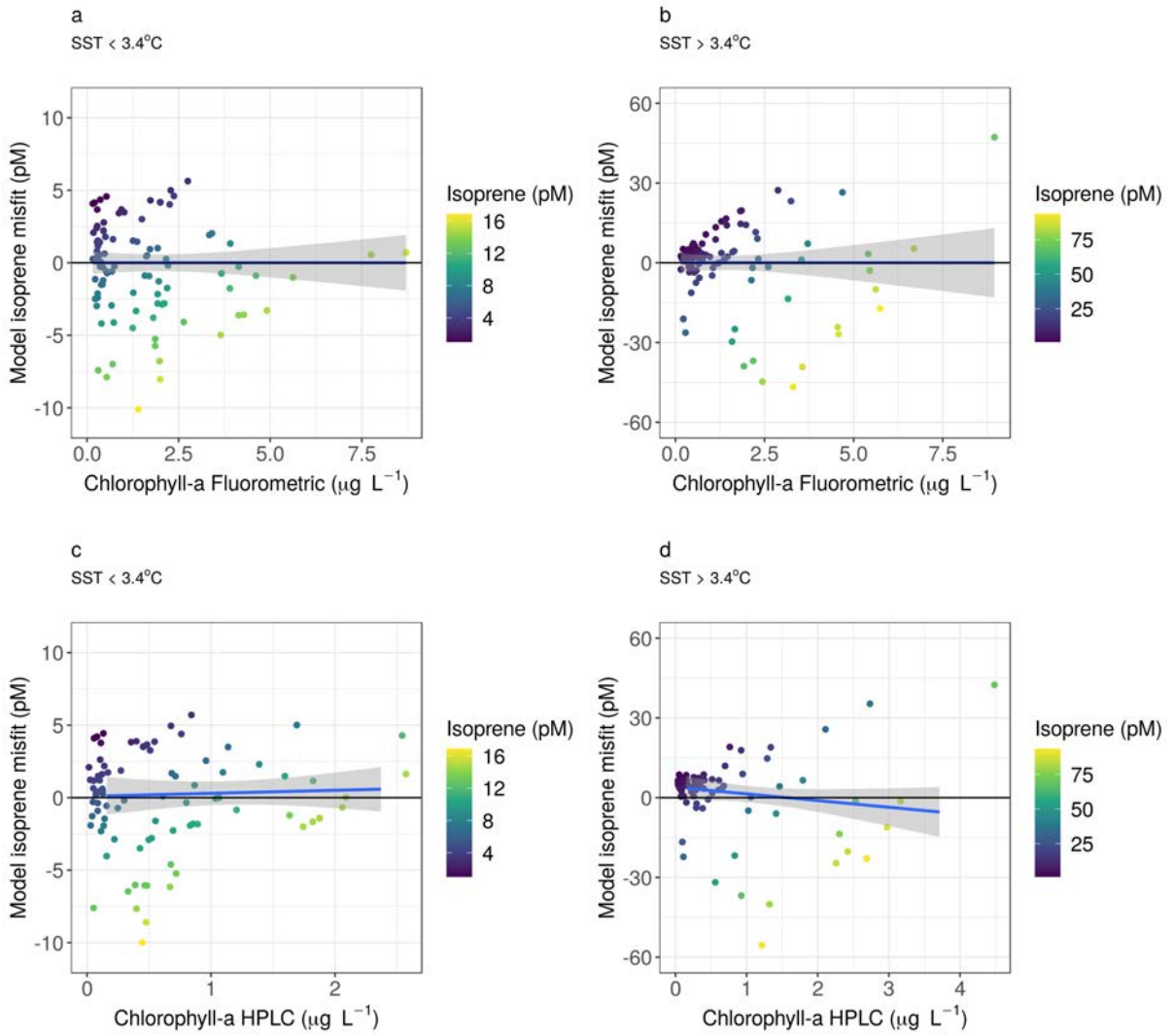


Figure 1.6: Scatterplot of misfit (residuals) among observed and predicted isoprene concentration values from PEGASO and ACE cruises versus chlorophyll-a levels (Fluorometric: a and b; and HPLC: c and d).

Statistical relationships between isoprene concentration and chlorophyll-a concentration and sea surface temperature

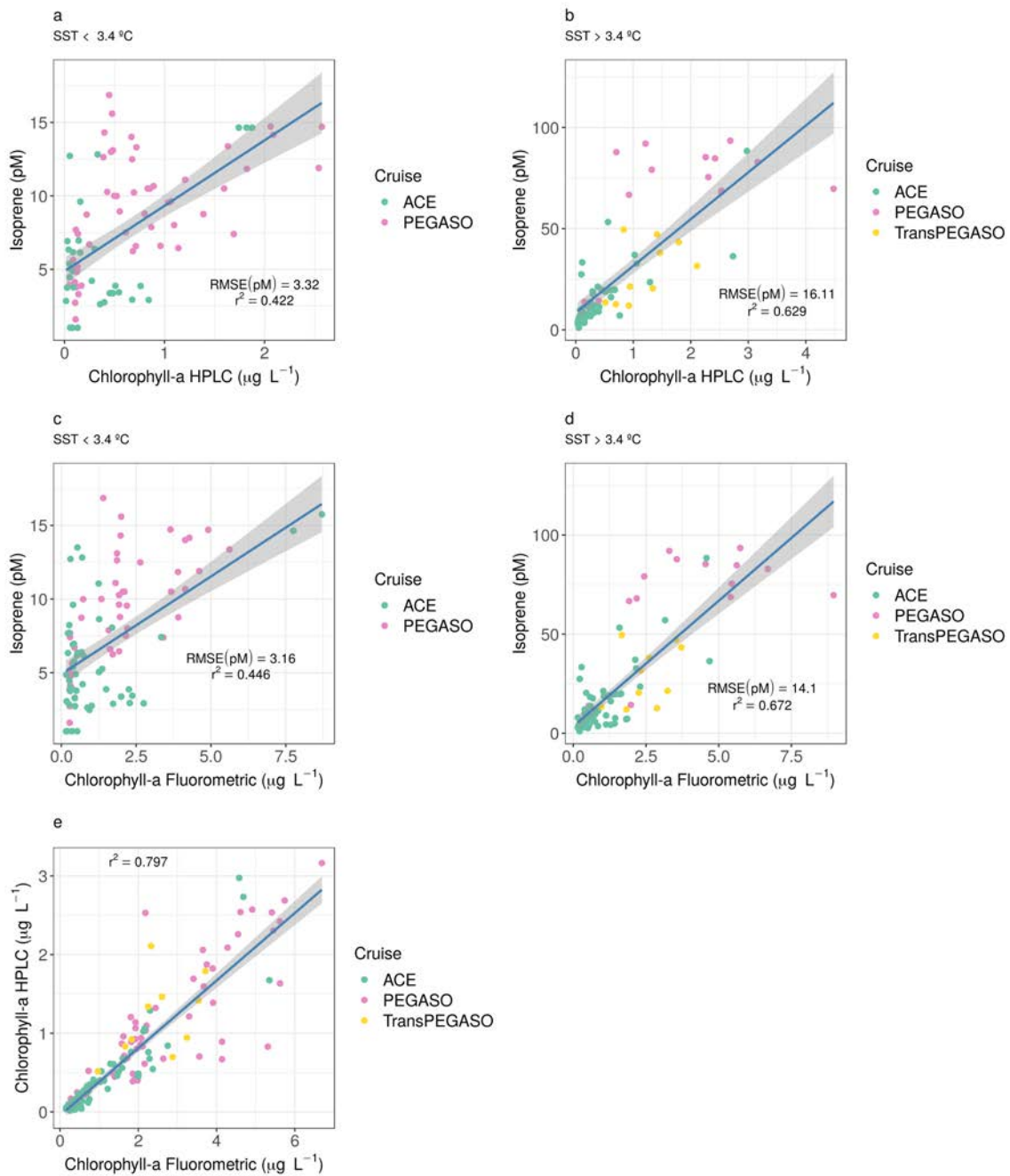
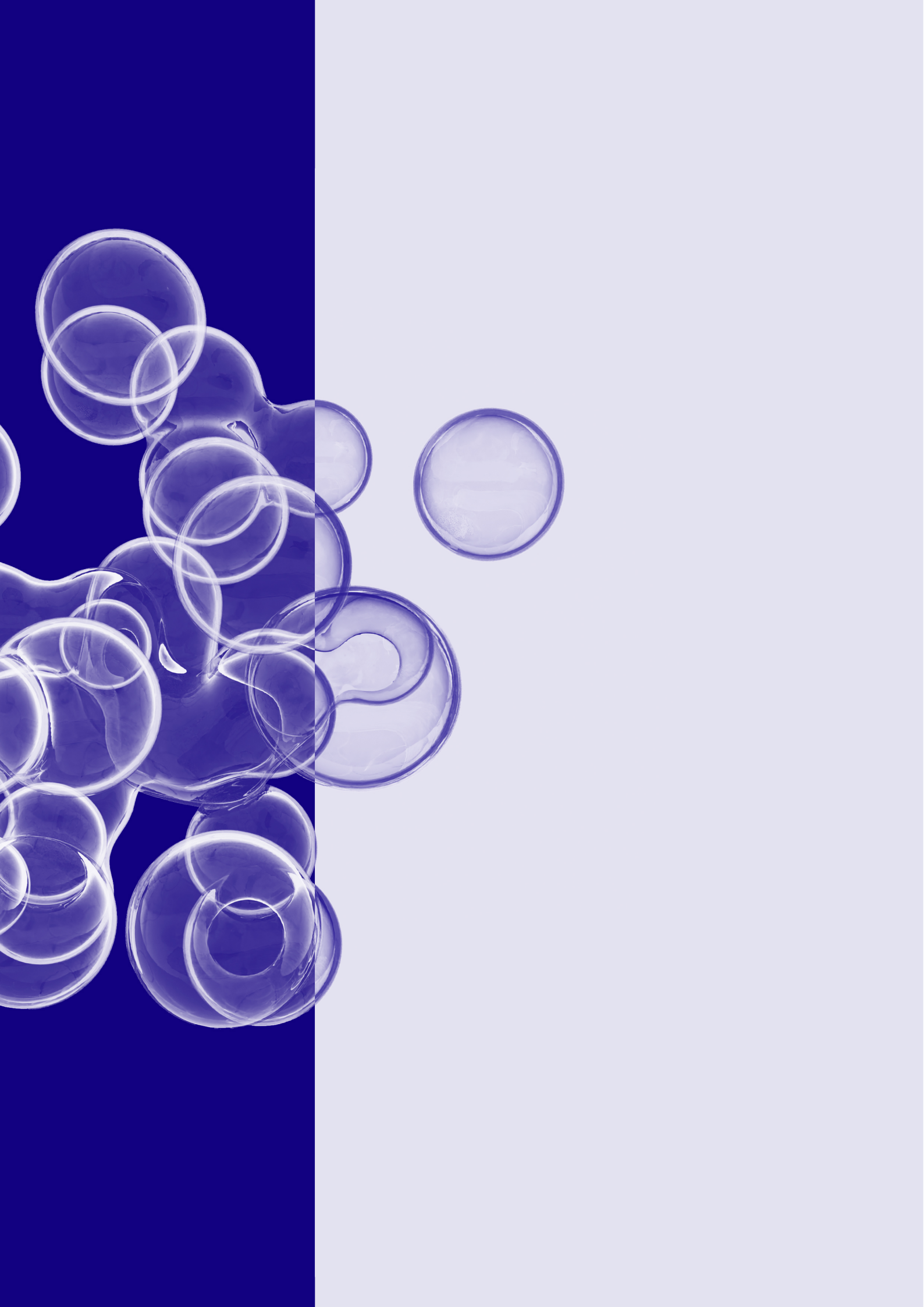


Figure 1.7: (a) and (b) Isoprene model based on CHLA-FLUO with the shifting regime based on a SST threshold of 3.4°C. (c) and (d) Isoprene model based on CHLA-HPLC with the shifting regime based on a SST threshold of 3.4°C. (e) CHLA-HPLC vs CHLA-FLUO. For these plots only data from TransPEGASO, PEGASO and ACE cruises were used (Figure 4.8, Table 3.3). RMSE = Root Mean Square Error (see equation 1.2).



Chapter 2

Remote sensing retrieval of isoprene concentrations in the Southern Ocean

Chapter 2

Remote sensing retrieval of isoprene concentrations in the Southern Ocean

Pablo Rodríguez-Ros¹, Martí Galí², Pau Cortés¹, Charlotte Mary Robinson³, David Antoine³, Charel Wohl⁴, MingXi Yang⁴, Rafel Simó¹

1. Institut de Ciències del Mar, ICM-CSIC, Passeig Marítim de la Barceloneta, 37-49, 08003, Barcelona, Catalonia, Spain
2. Earth Sciences Dept, Barcelona Supercomputing Center (BSC-CNS), Barcelona, Catalonia, Spain
3. Remote Sensing and Satellite Research Group, School of Earth and Planetary Sciences, Curtin University, Perth, Australia
4. Sorbonne Université, CNRS, Laboratoire d'Océanographie de Villefranche, LOV, F-06230 Villefranche-sur-Mer, France
5. Plymouth Marine Laboratory, Plymouth, United Kingdom

This chapter is published as:

Rodríguez-Ros, P., Galí, M., Cortés, P., Robinson, C. M., Antoine, D., Wohl, C., Yang, MingXi., & Simó, R. (2020). *Remote sensing retrieval of isoprene concentrations in the Southern Ocean*. *Geophysical Research Letters*, e2020GL087888. DOI: <https://doi.org/10.1029/2020GL087888>

—No es necesario haber estado en un sitio para saberlo todo sobre él—respondía Abdul—; si no, los marineros serían más sabios que los teólogos.

Baudolino – Umberto Eco.

Abstract

Isoprene produced by marine phytoplankton acts as a precursor of secondary organic aerosol and thereby affects cloud formation and brightness over the remote oceans. Yet, the marine isoprene emission is poorly constrained, with discrepancies among estimates that reach 2 orders of magnitude. Here we present ISOREMS, the first satellite-only based algorithm for the retrieval of isoprene concentration in the Southern Ocean. Sea surface concentrations from six cruises were matched with remotely-sensed variables from MODIS Aqua, and isoprene was best predicted by multiple linear regression with chlorophyll-a and sea surface temperature. Climatological (2002-2018) isoprene distributions computed with ISOREMS revealed high concentrations in coastal and near-island waters, and within the 40°-50°S latitudinal band. Isoprene seasonality paralleled phytoplankton productivity, with annual maxima in summer. The annual Southern Ocean emission of isoprene was estimated at 63 Gg C yr⁻¹. The algorithm can provide spatially and temporally realistic inputs to atmospheric and climate models.

Plain Language Summary

Isoprene is a marine trace gas with climatic relevance in remote regions of the ocean, because it reacts readily in the atmosphere to produce aerosols (atmospheric particles) that make clouds brighter. In the Southern Ocean, however, its regional emission is poorly quantified. We explored the capability of satellite observations (MODIS Aqua, NASA) to reconstruct isoprene concentrations measured in the Southern Ocean during various oceanographic cruises. We found an empirical relationship between isoprene and sea-surface chlorophyll and temperature, and used it to produce regional maps of isoprene emission. The new tool presented here, named ISOREMS, enables detailed exploration of the role of ocean-leaving isoprene in the Southern Ocean atmosphere.

Key points

- We present an algorithm for the retrieval of isoprene concentrations in the Southern Ocean from remote sensing.
- Isoprene peaks in mid-summer and is highest in coastal and near-island waters and in the 40°-50°S latitudinal band.
- The annual isoprene emission from the entire Southern Ocean amounts 63 Gg C yr⁻¹.

2.1 Introduction

Marine aerosols control cloud micro-physics and optics over the oceans (Andreae and Rosenfeld, 2008). Trace gases of marine origin, when oxidized in the lower atmosphere, form new aerosol particles and condense on pre-existing ones. These particles can eventually grow large enough to act as cloud condensation nuclei (CCN), increasing cloud brightness and lifetime (Carslaw et al., 2013). When the particle-forming oxidation products are mainly organic, the resulting aerosols are named Secondary Organic Aerosols (SOA) (O'Dowd et al., 2004). Ocean-emitted isoprene (2-methyl-1,3-butadiene, C_5H_8) contributes between 5-25 % of the natural SOA sources in the global marine atmosphere (Claeys et al., 2004; Liao et al., 2007; Gantt et al., 2009; Luo and Yu, 2010). Owing to its high reactivity (1–2 hours lifetime) (Medeiros et al., 2018), isoprene can impact the chemistry of the marine boundary layer (Palmer and Shaw, 2005; Lewis et al., 2005) and cool the climate (Claeys et al., 2004; Carslaw et al., 2013). This impact is thought to be stronger in the Southern Ocean (SO), away from land vegetation emissions, where isoprene can act synergistically with marine dimethylsulfide to form CCN (Meskhidze and Nenes, 2006; Vallina et al., 2007; Booge et al., 2016; Dani and Loreto, 2017).

Although it has been suggested that, depending on the regional magnitude of its emission fluxes, marine isoprene should be taken into account in climate models (Gantt et al., 2009; Shaw et al., 2010), this objective is currently hampered by the lack of knowledge about its drivers, spatio-temporal distribution, and atmospheric effects (Carslaw et al., 2013). Even the magnitude of marine isoprene emission is largely unconstrained, and there still are large discrepancies between the bottom-up ($0.085 - 1.2 \text{ Tg C yr}^{-1}$; (Bonsang et al., 1992; Milne et al., 1995; Broadgate et al., 1997; Palmer and Shaw, 2005; Arnold et al., 2009; Gantt et al., 2009; Booge et al., 2016)) and the top-down ($1.9 - 11.6 \text{ Tg C yr}^{-1}$; (Arnold et al., 2009; Luo and Yu, 2010)) estimates of the global oceanic flux. Most of the discrepancy stems from limited knowledge of isoprene production and loss processes in sea water (Shaw et al., 2010; Booge et al., 2016, 2018; Brüggemann et al., 2018), and the relationship between isoprene concentrations and biological and environmental parameters (Carpenter et al., 2012; Exton et al., 2013).

Due to the scarcity of in situ data, large-scale estimates of isoprene rely on either process-based ecosystem models or empirical models based on remote sensing data. Process-based isoprene parameterizations are currently limited by poor knowledge of the underlying processes. Therefore, empirical models linking directly observed sea-surface concentrations and remotely sensed variables offer a workable alternative for mapping isoprene, while allowing for uncertainty estimates. According to the available observations, higher marine isoprene concentrations tend to co-occur with phytoplankton blooms (Ooki et al., 2015). In the SO, local foci of iron supply lead to higher productivity and are expected to result in higher isoprene, as confirmed by deliberate iron fertilization experiments (Wingenter et al., 2004). The close relationship of isoprene to primary production and phytoplankton biomass, further tuned by environmental drivers such as temperature and light, has been demonstrated by both laboratory experiments and measurements at sea (Moore et al., 1994; Milne et al., 1995; McKay et al., 1996; Shaw et al., 2003; Exton et al., 2013; Liakakou et al., 2007; Bonsang et al., 2010; Meskhidze et al., 2015). Therefore, chlorophyll-a concentration has

been proposed, either alone or together with temperature or light, to empirically estimate isoprene concentration and emission from remote sensing observations (Bonsang et al., 1992; Booge et al., 2016; Ooki et al., 2015; Hackenberg et al., 2017). In their pioneering work, Palmer and Shaw (2005) used a mixed approach that combined MODIS (Moderate-resolution Imaging Spectroradiometer) chlorophyll-a (CHL) observations with a steady-state water-column model, parameterizing isoprene production from experimentally determined chlorophyll-a-specific production rates and prescribing microbial and chemical losses at fixed rate constants. Arnold et al. (2009), Luo and Yu (2010) and Booge et al. (2016) went a step further by using remote sensing estimates of phytoplankton functional types (PFT) and applying PFT-specific production rates from phytoplankton culture experiments.

The aforementioned models suggested that high southern latitudes are strong emitters of marine isoprene, by concurrence of high seasonal productivity and strong winds. Therefore, several circumstances concur in the SO that warrant a focused effort to assess isoprene emissions from remote sensing: potential for high emissions due to productivity and wind speed, cleanliness of the atmosphere and remoteness from continental influence. However, there has been a paucity of measurements of isoprene concentrations in the region (Kameyama et al., 2014; Ooki et al., 2015; Hackenberg et al., 2017). In the present work, we utilise an unprecedented dataset of isoprene concentrations from six research voyages (two of them reported here for the first time), which collectively span a much larger area than ever observed in-situ, to develop an algorithm for the retrieval of isoprene from remote sensing in the SO. The algorithm, here used to generate monthly synoptic distributions of isoprene concentration and emission fluxes, should allow the evaluation of interannual variability and decadal trends, and can be used to feed atmospheric models to assess ocean-climate interactions in this sensitive and critical region of the Earth.

2.2 In situ measurements

The PEGASO cruise was conducted in January 2015 on board the RV *Hesperides* in waters of the Atlantic sector of the SO, the Antarctic Peninsula and the Weddell Sea (Zamanillo et al., 2019a; Nunes et al., 2019a; Rodríguez-Ros et al., 2020a). The ACE cruise circumnavigated the SO between December 2016 and April 2017 on board the RV *Akademik Tryoshnikov* (Rodríguez-Ros et al., 2020a). During both cruises, seawater samples were collected from either the underway pumping system (intake at ≈ 4 -5 m depth) or the uppermost (≈ 5 m) bottle of the rosette on CTD casts. In either case, 0.5 L all-glass bottles were completely filled leaving no headspace, and analyzed within 1 hour after collection. Isoprene was measured, along with other volatile compounds, on a gas chromatography-mass spectrometry system (5975-T LTM-GC/MSL, Agilent Technologies). Aliquots of 25 mL were taken from the glass bottle with a glass syringe with a teflon tube, and filtered through a GF/F filter while introduced into a purge and trap system (Stratum, Tekmar Teledyne). Volatiles were stripped by bubbling with 40 mL min⁻¹ of ultrapure He for 12 minutes, trapped on solid adsorbent at room temperature and thermally desorbed (250°C) into the GC. Isoprene, monitored as m/z 67 in selected ion monitoring mode, had a retention time of 2.4 min in the LTM DB-VRX chromatographic column held at 35°C. The detection limit was 1 pmol L⁻¹. All samples were run in duplicates.

In PEGASO, calibration was performed by injections of a gaseous mixture of isoprene in N_2 . In ACE, a liquid standard solution prepared in cold methanol was used instead. In situ chlorophyll concentrations (CHL_{flu0}) were determined by filtration of 250 mL (PEGASO) or 2000 mL (ACE) of sea water through GF/F filters, extraction with cold 90% acetone for 24 h, and fluorescence measurement of extracts on a calibrated Turner Designs fluorometer.

For model development and validation, we also compiled surface (0-10 m depth) isoprene, CHL and temperature data from four other research cruises conducted entirely or partly in the SO ($> 40^\circ S$), namely: KH-09-5-2010 (Ooki et al., 2015), AMT23-2013 & AMT22-2012 (Hackenberg et al., 2017), and ANDREXII-2019 (Wohl et al., 2020) (Table 3.3, Figure 4.8). Description of measurement procedures can be found in the corresponding publications. Another cruise was discarded for this analysis because the reported isoprene concentrations were much higher than any other cruise's in the region (Kameyama et al., 2014), and there is the suspicion that they had a systematic offset (Kameyama, personal communication). A frequency distribution analysis reveals that isoprene measurements of the entire data set were evenly spread across the diel solar cycle (Figure 2.5), probably because a large proportion of the database is contributed by automated instruments or underway measurements at high temporal resolution (ANDREXII, KH-09-5, part of PEGASO).

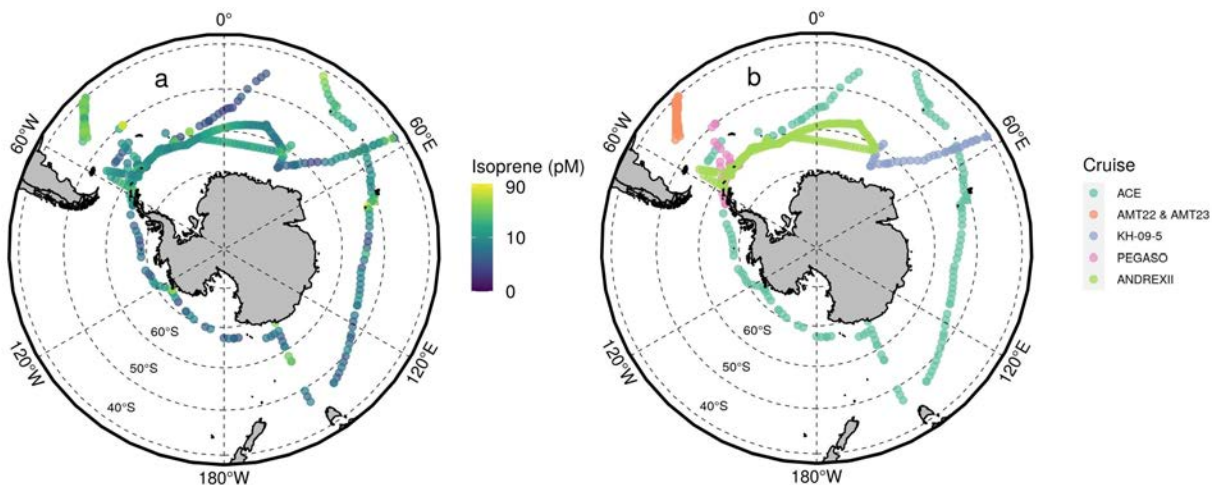


Figure 2.1: (a) Surface ocean isoprene concentrations from the six cruises. Note the log scale. (b) Cruise tracks. More information in Table 3.3

2.3 Remote sensing matchups

We matched the in situ measurements (Table 3.3) with several remotely sensed variables including chlorophyll-a (CHL), sea-surface temperature (SST), photosynthetically available radiation (PAR), euphotic layer depth (ZEU), particulate inorganic carbon (PIC) and particulate organic carbon (POC). MODIS-Aqua daily, 8-day and monthly composites at 4.64 km resolution were obtained from the NASA Ocean Color Website, accessed in February 2019 (2019), <https://oceancolor.gsfc.nasa.gov/>) (Table 2.2). The SO is challenging for remote sensing of ocean colour due to persistent heavy clouds, presence of sea ice, and low sun angles (Neukermans et al., 2018). To overcome the frequent satellite data gaps, match-ups were searched sequentially in order of decreasing

spatial-temporal resolution until a valid value was found. For the time and position of each in situ measurement, the search started with the daily single-pixel value, continued with the average of 3x3 and 5x5 pixel bins centered around it, and proceeded similarly for 8-day and monthly composites, ensuring that the best available resolution was used (Galí et al., 2018). Finally, in situ measurements that corresponded to the same satellite datum were averaged to avoid over-representation. The resulting database of isoprene and satellite measurements was matched to the mixed layer depth (MLD) obtained from a global monthly $1^\circ \times 1^\circ$ climatology (Holte et al., 2017).

2.4 ISOREMS: a new remote sensing-based model to predict isoprene concentrations in the Southern Ocean

We explored the predictive capacity of each remotely sensed variable for isoprene concentration through linear regression analysis. The best paired relationship was with CHL ($r^2 = 0.15$, p-value < 0.05 , $n = 408$), followed by SST ($r^2 = 0.09$, p-value < 0.05 , $n = 408$). A redundancy analysis (Legendre and Legendre, 2012) revealed that both CHL and SST contributed to the variance of isoprene concentration, while other variables were highly redundant to either CHL (POC, ZEU) or SST (PAR) (Figure 2.6). The fit improved indeed with a multiple regression model with CHL and SST together ($r^2 = 0.24$, p-value < 0.05). To further improve the model, we excluded three subsets that degraded the fit disproportionately, such that a total of 327 points were retained out of 408 (80%). Two of the subsets were removed owing to large discrepancies between in situ vs. satellite CHL, whose uncertainty propagated to the regression model. This was the case with some samples from the bloom north of South Georgia Islands, where diatoms represented more than 80% of the phytoplankton community (Nunes et al., 2019a); under these particular conditions, standard algorithms for CHL determination from satellite show poor agreement to in situ $\text{CHL}_{\text{fluor}}$ due to the interference of chlorophyll c pigments (Moutier et al., 2019). We also excluded from the database the cases where CHL values fell out of the 90% confidence prediction intervals of the regression between CHL and their $\text{CHL}_{\text{fluor}}$ match-ups ($r^2 = 0.63$, p-value < 0.05); this criterion removed points where the discrepancy could have been due either to optical reasons (which could not be assessed in the original datasets), or to poor match-up (e.g., due to strong small-scale variability). Finally, we also excluded two cases with CHL higher than $2 \mu\text{g L}^{-1}$ that were flagged outliers in the isoprene vs CHL regression. The resulting multiple regression model between isoprene and CHL + SST improved after these removals (Equation 2.1, $r^2 = 0.45$, MAPE = 46%, RMSE = 10.6 pM, relative RMSE = 0.73, relative BIAS = -0.5%, $n = 327$), and we named it ISOREMS (*Isoprene Southern Ocean Remote Sensing*) (numbers in brackets show the 95% confidence interval for each coefficient, estimated as described in section 2.5):

$$\text{ISO} = 3.0 [1.9 - 4.2] + 35.22 [29.35 - 40.08] \cdot \text{CHL} + 0.68 [0.59 - 0.77] \cdot \text{SST} \quad (2.1)$$

Where ISO is predicted isoprene concentration in pM (pmol L^{-1}), CHL is satellite-derived chlorophyll-a concentration, and SST is satellite-derived sea-surface temperature in degrees celsius

(°C). We note that ISOREMS is developed from observations within the following ranges: 0.04 – 1.54 $\mu\text{g L}^{-1}$ CHL, -1.8 – 24.5°C SST, 72.42°S – 40.00°S latitude, and its applicability is uncertain beyond these ranges. However, note that the proportion of 1x1 degree pixels with climatological CHL > 1.54 $\mu\text{g L}^{-1}$ is only 1.8 % in October through March and 0.7 % during the rest of the year. In Figure 2.2, we display the scatter plot of the predicted vs observed isoprene concentrations. In Figure 2.7 the residuals of ISOREMS predictions are shown to explore the misfit with observations along ranges of the potential predictor variables (CHL, SST, PAR, ZEU, PIC, POC and MLD). The misfit between predictions and observations is typically in the range of -30 to +30 pM, with the largest differences corresponding to six measurements from the diatom bloom in PEGASO (Nunes et al., 2019a; Zamanillo et al., 2019a). The analysis of the residuals (Figure 2.7) does not support the addition of any of the other potential predictors or the need for nonlinear terms in the multiple regression.

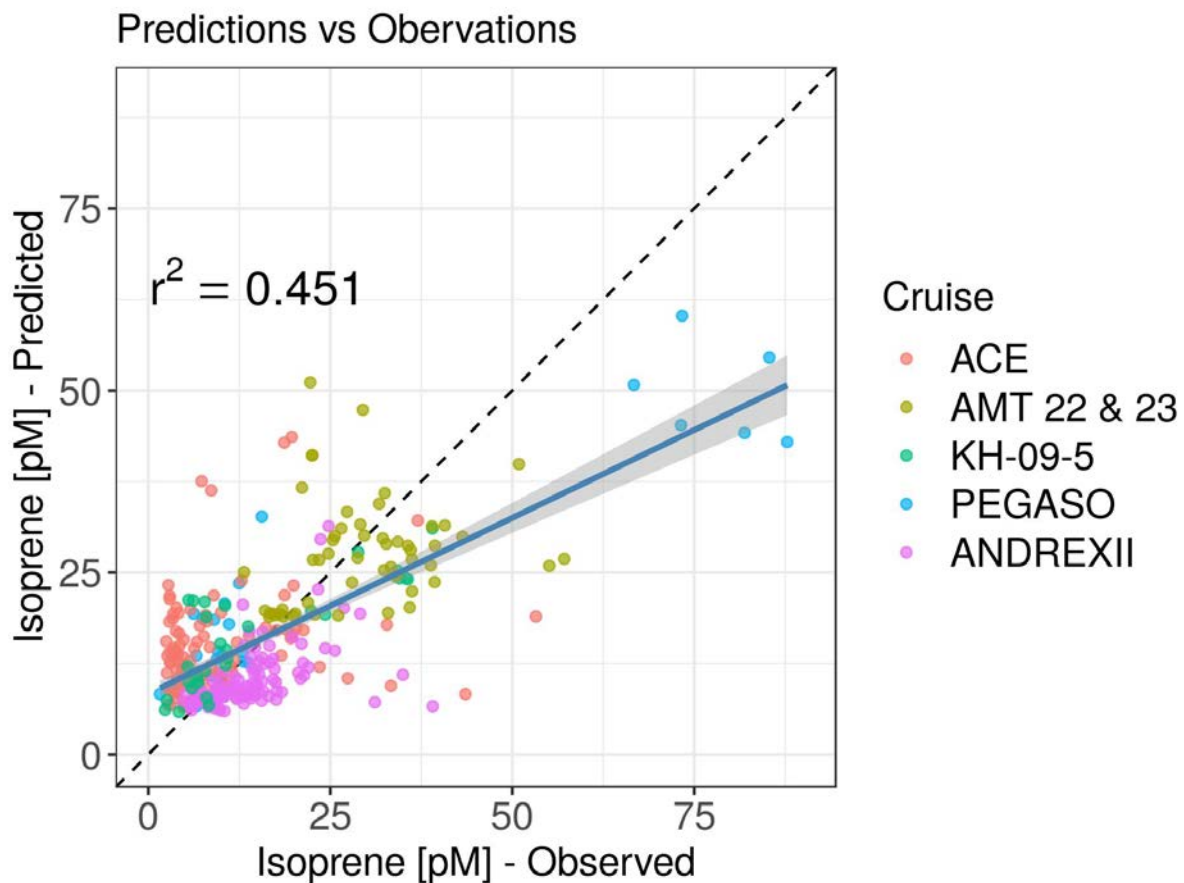


Figure 2.2: Scatter plot of ISOREMS predictions vs. observations of isoprene concentrations.

2.5 Validation of ISOREMS

Since all available data in the SO were used to develop ISOREMS, a random sampling approach was taken to validate the performance of the algorithm. First a multiple regression model equivalent to ISOREMS was performed on 80 % of in-situ isoprene and matched satellite CHL and SST dataset. The resulting equation was then applied to the remaining 20 % of the dataset, and predicted values were compared to observations using an array of skill metrics. We ran a total of 10,000 simulations following this process, which provided us with robust estimates of ISOREMS coefficients and skill metrics, along with their respective confidence intervals. Scatter plots of the randomly generated ISOREMS coefficients (Figure 2.8a) indicate a negative relationship between the intercept and the CHL coefficient in Equation 2.1, contrasting with the independent behavior of the SST coefficient. This exercise reveals a trade-off in the ability of ISOREMS to fit low isoprene concentrations (more influenced by the intercept) or high concentrations (more influenced by the CHL coefficient). Moreover, it suggests that additional predictor variables may be needed to obtain better fits. Unfortunately, inclusion of none of the other tested variables (Table 2.2) improved ISOREMS significantly. Finally, the histograms of the 10,000 randomly generated ISOREMS validation statistics (Figure 2.8b) are clearly centered around the statistics obtained when fitting the entire data-set (Table 3.3). Therefore, these statistics can reliably be used as uncertainty estimates of ISOREMS predictions on a pixel basis.

2.6 ISOREMS implementation to compute isoprene concentrations and emission fluxes

We implemented the ISOREMS model using monthly climatological fields of CHL and SST from MODIS-Aqua for the period 2002-2018 from NASA Ocean Colour service (<https://oceancolor.gsfc.nasa.gov/>). We then used the resulting concentrations of $ISO_{ISOREMS}$ to calculate the air-sea flux of isoprene (Palmer and Shaw, 2005):

$$F_{ISO} = k_{AS} \cdot \left(ISO_w - \frac{ISO_a}{K_H} \right) \approx k_{AS} \cdot ISO_w \quad (2.2)$$

Where ISO_w is isoprene concentration in sea water, ISO_a is isoprene concentration in the air, K_H is the Henry's Law constant for isoprene, and k_{AS} is the gas exchange velocity (cm h^{-1}). Air-side isoprene can be considered near zero and neglected for flux calculations because (a) isoprene is typically largely supersaturated in the surface ocean ($> 700\%$ during ANDREXII; (Wohl et al., 2020)), and (b) its short atmospheric lifetime (Medeiros et al., 2018) prevents that high airborne isoprene concentrations of continental origin occurred during our sampling. For k_{AS} we used the Wanninkhof (2014) parameterization:

$$k_{AS} = 0.251 \cdot \langle U_{10}^2 \rangle \cdot \left(\frac{S_C}{660} \right)^{-0.5} \quad (2.3)$$

Where $\langle U_{10}^2 \rangle$ is the average of the square of the wind speed at 10 m ($\text{m}^2 \text{s}^{-2}$), and Sc is the *Schmidt* number (non dimensional). We used monthly mean climatological fields of U_{10}^2 at 1×1 degrees spatial resolution constructed from the CCMPv2 product at 0.25×0.25 degrees and 6 h resolution for the period 1987-2018, which includes data from many inter-calibrated satellites (all the information and the most recent estimates are available at <http://www.remss.com/measurements/wind/>). To calculate Sc we used the equation proposed by Palmer and Shaw (2005):

$$S_C = 3913.15 - 162.13 \cdot \text{SST} + 2.67 \cdot \text{SST}^2 - 0.012 \cdot \text{SST}^3 \quad (2.4)$$

Where SST is in degrees celsius ($^{\circ}\text{C}$).

2.7 ISOREMS-derived isoprene concentrations and emission in the Southern Ocean

Our climatological monthly concentrations and air-sea fluxes of isoprene in the SO show remarkable coupling to biological productivity, with higher values in coastal regions, such as the Antarctic and South Atlantic Shelves, and next to subantarctic islands (Figures 2.3 and S5). This is expected from equation (1) and consistent with previous fieldwork studies (Broadgate et al., 2004; Ooki et al., 2015; Zindler et al., 2014; Hackenberg et al., 2017).

A band of higher isoprene concentrations and air sea-fluxes is observed around the Subantarctic front (approximately between 40°S and 50°S), as already depicted by Ooki et al. (2015) and Wohl et al. (2020). However, the air-sea fluxes show a more spread distribution than concentrations, with weaker gradients towards continental shelves and islands. This is consistent with the modelling simulations of Luo and Yu (2010) and Booge et al. (2016). Monthly average concentrations of $\text{ISO}_{\text{ISOREMS}}$ in the entire SO peak in January (13 pM), and the annual mean throughout the climatological year is 7 pM (Figure 2.4a). By latitudes, concentrations are higher in the $40\text{-}50^{\circ}\text{S}$ band (Figure 2.4b), reaching maximum values above 20 pM in November-December (Figure 2.4a). The $50\text{-}60^{\circ}\text{S}$ and $60\text{-}70^{\circ}\text{S}$ bands also show clear seasonality, yet their annual maxima are around 16 pM in December and 15 pM in January, respectively (Figure 2.4a).

As depicted by Figure 2.3, large portions of the SO are devoid of CHL data over the months of May through August. Consequently, isoprene concentrations cannot be computed in these areas. Similarly, large areas lack climatological wind speeds in May through August as well as near the Antarctic coasts all year round (Figure 2.9), impeding calculation of the air-sea flux. In order to circumvent this lack of data and be able to estimate SO-integrated isoprene emissions, we made two assumptions: (a) when light is not enough to allow remote sensing of CHL, we assume a minimum isoprene concentration of 3 pM, which is the intercept of Equation 1; (b) the gaps of remote sensing wind speed are filled with a fixed value of 7 m s^{-1} , considered a reasonable approximation to year-round conditions close to the Antarctic coasts (Bintanja et al., 2014). Moreover, following Peng et al. (2013) and Meier et al. (2017) we created a mask of sea ice coverage with monthly averages

for 2018, and assumed that isoprene emission is zero at sea ice concentrations above 10% (Galí et al., 2019). Integrating the resulting fluxes, monthly isoprene emissions from the entire SO peak in January ($7.9 \text{ Gg C month}^{-1}$, Figure 2.4c), where the highest monthly averaged isoprene fluxes (around $50 \text{ nmol m}^{-2} \text{ d}^{-1}$) occur in the latitudinal band of $40\text{-}50^\circ\text{S}$ (Figure 2.4d). Integrated over an entire climatological year, isoprene emission in the SO amounts 63 Gg C yr^{-1} . The latitudinal band of $40\text{-}50^\circ\text{S}$ contributes 57% of this emission, and the $50\text{-}60^\circ\text{S}$ and $60\text{-}70^\circ\text{S}$ bands contribute 33% and 8%, respectively. Note that the SO comprises 27% of the world's ocean area, and our annual isoprene emission (63 Gg C yr^{-1}) represents 5-74% of the bottom-up emission estimates for the global ocean (Bonsang et al., 1992; Milne et al., 1995; Broadgate et al., 1997; Palmer and Shaw, 2005; Arnold et al., 2009; Gantt et al., 2009; Booge et al., 2016), and 0.5-3% of the top-down estimates (Arnold et al., 2009; Luo and Yu, 2010). Therefore, ISOREMS supports the order of magnitude of the bottom-up approaches to marine isoprene emissions.

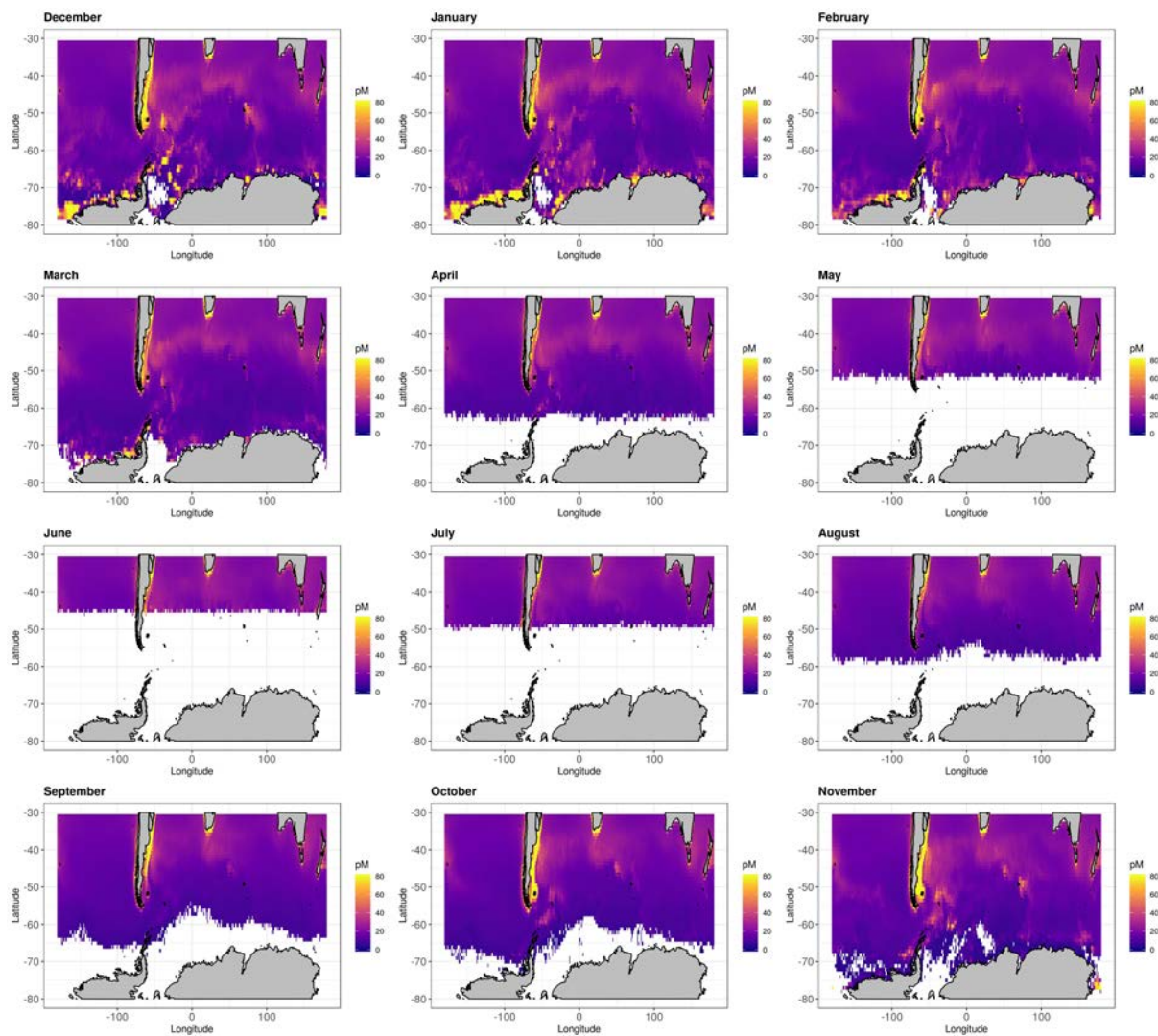


Figure 2.3: Monthly climatology of $\text{ISO}_{\text{ISOREMS}}$ concentration in the Southern Ocean.

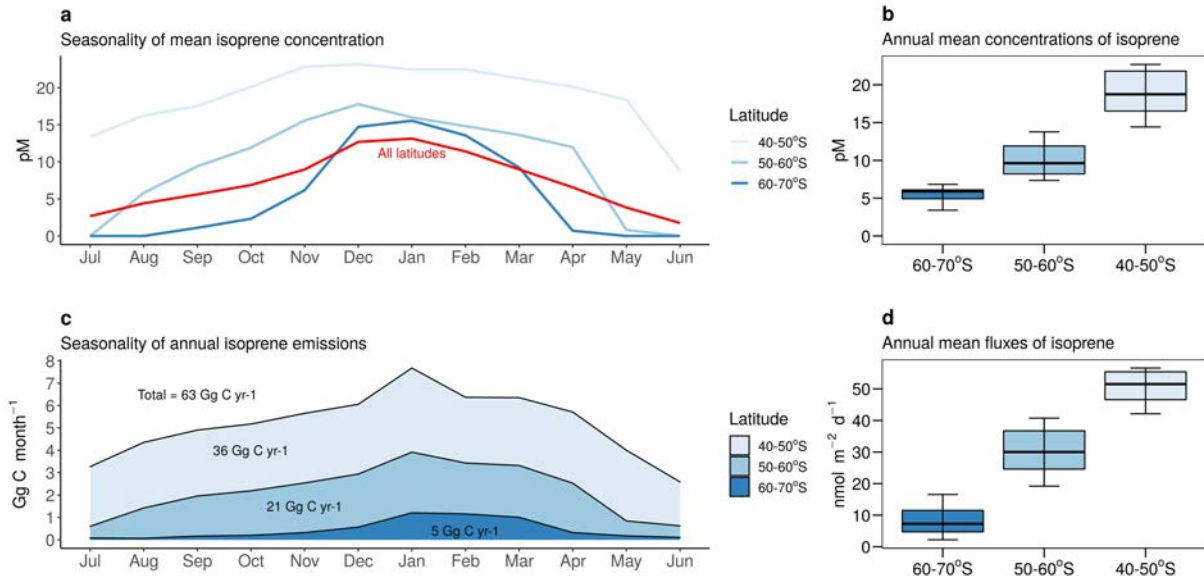


Figure 2.4: (a) Climatological seasonality of $ISO_{ISOREMS}$ concentrations in the entire Southern Ocean (red) and integrated by latitudinal bands (40 to 70°S). (b) Boxplot of annual mean concentrations of isoprene grouped by latitude. (c) Climatological accumulated emissions of $ISO_{ISOREMS}$ through the year. (d) Boxplot of annual mean isoprene emission fluxes grouped by latitude. In the boxplots (b and d), the horizontal black line inside the boxes is the median, the upper and lower limits of the boxes are, respectively, 75th and 25th percentiles; and the horizontal bars represent the upper and lower whiskers (largest values within 1.5 times interquartile range above 75th percentile and below 25th percentile).

2.8 Caveats of ISOREMS and future research

2.8.1 Lack of observations in a complex ocean

The surface waters of the SO are a complex mosaic in terms of biological, environmental and physical properties (Ardyna et al., 2017). Since Longhurst (1995) described oceanic biogeochemical provinces 35 years ago, there have been several attempts to revisit that concept, reaching different results depending on the criteria used and the purpose of the regionalization (Fay and McKinley, 2014; Ardyna et al., 2017). The conspicuous heterogeneity of the SO makes diagnostic isoprene parameterizations strongly dependent on the distribution of data used to build the statistical model. The paucity of measurements in the SO limited previous attempts to predict isoprene concentrations from in-situ CHL and SST: Ooki et al. (2015) pooled together data from the Arctic and the Antarctic, and Hackenberg et al. (2017) barely explored the northernmost area of the Atlantic sector of the SO (Figure 4.8, Table 3.3). We significantly increased the number of isoprene observations and covered most of the biogeochemical provinces, biomes and bioregions suggested by Fay and McKinley (2014) and Ardyna et al. (2017), yet only in summer or early fall. More observations in heavily undersampled regions like the Pacific sector, and at the beginning and end of the productive season,

are needed for a better representation of the spatial and temporal heterogeneity.

2.8.2 Uncertainties about potential sources of atmospheric isoprene from the Southern Ocean

In view of the enormous existing discrepancies between top-down and bottom-up approaches to isoprene emissions, a missing oceanic source has been invoked, and interpretation of laboratory experiments has partly attributed it to photoproduction reactions in the surface microlayer (SML), i.e., right at the air-sea interface (Ciuraru et al., 2015b). Brüggemann et al. (2018) provided a global map of SML isoprene photoproduction factors to calculate the relative contribution of this process to the isoprene production by phytoplankton. Conte et al. (2020) (in review in *Journal of Geophysical Research - Oceans*) implemented these factors in the PISCES global model and estimated that emissions of isoprene by SML photoproduction represent up to $\approx 60\%$ of the global emission. Therefore, our ISOREMS emission estimates probably set a lower limit for the total emission of isoprene from the SO, which may increase when a sound parameterization of the SML photoproduction is implemented. However, eddy covariance measurements of the oceanic flux of isoprene over the open ocean at relatively high wind speeds and low light levels have found no evidence for photochemical production of isoprene in the SML (Kim et al., 2017), and isoprene airborne concentrations in the Arctic did not correlate with a proxy of SML photoproduction either (Mungall et al. (2017)). It also must be noted that for oceanic regions with persistent high wind speeds, like the SO, the widespread occurrence of an SML is controversial (Brüggemann et al., 2018).

2.9 Closing remarks

- ISOREMS is the first published statistical model to predict isoprene concentrations based solely on remote sensing data, which allows synoptic distributions of isoprene concentrations to be computed over the entire SO.
- Similar regional models should be developed for other oceanic regions in order to predict the global patterns of isoprene concentration and its emission to the atmosphere. A mosaic of regional models holds better potential than a single model to accurately constrain global isoprene emissions and contribute to close the current existing gap between bottom-up and top-down approaches.
- Our results do not resolve the aforementioned discrepancy but support the order of magnitude of the bottom-up estimates.
- Even though the SO has areas and months of high productivity due to abundance of macronutrients and localised iron supply, isoprene concentrations and emissions are moderated by the low temperatures. This does not preclude they may be important for the SOA budget in a region that is particularly sensitive to aerosols of marine origin.

- ISOREMS represents a useful tool to study the role of oceanic isoprene emissions in climate and the oxidative capacity of the atmosphere over the SO.

Aknowledgements

This research was funded by the Spanish Ministry of Economy and Competitiveness through project PEGASO (CTM2012–37615) to RS, and partially by the Australian Government through the Australian Research Council's Discovery Projects funding scheme (project DP160103387). The Antarctic Circumnavigation Expedition was made possible by funding from the Swiss Polar Institute and Ferring Pharmaceuticals. PRR was supported by a "la Caixa" Foundation PhD Fellowship (2015-2019). Members of the ACE1 research team are greatly acknowledged for providing data and technical support. We are grateful to NASA's Ocean Biology Processing Group (OBPG) for MODIS Aqua data, and to the British Oceanographic Data Centre (BODC). We thank R. Wanninkhof (NOAA/AOML) and J. Triñanes (Universidade de Santiago de Compostela) for providing the CCMP2 monthly climatology. PRR would like to thank M. Babin, M. Levasseur and M. Lizotte for hosting and training him at Takuvik Joint International Laboratory (Université Laval (Canada) – CNRS (France)) during 2016. We also want to thank the captain, officers and crew of RV Hespérides and RV Akademik Tryoshnikov, engineers of the Marine Technology Unit (CSIC) and research colleagues for their support and help during the cruises. Data are available at the *Zenodo* repository (<https://doi.org/10.5281/zenodo.3822547>, DOI: 10.5281/zenodo.3822547).

2.10 Appendix

Measurements of isoprene concentration

Table 2.1: Surface (0 – 10 m) isoprene concentration measurements (pM) in the SO (>40°S) used for ISOREMS model development. *GC-MS: Gas Chromatography-Mass Spectrometry. **PTR-MS: Proton Transfer Reaction - Mass Spectrometry.

Mean [Min – Max]	Southern Ocean Area	Cruise name	Method	Source
10.7 [2.1 – 88.4]	Southern Ocean Circumnavigation	ACE	GC-MS*	This work
22.4 [1.6 – 93.5]	Atlantic sector and Weddell Sea	ACE	GC-MS*	This work
29.1 [13.2 – 57.1]	Atlantic sector	AMT22 & AMT23	GC-MS*	Hackenberg et al. (2017)
9.5 [2.3 – 39.0]	Indian sector	KH-09-5	GC-MS*	Ooki et al. (2015)
13.5 [4.8 – 39.1]	Atlantic sector	ANDREXII	PTR-MS**	Wohl et al. (2020)

Remote sensed variables

Table 2.2: Variables used in this work and their sources.

Abbreviation	Name	Source	Units	% matchup	Mean [Minx – Max]	Reprocessing status
ISO	Isoprene concentration	Table 3.3	pM	–	14.6 [1.0 – 93.5]	-
CHL	Chlorophyll-a concentration	MODIS aqua	$\mu\text{g L}^{-1}$	86.84	0.45 [0.07 – 3.20]	R2018.0
SST	Sea surface temperature	MODIS aqua	Deg. C	84.65	3.02 [-1.80 – 12.30]	R2014.0
PIC	Particulate Inorganic Carbon	MODIS aqua	Mol m ⁻³	86.84	4.17×10^{-4} [1.19×10^{-5} - 2.5×10^{-3}]	R2018.0
PAR	Photosynthetically Active Radiation	MODIS aqua	Einstein m ⁻² d ⁻¹	96.93	33.62 [8.81 – 66.49]	R2018.0
POC	Particulate Organic Carbon	MODIS aqua	mg m ⁻³	86.40	91.85 [33.65 – 254.04]	R2018.0
ZEU	Depth of the Euphotic Layer	MODIS aqua	m	93.86	57.54 [17.71 – 112.32]	R2018.0
MLD	Mixing Layer Depth	Holte et al. (2017)	m	100	38.43 [10.98 – 145.72]	R2018.0

Solar time frequency of measurements

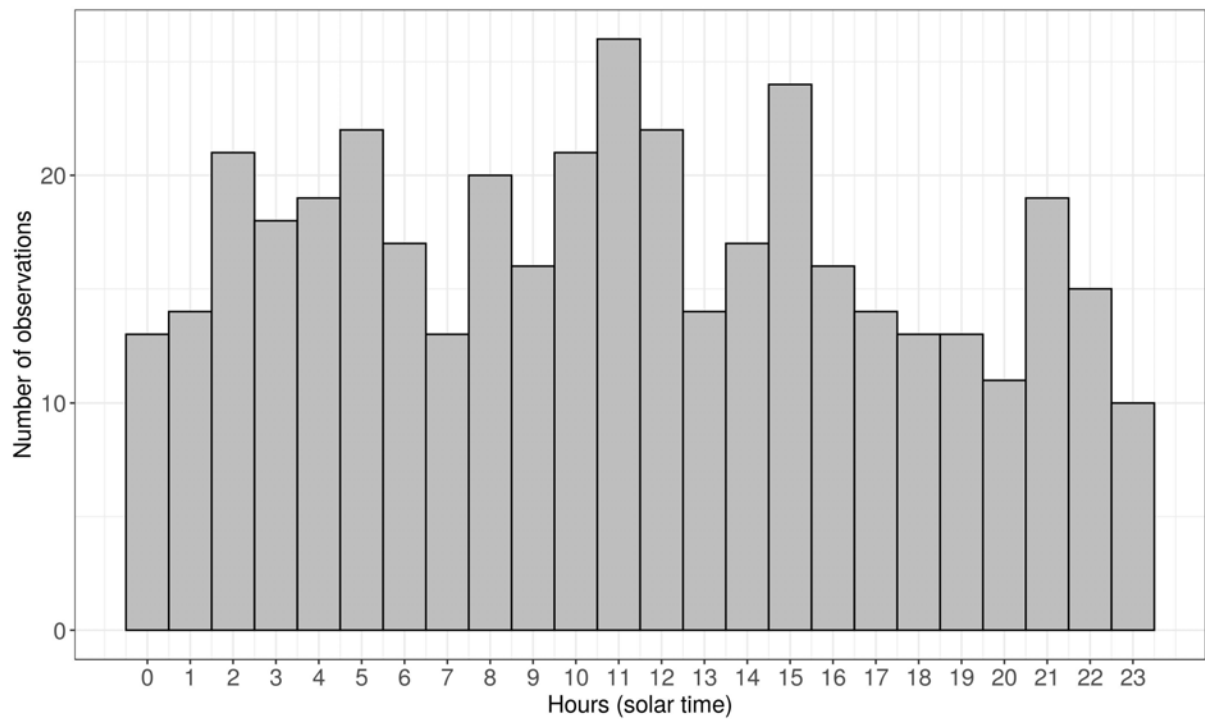


Figure 2.5: Number of isoprene concentration measurements over the diel cycle of solar times. Solar times were calculated from GMT time and longitude using the *solaR* package on R.

Redundancy analysis

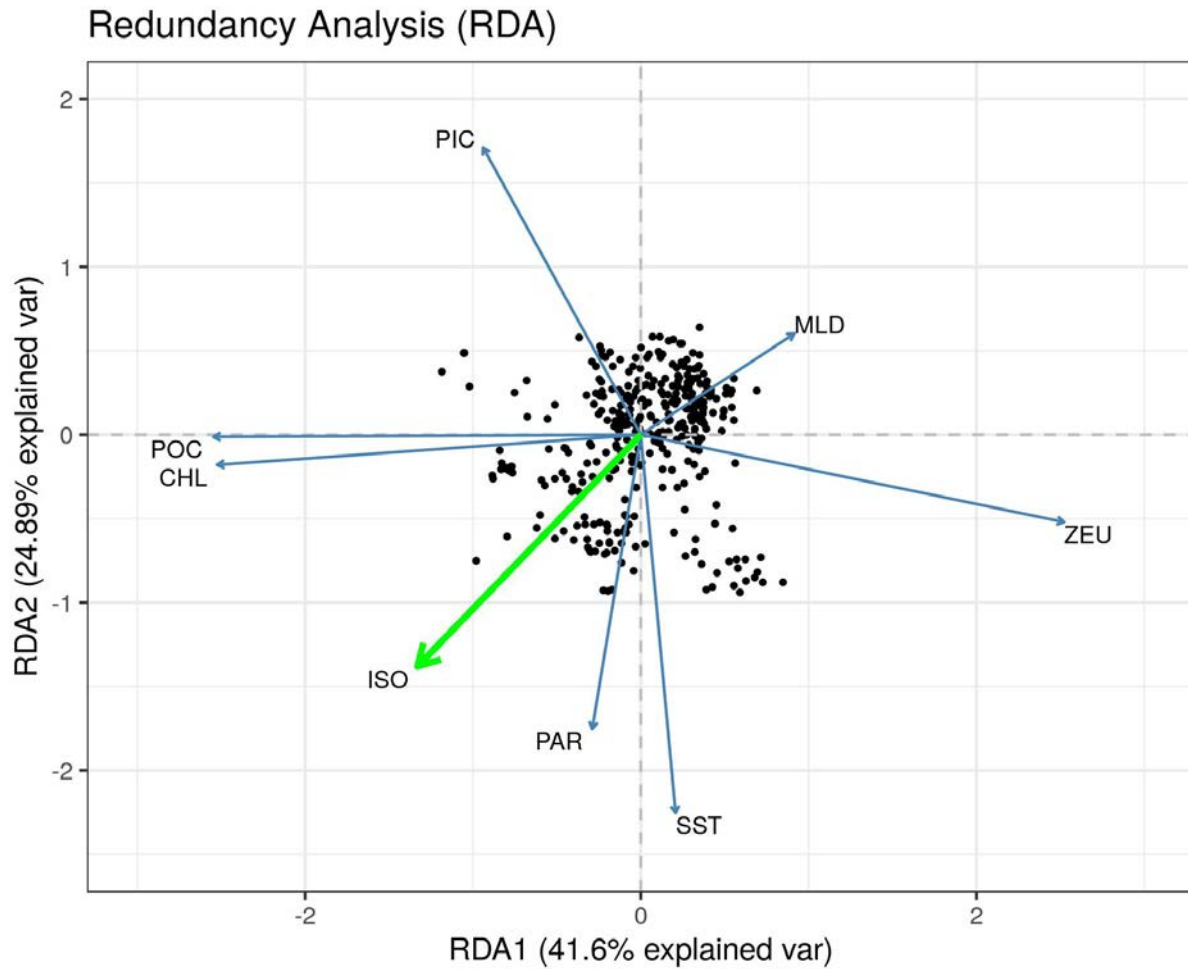


Figure 2.6: Redundancy analysis (RDA) (Legendre and Legendre, 2012) of isoprene concentration and remote sensing variables using *vegan* package on R. After checking the non-normality distribution of our variables using Shapiro-Wilk's test, data were log-transformed. See Table 2.2 for abbreviations.

Residuals of ISOREMS

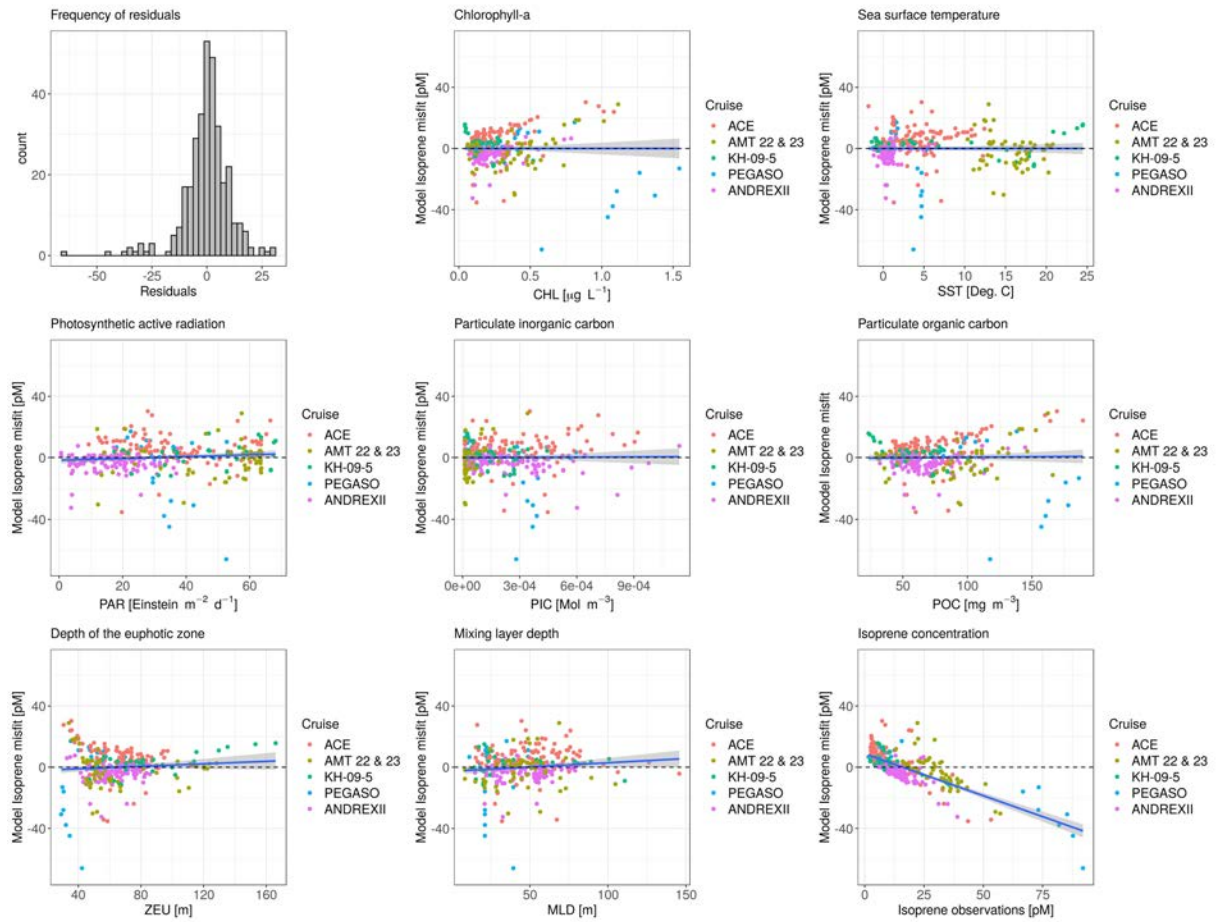


Figure 2.7: Misfit (residuals) of ISOREMS-predictions vs. each of the potential predictive variables tested (ISO, CHL, SST, PIC, PAR, POC, ZEU, MLD; Table 2.2). Last panel: Misfit of ISOREMS-predictions vs. observed isoprene concentrations.

Validation of ISOREMS

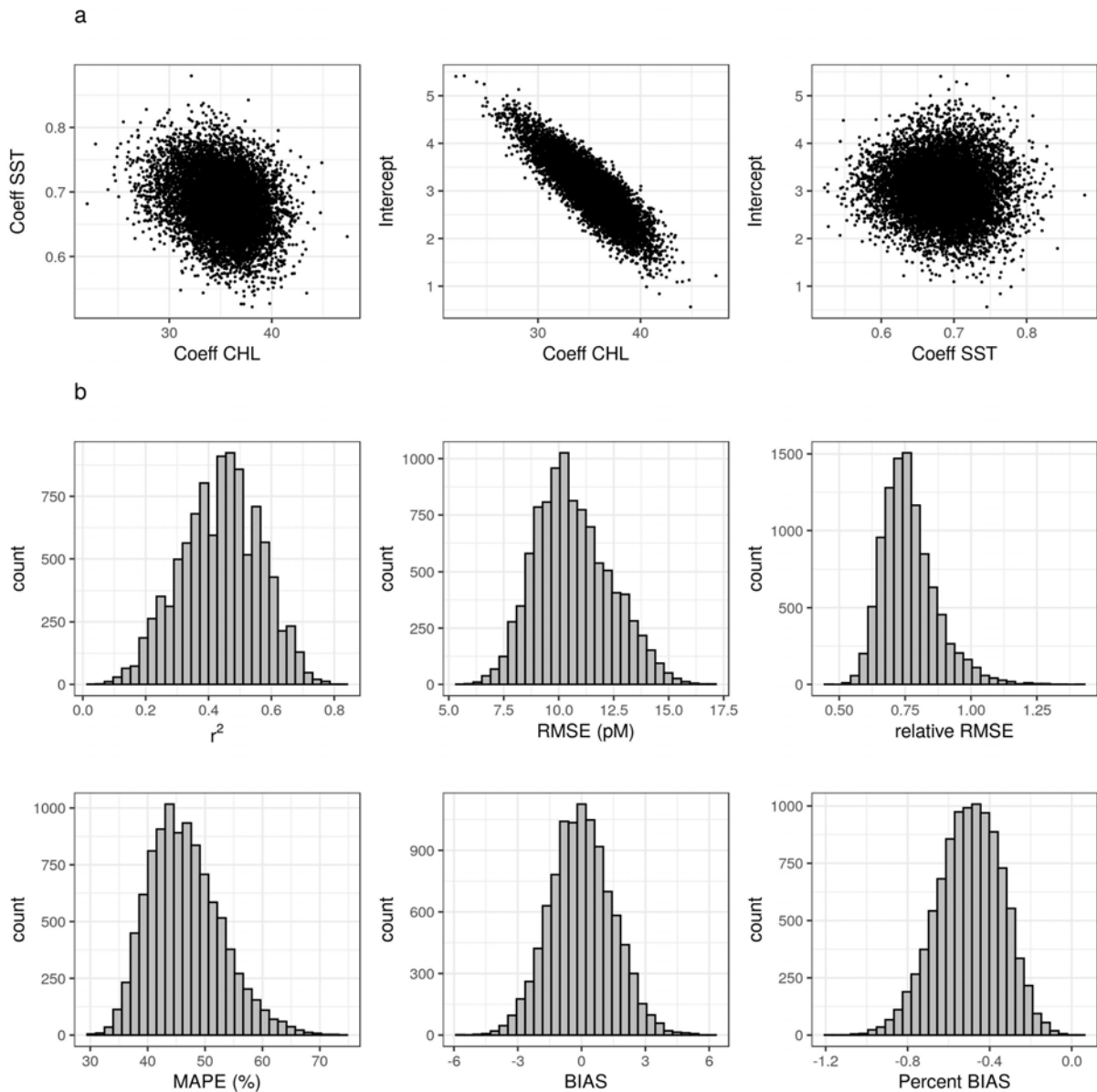


Figure 2.8: (a) Scatter-plot of the coefficients of CHL and SST and the intercepts of the multiple linear regressions of random-sampling (80%) simulations (see text for details). (b) Histograms of the validation statistics (r^2 , RMSE, relative RMSE, BIAS, percent BIAS, and MAPE) randomly generated by the above simulations on 20% of the data. Number of simulations = 10,000.

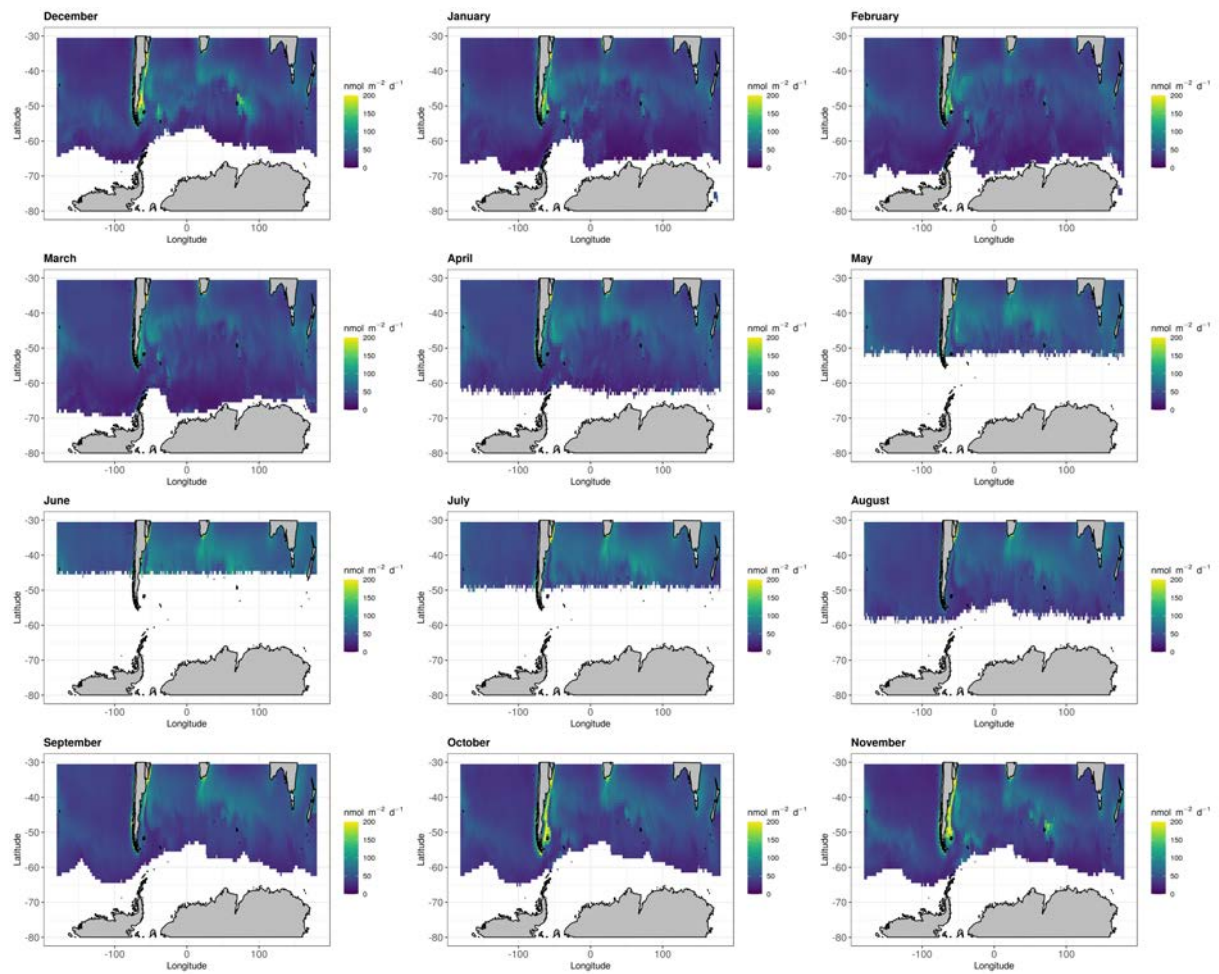
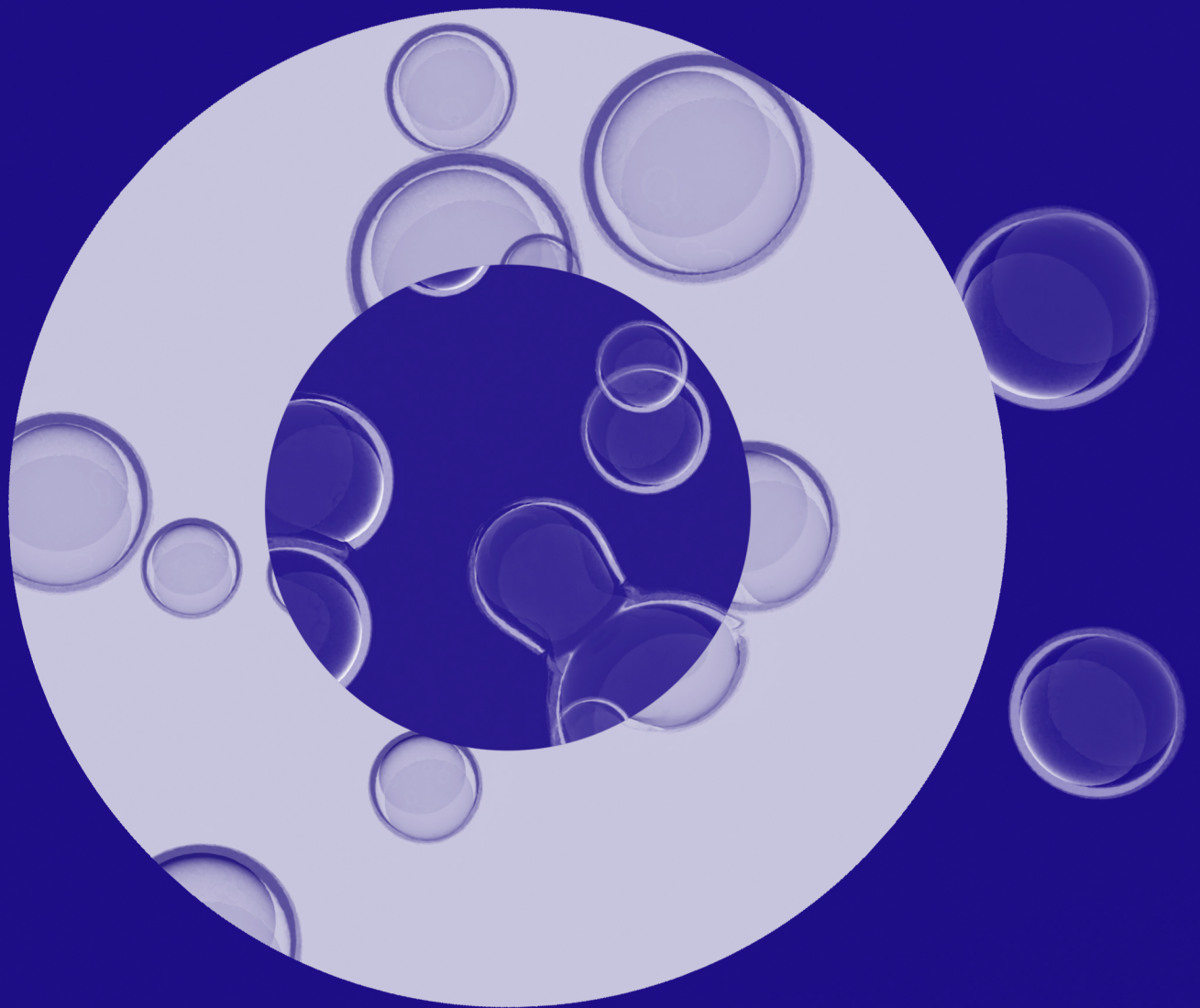
Climatological emission of ISO_{ISOREMS}

Figure 2.9: Monthly climatology of ISO_{ISOREMS} emission fluxes in the Southern Ocean. Blank spaces are pixels where either satellite CHL or wind speed are lacking.



Chapter 3

Ecological modelling of marine isoprene in the Southern Ocean

Chapter 3

Ecological modelling of marine isoprene in the Southern Ocean

Pablo Rodríguez-Ros¹, Cara Nissen², Pau Cortés¹, Nicolas Gruber², Sergio Vallina³, Meike Vogt², Rafel Simó¹

1. Institut de Ciències del Mar. Passeig Marítim de la Barceloneta, 37-49, 08003 Barcelona, Spain
2. Institute for Biogeochemistry and Pollutant Dynamics, ETH Zurich, Zurich, Switzerland
3. Gijon Oceanographic Centre (IEO) - Spanish Institute of Oceanography, Gijon, Asturias, Spain

I don't have any particular recipe... It is like being lost in a jungle and trying to use all the knowledge that you can gather to come up with some new tricks, and with some luck, you might find a way out.

Maryam Mirzakhani - Fields Medal winner (2014)

Abstract

Isoprene (C_5H_8) is a volatile organic compound produced by vegetation on land and phytoplankton in the ocean. Upon emission to the atmosphere, isoprene acts as a precursor of secondary organic aerosols and influences cloud formation and microphysics. This influence is larger in oceanic regions remote from continental emissions, like the Southern Ocean. Up to date, global estimates of marine isoprene emissions to the atmosphere still show a substantial uncertainty, spanning two orders of magnitude. Using new in situ measurements of isoprene biological cycling over Lagrangian studies in the Southern Ocean, we implemented chlorophyll-specific isoprene production rates of three phytoplankton functional types (Diatoms, Coccolitophores and a group of *Small Mixed Phytoplankton*) into a regional ecosystem model for the Southern Ocean (ROMS-BEC). Furthermore, isoprene consumption rates calculated in the model were based on new experiments. The model simulated monthly regional distributions of isoprene concentrations and emissions to the atmosphere. We compared these model outputs with those obtained using a compilation of published laboratory-derived PFT-specific production rates as well as prescribed consumption rates from previous works. Altogether, isoprene concentration peaks in summer, which agrees with the observations, although the highest concentrations are found in the latitudes from 60 to 70°S, which disagrees with the observations. The modelled annual emission of isoprene from the SO (>40°S) amounts 0.071 Tg C yr⁻¹. The model results suggest that that phytoplankton isoprene production rates and microbial degradation rates must be better constrained if we are to improve our predictive capacity to isoprene emission changes in the current global warming scenario.

3.1 Introduction

Isoprene (C_5H_8) is a biogenic volatile organic compound produced in the biosphere by photosynthetic organisms. Its main source are terrestrial plants (Zimmerman et al., 1988; Sharkey and Yeh, 2001), accounting for a flux to the atmosphere of up to $400\text{-}750 \text{ Tg C yr}^{-1}$ (Guenther et al., 2006; Müller et al., 2008). Estimated marine emissions of isoprene are 2-3 orders of magnitude lower ($0.1\text{-}11.6 \text{ Tg C yr}^{-1}$, Palmer and Shaw (2005); Gantt et al. (2009); Luo and Yu (2010); Shaw et al. (2010); Brüggemann et al. (2018)). The large discrepancies in the global marine isoprene emission estimates can to some extent be attributed to our incomplete understanding of the magnitude and spatio-temporal variability of marine isoprene concentrations due to limitations in data availability (Hackenberg et al., 2017; Booge et al., 2018). Despite comparatively low marine emissions, oxidation of ocean-leaving isoprene (Cui et al., 2019) represents a major source of secondary organic aerosols (SOA) in remote marine atmospheres (Claeys et al., 2004; Meskhidze and Nenes, 2006; Gantt et al., 2009; Luo and Yu, 2010; Huang et al., 2011; Cui et al., 2019). SOA contribute to the pool of cloud condensation nuclei, thus affecting cloud formation properties (Moore et al., 1994) and resulting in reduced radiative forcing and cooling or reduced warming (Claeys et al., 2004; Rosenfeld et al., 2019). Consequently, isoprene has been highlighted as an important component for global climate change projections (Meskhidze and Nenes, 2006; Arnold et al., 2009).

As a result of the remoteness of the Southern Ocean (SO) atmosphere from landmasses and hence continental emissions of isoprene, its chemical and optical properties in general and the formation of SOA in particular mainly depend on oceanic emissions (Claeys et al., 2004; Matsunaga et al., 2005; Henze and Seinfeld, 2006; Meskhidze and Nenes, 2006). Some studies have suggested that polar oceans are important sources of isoprene (Luo and Yu, 2010; Meskhidze and Nenes, 2006), while others have shown that its emissions are restricted to productive coastal polar waters (Palmer and Shaw, 2005; Booge et al., 2016), contrasting with a much lower contribution from the oligotrophic polar oceans (Arnold et al., 2009; Hackenberg et al., 2017, Chapter 1). However, measurements of marine isoprene concentration in the SO are scarce and no field-work experiments of isoprene production and degradation have been conducted in the area, impeding a reliable extrapolation from these few measurements to the regional scale. The highest isoprene concentrations in the SO have been measured in spring and summer in coastal and highly productive areas, never exceeding a concentration of 65 pM (Ooki et al., 2015; Hackenberg et al., 2017), or upon iron fertilization experiments where isoprene was correlated with biological productivity and concentrations increased by a factor of four in the fertilized patch (Wingenter et al., 2004). Overall, these studies suggest that phytoplankton productivity plays a dominant role in governing isoprene concentrations. However, there have been no studies to date of the characterization and magnitude of isoprene cycling processes in the SO.

Isoprene production has been confirmed for microalgae (collection of ≈ 124 strains from Shaw et al. (2003); Bonsang et al. (2010); Exton et al. (2013); Booge et al. (2016); Meskhidze et al. (2015)), and macroalgae (Broadgate et al., 2004). Production by heterotrophic bacteria has also been demonstrated (Fall and Copley, 2000) but the occurrence and significance of this process in the ocean is unknown. Based on this relationship with biological production, three dif-

ferent approaches have been proposed to estimate isoprene production rates by phytoplankton functional groups (PFTs) in the oceans: using isoprene:chlorophyll-a relationships from cultured strains, using isoprene:chlorophyll-a:irradiance functions from cultured strains, and using specific isoprene:chlorophyll-a ratios from in situ measurements in the field. Thus, measurements of isoprene production by phytoplankton are typically from laboratory experiments showing remarkable differences in the production rates across and within PFTs, varying up to 2 orders of magnitude even between strains of the same species (Shaw et al., 2003; Exton et al., 2013; Booge et al., 2016). Only recently, Booge et al. (2018) have estimated isoprene production rates by PFTs in field conditions, finding discrepancies (≈ 1 order of magnitude) with the values compiled in Booge et al. (2016). Concretely, they found lower values of production rates of isoprene for *Prochlorococcus*, chlorophytes and diatoms; and higher rates for haptophytes and cyanobacteria (mainly *Synechococcus*). Furthermore, following the approach suggested by Gantt et al. (2009), Booge et al. (2018) calculated new PFT isoprene production rates from field measurements by relating production to irradiance. Regarding the main loss processes of marine isoprene, they are thought to be bacterial degradation, chemical oxidation and emission to the atmosphere, with a negligible contribution of vertical mixing (Booge et al., 2018). However, due to the lack of in-situ experiments, the relative importance of bacterial and chemical losses in controlling marine isoprene concentrations is still rather uncertain (Booge et al., 2018).

Several statistical modelling and remote sensing studies have been performed on a global scale to estimate marine isoprene emissions. Two studies have developed statistical models to predict surface ocean isoprene concentrations from environmental parameters such as light, pigments and/or temperature (Ooki et al., 2015; Hackenberg et al., 2017), but their applicability in the SO is uncertain as few data from this region were used in the development of the models. In parallel, top-down estimates of isoprene emission to isoprene (balancing atmospheric observations with model outputs) have rendered much higher values than bottom up estimates (1 or 2 orders of magnitude, see compilation in Brüggemann et al. (2018)). Arnold et al. (2009) compared the emissions needed to satisfy the isoprene concentration levels in the marine boundary layer generated in a global chemical transport model (GEOS-CHEM) in which they implemented lab-based PFT production rates in a remote sensing product (PHYSAT). A similar methodology (PFT and PHYSAT), but this time exclusively bottom-up, was used by Booge et al. (2016) showing that the SO is a relevant area for isoprene concentration and emission. Furthermore, there have been attempts to quantify the distribution and emission of marine isoprene using remote sensing data. Palmer and Shaw (2005) were the first to quantify global isoprene marine emissions using remote sensing data of chlorophyll-a and sea surface temperature, and a simple model of isoprene cycling. Recently, Rodríguez-Ros et al. (2020b) used the same satellite variables to developed an algorithm for surface isoprene concentration retrieval specific for the SO. However, remote sensing products are known to have a huge degree of uncertainty in polar waters (Neukermans et al., 2018), and specifically in the SO, due to solar angle, heavy cloudiness and the presence of sea ice.

Prognostic modelling based on coupled physical-ecosystem models and isoprene production and cycling rates is a challenging but potentially powerful tool to simulate global or regional distributions of isoprene concentration and emission. Prognostic models offer the possibility to project future and past scenarios, an essential step in the current state of global change. Since

the uncertainty of these models will be inversely proportional to our knowledge of the cycling processes involved, it is vital to shed light on the isoprene degradation and production processes that remain unknown. In this study, we conducted field and modelling work with the aim to advance our knowledge of isoprene cycling processes in the SO and build a predictive tool for isoprene distribution over the entire region. First, we measured isoprene concentrations and loss rates during Lagrangian occupations of three oceanographic stations near the South Orkney and South Georgia Islands, and budgeted them to estimate in situ PFT-specific isoprene production rates. Then, we implemented these production and loss rates as an isoprene module into a physical-biogeochemical model ROMS-BEC specifically developed for the SO (Nissen et al., 2018). The model provided regional and seasonal distributions of isoprene concentrations and emission to the atmosphere.

3.2 Methods

3.2.1 Sampling and physical measurements

The TransPEGASO cruise crossed the Atlantic Ocean from North to South on the R/V *Hesperides*, between 20 October and 21 November 2014 (Zamanillo et al. (2019b); Nunes et al. (2019b)). Surface seawater was sampled using the ship's underway pumping system, which had the water intake located 4-5 m below sea level. All the parts of the centrifugal pump (BKMKC-10.11, Tecnum) that were in contact with the fluid were made of polypropylene and glass. Seawater temperature and salinity were recorded continuously via the flow-through thermosalinograph SBE21 SeaCAT (Sea Bird Sci.). The PEGASO cruise was conducted on board the R/V *Hesperides* in the regions of Antarctic Peninsula, South Orkney and South Georgia Islands from 2 January to 11 February 2015 (Dall'Osto et al. (2017); Zamanillo et al. (2019a); Nunes et al. (2019a)). Seawater samples were collected from either the underway pumping system intake (same as above) or the uppermost (\approx 4 m) bottle of the rosette on SBE911+ CTD casts, which recorded temperature and salinity. The Antarctic Circumnavigation Expedition (ACE) completed the full circumnavigation to the antarctic continent while visiting a large number of sub-antarctic islands between 20 December 2016 and 21 March 2017 on board R/V *Akademik Treshnikov*. In a similar way than TransPEGASO and PEGASO cruises, surface seawater was sampled using the ship's underway pumping system (intake located 5 m below sea level) and CTD cast deployments (Henry et al., 2020).

3.2.2 Lagrangian studies during PEGASO

During PEGASO, three regions were occupied for several days following a Lagrangian approach: north of the South Orkney Islands (NSO), southeast of the South Orkney Islands (SSO), and northwest of South Georgia (NSG) (Dall'Osto et al., 2017; Zamanillo et al., 2019a; Nunes et al., 2019a). NSO and NSG were selected due to their high levels of chlorophyll-a (Chl a) based on previous 8-day average composite images of satellite data (NASA Ocean Colour). SSO was selected for its vicinity to the sea ice edge. To track the water bodies in NSO and NSG, WOCE (World Ocean Circulation Experiment) standard drifters provided with Iridium communication system were used. In SSO, two

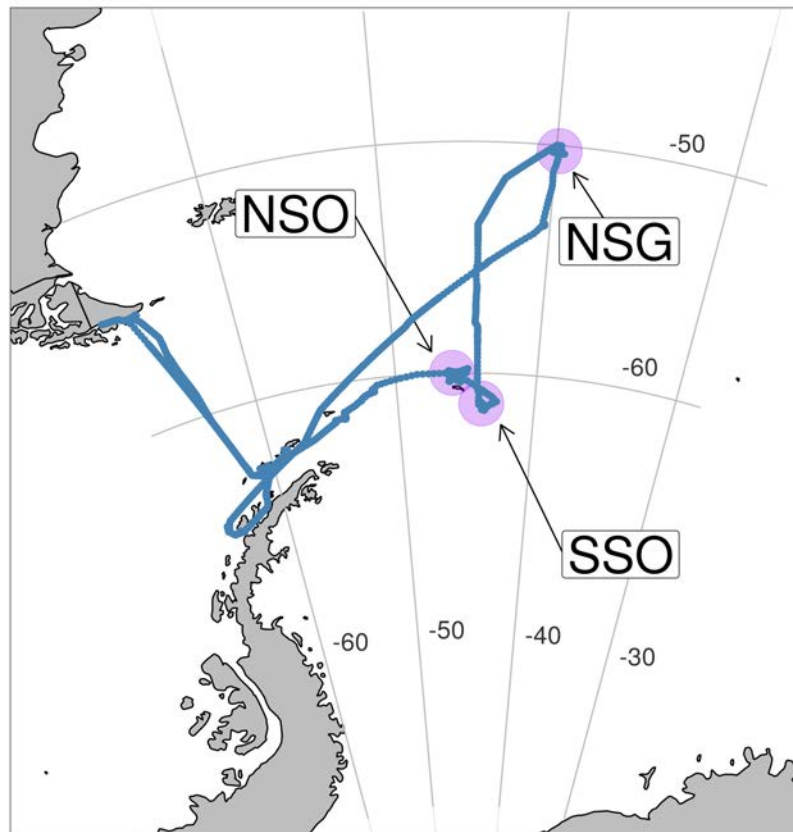


Figure 3.1: Location of the three blooms during the PEGASO Cruise (pink circles) and track (blue line): North of the South Orkney Islands= **NSO**, Southeast of the South Orkney Islands = **SSO** and Northwest of South Georgia = **NSG**.

icebergs were used as natural Lagrangian drifters. During each Lagrangian occupation over more than 24 hours, seawater samples were taken every 30 min. with the ship's clean underway pumping system, and every 4 hours with CTD casts. Surface ocean isoprene concentrations were measured every 30 min., whereas chlorophyll-a and biomarker pigments were measured every 4 hours.

3.2.3 Phytoplankton pigments and taxonomy

For chlorophyll-a analyses, 250-mL seawater samples were filtered on glass fibre filters (Whatman GF/F), which were extracted with 90% acetone at 4°C in the dark for 24 hours. Fluorescence of extracts was measured with a calibrated Turner Designs fluorometer (Yentsch and Menzel, 1963). No phaeopigment corrections were applied. Taxonomy-related pigments were measured with HPLC as described in Nunes et al. (2019a). The CHEMTAX chemical taxonomy software was run on the pigment distributions to derive the contribution of microalgal groups to the total Chl a biomass (ngChlaL^{-1}). Eight main pigmentary classes were quantified: chlorophytes, cryptophytes, dinoflagellates, diatoms, haptophytes, *Phaeocystis*-like haptophytes, pelagophytes, and prasinophytes.

3.2.4 Isoprene concentration

During the TransPEGASO, PEGASO and ACE cruises, isoprene was measured on a gas chromatography-mass spectrometry system (5975-T LTM GC/MS, Agilent Technologies). Aliquots of 25 mL were drawn from the glass bottle with a glass syringe with a teflon tube, and filtered through a 25 mm glass fibre filter while introduced into a purge and trap system (Stratum, Tekmar Teledyne). Volatiles were stripped by bubbling with 40 mL min⁻¹ of ultrapure He for 12 minutes, trapped on solid adsorbent at room temperature and thermally desorbed (250°C) into the GC. Isoprene, monitored as m/z 67 in selected ion monitoring mode, had a retention time of 2.4 min in the LTM DB-VRX chromatographic column held at 35°C. The detection limit was 1 pmol L⁻¹, and the median analytical precision was 5%. In TransPEGASO and PEGASO, calibration was performed by injections of a gaseous mixture of isoprene in N₂. In ACE, a liquid standard solution prepared in cold methanol and subsequently diluted in MilliQ water was used instead.

3.3 Isoprene cycling processes from Lagrangian series

3.3.1 The isoprene budget in the surface mixed layer

The daily change in isoprene concentration in the surface mixed layer ($\frac{dISO}{dt}$, nmol m⁻³ d⁻¹) is the net result of production and consumption processes as described as follows:

$$\frac{dISO}{dt} = P - L = P_{PFT} - L_{BIO} - L_{CHEM} - L_{ATM} - L_{MIX} \quad (3.1)$$

where P_{PFT} (nmol m⁻³ d⁻¹) is isoprene production by phytoplankton organisms, L_{BIO} (nmol m⁻³ d⁻¹) is the biological degradation of isoprene, L_{CHEM} (nmol m⁻³ d⁻¹) is the chemical reaction with radicals O₂ and OH; L_{ATM} (nmol m⁻³ d⁻¹) is the emission of isoprene to the atmosphere, and L_{MIX} (nmol m⁻³ d⁻¹) is the vertical mixing of isoprene.

3.3.2 Bacterial degradation and chemical oxidation rates

Isoprene biological and chemical losses rates (L_{CHEM} & L_{CHEM}) are defined as:

$$L_{BIO} = ISO \cdot k_{BIO} \quad (3.2)$$

$$L_{CHEM} = ISO \cdot k_{CHEM} \quad (3.3)$$

where k_{BIO} (d⁻¹) and k_{CHEM} (d⁻¹) are the respective rate constants. Previous studies have used values of L_{CHEM} and L_{CHEM} derived from other gases or in other media (Palmer and Shaw, 2005; Booge et al., 2016). Alvarez et al. (2009) provided evidence of bacterial consumption of isoprene in temperate and tropical marine and coastal environments, but used isoprene additions orders of magnitude higher than natural concentrations. Moore (2006) and Booge et al. (2016) used a k_{BIO} value of 0.06 d⁻¹, taken from the biological degradation rate constant of methyl bromide, a

completely different trace gas (Tokarczyk et al., 2003; Yvon-Lewis et al., 2002). More recently, Booge et al. (2018) the need for a variable k_{BIO} spanning at least between 0.01 and 0.1 d^{-1} was invoked to close the balance between observed concentrations and a semiempirical model. All in all, most of the studies agree that consumption by bacteria must be taken into account to estimate isoprene concentration in the oceans (Exton et al., 2013; Booge et al., 2016). Nevertheless, no k_{BIO} values have been experimentally determined anywhere in the global ocean. Regarding chemical degradation, in previous works it has been implemented as a constant k_{CHEM} value of 0.0527 d^{-1} derived from reaction rate constants and estimated concentrations of reactive oxygen species in the surface ocean (Riemer et al., 2000; Palmer and Shaw, 2005).

At the three locations of Lagrangian occupation during PEGASO (NSO, NSG and SSO; Figure 3.1 and Table 3.1), duplicate all-glass bottles (0.5 L) were completely filled, leaving no headspace. One of the bottles was analyzed in duplicate for isoprene within 1-2 hours after collection, to set the initial concentration. The other bottle was dark-incubated for 24 hours in a tank with constant flushing of pumped-in surface ocean water, to keep incubation temperature the same as in situ. At the conclusion of the incubation time isoprene concentration was analysed in duplicate. In one case (NSG), an intermediate point was sampled and analysed after 9h. In these experiments, L_{BIO} and L_{CHEM} occurred simultaneously in the incubation bottle. Therefore, the observed loss over time was, in fact, the result of both K_{BIO} and K_{CHEM} , and was named the loss rate constant k_{LOSS} (d^{-1}) (Table 3.1). k_{LOSS} was calculated as the slope of $\text{Ln}(\text{concentration})$ vs. time (Simó et al. 2020):

$$L_{\text{BIO}} + L_{\text{CHEM}} = \text{ISO} \cdot k_{\text{LOSS}} \quad (3.4)$$

3.3.3 Air-sea exchange fluxes and rates

The isoprene flux to the atmosphere (F_{ATM} , in $\text{nmol m}^{-2} \text{d}^{-1}$) was calculated as:

$$F_{\text{ATM}} = k_{\text{AS}} \cdot \left(\text{ISO}_w - \frac{\text{ISO}_a}{K_{\text{H}}} \right) \approx (k_{\text{AS}} \cdot \text{ISO}_w) \quad (3.5)$$

where ISO_w is the isoprene concentration in surface sea water, ISO_a is the isoprene concentration in the air, K_{H} is the Henry's Law constant for isoprene, and k_{AS} is the gas exchange velocity (cm h^{-1}). Air-side isoprene can be considered near zero and neglected for flux calculations because isoprene is highly reactive in the atmosphere and it is largely supersaturated in the surface ocean. k_{AS} was estimated from Wanninkhof (1992):

$$k_{\text{AS}} = 0.31 \cdot U_{10}^2 \left(\frac{S_{\text{C}}}{660} \right)^{-0.5} \quad (3.6)$$

where U_{10} is the wind speed at 10 m (ms^{-1}), and S_{C} is the Schmidt number (non-dimensional). On cruises, wind speed was measured by the ships' meteorological stations. S_{C} was computed as (Palmer and Shaw, 2005):

$$S_{\text{C}} = 3913.15 - (162.13 \cdot \text{SST}) + (2.67 \cdot \text{SST}^2) - (0.012 \cdot \text{SST}^3) \quad (3.7)$$

where SST is in degrees Celsius ($^{\circ}\text{C}$). F_{ATM} was determined every 30 minutes and then it was integrated for a 24 hour period. To convert the ventilation flux F_{ATM} ($\text{nmol m}^{-2} \text{d}^{-1}$) into the emission

rate (L_{ATM} , $\text{nmol m}^{-3} \text{d}^{-1}$), the flux was divided by the mixed layer depth (Z_{ML} , m):

$$L_{ATM} = \frac{F_{ATM}}{Z_{ML}} \quad (3.8)$$

Z_{ML} was determined from CTD profiles as the depth at which density was 0.125 kg m^{-3} higher than that at 5 m.

3.3.4 Vertical mixing fluxes and rates

At the three PEGASO Lagrangian occupations, the rate of vertical mixing by turbulent diffusion (F_{MIX}) was estimated from measured vertical profiles of isoprene concentration and the turbulent diffusion across the pycnocline (K_Z). Thus, the vertical mixing flux at the bottom of the ML (F_{MIX} , $\text{nmol m}^{-2} \text{d}^{-1}$) was calculated as:

$$F_{MIX} = K_Z \cdot \left(\frac{\Delta ISO}{\Delta Z} \right) \quad (3.9)$$

where a $K_Z = 2.6 \text{ m}^2 \text{d}^{-1}$ (or $0.3 \text{ cm}^2 \text{s}^{-1}$) was considered appropriate for the Southern Ocean (Yang et al., 2013), ΔISO (nmol m^{-3}) was the isoprene concentration gradient across the upper pycnocline, and ΔZ (m) was the distance covered by this gradient. To convert mixing flux into a mixing rate (L_{MIX}), F_{MIX} was multiplied by the Z_{ML} (determined from the CTD profiles as above). Depending on the location of the concentration maximum, L_{MIX} was positive (loss term, export from the ML) or negative (gain term, import into the ML):

$$L_{MIX} = \left(\frac{K_Z}{Z_{ML}} \right) \left(\frac{\Delta ISO}{\Delta Z} \right) \quad (3.10)$$

3.3.5 PFT-specific production rates

Reordering equation 3.1 and implementing all the defined loss terms, production of isoprene (P , $\text{nmol m}^{-3} \text{d}^{-1}$) on each bloom is described as follows:

$$P = \frac{\Delta ISO_w}{d} + \overline{ISO} \cdot k_{LOSS} + \frac{F_{ISO}}{Z_{ML}} + \left(\frac{K_Z}{Z_{ML}} \right) \left(\frac{\Delta ISO}{\Delta Z} \right) \quad (3.11)$$

where $\frac{\Delta ISO_w}{d}$ ($\text{nmol m}^{-3} \text{d}^{-1}$) is the daily isoprene budget, taken as the change in isoprene concentration (ISO, nmol m^{-3}) within 24 hours, \overline{ISO} (nmol m^{-3}) is the mean of isoprene concentration in sea water over the 24 hours.

We calculated all the terms in equation 3.11 as described (Table 3.1), and obtained the isoprene production rate P from each site. Isoprene is produced inside the plastids of phytoplanktonic organisms and released into the marine environment through their cellular membrane (Dani et al., 2017). Therefore, following Exton et al. (2013) and Booge et al. (2016), the isoprene production rate P_{PFT}^i ($\text{nmol m}^{-3} \text{d}^{-1}$) of each phytoplankton functional type (PFT i) which contributes to the total production of isoprene (P) is considered linearly coupled to their respective chlorophyll concentration (B_{CHLA}^i , $\mu\text{g L}^{-1}$) through a constant rate specific to each PFT i (ρ_{CHLA}^i , $\text{nmol m}^{-3} \text{mg Chl}^{-1}$

d^{-1}). Consequently, the total isoprene production by all PFTs (P_{PFT} , $nmol\ m^{-3}d^{-1}$) at each site was calculated as:

$$P = P_{PFT} = \sum_{i=1}^3 \rho_{CHLA}^i \cdot B_{CHL}^i \quad (3.12)$$

In previous works, ρ_{CHLA}^{PFT} values have been obtained from laboratory culture experiments (Milne et al., 1995; Shaw et al., 2003; Bonsang et al., 2010; Exton et al., 2013). However, these lab experiments have the limitation of focusing on exponential growth, being conducted in conditions regarding light, temperature and turbulence that may differ notably from conditions of the surface SO, and being conducted with cultured strains that may behave differently from natural populations. Instead, we took advantage of the Lagrangian approach during the PEGASO cruise to estimate new values based on in situ measurements. In Figure 3.2 and Table 3.1 we show a synthesis of the community composition of the different phytoplankton groups on each site (NSO, SSO and NSG). SSO was mainly dominated by haptophytes (62.08%), NSG by diatoms (81.17%) and NSO by a more diverse assemblage, being cryptophytes the largest contributor (32.08%). To calculate

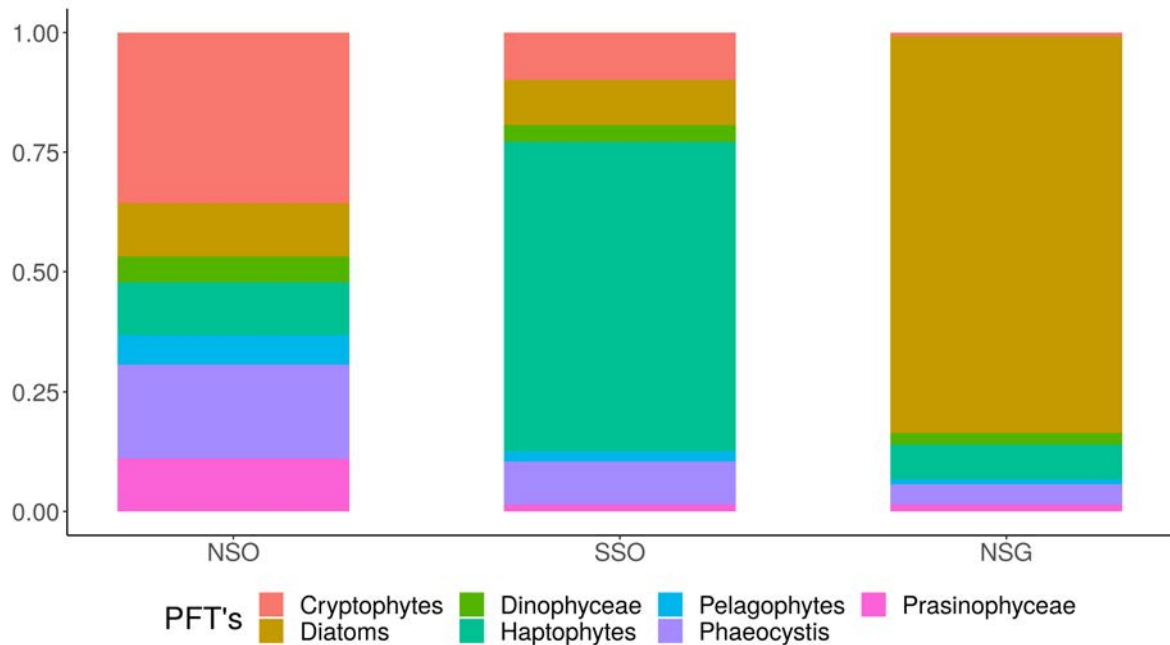


Figure 3.2: Phytoplankton community composition based on CHEMTAX-HPLC analyses (Nunes et al., 2019a) for the three blooms during the PEGASO cruise (See Figure 3.1: North of the South Orkney Islands = **NSO**, Southeast of the South Orkney Islands = **SSO** and Northwest of South Georgia = **NSG**).

ρ_{CHLA}^{PFT} during PEGASO's blooms, we solved the system of equations 3.13 formed by the isoprene

production equation for each site (Table 3.1, Figure 3.1):

$$\begin{cases} P^{NSO} = \left(\frac{B_{DIAT}^{NSO}}{100} \cdot \rho_{CHLA}^{DIAT} \right) + \left(\frac{B_{COCC}^{NSO}}{100} \cdot \rho_{CHLA}^{COCC} \right) + \left(\frac{B_{SP}^{NSO}}{100} \cdot \rho_{CHLA}^{SP} \right) \\ P^{SSO} = \left(\frac{B_{DIAT}^{SSO}}{100} \cdot \rho_{CHLA}^{DIAT} \right) + \left(\frac{B_{COCC}^{SSO}}{100} \cdot \rho_{CHLA}^{COCC} \right) + \left(\frac{B_{SP}^{SSO}}{100} \cdot \rho_{CHLA}^{SP} \right) \\ P^{NSG} = \left(\frac{B_{DIAT}^{NSG}}{100} \cdot \rho_{CHLA}^{DIAT} \right) + \left(\frac{B_{COCC}^{NSG}}{100} \cdot \rho_{CHLA}^{COCC} \right) + \left(\frac{B_{SP}^{NSG}}{100} \cdot \rho_{CHLA}^{SP} \right) \end{cases} \quad (3.13)$$

After solving the system of equations 3.13, the resulting isoprene production rates (in $\text{nmol C}_5\text{H}_8 \text{ mg Chl d}^{-1}$) were: $\rho^{DIAT} = 12.14$, $\rho^{COCC} = 10.98$, and $\rho^{SP} = 0.69$.

Table 3.1: Parameters used to estimate the isoprene production rates of each PFT (diatoms, coccolithophores and small mixed phytoplankton) calculated from *in situ* data in three different blooms studied in the PEGASO cruise (See Figure 3.1: North of the South Orkney Islands = **NSO**, Southeast of the South Orkney Islands = **SSO** and Northwest of South Georgia = **NSG**). *Mean of k_{LOSS} in the PEGASO cruise experiments = 0.29 d^{-1} .

Parameter	Units	NSO	SSO	NSG
P	$\text{nmol m}^{-3} \text{ d}^{-1}$	5.63	2.24	57.87
CHLA	mg m^{-3}	1.96	0.28	5.37
P_{CHLA}	$\text{nmol mgchla}^{-1} \text{ d}^{-1}$	2.87	7.77	10.77
\overline{ISO}_w	nmol m^{-3}	21.75	17.55	89.31
$\frac{\Delta ISO_w}{d}$	$\text{nmol m}^{-3} \text{ d}^{-1}$	-0.14	-0.75	-9.96
k_{LOSS}	d^{-1}	0.19 *	0.06 *	0.64 *
F_{ATM}	$\text{nmol m}^{-2} \text{ d}^{-1}$	26.05	27.37	320.53
Z_{ML}	m	36.70	17.85	47.35
ΔC	nmol m^{-3}	-4.9	-5.6	49.5
ΔZ	m	15	20	56
F_{VENT}	$\text{nmol m}^{-2} \text{ d}^{-1}$	-7.96	-9.28	2.94
SRD	W m^{-2}	65	105	24
Diatoms	% HPLC-CHEMTAX	10.32	8.89	81.17
Haptophytes	% HPLC-CHEMTAX	10.362	62.08	7.67
Phaeocystis	% HPLC-CHEMTAX	17.29	7.27	3.97
Cryptophyceae	% HPLC-CHEMTAX	32.08	8.89	0.86
Prasinophytes	% HPLC-CHEMTAX	9.93	1.25	1.42
Dinophyceae	% HPLC-CHEMTAX	4.83	3.23	2.44
Pelagophyceae	% HPLC-CHEMTAX	5.65	2.42	1.14

3.4 An ecosystem model for isoprene concentration and emission in the Southern Ocean

3.4.1 Description of the ROMS-BEC model and setup

We used the regional setup for the SO of the UCLA-ETH version of ROMS (Regional Ocean Modeling System, Shchepetkin and McWilliams, 2005; Haumann, 2016), which is a circumpolar model with a latitudinal range from $\approx 24^{\circ}\text{S}$ - 78°S and an open northern boundary. The spatial resolution for this study is 0.5 degrees and the water column is divided into 64 sigma layers. The primitive equations are solved with a time step of 2700 seconds. Coupled to ROMS is an extended version of the biogeochemical model BEC (Moore et al., 2013b), which has recently been extended by an explicit parametrization of coccolithophores (Nissen et al., 2018) and which we further extended by an explicit parametrization of isoprene for this study. BEC resolves the cycling of all major biogeochemical cycles (C, N, P, Si, Fe, O_2) and includes four PFT's (diatoms, coccolithophores, mixed small phytoplankton and diazotrophs), whose growth and loss parameters are chosen based on available in-situ and laboratory studies (see Nissen et al., 2018). Furthermore, BEC includes one zooplankton PFT which grazes on all phytoplankton groups and which is parametrized to describe the characteristics of both microzooplankton and macrozooplankton (Moore et al., 2002; Sailley et al., 2013). A more detailed description of the SO setup of ROMS-BEC used here can be found in Nissen et al. (2018).

Our model setup is identical to the one described in Nissen et al. (2018) regarding its atmospheric forcing, boundary and initial conditions, and BEC parameters. But in the present work, we used a lower horizontal resolution (0.5 as compared to 0.25 degrees in Nissen et al., 2018). For the initial conditions of isoprene, we computed surface isoprene concentration values by applying the equation proposed by Hackenberg et al. (2017) for surface waters with a temperature below 20°C (Equation 3.14) to MODIS Aqua monthly climatologies of sea surface temperature and chlorophyll-a concentration (9x9 km spatial resolution, MODIS Aqua, "NASA's OceanColor Web", <https://oceancolor.gsfc.nasa.gov/>):

$$\text{ISO} = 33.2 \cdot \times [\text{Chl} - \text{a}, \text{mg m}^{-3}] + 13.7 \quad (3.14)$$

The mean value supplied for surface ocean waters over the antarctic summer period (December, January and February) was 23.07 pM ($>40^{\circ}\text{S}$), which lies within the range of in situ measurements (9.48 - 29.05 pM, Table 3.3). Below the surface, for both initial fields and the boundary conditions, we assumed a constant value of 0.001 pM. Same as in Nissen et al. (2018), we first did a physics only spin up of 30 years and, thereafter, we ran the coupled ROMS-BEC setup for another 20 years, of which a monthly climatology over the last 5 full seasonal cycles was analyzed.

3.4.2 An isoprene module for ROMS-BEC

In ROMS-BEC, changes over time of isoprene concentrations in sea water (ISO, pM) result from the balance of its production (P, $\text{nmol m}^{-3} \text{d}^{-1}$) and loss rates (L, $\text{nmol m}^{-3} \text{d}^{-1}$), as described in

equation 3.1 in previous sections. Isoprene is generally produced by the phytoplankton PFTs (P_{PFT} , $\text{nmol m}^{-3} \text{ d}^{-1}$) and is lost via biological degradation by bacteria (L_{BIO} , $\text{nmol m}^{-3} \text{ d}^{-1}$), chemical reaction with radicals O_2 and OH (L_{CHEM} , $\text{nmol m}^{-3} \text{ d}^{-1}$), and emission to the atmosphere (L_{ATM} , $\text{nmol m}^{-3} \text{ d}^{-1}$, equation 3.8, following Wanninkhof (1992)). Finally, L_{MIX} , the vertical mixing of isoprene, which was dynamically resolved in ROMS-BEC. In our BASELINE ROMS-BEC configuration, k_{BIO} and k_{CHEM} are implemented together as $k_{\text{LOSS}} = 0.29 \text{ d}^{-1}$ (BASELINE, Table 4.2), which is the average of the three values obtained from incubations at the three Lagrangian sites of the PEGASO cruise (Table 1; Simó et al. 2020). Note that these experimental results spanned on order of magnitude ($0.06\text{--}0.64 \text{ d}^{-1}$), which is indicative of the limitations of using fixed values for k_{BIO} and k_{CHEM} . In our BASELINE simulation we used a fixed isoprene degradation rate derived from a variety of biological and environmental conditions in the region. In some of our other simulations, we used the values previously proposed in other regions of the global ocean ($0.01\text{--}0.06 \text{ d}^{-1}$, see below).

3.4.3 BASELINE simulation and model experiments

To study the effects of parameter choices on model outputs, we performed a set of modelling experiments where we implemented one or another method of isoprene production estimation, or one or another k_{BIO} (Table 4.2). These experiments were grouped in four categories: *BASELINE* (where PFT-specific production rates as well as k_{LOSS} were the ones experimentally determined in PEGASO); *Direct* (which differed from the BASELINE in that two extremes of k_{BIO} were taken from previous works, while k_{CHEM} was fixed); *Laboratory* (which incorporated light-independent variable PFT-specific production rates from laboratory experiments); and *Light* (which incorporated light-dependent, variable PFT-specific production rates from laboratory experiments). The modelling experiments are summarized in Table 4.2. The PFT Chl a shares required to apply specific production rates upon, were provided by the ROMS-BEC simulations. We excluded diazotrophs in the calculation of isoprene production since their contribution to the total phytoplankton biomass in the model is negligible at latitudes higher than 40°S (Hirata et al., 2011; Nissen et al., 2018) (Figure 3.19).

For *Laboratory* experiments, we implemented values of $\rho_{\text{CHLA}}^{\text{PFT}}$ derived from the ones compiled in Booge et al. (2016) (*Laboratory*, Table 4.2). These rates were obtained as the daily increase of isoprene per unit or chlorophyll-a during the exponential growth phase of phytoplankton cultured strains. We averaged the individual values of $\rho_{\text{CHLA}}^{\text{PFT}}$ for each of the three PFT's selected in ROMS-BEC (diatoms, coccolitophores and small phytoplankton), only considering species known to occur in the SO (LAB, Table 4.2). Thus, for diatoms we used the values belonging to the "cold adapted diatoms" field, while for coccolitophores we used the values of *Emiliana huxleyi* strains, since it is the dominant species among SO coccolitophores (Saavedra-Pellitero et al., 2014; Balch et al., 2016). Lastly, for small mixed phytoplankton communities we used *Chlorophyceae* species values. We also implemented the minimum and maximum $\rho_{\text{CHLA}}^{\text{PFT}}$ values for every PFT present in polar waters among the values provided in Booge et al. (2016) (runs RHO.LOW and RHO.HIGH, respectively, in Table 4.2). Moreover, we used the specific value for "Diatoms of the Southern Ocean" compiled in Booge et al. (2016) (DIAT.SO, Table 4.2). Then, for *Laboratory* experiments we also tested the k_{BIO} values of 0.01 and 0.06 d^{-1} . For *Direct* experiments, since the values used in our BASELINE obtained

during the PEGASO cruise are unique, we just varied the value of k_{BIO} based on the reported in literature (Booge et al., 2016) (*Direct*, Table 4.2). For *Light* experiments, we calculated and implemented the values of $\rho_{\text{CHLA}}^{\text{PFT}}$ retrieved from the light emission factors provided by Gantt et al. (2009) and Booge et al. (2018), following the equation 3.15 (*Light*, Table 4.2). This parametrization uses an unique factor for each PFT (EF), which relates with the intensity of PAR radiation (I , $\mu\text{E m}^{-2} \text{d}^{-1}$).

$$\rho_{\text{CHLA}}^{\text{PFT}} = \text{EF}^{\text{PFT}} * \ln(\text{SRD} * 2)^2 \quad (3.15)$$

During PEGASO, the solar radiation dose was calculated at every sampling site using equation 3.16, where I is the average surface intensity radiation in the 24 hours previous to sampling (Wm^{-2}), k is the light attenuation coefficient (m^{-1}), and Z_{ML} is the mixed layer depth (m):

$$\text{SRD} = \frac{I}{k \cdot Z_{\text{ML}}} \cdot (1 - e^{-k \cdot Z_{\text{ML}}}) \quad (3.16)$$

The phytoplankton community of NSG was dominated by diatoms (81 %, Figure 3.2), and SSO by *Haptophytes* (69 %, Figure 3.2). Therefore, we made the assumption that P_{CHLA} of NSG and SSO are equal to $\rho_{\text{CHLA}}^{\text{DIAT}}$ and $\rho_{\text{CHLA}}^{\text{COC}}$, respectively. Then, we applied the EF values from (Gantt et al., 2009) and (Booge et al., 2018): 0.0064 and 0.042 for NSG, and 0.0099 and 0.019 for SSO (Table 4.2). Finally, we estimated $\rho_{\text{CHLA}}^{\text{SP}}$ from NSO using the EF values resulting of taking into account together *Chlorophytes*, dinoflagellates and *Cryptophytes*: 0.015 and 0.028 (Table 4.2). We chose NSO for $\rho_{\text{CHLA}}^{\text{SP}}$ calculation since it had the most diverse representation of the different PFT's belonging to the small phytoplankton category. Since the values of $\rho_{\text{CHLA}}^{\text{PFT}}$ used *Light* experiments were calculated with the same measurements as for *Direct* experiments, we also tested the effects of implementing k_{CONC} .

Table 3.2: Overview of model parameters used in BASELINE simulation and model experiments. Annual means of isoprene concentration (0-10 m), and integrated annual flux values in surface waters are shown for latitudes $> 40^\circ\text{S}$.

	Run name	$\rho_{\text{CHLA}}^{\text{DIAT}}$ nmol C ₅ H ₈ mg Chl · d	$\rho_{\text{CHLA}}^{\text{COC}}$ nmol C ₅ H ₈ mg Chl · d	$\rho_{\text{CHLA}}^{\text{SP}}$ nmol C ₅ H ₈ mg Chl · d	k_{BIO} d ⁻¹	k_{CHEM} d ⁻¹	Flux Tg C yr ⁻¹	Concentration nmol m ⁻³
	BASELINE	12.14	10.98	0.69	$k_{\text{LOSS}} = 0.297$		0.071	68.92
Direct	DIRECT	12.14	10.98	0.69	0.06	0.0527	0.142	143.17
	DIRECT.KBIO.LOW	12.14	10.98	0.69	0.01	0.0527	0.199	207.81
Laboratory	LAB	2.06	5.54	5.73	0.06	0.0527	0.045	46.12
	KBIO.LOW	2.06	5.54	5.73	0.01	0.0527	0.044	40.57
	RHO.LOW	0.56	1.00	1.4	0.06	0.0527	0.0077	7.15
	RHO.HIGH	9.36	11.2	9.66	0.06	0.0527	0.119	115.67
	DIAT.SO	1.21	5.54	5.73	0.06	0.0527	0.021	17.83
Light	EF.BOOGE	1.2	2.5	3.5	0.06	0.0527	0.017	16.13
	EF.BOOGE.KBIO.NEW	1.2	2.5	3.5	$k_{\text{LOSS}} = 0.297$		0.0078	7.69
	EF.BOOGE.KBIO.LOW	1.2	2.5	3.5	0.01	0.0527	0.025	23.61
	EF.GANTT	7.8	4.9	6.5	0.06	0.0527	0.095	94.91
	EF.GANTT.KBIO.NEW	7.8	4.9	6.5	$k_{\text{LOSS}} = 0.297$		0.041	45.50
	EF.GANTT.KBIO.LOW	7.8	4.9	6.5	0.01	0.0527	0.134	138.06

The BASELINE simulation produced the maximum isoprene concentrations (sometimes exceeding 100 pM) in spring and summer periods in coastal and blooming areas, mostly occurring

within the 60–70 °S latitudinal band (Figures 3.3 A and B, and 3.15). This distribution parallels the distribution of diatoms, which dominate the phytoplankton community across the SO in ROMS-BEC (Nissen et al., 2018) (Figures 3.18). Our BASELINE simulation gave a year-averaged surface concentration of 68.9 pM (Table 4.2), which is high in comparison with the existing measurements (Table 3.3). Among all experiments, the highest annual mean isoprene concentration was obtained by DIRECT.KBIO.LOW (207.81 pM, Table 4.2), which is far off the mean of observations (Table 3.3). In contrast, the lowest annual mean isoprene concentrations were obtained by RHO.LOW (7.15 pM, Table 4.2) and EF.BOOGE.KBIO.NEW (7.69 pM, Table 4.2). These values are rather low compared with the mean of observations (Table 3.3).

Regarding the emission of isoprene, the highest values were also obtained during the summer period but their spatial patterns showed differences with isoprene surface concentration. Fluxes of isoprene peak at lower latitudes than isoprene concentration (40-60°S, Figure 3.3 C and 3.14), where wind speed and sea surface temperature are higher, and sea ice is not present all over the year (Haumann, 2016). This contrasting geographical pattern between isoprene concentration and fluxes reflects the dominance of the open ocean over the coastal areas or islands for the annual emission of isoprene from the SO in contrast to other oceans, agreeing with previous works (see Figure S2 in Booge et al. (2016)). Among the model experiments, the highest isoprene fluxes of isoprene were simulated in the experiment EF.GANTT.KBIO.LOW (0.199 Tg C yr⁻¹) and DIRECT (0.142 Tg C yr⁻¹), while the lowest in RHO.LOW (0.0071 Tg C yr⁻¹) and EF.BOOGE.KBIO.NEW (0.0078 Tg C yr⁻¹), with differences that reached to 2 orders of magnitude (Table 4.2).

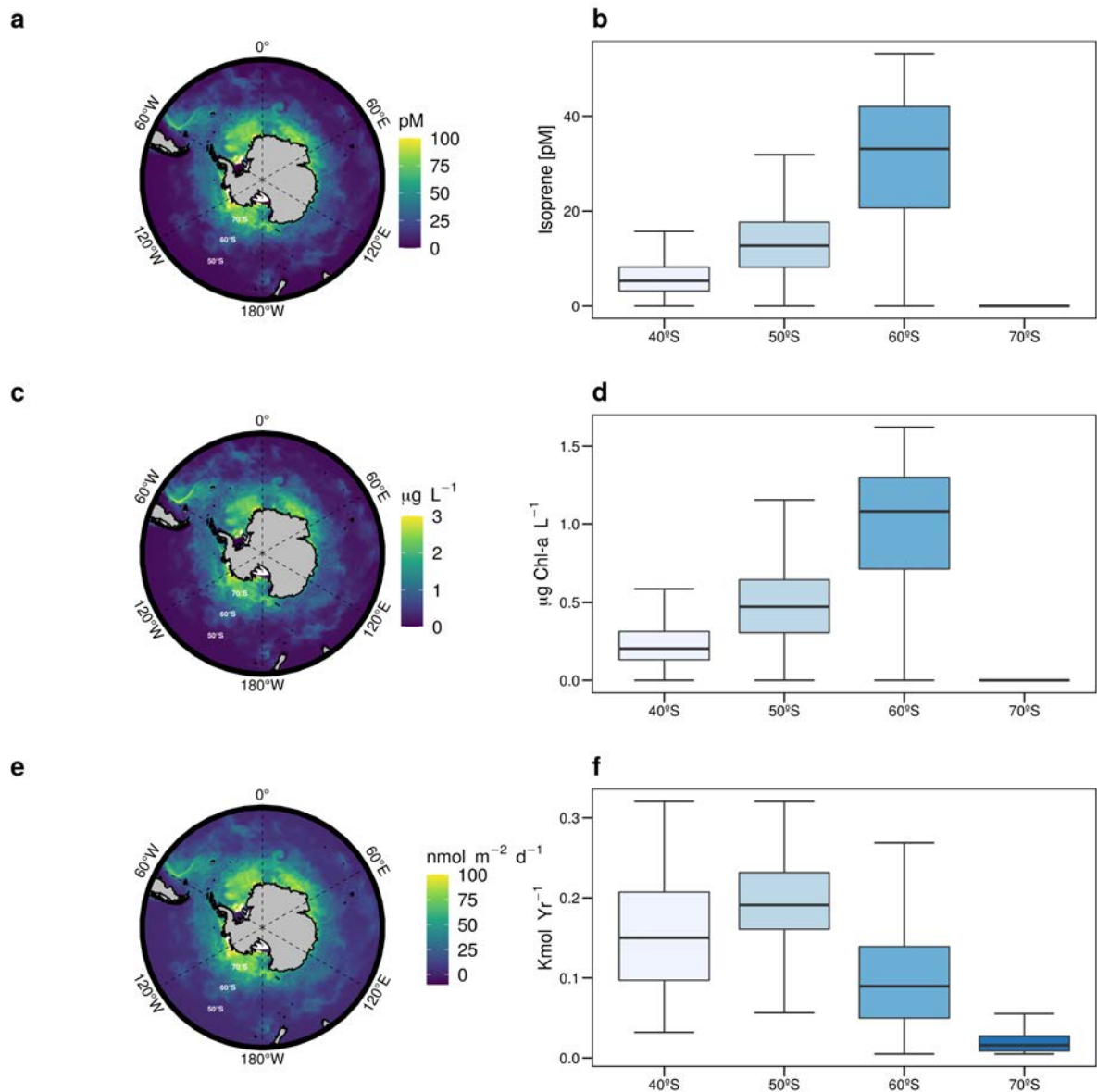


Figure 3.3: Overview of the mean isoprene surface (0–10 m) concentration (a), chlorophyll-a biomass (c) and isoprene emission (e) patterns in ROMS-BEC from the BASELINE run (Table 4.2). Boxplots representing the latitudinal distribution of the year integration of isoprene surface concentration (b), total chlorophyll-a biomass (d) and emission of isoprene (f). In the boxplots only values within percentile 5% and 95% are shown.

Direct

The biggest changes in surface isoprene concentration were simulated when applying the value of $\rho_{\text{CHLA}}^{\text{PFT}}$ calculated from the PEGASO cruise, due to the change of k_{BIO} from 0.297 d^{-1} to 0.06 d^{-1} and 0.01 d^{-1} , in DIRECT and DIRECT.KBIO.LOW respectively (Table 4.2). Thus, these runs triggered an increase in isoprene concentration of 108% (DIRECT) and 202% (DIRECT.KBIO.LOW) (Figure 4.7a). We also observed that changes in isoprene concentration in DIRECT.KBIO.LOW and

DIRECT runs showed their highest values in the latitudinal bands of 60-70°S (Figure 4.7a).

Laboratory

Among all the experiments performed using the values of production and degradation rates from Booge et al. (2016), RHO.HIGH resulted in the highest changes in isoprene concentration in surface waters of the whole SO (68%, Figure 4.7c). When looking at latitudinal differences, we observed that RHO.HIGH triggers a more intense effect on isoprene concentrations at low latitudes (40-50°S, 68%, Figure 4.7c), rather than higher ones (60-70°S, 65%, Figure 4.7c). In contrast, isoprene concentrations in surface waters decreased in runs RHO.LOW and DIAT.SO (-41% and -74%, respectively, Figure 4.7c). However, latitudinal differences in RHO.LOW run are much more smaller than the ones for RHO.HIGH (40-50°S: -88%, and 60-70°S: -90%, Figure 4.7c). Finally, setting k_{BIO} to 0.01 d^{-1} (KBIO.LOW) increased, respectively, the concentration or surface isoprene in the SO but in a weaker way than when increasing the production rates by diatoms (Figure 4.7c).

Light

When incorporating the values of k_{BIO} and $\rho_{\text{CHLA}}^{\text{PFT}}$ derived from PEGASO following the light approach described in Gantt et al. (2009) and Booge et al. (2018), we observed dramatic changes in isoprene concentration, reaching up to more than 100% (60-70°S, EF.GANTT.KBIO.LOW, Figure 4.7b). The highest isoprene concentrations were obtained when implementing the light approach values derived from the factors from Gantt et al. (2009) (EF.GANTT and EF.GANTT.KBIO.LOW, 38% and 100%, respectively, Figure 4.7b). In contrast, when using the light factor from Booge et al. (2018) we observed a decrease in isoprene concentration levels (EF.BOOGE, EF.BOOGE.KBIO.LOW and EF.BOOGE.KNEW: -77%, -66%, and -89%, respectively, Figure 4.7b), which are values similar to RHO.LOW (Figure 4.7A). However, the simulated change in the lat bands is different across simulations. Thus, while EF.BOOGE and EF.BOOGE.KBIO.LOW triggered the biggest effects between 40-50°S, EF.BOOGE.KNEW showed the biggest changes in the latitudinal band of 40-50°S. Overall, the runs using the light factors from Gantt et al. (2009) gave higher isoprene concentrations even when applying the highest k_{BIO} ($k_{\text{BIO}} = 0.29 \text{ d}^{-1}$, Table 4.2). Finally, in EF.GANTT.NEW run simulated isoprene levels in the latitudinal band of 50-60°S were higher than in the other latitudes.

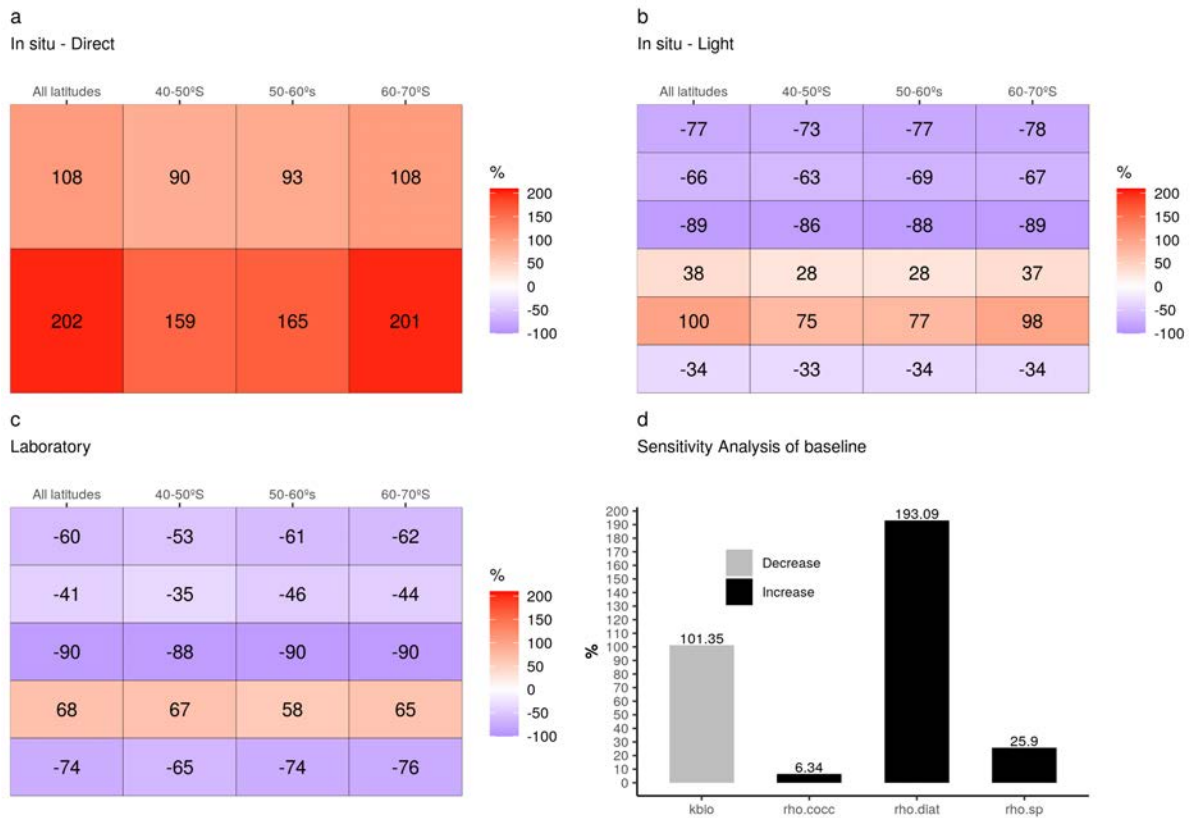


Figure 3.4: Changes in annual mean isoprene concentration (0-10), as percent difference, among all experiments (**a**: In situ - Direct; **b**: In situ - Light; **c**: Laboratory) (Table 4.2) for all latitudes higher than 40°S, and 10° latitudinal bands (40-50°S, 50-60°S, 60-70°S). BASELINE run is taken as reference (white color in a, b and c). **d**: Sensitivity Analysis results of BASELINE simulation to changing parameter by $\pm 50\%$ (Table 3.4). The state variable selected to that aim was isoprene concentration. Black bars indicate that an increase of the parameter causes an increase of the state variable, while grey bars indicate that an increase of the parameter causes a decrease of the variable state.

3.4.4 Model evaluation

For the model evaluation, we compiled a data set of isoprene concentrations in the SO ($>40^{\circ}\text{S}$) from six different cruises (Table 3.3): ACE (Antarctic Circumnavigation Expedition), PEGASO (South Georgia Island, South Orkney Islands and Antarctic Peninsula), TransPEGASO (South Atlantic Ocean, Nunes et al. (2019b), Zamanillo et al. (2019a)), AMT23 & AMT23 (South Atlantic Ocean and SO, Hackenberg et al. (2017)), KH-09-5 (South Indian Ocean and SO, Ooki et al. (2015); Schlitzer et al. (2018)), and ANDREXII cruise (Wohl et al., 2019). In total, this data set amounts up to ≈ 330 observations in the SO (Figure 3.6), making it the most complete data set compiled for this oceanic region ($>40^{\circ}\text{S}$) up to date. It covers all latitudes and longitudes of the SO (Figure 3.6 A), and includes some sub-antarctic islands. Nevertheless, some areas are still greatly under-sampled, mostly the Pacific sector of the SO.

In ROMS/BEC, the highest values of isoprene concentration were found in highly produc-

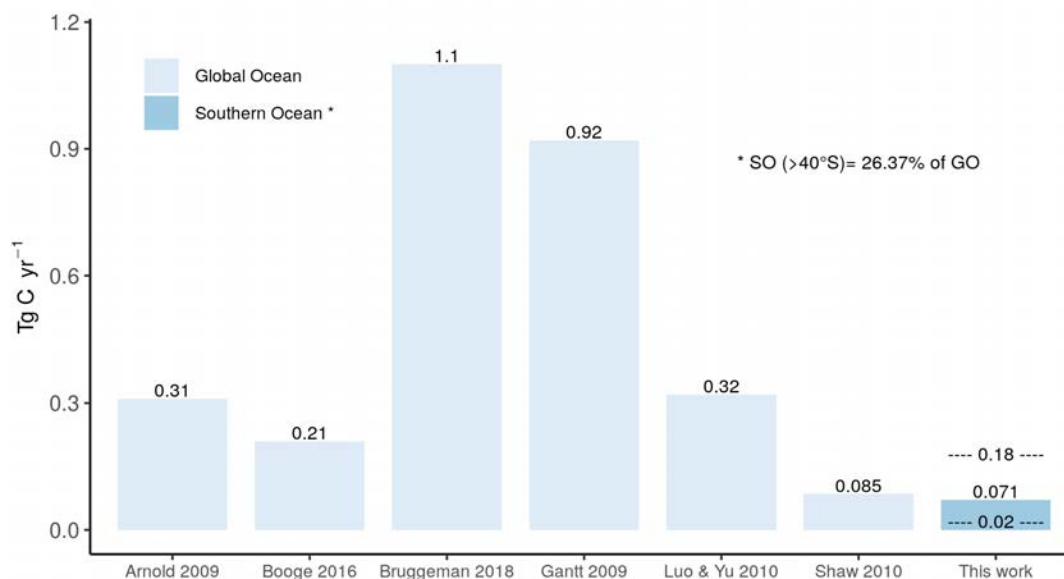


Figure 3.5: Global estimates (light blue) vs estimates from this work (blue). Dash lines in the results from this work represents the maximum and minimum values of isoprene emission from our experiments. The estimates from published works included in this graphs are bottom-up approaches.

Table 3.3: Surface isoprene concentration (0 – 10 m, pM) in the SO (>40°S) along the research cruises represented in Figure 3.6 A: PEGASO, TransPEGASO, ACE Expedition, AMT23, AMT22, KH-09-5 and ANDREXII.

Range (Mean)	Southern Ocean Area	Cruise
2.12 – 88.38 (10.68)	Southern Ocean Circumnavigation	ACE Expedition
1.6 – 93.46 (22.42)	South Atlantic Ocean and Weddell Sea	PEGASO cruise
12.01 – 49.52 (25.25)	Southwestern Atlantic Self	TransPEGASO cruise
13.15 – 57.14 (29.05)	South Atlantic Ocean	AMT23 & AMT22 cruises
2.3 – 39.03 (9.48)	South Indian Ocean	KH-09-5
4.82 – 39.07 (13.53)	South Atlantic Ocean	ANDREXII

tive waters being especially high in large scale bloom and coastal areas of Antarctica, contrasting with a low concentration background in most of the open ocean (Figure 3.6 A, Figure 3.3 A and B, Figure 3.22, and Table 3.3). Regarding the depth distribution of isoprene concentrations, the highest values were typically confined above 20 meters depth (Figure 3.15). In fact, $\approx 80\%$ of isoprene production was constrained to the first 10 meters depth (data not shown, Figure 3.16).

In the BASELINE simulation, there is a strong discrepancy between model results and observations regarding the latitudinal pattern. We noticed that there is a bias in the dataset, with many more observations in the latitudes where ROMS-BEC yields the highest isoprene concentrations (> 60°S, Figure 3.6 B). We also observed that our model overestimates concentrations at high latitudes (> 60°S) and, in contrast, underestimates at low latitudes (40-50°S, Figure 3.6C). The best agreement between observations and model results was found at latitudes of 50 and 55°S (Fig-

ure 3.6 C). Pairwise comparison showed that model outputs and observations of isoprene surface concentrations fall within the same overall range (0-150 pM). However, differences up to 2 orders of magnitude were found (Figure 3.6 D). When the published statistical models (Ooki et al., 2015; Hackenberg et al., 2017) were pairwise compared to observations, the models generally overestimated concentrations, more so with the lowest observed concentrations (Figure 3.6 E and F).

The patterns of simulated phytoplankton biogeography were comparable in the setup for this work and for Nissen et al. (2018) (compare Figure 3.3 B to Figure 1a in Nissen et al., 2018) showing the same positive bias of chlorophyll-a and sea surface temperature in high latitudes (Nissen et al., 2018) (Figure 3.3 A). In our ROMS-BEC configuration, diatoms were the main contributor to biomass of total chlorophyll-a in the SO (Figures 3.3 and 3.18). Concretely, they represented the 93.45% in terms of chlorophyll-a, are the strongest producers of isoprene representing the 98.01% of the total production in the Southern Ocean (Figure 3.7). Small mixed phytoplankton were the second contributors (4.83% of total isoprene production, 0.32% of chlorophyll-a in ROMS-BEC), while coccolithophores were the lowest contributors among the three modelled PFT's (1.72% of total production, 1.67% of chlorophyll-a). While coccolithophore biogeography looked different from that of diatoms, showing higher values at 40-50°S in summer, covering the area known as the "Great Calcite Belt" (Balch et al., 2011), small phytoplankton peaked in high latitudes (60-80°S). Regarding the seasonal patterns, the highest values of diatom biomass (monthly integrated mean values up to 5 $\mu\text{g L}^{-1}$) and chlorophyll-a concentration occurred in December in the latitudinal band of 60-70°S and, with a lower magnitude, also in the band 70-80°S that includes coastal Antarctica (Figure 3.15). This pattern matched the peaks of modelled isoprene concentration and production in the summer period, indicating that diatoms are the main drivers of isoprene in the model. A more detailed description of phytoplankton biogeography in the SO and its implementation in ROMS-BEC model can be found in (Nissen et al., 2018).

3.4.5 Sensitivity experiments

To assess the sensitivity of the simulated isoprene concentration levels to critical parameters, we conducted a set of sensitivity analysis (SA) experiments by increasing/decreasing each parameter (k) by 50% in our BASELINE configuration (Table 3.4). Since the focus of this study were the surface concentrations and the fluxes to the atmosphere, we restricted the analysis to the upper 10 meters of the SO for all sensitivity simulations performed to our BASELINE simulation (Table 4.2). Furthermore, it is in the first ten meters where the highest concentration of the three PFTs implemented in ROMS-BEC are found (Figure 3.18, 3.20, and 3.21). Therefore, we quantified the sensitivity as a change in annual means of isoprene concentration integrated over the upper 10 meters, since (1) it reflects the available isoprene to be transferred to the atmosphere and (2) isoprene production is typically constrained to surface waters (in our BASELINE simulation, 67 % of the total isoprene production (*data not shown*) occurred within the first 10 meters of the water column); and (3) all of our in situ measurements to validate the model lie within the first ten meters of the surface SO (Section 3.4.4). The SA index, describing the percentage change of a target model output variable when varying an initial model parameters value, was taken from Le Clainche et al. (2004) and was defined as follows:

$$S_k = \frac{ISO_{k_{\max}} - ISO_{k_{\min}}}{ISO_{\text{BASELINE}}} * 100 \quad (3.17)$$

where $ISO_{k_{\text{BASELINE}}}$, $ISO_{k_{\max}}$ and $ISO_{k_{\min}}$ are the annual means of isoprene concentration integrated over the upper 10 meters obtained for the each sensitivity simulation (Table 3.4): BASELINE (reference value of parameter k), 50% increase in the parameter k ($k_{\max} = 1.5 * k$), and 50% decrease in the parameter k ($k_{\min} = 0.5 * k$). All sensitivity runs start from the common spin-up described in section 3.4.1 and only differ in the chosen isoprene production or loss rates (Table 4.2). Each of the sensitivity simulations was started from the 10-year restart file of the BASELINE run, and then run for ten years. As for the BASELINE, we assessed the annual means of isoprene concentration obtained from the monthly climatology of the last 5 seasonal cycle.

Table 3.4: Overview of sensitivity experiments (as described in Section 4.2.4) for BASELINE simulation (Table 4.2).

Run name	$\rho_{\text{CHLA}}^{\text{DIAT}}$ $\frac{\text{nmol C}_5\text{H}_8}{\mu\text{gChl d}}$	$\rho_{\text{CHLA}}^{\text{COC}}$ $\frac{\text{nmol C}_5\text{H}_8}{\mu\text{gChl d}}$	$\rho_{\text{CHLA}}^{\text{SP}}$ $\frac{\text{nmol C}_5\text{H}_8}{\mu\text{gChl d}}$	k_{LOSS} d^{-1}
DIAT.50+	18.21	10.98	0.69	0.29
DIAT.50-	6.07	10.98	0.69	0.29
COCC.50+	12.14	16.47	0.69	0.29
COCC.50-	12.14	5.49	0.69	0.29
SP.50+	12.14	10.98	1.03	0.29
SP.50-	12.14	10.98	0.34	0.29
KBIO.50+	12.14	10.98	0.69	0.45
KBIO.50-	12.14	10.98	0.69	0.15

For isoprene surface concentrations (Figure 4.7.D), $\rho_{\text{CHLA}}^{\text{DIAT}}$ has the largest effects, which is not surprising due to the dominance of diatoms in the total production of isoprene (Figure 3.7.A), but

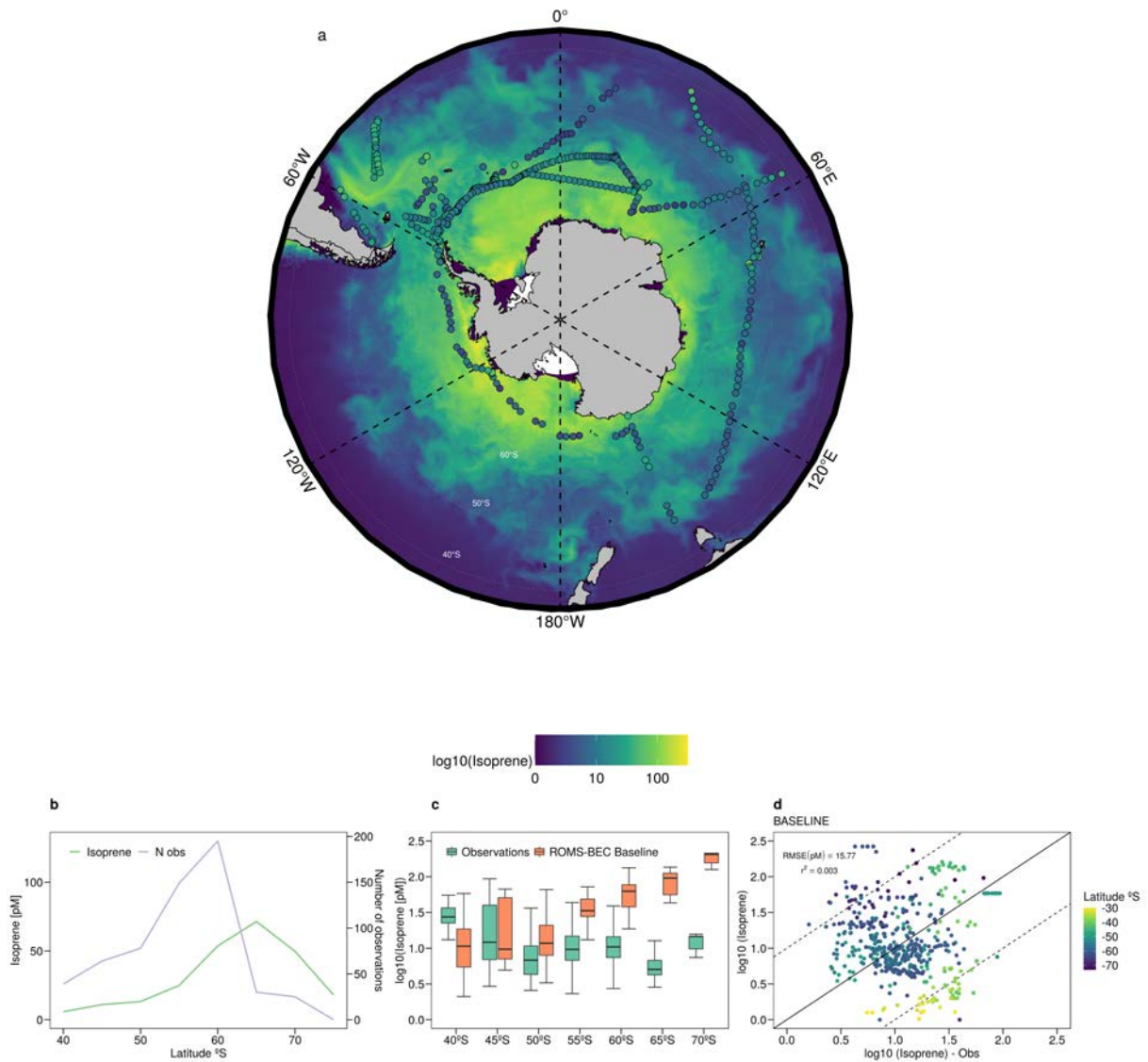


Figure 3.6: **a:** Validation data set of isoprene concentration for the cruises compiled in Table 3.3 plotted together with the monthly average of isoprene surface concentration for the months of December, January, February and March (BASELINE run, Table 4.2). **b:** Latitudinal distribution of monthly averaged isoprene surface (0-10 m) concentrations for the months of concentration December, January, February and March and number of observations in our data set (Table 3.3). **c:** Boxplot of latitudinal values of observations and BASELINE run for the climatological period November - March, and latitudes higher than 40°S . **d:** Scatterplot of observations of isoprene concentration and model results from BASELINE run (Table 4.2).

also on every latitudinal band (Figure 3.7.B). The effects of changes in $\rho_{\text{CHLA}}^{\text{COCC}}$ and $\rho_{\text{CHLA}}^{\text{SP}}$ groups were much smaller compared with changes in diatoms production rate. Moreover, the K_{LOSS} triggered a stronger effect than $\rho_{\text{CHLA}}^{\text{COCC}}$ and $\rho_{\text{CHLA}}^{\text{SP}}$ on isoprene concentration levels. Overall, changes in all tested parameters affected the isoprene surface concentration levels at high latitudes (60-70°S, Figure 4.7) more strongly rather than in low latitudes of the SO (40-60°S, Figure 4.7).

Testing the sensitivity of isoprene concentration in ROMS-BEC to changes in the main parameters can be useful to detect the main uncertainties in our modelling capability of isoprene emission from the SO. The huge variability of the tested parameters, k_{BIO} , k_{CHEM} and $\rho_{\text{CHLA}}^{\text{PFT}}$, obtained from in situ measurements and/or laboratory experiments, must be better constrained if we are to improve the predictability of isoprene production and degradation. Hence, these ROMS-BEC results will help to point where future efforts in experimental works must be performed, if we aim to characterize isoprene in the SO, in particular, and in the global ocean, in general.

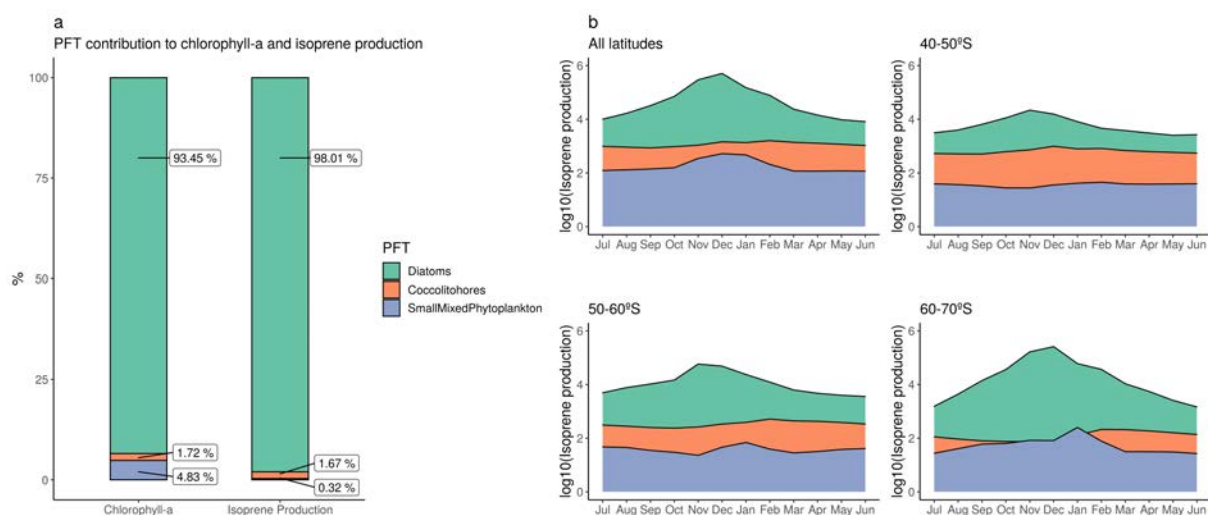


Figure 3.7: **a**: Comparison of the relative contribution (%) of each PFT to chlorophyll-a and to isoprene production. **b**: Time series of isoprene production (logarithm of 10) per PFT throughout the climatological months. Data used for A and B is BASELINE (Table 4.2).

3.5 Discussion

3.5.1 Sources and sinks of isoprene

The laboratory-derived isoprene production rates used in this study (Table 4.2), compiled in (Booge et al., 2016), were measured during the exponential growth phase of phytoplankton monocultures (Shaw et al., 2003; Exton et al., 2013). Consequently, they may not necessarily be applicable to natural conditions of the surface ocean, because it has been shown that isoprene production changes depending on the growth stage (Milne et al., 1995). Moreover, the strains used in laboratory experiments are usually a product of generations grown in laboratory conditions. We checked in <http://www.algaebase.org/> the presence in the SO of the phytoplankton species compiled in Booge

et al. (2016). Among the compiled species, 33 are present in polar waters and 21 in the SO. Therefore, we believe that the data of this broad range of cultured strains can be a good approximation to isoprene production in the SO. However, measurements in natural communities of the SO had never been performed; before the PEGASO cruise, no production rates had been proposed specifically for this area. Likewise, we determined for the first time the rates of chemical and biological isoprene losses in the SO (Simó et al. 2020). Degradation processes in the marine environment have been discussed in several works in the past (Shaw et al., 2003; Alvarez et al., 2009; Booge et al., 2018). Despite early laboratory experiments suggested that biological consumption was negligible (Shaw et al., 2003), recent studies pointed out that it may be the most important isoprene sink from the surface ocean (Booge et al., 2018) (Simó et al. 2020). In this work we determined production and loss rates that were higher than those used hitherto, suggesting that isoprene cycling is faster than believed.

3.5.2 The role of community structure in the production of isoprene

Phytoplankton communities in the SO are diverse in terms of both its biogeochemical triggers (Ardyna et al., 2019) and its species composition (Table 3.1). In our ROMS-BEC configuration, isoprene production and concentration levels are constrained to surface waters (Figure 3.16 & 3.15), coinciding with chlorophyll-a (Figure 3.22), although it is also produced and transported from deeper levels. Among the three PFTs implemented in our isoprene-ROMS-BEC model, diatoms dominate the total isoprene production in the SO (Figure 3.7.A). This agrees with previous works that have suggested that diatoms are the most important producers of isoprene in the ocean (Arnold et al., 2009; Dani et al., 2017). In contrast, the production of isoprene from coccolithophores and small mixed phytoplankton represents a much lower contribution than the one from diatoms, with differences of several orders of magnitude (Figure 3.7.B). However, the PFT-specific production rates we determined in PEGASO were very similar for diatoms and coccolithophores; therefore, the prominent role of diatoms obeys to their prominent abundance, not to an isoprene-prone physiology. The small mixed phytoplankton, conversely, have a much lower specific isoprene production.

For all latitudinal bands from 40 to 70 °S, isoprene production by coccolithophores is higher than the one by small mixed phytoplankton, except for the climatological months of November, December and January and February in latitudes 60-70 °S (Figure 3.7.B). This agrees with previous works that have reported that assemblages of mixed phytoplankton are more common at subantarctic latitudes, with substantial contributions of coccolithophores (Balch et al., 2011, 2016). Overall, our experimental results revealed that marine phytoplankton production of isoprene may be significantly higher than that estimated from monoculture experiments in the laboratory.

3.5.3 Limitations within the model

In our ROMS-BEC configuration we implemented the specific isoprene production rates for three PFTs: diatoms, coccolithophores, and small mixed phytoplankton. We may be missing the isoprene production of some taxa that play a relevant role in phytoplankton blooms in the SO, like *Phaeocystis*

(DiTullio et al., 2000). Isoprene production by *Phaeocystis* has been neglected so far in modelling works since Broadgate et al. (1997) suggested that this taxon inhibits the production of isoprene. We suggest that it should be experimentally re-visited. Our measurements in NSO, that we attributed to small mixed phytoplankton, corresponded to a phytoplankton assemblage with 17% of the chlorophyll-a contributed by *Phaeocystis* (Table 3.1). Unfortunately, it is not possible to provide a specific isoprene production rate by *Phaeocystis*.

Moreover, it must be taken into account that, as described in Nissen et al. (2018), the ROMS-BEC model configuration has a positive chlorophyll bias at high SO latitudes, resulting partly from high temperatures, shallow mixed layer depth and missing ecosystem complexity, which may result in an overestimation of the simulated isoprene production. Consequently, further versions of ROMS-BEC model have to be improved in order to correct these biases. Furthermore, the shortage of data in relevant regions directly affects the validation of our results (Figure 3.12) in an ocean which is quite complex in terms of biogeochemistry dynamics (Ardyna et al., 2017, 2019).

3.5.4 Paucity of in situ measurements and experiments

The database of isoprene concentrations in the SO compiled for this work, despite being the most complete up to date, it is still quite scarce in terms of spatial and temporal coverage (Figure 3.6A), which causes seasonal and geographical biases. As shown in Figure 3.13, in ROMS-BEC the Pacific sector is the main contributor to isoprene emissions from the SO ($>40^{\circ}\text{S}$) because it comprises the largest area. However, the number of isoprene measurements in this sector is the smallest one ($n = 38$, Figure 3.13). In contrast, the Atlantic sector ($n = 241$, Figure 3.13) is the lowest emitter of isoprene and contains the highest number of isoprene measurements. The Indian sector falls somewhere between the Pacific and the Atlantic sectors ($n = 38$, Figure 3.13).

The validation of isoprene concentrations in the vertical column is even more challenging since less than 10 measured profiles are available in the whole SO. The small number of isoprene measurements in the SO in particular, and the global ocean in general, can be easily noticed when comparing with another trace gas like DMS, whose dataset in the SO amounts more than 8,000 measurements (Lana et al., 2011). In consequence, despite the available data cover all latitudes and longitudes of the ocean, it is not enough to disentangle biogeochemical processes and ecological patterns related to isoprene production and consumption. Another bias is that the different cruises performed in the SO have followed different sampling approaches. Some of the cruises consisted of untargeted transects (Ooki et al., 2015; Hackenberg et al., 2017), while others targeted areas of particular characteristics such as blooming or ice edge waters, like PEGASO. Both strategies are required if we are to achieve a better coverage in an oceanic region that is quite complex in terms of biogeochemical dynamics (Longhurst, 1995; Ardyna et al., 2017, 2019).

3.5.5 The annual emission of isoprene from the SO

The year integrated emission obtained from our BASELINE simulation ($0.071 \text{ Tg C yr}^{-1}$, Table 4.2) for the SO ($> 40^\circ\text{S}$) represents from 6 to 84% of previous global estimates (see compilation in Brüggemann et al. (2018)). Note that the upper limit exceeds the percentage of the global ocean represented by the SO waters ($\approx 27\%$). The highest emission estimates were obtained with the DIRECT.KBIO.LOW run ($0.199 \text{ Tg C yr}^{-1}$, Table 4.2). In this configuration we implemented the specific production rates derived from the PEGASO cruise, and the k_{BIOL} from Palmer and Shaw (2005). This illustrates how the parameter choice in model configurations have a big impact in isoprene emissions. Field-work derived specific production rates, which were higher than lab-derived values, must be accompanied with field-work derived loss rate constants, which were also higher than prescribed ones; otherwise, the big imbalance leads to emission overestimates. Regarding the runs using the light-dependent emission factors from lab experiments Gantt et al. (2009); Booge et al. (2018), there are also remarkable differences among them. So there are among configurations that used light-independent PFT-specific production rates from lab experiments Booge et al. (2016), which yielded emissions that spanned up to two orders of magnitude (from 0.0077 to $0.119 \text{ Tg C yr}^{-1}$, Table 4.2). We must stress that all these isoprene production parameterizations were not derived from polar water measurements. Moreover, the differences in the lab-derived production rates of isoprene even within strains of the same species (e.g. *Emiliana huxleyi*, see Table 2 in Booge et al. (2016)), reflect that isoprene production is dependent on culture conditions and the physiological state of the organism. Consequently, in-situ isoprene production by phytoplankton may also vary also depending on the place and season. In any case, overall our emissions estimates are more coincident with the range of bottom-up rather than top-down estimates (see compilation in (Brüggemann et al., 2018)).

Global emissions of isoprene have been a widely discussed topic among atmospheric and marine research communities (Palmer and Shaw, 2005; Arnold et al., 2009; Luo and Yu, 2010; Hackenberg et al., 2017). Recently, Brüggemann et al. (2018) synthesized all previous estimates of global marine isoprene emissions revealing strong discrepancies among the published studies (Figure 5.5). These differences are due to methodological approaches, from the combination of remote sensing and modelling (Palmer and Shaw, 2005) to the use of PFT-specific isoprene production rates (Booge et al., 2016). All of them, moreover, suffer from a poor knowledge of how production and degradation processes actually occur in the ocean.

3.6 Conclusions

For the first time, we have quantified the emission of isoprene from the SO using a PFT-based biogeochemical modelling approach into which we implemented PFT-specific isoprene production rates determined from in-situ measurements. Mechanistic (prognostic) modelling approaches are complementary to statistical (diagnostic) models to assess isoprene emissions at the regional and

Table 3.5: Global estimates of isoprene emissions for the global ocean in comparison with our results for the Southern Ocean. A more complete version of global estimates of isoprene emission can be found in (Brüggemann et al., 2018).

Area	Ref	Flux (Tg C yr^{-1})	Type
S. Ocean ($>40^\circ\text{S}$, 26.37 % of GO)	This work - mean (range)	0.071 (0.002 - 0.18)	Bottom-up
Global ocean	Palmer and Shaw (2005)	0.1	Top-down
Global ocean	Booge et al. (2016)	0.21	Bottom-up
Global ocean	Arnold et al. (2009)	0.31 - 1.9	Bottom-up – Top-down
Global ocean	Luo and Yu (2010)	0.32 - 11.6	Bottom-up – Top-down
Global ocean	Gantt et al. (2009)	0.92	Bottom-up
Global ocean	Brüggemann et al. (2018)	1.1	Bottom-up
Global ocean	Shaw et al. (2010)	0.085 - 11.6	Bottom-up – Top-down

global scales, adding the capability to make projections into the past or future. To improve prognostic models, our sensitivity analysis highlights that there is a need for better-constrained production rates of isoprene by different PFT's, not only from lab experiments but also from in situ data. There is also a need to better evaluate and parameterize isoprene degradation rates by marine microbes and chemical radicals. Moreover, increasing the data set of measurements of isoprene concentrations in the SO will improve further validation of model results. We call for making all isoprene data in the SO publicly available to facilitate model developments and validations and to look for weaknesses and strengths in existing modelling approaches.

Ecological-biogeochemical modelling approaches are an accurate tool to understand isoprene levels and emission patterns at the regional scale. Temperature increase due to global warming will impact on the marine ecosystem of the SO in many different ways either by temperature itself or through sea ice changes, stratification of the water column, and ocean acidification (Hoegh-Guldberg and Bruno, 2010; Stocker et al., 2013). These changes will result in shifts in the phytoplankton community composition (Tortell et al., 2008; Montes-Hugo et al., 2009; Boyce et al., 2010), thereby expanding or contracting the geographic range of marine isoprene-emitters like diatoms or coccolithophores (Dani and Loreto, 2017; Pinkernell and Beszteri, 2014). Only numerical prognostic models that incorporate a better knowledge of isoprene cycling processes will be able to anticipate future changes in isoprene emission patterns in this relevant region for global climate.

Aknowledgements

This research was supported by the Spanish Ministry of Economy and Competitiveness through project PEGASO (CTM2012–37615) and the Swiss Polar Institute and Ferring Pharmaceuticals through projects SORPASSO–ACE8 to RS and ACE1 to DA. It was also partially funded by the Australian Government through the Australian Research Council's Discovery Projects funding scheme (project DP160103387). PRR was supported by a "la Caixa" Foundation PhD Fellowship (2015–2019). This research is the result of the *COPLA* research project funded by the Polytechnic University of Catalonia (UPC) through two fellowships from its program for International Research Mobility

(editions 2017 and 2018) which were awarded to PRR. Members of the ACE 1 research team are greatly acknowledged for providing data and technical support. PRR would like to thank Doctor Nicolai Gruber and Meike Vogt, as well as the rest of his team, for hosting and training him at Environmental Physics Group (ETH Zürich (Switzerland)) during 2017 and 2018. CN, MV and NG acknowledge funding from the Swiss Federal Institute of Technology Zürich (ETH Zürich) and the Swiss National Science foundation (project SOGate, grant no.20021_153452). The simulations were performed at the HPC cluster of ETH Zürich, Euler, which is located in the Swiss Supercomputing Center (CSCS) in Lugano and operated by ETH ITS Scientific IT Services in Zürich. The authors are grateful to the British Oceanographic Data Centre (BODC). The authors would like to thank to Marina Zamanillo (ICM-CSIC) for Solar Radiation Dose data. The authors also want to thank the captain, officers and crew of RV Hespérides and RV Akademik Tryoshnikov, engineers of the Marine Technology Unit (CSIC) and research colleagues for their support and help during the cruises. Model output and in situ data are available and data of in situ measurements are available upon request to the corresponding author.

3.7 Appendix

General patterns

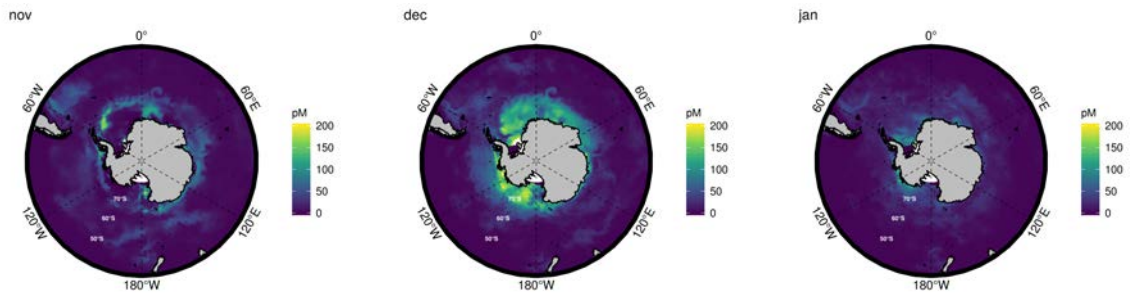


Figure 3.8: Monthly climatologies of isoprene concentration (pM) for the BASELINE run (Table 4.2).

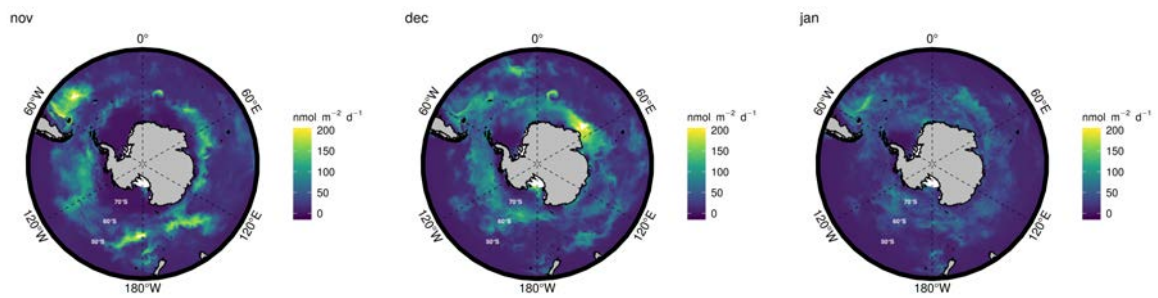


Figure 3.9: Monthly climatologies of flux of isoprene ($\text{nmol m}^{-2} \text{d}^{-1}$) for the BASELINE run (Table 4.2).

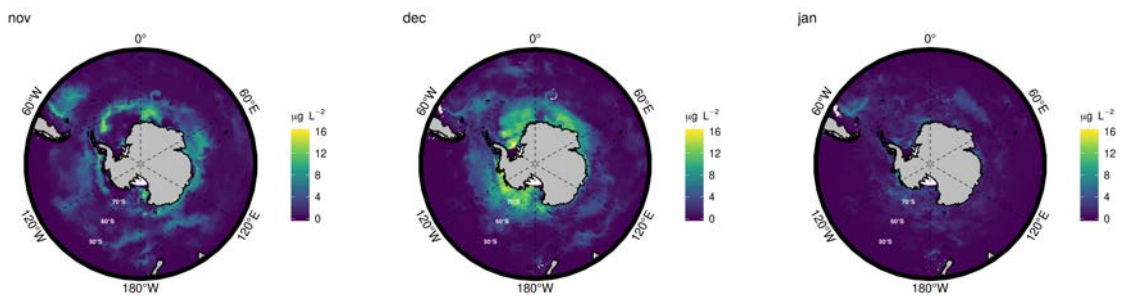


Figure 3.10: Monthly climatologies of total chlorophyll-a concentration ($\mu\text{g L}^{-1}$) for the ROMS-BEC configuration used in this work.

Model experiments

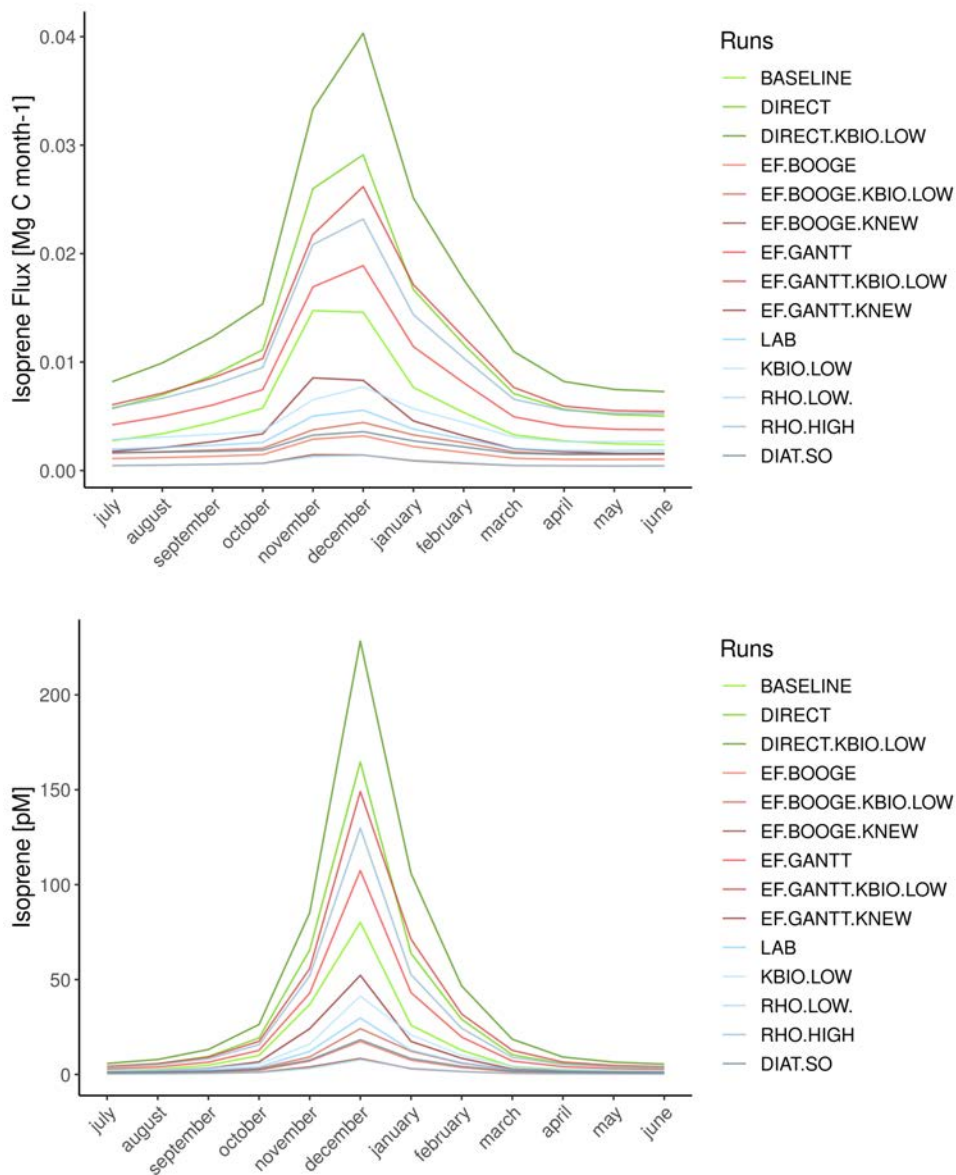


Figure 3.11: Time series of monthly integrated isoprene concentration (left) and flux (right) in the Southern Ocean (>40°S) from ROMS-BEC runs. Note that the results of applying the statistical models from Ooki et al. (2015) (blue) and Hackenberg et al. (2017) are not shown.

Validation of experiments

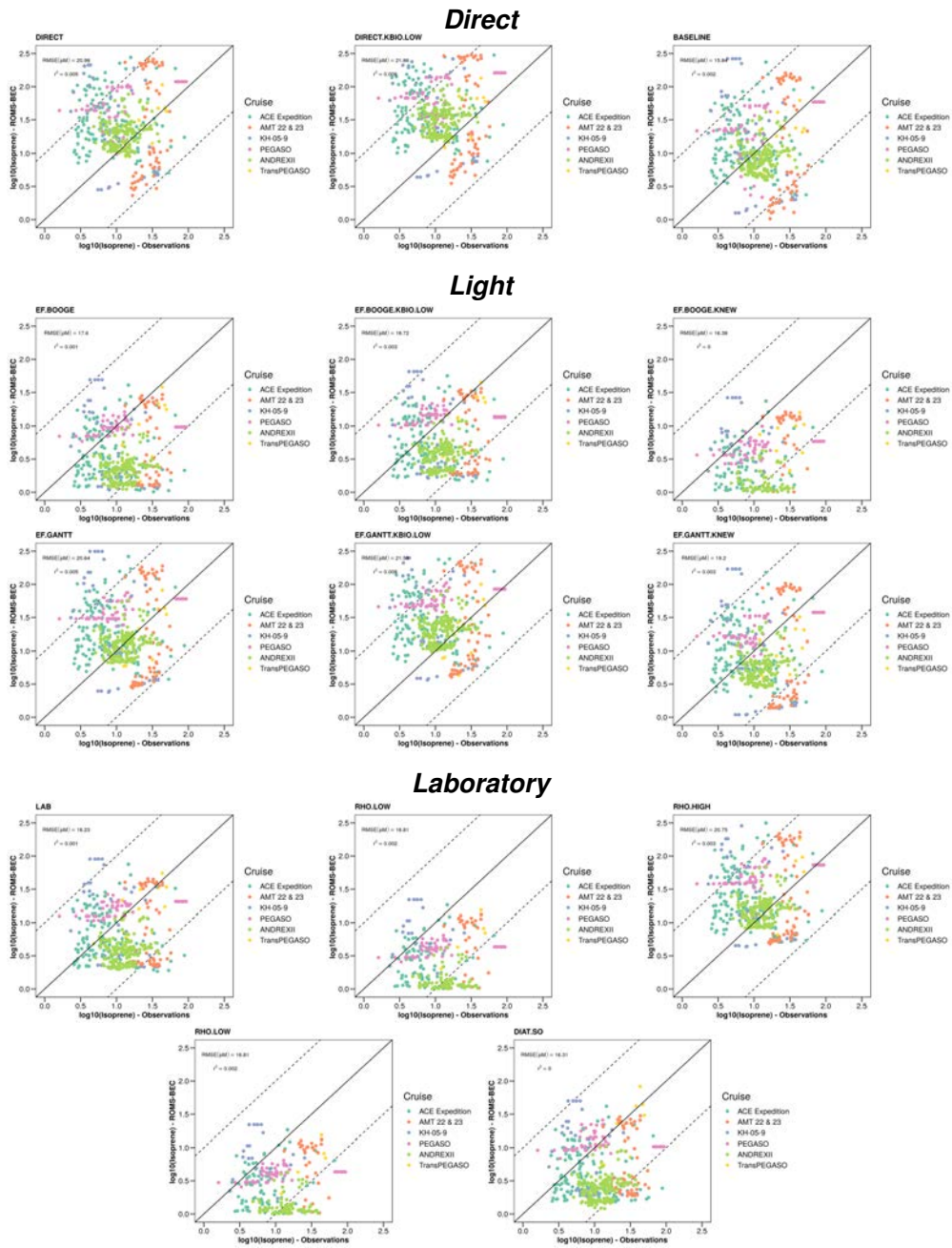


Figure 3.12: Validation of isoprene concentration results from our simulations (Table 4.2) with observations of isoprene concentration from the cruises compiled in 3.3. RMSE = Root Mean Squared Error.

Ocean basins

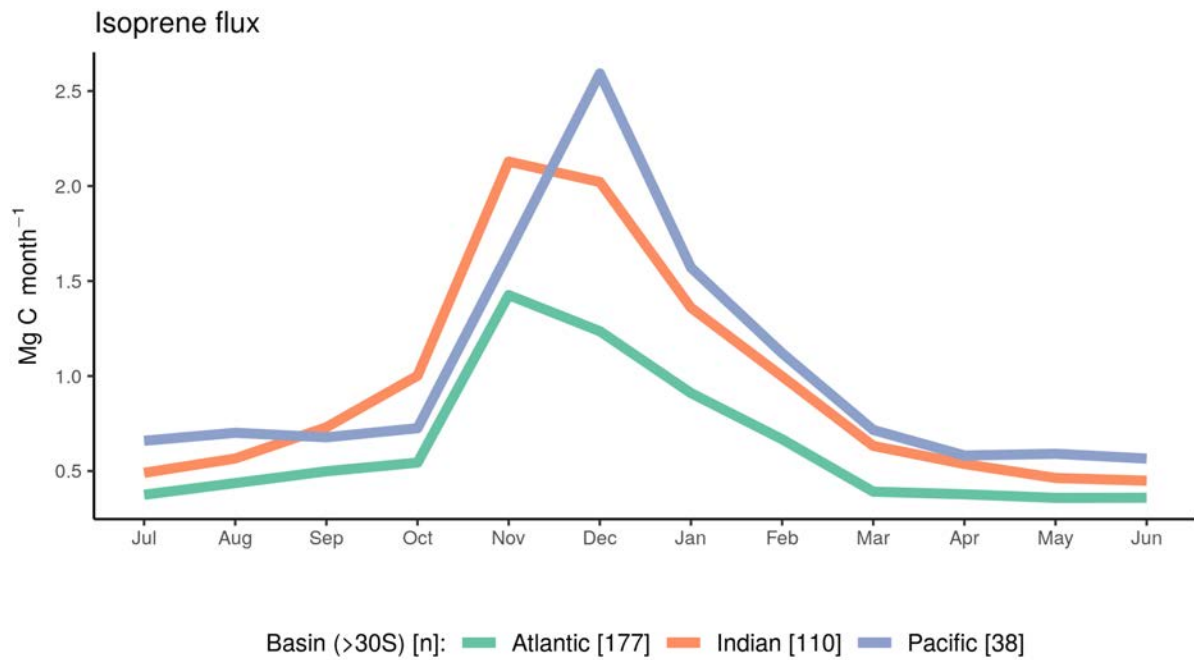


Figure 3.13: Relative contribution of every oceanic basin: Atlantic, Indian and Pacific Ocean (limits are defined according to NODC-NOAA: https://www.nodc.noaa.gov/woce/woce_v3/wocedata_1/woce-uot/summary/bound.htm) when latitude was below 40 °S (3.13). The marine emission of isoprene is proportional to the size of each ocean basin. Thus, for our BASELINE run, the Pacific Ocean is the main emitter (12.15 Mg C y⁻¹) followed by the Indian Ocean (11.37 Mg C y⁻¹) and the Atlantic Ocean (7.58 Mg C y⁻¹).

Hovmoller diagrams

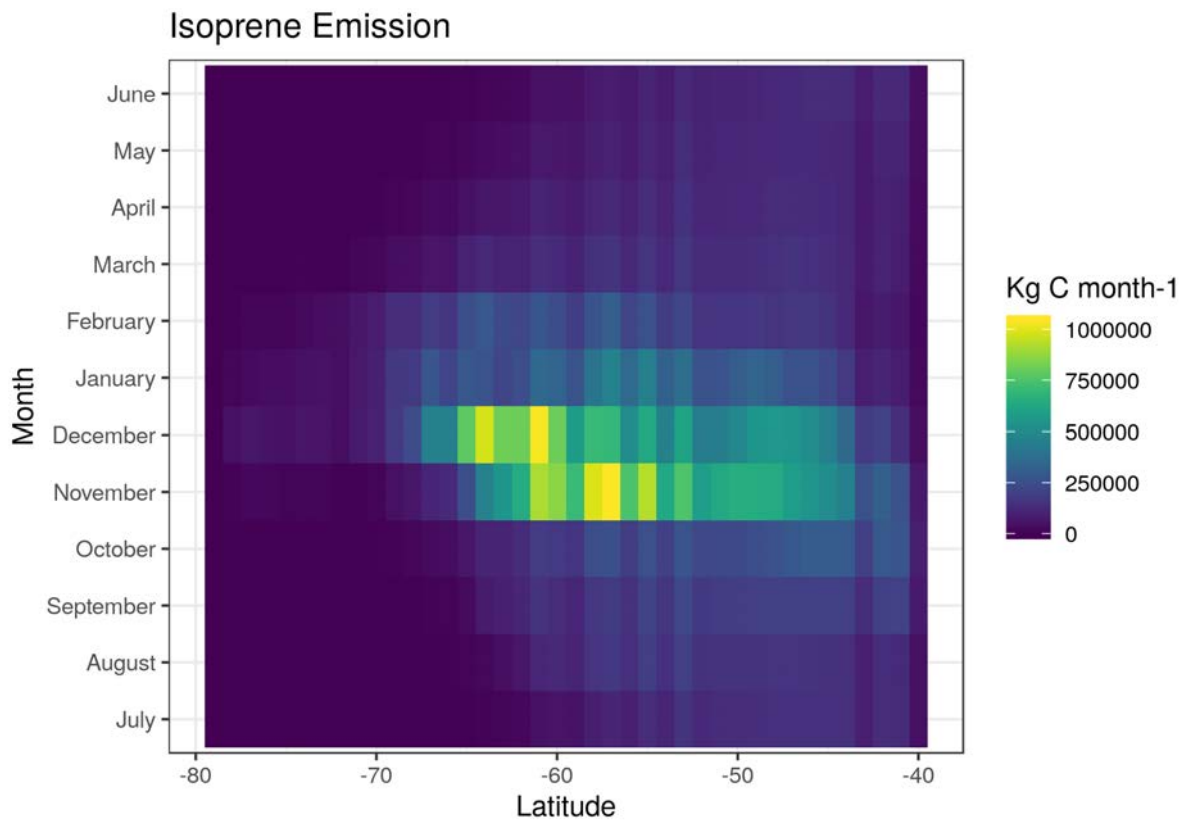


Figure 3.14: Hovmoller diagram of isoprene emission in the Southern Ocean ($>40^{\circ}\text{S}$) from the BASELINE simulation.

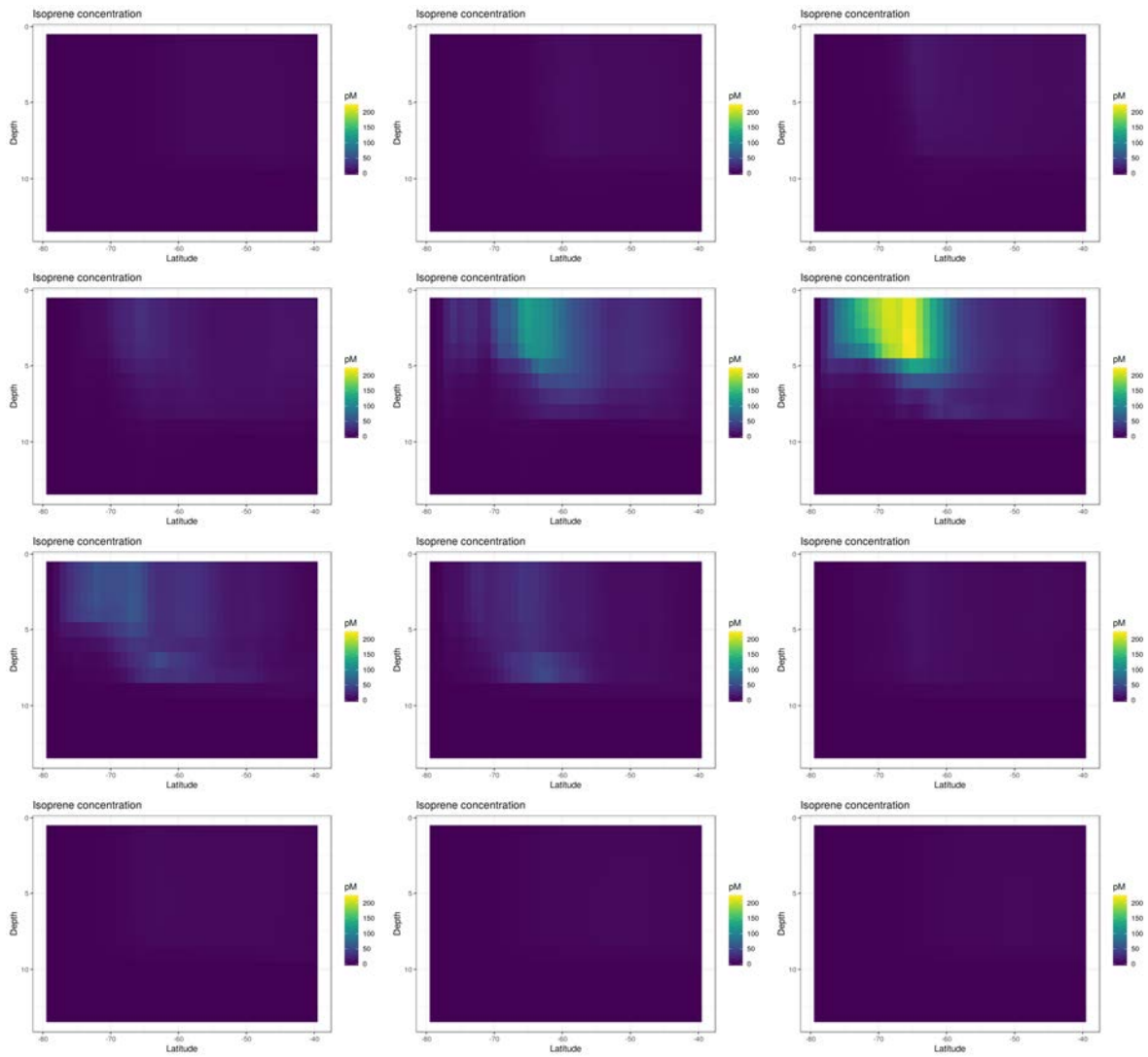


Figure 3.15: Hovmoller diagram of the vertical distribution of isoprene concentration in the Southern Ocean from the BASELINE simulation.

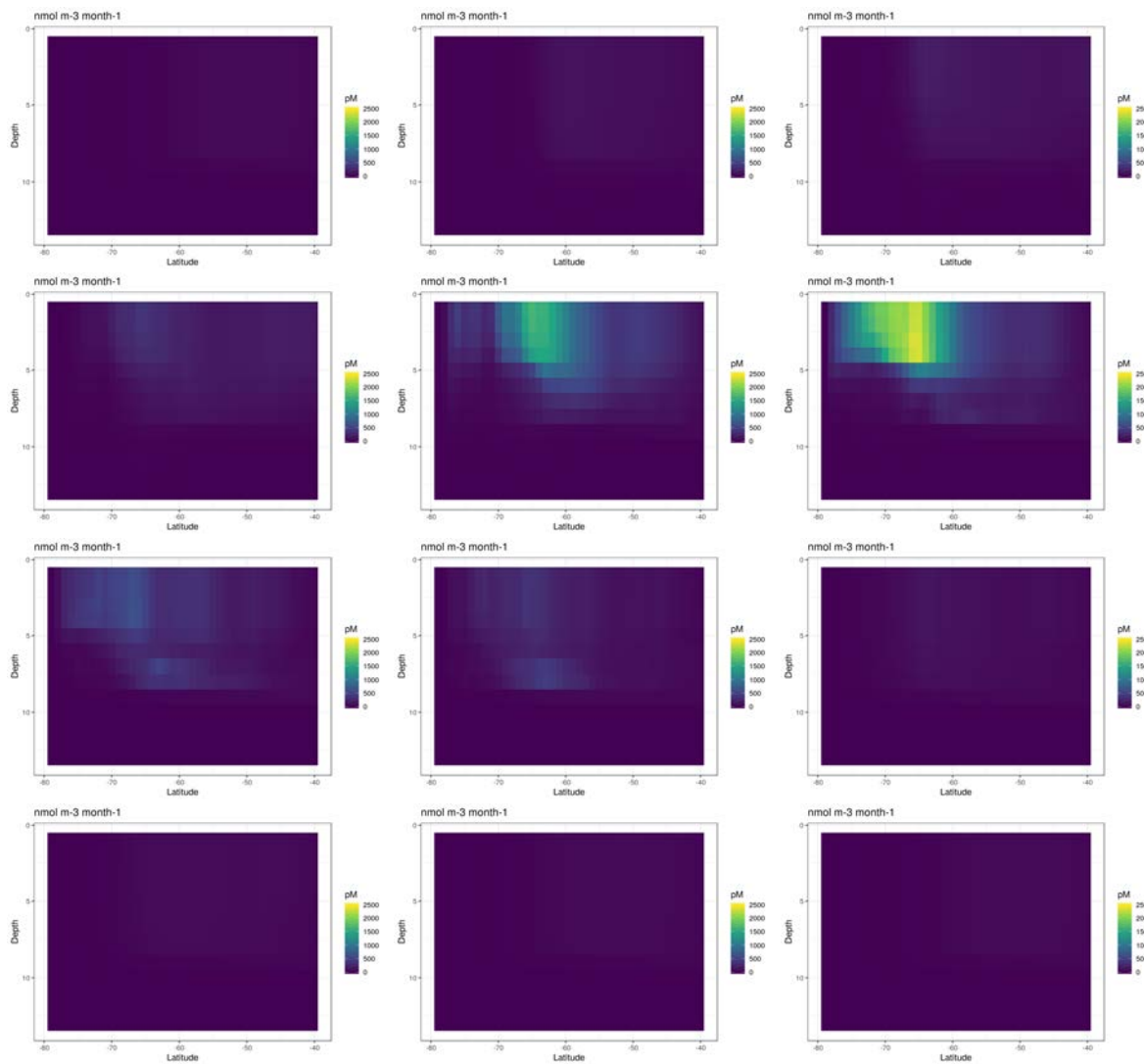


Figure 3.16: Hovmoller diagram of the vertical distribution of isoprene production in the Southern Ocean from the BASELINE simulation.

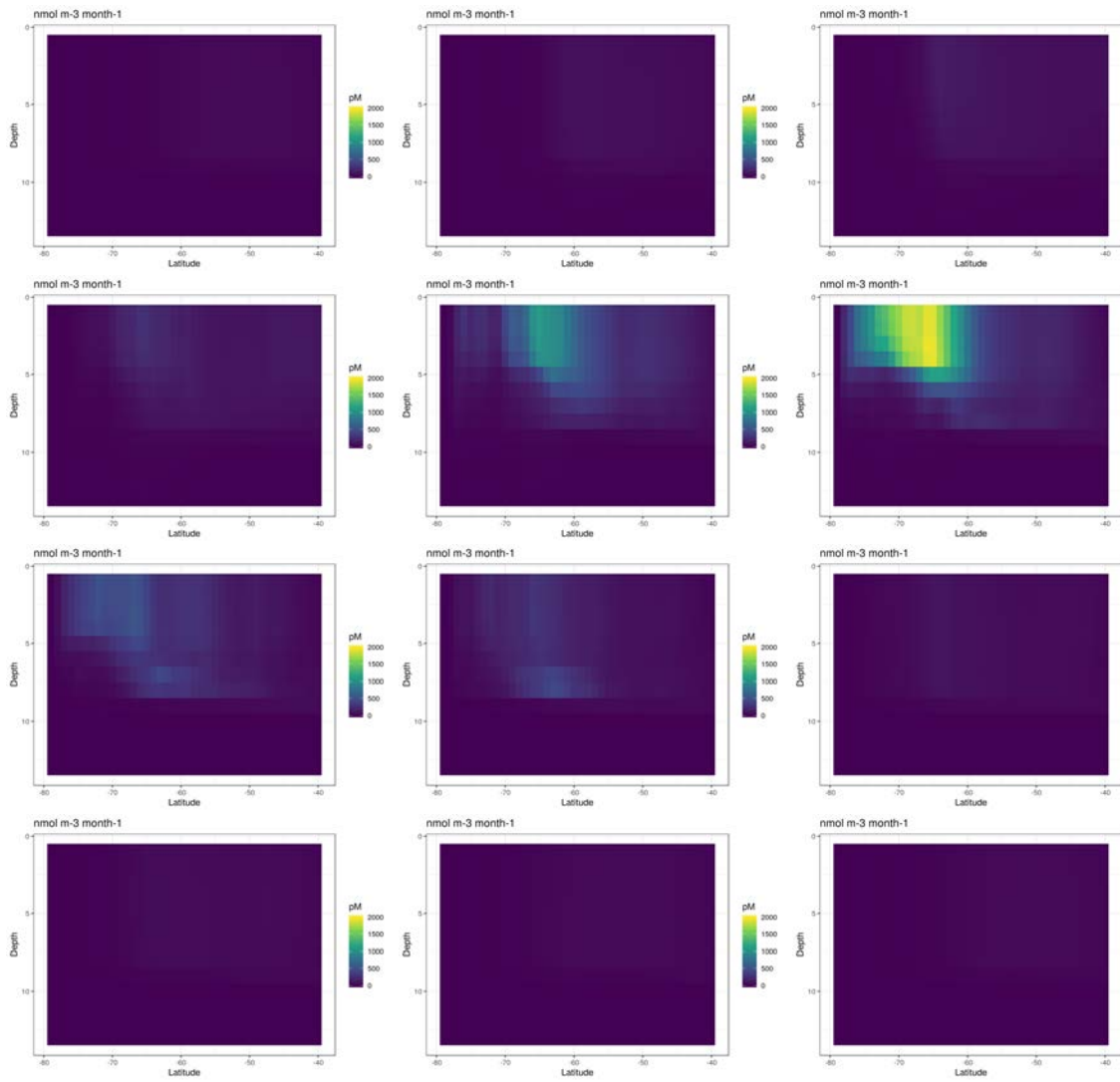


Figure 3.17: Hovmoller diagram of the vertical distribution of isoprene biological + chemical degradation (k_{LOSS} , see Section 3.4) in the Southern Ocean from the BASELINE simulation.

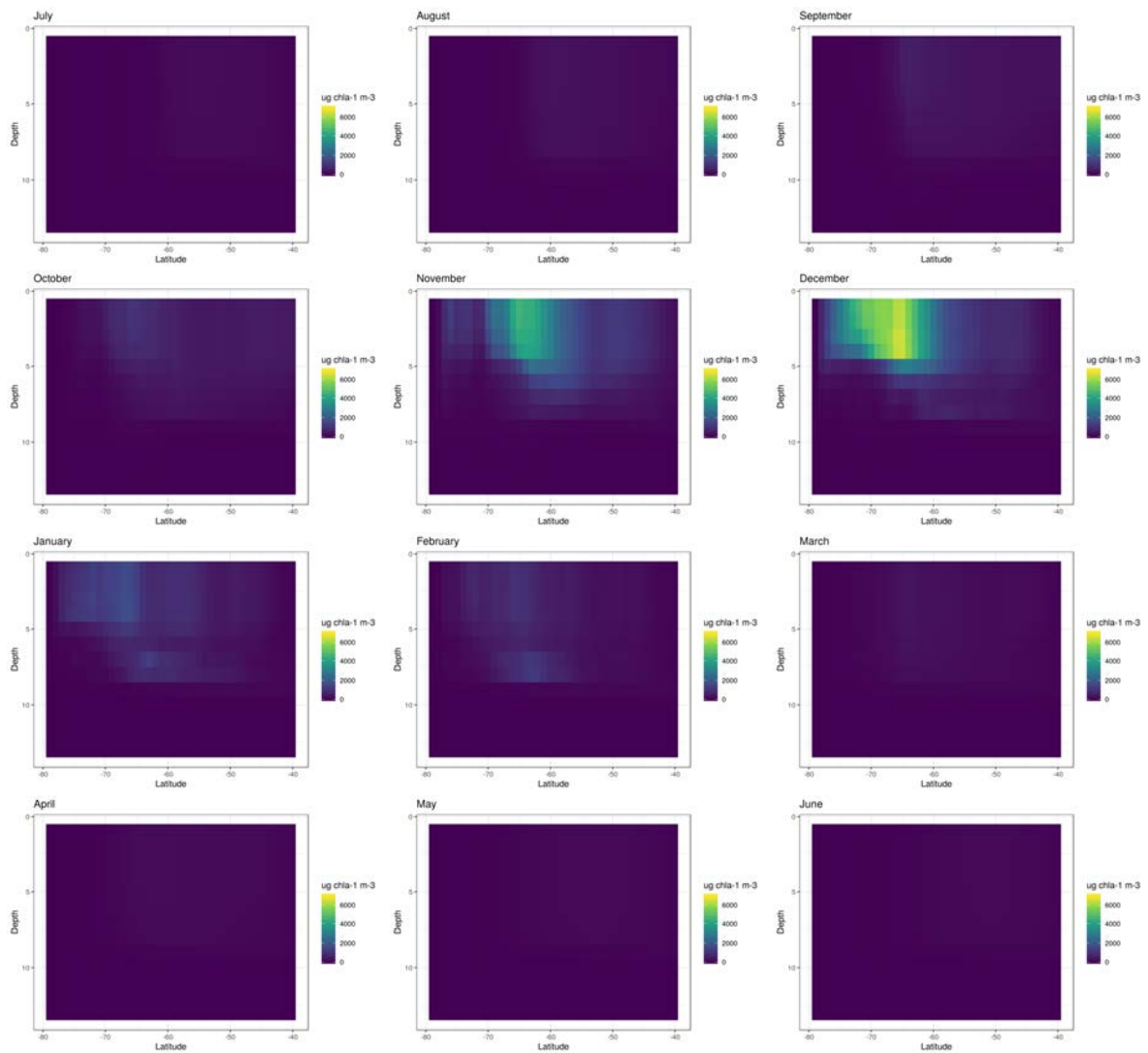


Figure 3.18: Hovmoller diagram of the vertical distribution of diatom biomass in the Southern Ocean from the BASELINE simulation.

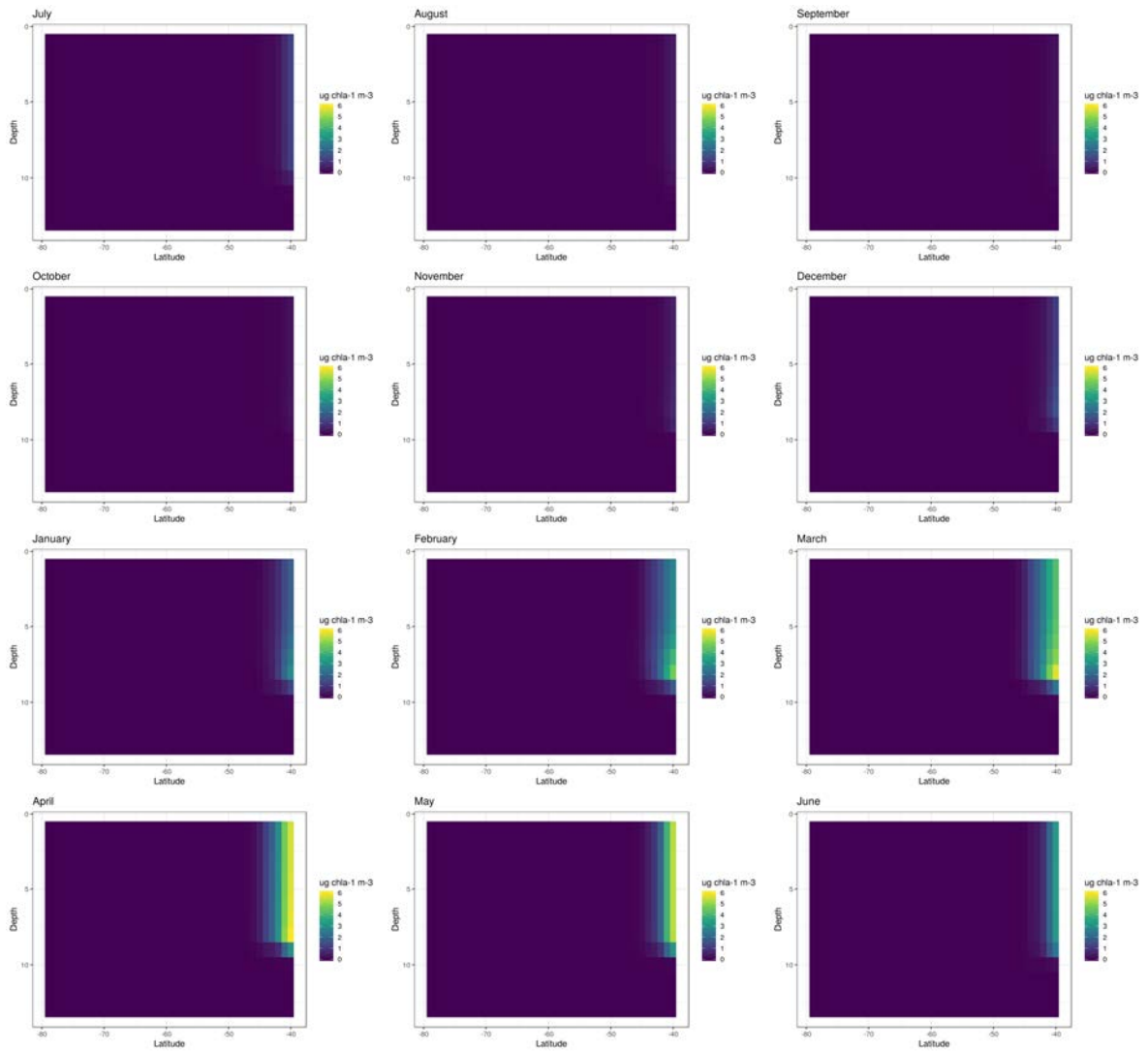


Figure 3.19: Hovmoller diagram of the vertical distribution of diazotroph biomass in the Southern Ocean from the BASELINE simulation.

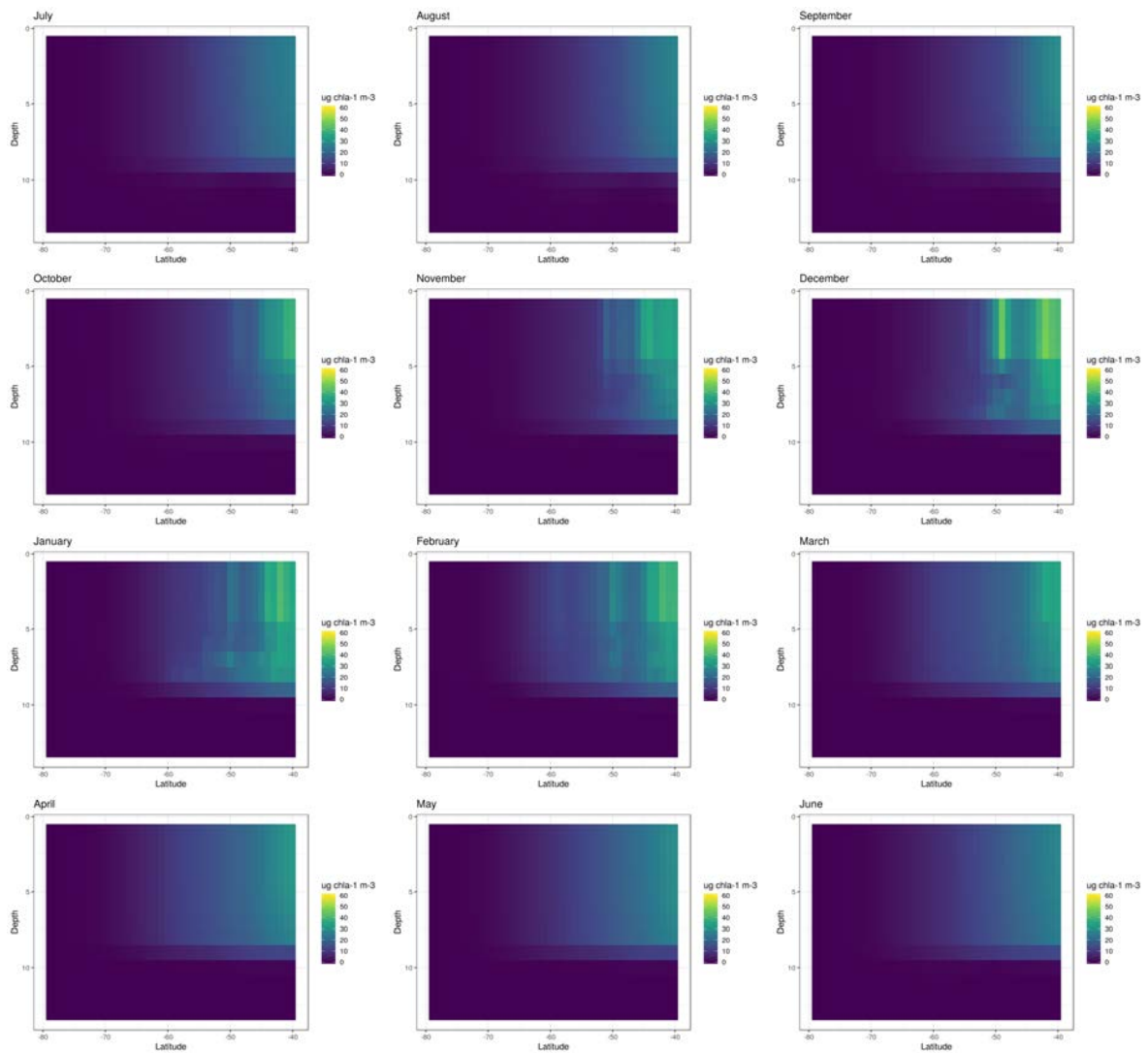


Figure 3.20: Hovmoller diagram of the vertical distribution of coccolithophore biomass in the Southern Ocean from the BASELINE simulation.

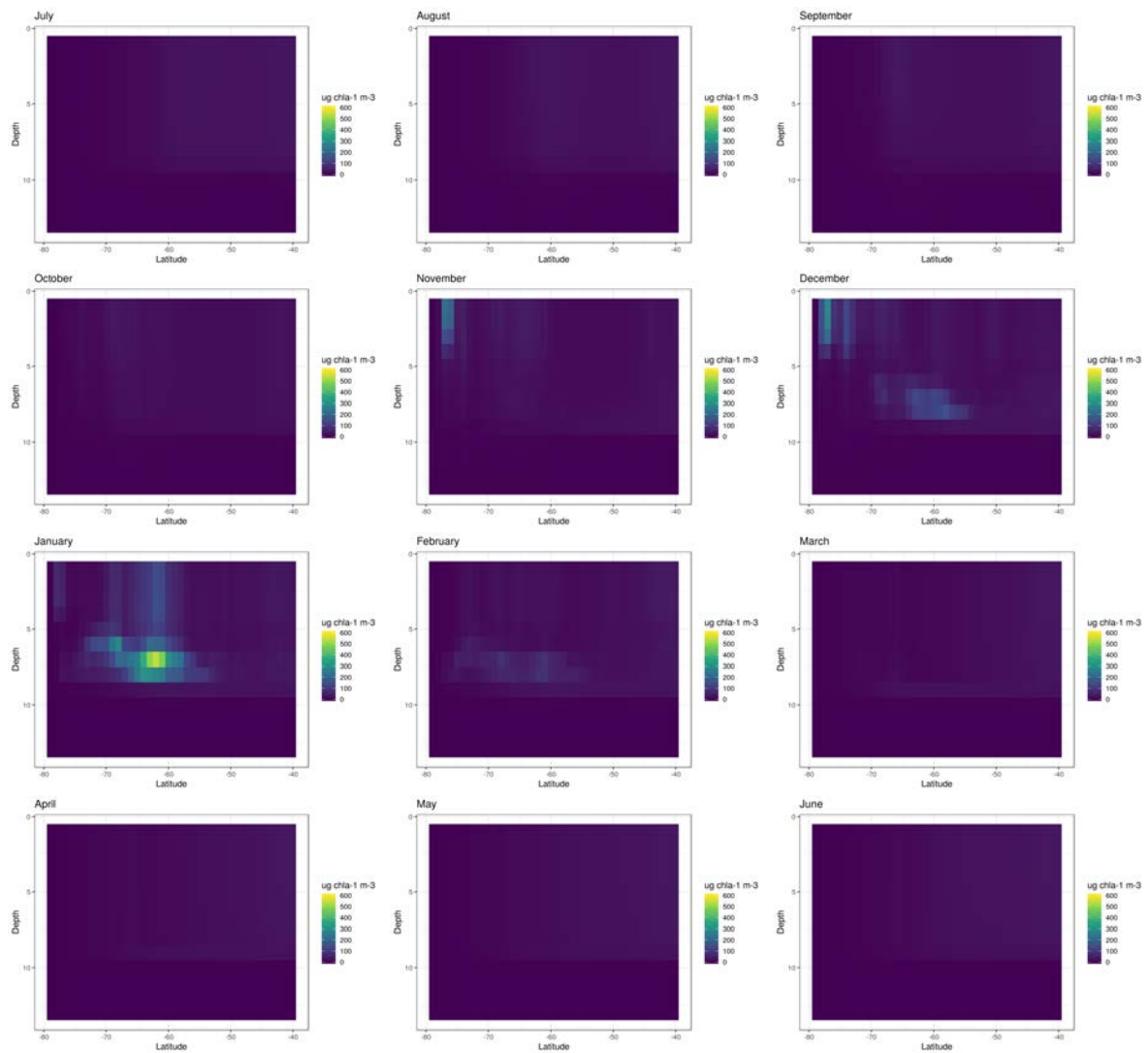


Figure 3.21: Hovmoller diagram of the vertical distribution of small phytoplankton biomass in the Southern Ocean from the BASELINE simulation.

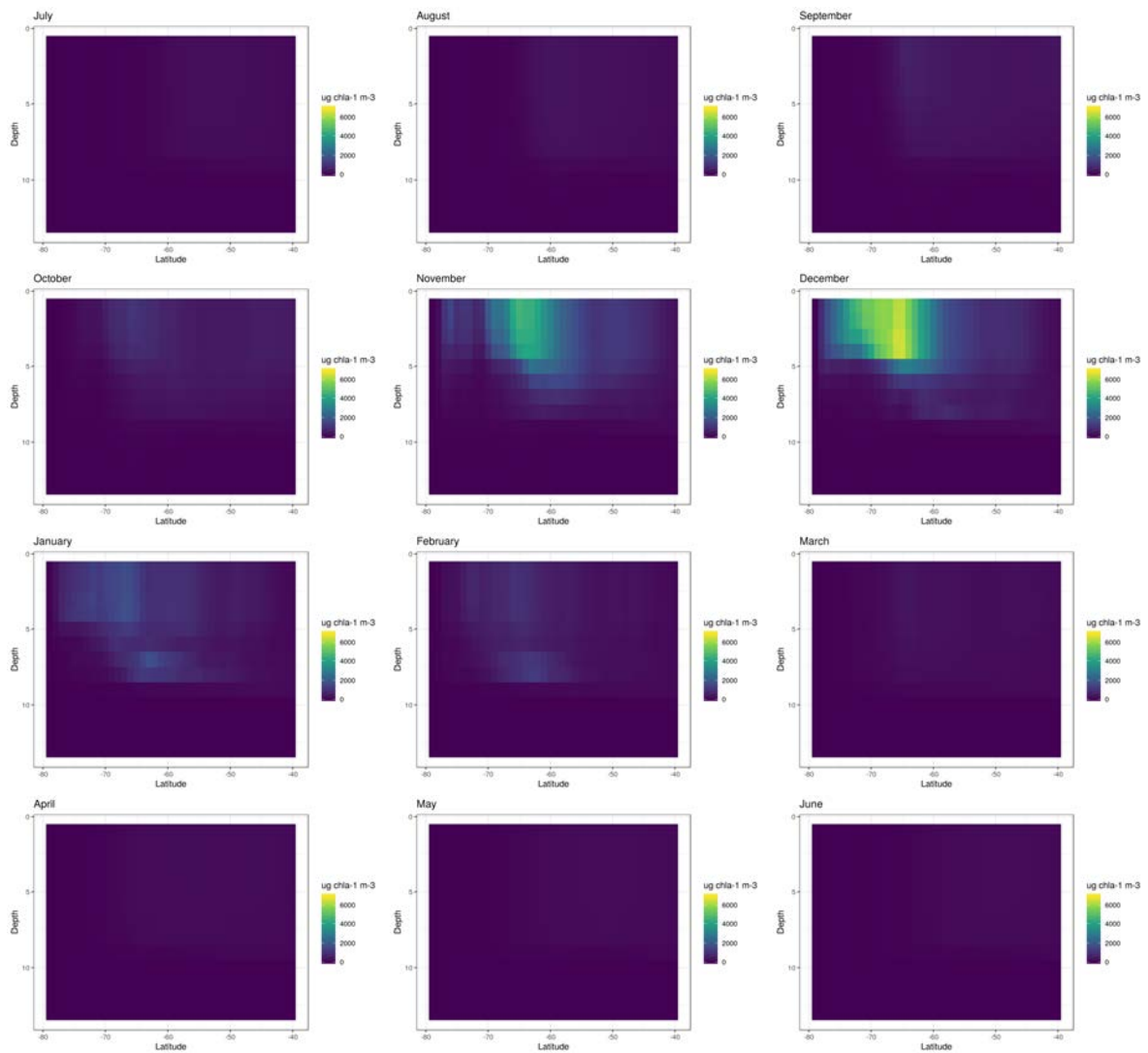
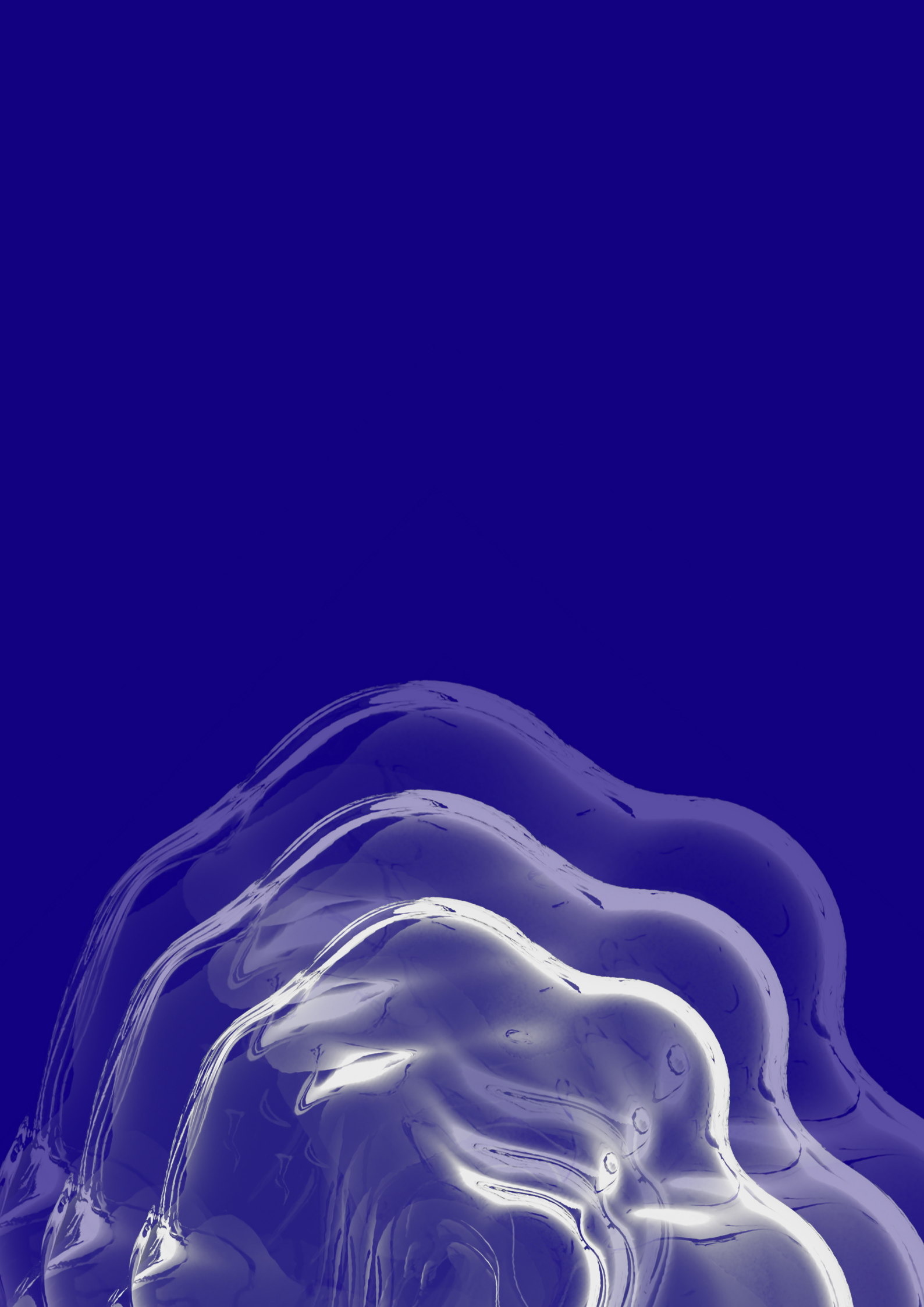


Figure 3.22: Hovmoller diagram of the vertical distribution of total chlorophyll-a biomass in the Southern Ocean from the BASELINE simulation.



Chapter 4

Global ecological modelling of marine isoprene production

Chapter 4

Global ecological modelling of marine isoprene production

Pablo Rodríguez-Ros^{1,2}, Andrew Barton², Sergio Vallina³, Stephanie Dutkiewicz⁴, Oliver Jahn⁴, Rafel Simó¹

1. Institut de Ciències del Mar. Passeig Marítim de la Barceloneta, 37-49, 08003 Barcelona, Spain
2. Integrative Oceanography Division, Scripps Institution of Oceanography, University of California San Diego
3. Gijon Oceanography Centre (IEO) - Spanish Institute of Oceanography, Gijón, Asturias, Spain
4. Department of Earth, Atmospheric and Planetary Sciences. Massachusetts Institute of Technology

*Our imagination is struck only by what is great; but the lover of natural philosophy should reflect
equally on little things.*

Alexander von Humboldt

Abstract

Isoprene is a marine biogenic trace gas which may play relevant atmospheric and climatic roles in the marine atmosphere of remote oceanic regions. Although several studies have attempted to model its cycling in the ocean, some of its production and degradation processes are still unknown. We use the phytoplankton functional type (PFT) outputs of the ecological-biogeochemical DARWIN model to explore the spatial and seasonal patterns of isoprene production in the global ocean. To this aim, we implemented PFT-specific isoprene production rates normalized per chlorophyll-*a* from laboratory experiments to the abundances of 6 PFTs predicted by DARWIN. We found that phytoplankton taxa dominating isoprene production differ among the oceanic regions. The highest levels of isoprene production occur in the productive waters of coastal areas, islands and upwelling regions. Diatoms dominate isoprene production in polar regions while prokaryotes and picoeukaryotes in the tropical oceans. We suggest that complex models like DARWIN, with a larger number of PFT's, are valid tools to disentangle the key processes and role players of isoprene production across different oceanic regions. Furthermore, we point out to the main gaps to be solved if aiming to model isoprene production using prognostic ecological-biogeochemical models.

4.1 Introduction

Isoprene is a marine trace gas produced eminently by phytoplankton all over the oceans (Carpenter et al., 2012). Despite its oceanic emission is two orders of magnitude lower than terrestrial emissions, in the atmosphere of remote oceanic regions isoprene can play a relevant role in cloud formation processes and brightness, therefore influencing climate at the local and the global scale (O'Dowd et al., 2004; Arnold et al., 2009). Despite all the previous efforts in quantifying the marine emission of isoprene (see compilation in Brüggemann et al. (2018)), there is a discrepancy up to 2 orders of magnitude (see compilation in (Brüggemann et al., 2018)). Thus, top-down estimates suggest values up to 11.6 Tg C yr⁻¹ (Arnold et al., 2009; Luo and Yu, 2010); while bottom-up approaches have provided lower values, typically ≈ 1 Tg C yr⁻¹ (Palmer and Shaw, 2005; Booge et al., 2016). This issue has been pointed to be due to a poor description and quantification of isoprene sources and sinks (Hackenberg et al., 2017; Booge et al., 2018; Brüggemann et al., 2018).

Isoprene production is directly linked to biological activity (Booge et al., 2016, 2018), and it has been confirmed for many phytoplankton species in laboratory conditions (Milne et al., 1995; Shaw et al., 2003; Bonsang et al., 2010; Colomb et al., 2009; Exton et al., 2013; Dani et al., 2017). From these studies, a set of isoprene production rates normalized per chlorophyll-a were compiled in (Booge et al., 2016), which showed discrepancies up to 2 orders of magnitude among cultured strains of the same species. Soon after that, Meskhidze et al. (2015) tested the effects of physiological stressors such as light irradiance and temperature in culture experiments. Just recently, isoprene production rates have been directly retrieved from measurements in the field by Booge et al. (2018) following the approach of Gantt et al. (2009, described in Chapter 3). Very recently, (Conte et al., 2020) have modeled the global cycle of isoprene using the culture-based isoprene production rates from Booge et al. (2016) and Meskhidze et al. (2015). Moreover, they have tested the effects of including an extra photochemical production for isoprene, using the factor provided by Brüggemann et al. (2018), and assess how this impact on the global emission values. Overall, they shed light on many uncertainties related to production and degradation of isoprene which still make it difficult to model the cycling of isoprene in the global ocean. Specifically, they suggested that isoprene production and degradation rates must be modulated by environmental and biological parameters such as temperature, light or chlorophyll-a.

Taking into account the present discrepancies among the published PFT-specific isoprene production rates, it remains essential to constrain the relative importance of each PFT to regional and global isoprene production levels. Up to date, the only study that has attempted an assessment of which phytoplankton functional type (PFT) dominates isoprene production levels on each oceanic region using a global ecological-biogeochemical model (NEMO-PISCES; Conte et al. (2020)) only included two PFT's (Diatoms and *others*). In this work, we used the DARWIN model (Dutkiewicz et al., 2019; Kuhn et al., 2019) to estimate the isoprene production of 35 phytoplankton taxa grouped in 6 major PFTs: *Prokaryotes*, *Mixotrophic dinoflagellates*, *Diatoms*, *Coccolitophores*, *Diazotrophs* and *Pico-Eukaryotes*. To this aim, we performed a set of modelling experiments using the PFT-specific isoprene production rates compiled in Booge et al. (2016) and Meskhidze et al. (2015). We evaluated the spatial patterns of isoprene production, in terms of latitude and vertical distribution,

as well as the differences among oceanic basins. Additionally, we assessed whether the PFT that dominate the phytoplankton communities in terms of chlorophyll-a levels also dominate the isoprene production. Finally, we compared the climatological values of isoprene production with an updated data set of ≈ 1400 isoprene concentration measurements across the global ocean.

4.2 Methods

4.2.1 DARWIN model setup

We used the outputs of the DARWIN model to study the global patterns of isoprene production by the different PFT's whose isoprene production has been confirmed on laboratory experiments (Meskhidze et al., 2015; Booge et al., 2016). The DARWIN model setup is the one described in Dutkiewicz et al. (2019) and Kuhn et al. (2019). It includes a total of 35 phytoplankton taxa that are grouped in 6 major PFTs: Prokaryotes (PRO), Pico-Eukaryotes (PIC), Coccolitophores (COCC), Diazotrophs (DIAZ), Diatoms (DIAT), and Mixotrophic dinoflagellates (MIX). The horizontal resolution is 1x1 degrees, the vertical scale ranges from 0 to 5700 m, and the temporal scale is climatological months. Regarding the latitudinal range, this DARWIN configuration goes from 80°S to 80°N, which covers practically all oceanic waters of the Earth ($\approx 95\%$, estimated with *marelac* package in *R*). A broader description of DARWIN can be found in the Appendix 4.4.

Table 4.1: Overview of the PFT's implemented in the configuration of the DARWIN model used in this work (Dutkiewicz et al., 2019; Kuhn et al., 2019)

Minor PFT	Major PFT	Number of minor PFT's
CHL_1 to CHL_2	Prokaryotes (PRO)	2
CHL_3 to CHL_4	Pico-eukaryotes (PIC)	2
CHL_5 to CHL_9	Coccolitophores (COCC)	5
CHL_10 to CHL_14	Diazotrophs (DIAZ)	5
CHL_15 to CHL_25	Diatoms (DIAT)	11
CHL_26 to CHL_35	Mixotrophic dinoflagellates (MIX)	10

4.2.2 Isoprene production in DARWIN

Isoprene production is implemented in DARWIN in the same way as for ROMS-BEC in Chapter 3 of this thesis. Isoprene is produced inside the plastids of phytoplanktonic organisms and released into the marine environment through their cellular membrane (Dani et al., 2017). Therefore, the isoprene production rate P_{PFT}^i ($\text{nmol m}^{-3} \text{d}^{-1}$) of each phytoplankton PFT i in DARWIN can be considered linearly coupled to their respective cellular chlorophyll concentration (B_{CHLA}^i , μgL^{-1}) through a constant rate specific to each PFT i (ρ_{CHLA}^i , $\text{mmol mgChl}^{-1} \text{d}^{-1}$) (Shaw et al., 2003; Bonsang et al., 2010; Exton et al., 2013; Meskhidze et al., 2015; Booge et al., 2016). Consequently,

the total isoprene production by all PFTs present in a community (P_{PFT} , $\text{nmol m}^{-3} \text{d}^{-1}$) is calculated as:

$$P_{\text{PFT}} = \sum_{i=1}^n \rho_{\text{CHLA}}^i \cdot B_{\text{CHL}}^i \quad (4.1)$$

Where n is the number of phytoplankton species in the community, which in the case of this work is 35 grouped in 6 major groups (Table 4.1).

4.2.3 Baseline simulation and experiments

For our BASELINE simulation, we compiled all the production rates from Meskhidze et al. (2015) and Booge et al. (2016) ($n = 124$, Table 4.4). These rates were obtained as the daily increase of isoprene per unit of chlorophyll-a during the exponential growth phase of cultured phytoplankton strains. Although this DARWIN model configuration accounts for a total of 35 PFT's, it is not possible to assign specific isoprene production rates to each of them due to the small number of published measurements and the little comprehension about the relation of these rate with environmental (e.g. temperature or light) and physiological (e.g. cell size) parameters. Thus, we averaged the individual values of $\rho_{\text{CHLA}}^{\text{PFT}}$ from Booge et al. (2016) and Meskhidze et al. (2015) that could be assigned to the six major PFT's in DARWIN (Table 4.1), and implemented them following equation 4.1. Specifically, taking Table 4.4 as a reference, we used *Bacillariophyceae* for DIAT ($\rho_{\text{CHLA}}^{\text{DIAT}}$), *Prasinophyceae* for PIC ($\rho_{\text{CHLA}}^{\text{PIC}}$), *Cyanophyceae* (*Prochlorococcus* + *Synechococcus*) for PRO ($\rho_{\text{CHLA}}^{\text{PRO}}$), *Prymnesiophyceae* for COCC ($\rho_{\text{CHLA}}^{\text{COCC}}$), and *Dinophyceae* for MIX ($\rho_{\text{CHLA}}^{\text{MIX}}$). Finally, for DIAZ ($\rho_{\text{CHLA}}^{\text{DIAZ}}$) we used the isoprene production rates for *Trichodesmium* from Bonsang et al. (2010), which are the only ones published up to date for this PFT.

Furthermore, we ran three experiments (Table 4.2) to assess the uncertainty associated with the implementation of these parameters in DARWIN. We first tested the effects on isoprene production of assuming that all PFT's produce the same amount of isoprene per unit of chlorophyll-a (CHLA, Table 4.2). For this, we averaged all $\rho_{\text{CHLA}}^{\text{PFT}}$ compiled in Table 4.4, obtaining a value of $4.53 \text{ mmol mgChl}^{-1} \text{d}^{-1}$. Subsequently, in the experiments named RHO.MAX and RHO.MIN (Table 4.2), we implemented in equation 4.1 the minimum and maximum published values of $\rho_{\text{CHLA}}^{\text{PFT}}$ values (Booge et al. (2016), Meskhidze et al. (2015), Arnold et al. (2009)).

Table 4.2: Overview of model experiments using DARWIN model.

Run name	$\rho_{\text{CHLA}}^{\text{DIAT}}$	$\rho_{\text{CHLA}}^{\text{PRO}}$	$\rho_{\text{CHLA}}^{\text{COCC}}$	$\rho_{\text{CHLA}}^{\text{DIAZ}}$	$\rho_{\text{CHLA}}^{\text{PIC}}$	$\rho_{\text{CHLA}}^{\text{MIX}}$
	$\text{mmol mgChl}^{-1} \text{d}^{-1}$					
BASELINE	3.79	5.38	5.16	3	12.46	6.94
CHLA	4.53					
RHO.MAX	28.48	11.76	15.36	4.7	32.16	27.6
RHO.MIN	1.12	1.4	1	1.6	1.4	4.56

4.2.4 Sensitivity experiments

To assess the sensitivity of simulated isoprene production to model parameters, we conducted a sensitivity analysis (SA) by increasing/decreasing each parameter (k) by 50% of the BASELINE configuration described in Table 4.2). Since the focus of this study was isoprene production, we restricted the analysis to the upper 20 meters of the water column. Sensitivity was quantified as a change in total annual production of isoprene integrated over the upper 20 meters, since (1) it reflects the available isoprene to be eventually transferred to the atmosphere, and (2) isoprene production (P_{PFT}) is typically constrained to surface waters (Figure 4.4). The SA index, describing the percentage change of a target model output variable when varying an initial model parameter, was taken from Le Clainche et al. (2004) and is defined as follows:

$$S_k = \frac{P_{PFT_{k_{50+}}} - P_{PFT_{k_{50-}}}}{P_{PFT_{Baseline}}} * 100 \quad (4.2)$$

Where $P_{PFT_{k_{Baseline}}}$, $P_{PFT_{k_{50+}}}$ and $P_{PFT_{k_{50-}}}$ are the annual total productions of isoprene integrated over the upper 20 meters obtained for the each sensitivity simulation: BASELINE (reference value of parameter k), 50% increase in the parameter k ($k_{50+} = 1.5 * k$), and 50% decrease in the parameter k ($k_{50-} = 0.5 * k$).

4.2.5 Data of isoprene concentration

We compiled data of isoprene measurements from the cruises listed in Table 4.3 to test the predictive capacity of isoprene production, chlorophyll-a concentration and sea surface temperature from DARWIN for isoprene concentration levels. Measurements from TransPEGASO, PEGASO and ACE cruises have been broadly described in Chapters 1, 2 and 3 of this thesis. The measurements taken during the BIOGAPS expedition near Moorea Island (French Polynesia) were conducted following the same instrumental setup and analytical procedure (Chapter 5). The information regarding the methodology followed on the rest of cruises can be found in their respective publications, which are listed in the last column of Table 4.3. Additionally, this dataset aims to contribute to a better description of the global spatial and temporal patterns of isoprene concentration and to constrain the uncertainty in our models parameters. Moreover, this dataset will serve as a resource to be used in the development and validation processes of future modelling works.

4.3 Results and Discussion

4.3.1 Assessment of published isoprene production rates

The specific production rates of isoprene (ρ_{CHLA}^{PFT}) compiled for this work amount 124 data (Figure 4.1, Table 4.4). *Prasinophytes* ($n = 3$) shows the highest mean values of ρ_{CHLA}^{PFT} , and *Cyanophyceae*

Table 4.3: Isoprene concentration measurements compiled for this work.

Mean [Min - Max] (pM)	Oceanic region	Cruise	Reference
10.9 [1.0 - 88.4]	Southern Ocean Circumnavigation	ACE Expedition	Rodríguez-Ros et al. (2020a)
22.6 [1.6 - 93.5]	South Atlantic Ocean	PEGASO cruise	Rodríguez-Ros et al. (2020a)
37.5 [9.8 - 115.8]	South Atlantic Ocean	TransPEGASO cruise	Rodríguez-Ros et al. (2020a)
37.0 [16.0 - 82.4]	Mediterranean Sea	HOTMIX cruise	Cortés and Simó (Non-published)
18.72 [14.48 - 22.39]	Moorea, French Polynesia	BIOGAPS Expedition	Masdeu and Simo (Non-published)
11.21 [0.28 - 93.51]	South Atlantic Ocean	AMT22 cruise	Hackenberg et al. (2017)
9.61 [0.13 - 123.52]	South Atlantic Ocean	AMT23 cruise	Hackenberg et al. (2017)
5.35 [0.03 - 146.46]	Arctic Ocean	ACCACIA1 cruise	Hackenberg et al. (2017)
21.19 [2.41 - 70.61]	Arctic Ocean	ACCACIA2 cruise	Hackenberg et al. (2017)
88.34 [37.26 - 144.10]	NW Pacific	KT-09-5	Ooki et al. (2015)
26.44 [6.63 - 73.15]	NW Pacific	KH-08-2	Ooki et al. (2015)
25.64 [2.16 - 74.7]	NW Pacific Indian Ocean to Southern Ocean	KH-09-5	Ooki et al. (2015)
26.07 [13.16 - 50.17]	NW Pacific	KH-10-1	Ooki et al. (2015)
16.67 [1.33 - 71.52]	NW Pacific Bering Sea and Arctic Ocean	MR12-E03	Ooki et al. (2015)
23.46 [8.40 - 47.80]	Tropical Pacific Ocean	R/V Science	Li et al. (2019)
24.12 [1.25 - 81.26]	Tropical Pacific Ocean	SPACES, OASIS, ASTRA-OMZ	Booge et al. (2018)
2.40 [1.02 - 5.09]	Arctic Ocean	Transsiz	V. Gros (Non-published)
30.10 [8.70 - 83.28]	Arctic Ocean	ARKXXV	V. Gros (Non-published)
13.53 [4.82 - 39.07]	Antarctic Ocean	ANDREXII	Wohl et al. (2020)

($n = 6$) and *Chlorophyceae* ($n = 3$) the lowest (Figure 4.1a). Note, however, that in both cases the number of $\rho_{\text{CHLA}}^{\text{PFT}}$ estimates is very small (Figure 4.1a). Diatoms are the PFT with the highest number of estimates of $\rho_{\text{CHLA}}^{\text{PFT}}$ ($n = 75$). When splitting the estimates of $\rho_{\text{CHLA}}^{\text{PFT}}$ by species, differences are much larger (Figure 4.1b), even of one order of magnitude among strains (Figure 4.1b). This fact was already pointed out by Booge et al. (2018), who suggested that this is due to the different environmental forcing conditions experienced by the phytoplankton cells during the previous acclimation process. Among all estimates, *Symbiodinium sp* ($n = 4$), *Emiliana huxleyi* ($n = 5$) and *Chatoceros neoglacialis* ($n = 2$) are the species that show the largest intraspecific differences (Figure 4.1b, Table 4.4). However, we can not be certain that the rest of species would not show similar variability, because species with multiple experimental estimates are very scarce (Figure 4.1.B and C). The maximum n of a $\rho_{\text{CHLA}}^{\text{PFT}}$ is 29 for *Thalassiosira pseudonana* and *Thalassiosira weissflogii* ((Meskhidze et al., 2015)).

Values of $\rho_{\text{CHLA}}^{\text{PFT}}$ increased exponentially with temperature (Figure 4.1c) and light intensity (Figure 4.1d) until reaching a threshold value (respectively, $\approx 26^\circ\text{C}$ and $300 \mu\text{E s}^{-1} \text{m}^{-2}$) beyond which $\rho_{\text{CHLA}}^{\text{PFT}}$ started to decrease. Unfortunately, the culture conditions of many of the experiments were not reported, making this relationship still preliminary. Most of these values came from Meskhidze et al. (2015), who tested the changes of $\rho_{\text{CHLA}}^{\text{PFT}}$ along gradients of temperature (for two diatom species: *Thalassiosira weissflogii* and *Thalassiosira pseudonana*) and light irradiance (for *Thalassiosira eissflogii* and *Thalassiosira pseudonana*, and also for one prymnesiophyte: *Pleurochrysis carterae*; two dinoflagellates: *Karenia brevis* and *Prorocentrum minimum*; and one cryptophyte: *Rhodomonas salina*). They found an enhancement of $\rho_{\text{CHLA}}^{\text{PFT}}$ with increasing temperature and light intensity until reaching a saturation limit, which was different for each tested strain. Therefore, probably a much clearer relationship between $\rho_{\text{CHLA}}^{\text{PFT}}$ and light and/or temperature will appear when more species are tested.

We also explored the relationship of $\rho_{\text{Cells}}^{\text{PFT}}$ with cell volume, firstly observed by Bonsang

et al. (2010) with a limited set of strains. When possible, we attributed cell volumes to the aforementioned assayed species using the tables from Harrison et al. (2015) (Figure 4.1e). We found a relationship similar but weaker than that proposed by Bonsang et al. (2010) ($r^2 = 0.77$), which suggests that isoprene production rates could be parameterized as a function of cell size. Unfortunately, the low numbers of available $\rho_{\text{Cells}}^{\text{PFT}}$ concomitant with cell sizes makes this implementation in prognostic ecological models still uncertain.

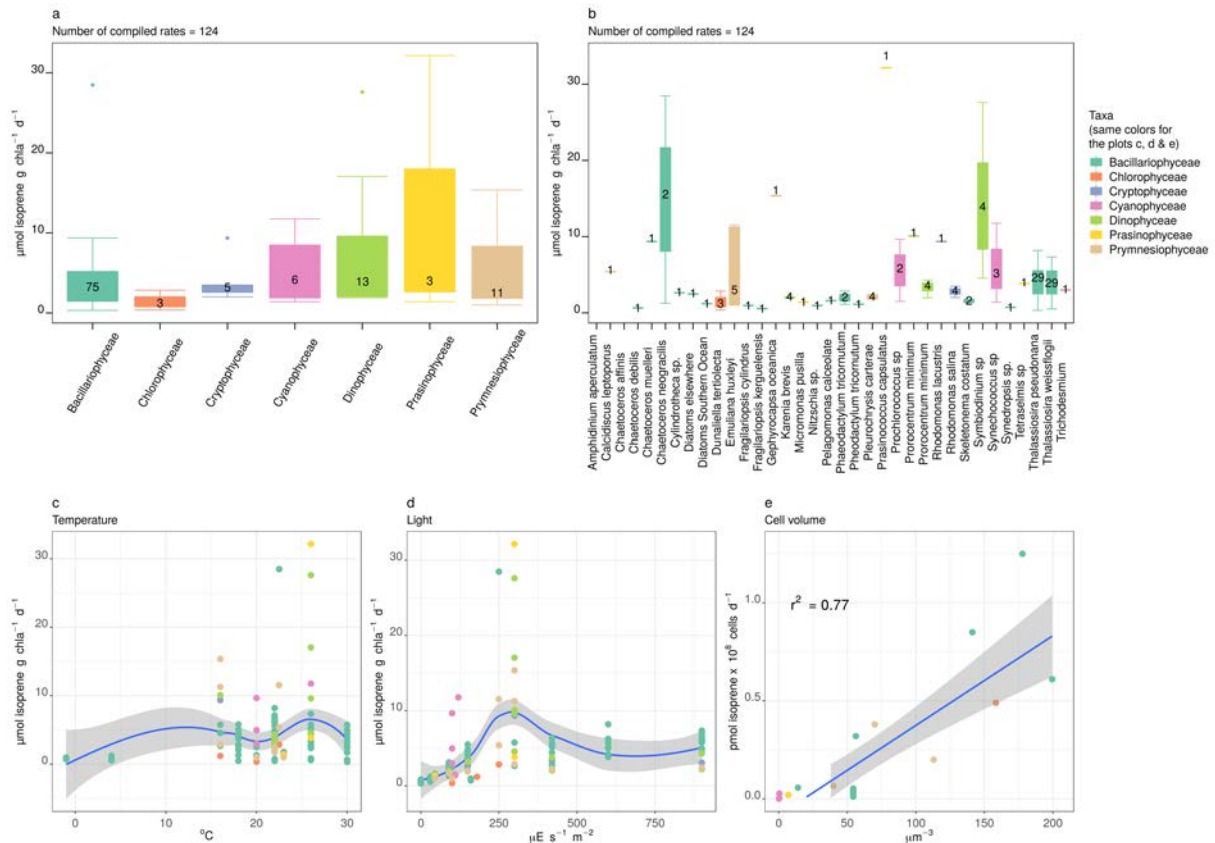


Figure 4.1: Isoprene production rates normalized by chlorophyll-a from lab experiments by taxon (a), by species (b), and a combination of both (c). Isoprene production rates vs (d) temperature in the cultures, and vs (e) light conditions in the cultures. (e) Isoprene production rates per cell vs cell volume. The values used for this Figure can be found in Table 4.4.

4.3.2 Seasonality and spatial distribution of isoprene production in the global ocean

To analyze the seasonal patterns of isoprene production on a monthly basis from our BASELINE simulation (Table 4.2), we integrated the isoprene production over the first 20 meters of the water column for each PFT (Figure 4.2). Overall, we did not observe a strong seasonality for the specific isoprene production of the following PFTs: COCC, DIAZ, MIX, PIC and PRO (Figure 4.2). In contrast, isoprene produced by DIAT shows a clear seasonal behaviour, with higher production rates during summer in the Southern Hemisphere (Figure 4.2). This is not surprising since species belonging to DIAT dominate in polar waters of the Southern Ocean, blooming in the austral summer (Saavedra-Pellitero et al., 2014; Balch et al., 2016). Along the climatological year, only PIC and PRO dominate

over DIAT at the global scale during boreal summer months (May – September). DIAZ are by much the lowest producers of isoprene in the global surface ocean (Figure 4.2).

Regarding the spatial distribution, the highest isoprene production rates are found in highly productive waters from upwelling regions and coastal areas (Figure 4.11 and 4.3). A significant portion of the total isoprene production budget takes place in the temperate regions around the latitudes of 40 °S and 40 °N, as observed in models for production Conte et al. (2020) and in models and data compilations for concentration (Luo and Yu, 2010; Ooki et al., 2015; Booge et al., 2016). Our results also agree with (Conte et al., 2020) in suggesting that oligotrophic oceans are the least important areas in terms of total isoprene production along the climatological year. In contrast, we observed an intense hot-spot of isoprene production in the eastern tropical Atlantic which was not detected in (Conte et al., 2020).

Looking at the relative contribution of each PFT to total isoprene production levels across the global surface ocean (Figure 4.3), Isoprene production by DIAT is clearly constrained within high latitudes of Northern and Southern Hemispheres, being more intense in the North Pacific area. Production of isoprene by DIAZ essentially occurs in warm waters at low and middle latitudes, being specially high in waters of the North Indian Ocean. Isoprene production by COCC is higher in the eastern tropical Atlantic, contributing to the aforementioned hot-spot in production; it is also higher in the area of the Southern Ocean known as the "Great Calcite Belt" (Balch et al., 2011). Regarding isoprene production by MIX, it occurs over most of the ocean with the exception of the subtropical gyres, and also shows higher values in the North Atlantic Ocean, the Southern Ocean and north of Australia. Isoprene production by PRO, it is dominant in tropical and sub-tropical waters (Figure 4.2).

In our BASELINE simulation, isoprene production is confined to surface waters and rarely present at deeper than 100 meters (Figure 4.4). Moreover, the most relevant areas in terms of annual isoprene production are the transitional waters of the sub-polar and polar fronts in the Southern Ocean. Also, isoprene is highly produced in the Arctic Ocean and Equatorial waters. In contrast, the oligotrophic subtropical gyres are the weakest contributors to global isoprene production, and show maximum production in deeper waters, co-occurring with deep chlorophyll maxima, probably due to the strong stratification and the deeper penetration of light.

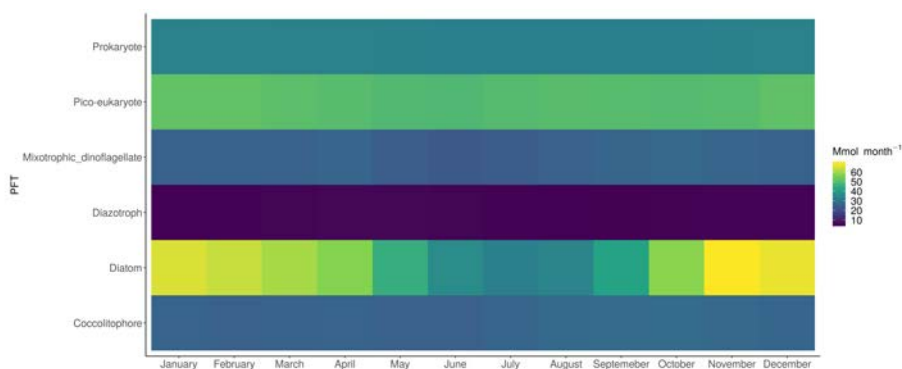


Figure 4.2: Seasonality of isoprene production in the surface global ocean (0-20 m) for each PFT (BASELINE simulation, Table 4.2).

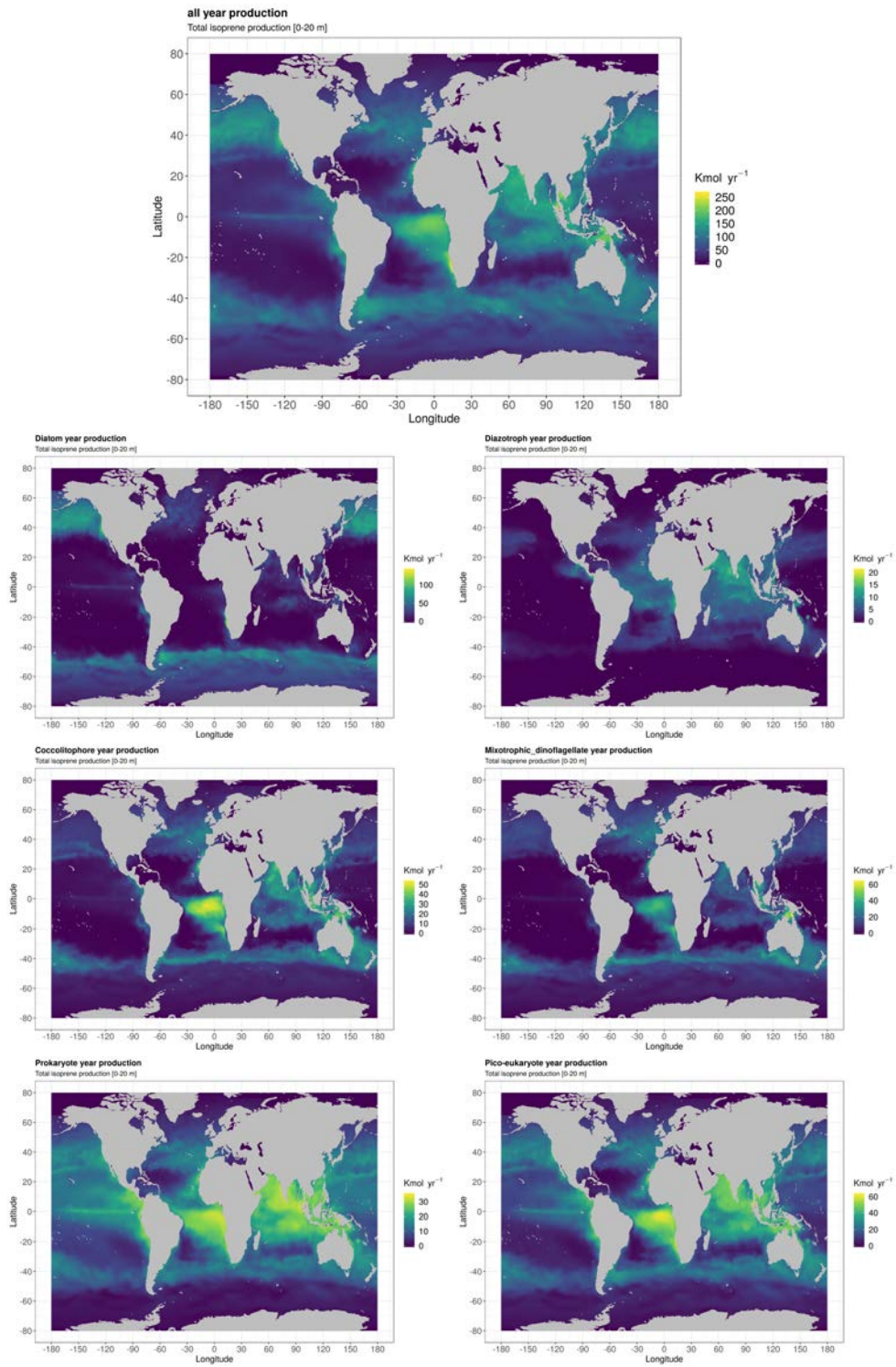


Figure 4.3: Total surface isoprene production (0-20 meters depth) along the full climatological year for all PFTs (TOP) and each of them individually (BASELINE simulation, Table 4.2).

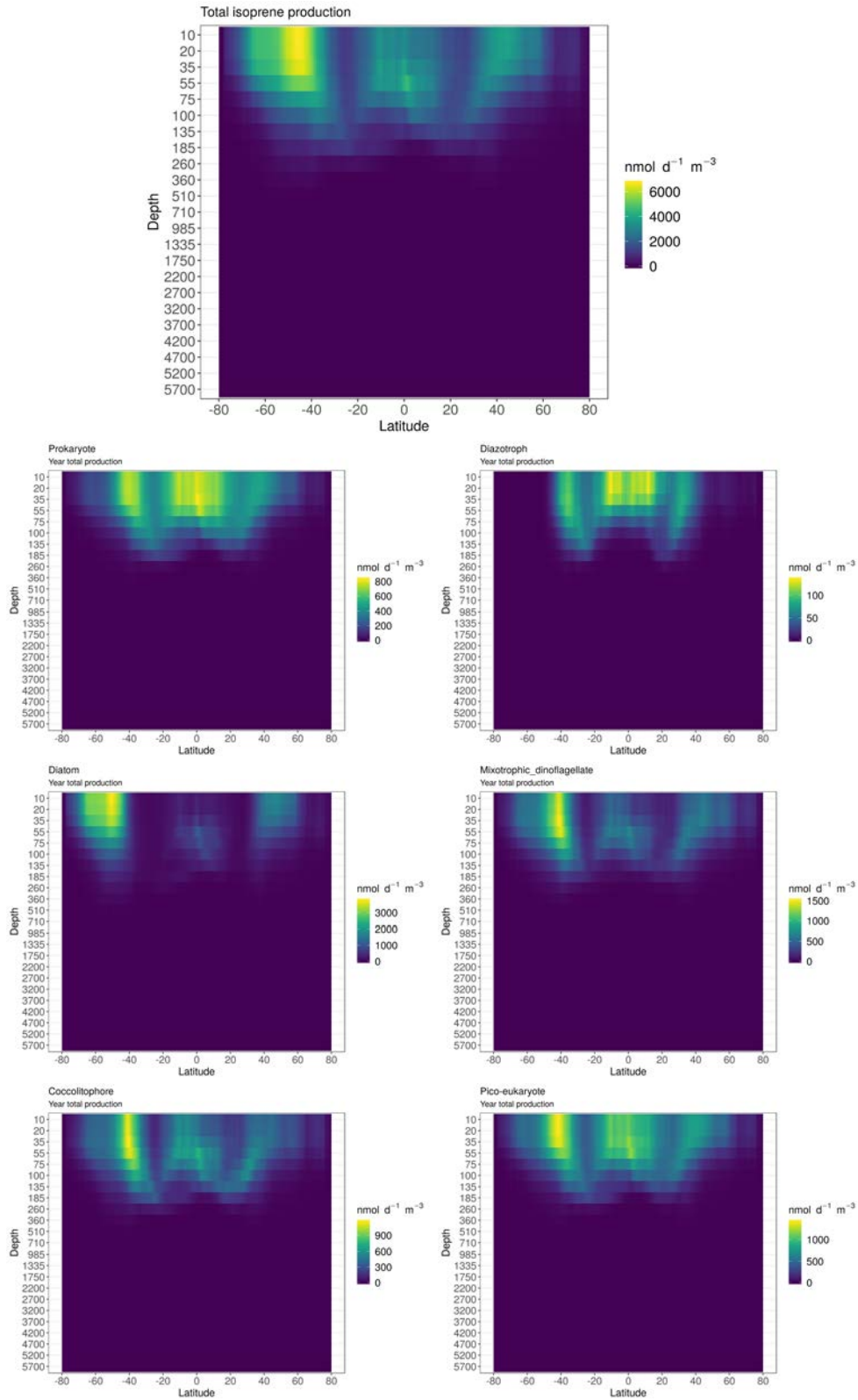


Figure 4.4: Hovmoller diagrams of the vertical distribution of isoprene production integrated along the full climatological year for all PFTs (TOP) and each of them individually (BASELINE simulation, Table 4.2).

4.3.3 Which PFT dominates isoprene production in each oceanic region?

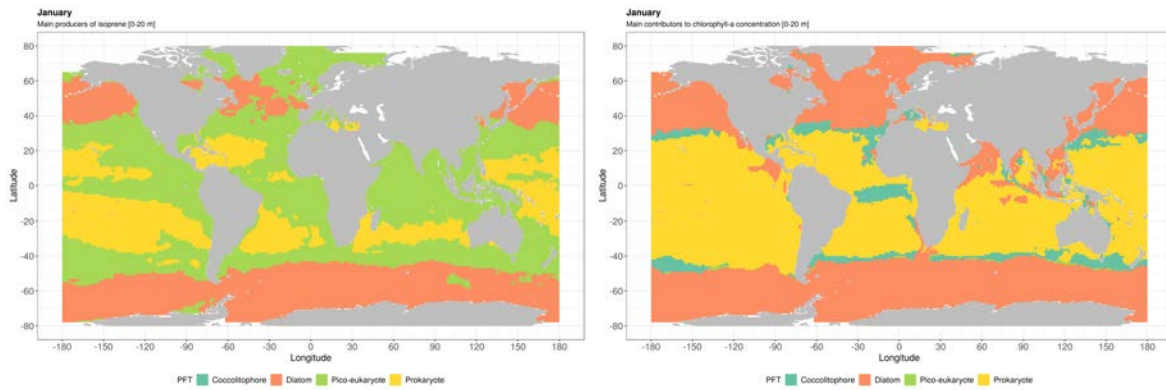
Figure 4.5 compares the PFT that dominate isoprene production with the PFT that dominate chlorophyll-a concentrations in the BASELINE simulation. Over the climatological year, PRO (*yellow* in Figure 4.5) dominate isoprene production in surface waters of the oligotrophic oceans, mainly confined to the subtropical gyres. PIC (*green* in Figure 4.5) dominate the production of isoprene in coastal areas of tropical and sub-tropical latitudes, but also in polar regions and open ocean regions. The fact that PIC make a large and widespread contribution to isoprene production but only dominate chlorophyll-a levels in some locations during summer is due to their high $\rho_{\text{CHLA}}^{\text{PIC}}$ (Table 4.2). DIAT (*orange* in Figure 4.5) are the dominant PFT in polar regions, showing a larger contribution to chlorophyll-a in spring and summer in both hemispheres. Despite DIAT dominate the phytoplankton communities in coastal upwelling areas, PIC dominate the production of isoprene. Regarding COCC (*dark green* in Figure 4.5), despite being the largest contributor to total chlorophyll-a levels in the Great Calcite Belt and the eastern tropical Atlantic, their dominance of isoprene production is rare.

The BASELINE simulation results provide a total production of isoprene in the surface ocean (0-50 m) that amounts $1.43 \text{ Tg C yr}^{-1}$ while the CHLA, RHO.MIN, RHO.MAX experiments gave values of 1.15, 0.24 and $5.88 \text{ Tg C yr}^{-1}$, respectively. This remarkable difference up to one order of magnitude is the consequence of the poorly constrained isoprene production rates from the different PFT's. Looking into the spatial patterns of the total production in our BASELINE simulation, the highest isoprene production rates are placed in the latitudinal band of 30-60°S, while the lowest are found in polar regions, mainly in waters of the Arctic Ocean (>60°N) (respectively, 8.25 and $1.34 \mu\text{mol m}^{-2} \text{ yr}^{-1}$, Figure 4.6a, left). DIAT is the largest contributor to isoprene production at a global scale (Figure 4.6a, right). While DIAT dominate production in latitudes higher than 30°N and 30°S, PIC dominate the tropical regions (from 30°S to 30°N), which represent a larger area than the polar oceans. As expected, the MAX experiment (Table 4.2) shows an increase in isoprene production in all latitudinal bands, peaking in 30-60°S ($39.72 \mu\text{mol m}^{-2} \text{ yr}^{-1}$, Figure 4.6a, left). In contrast to BASELINE, MAX replaces the dominance of PIC with PRO in tropical waters, except in the bands where DIAT dominate (Figure 4.6a, right). In the MIN experiment, isoprene production decreases one or two orders of magnitude at all latitudes (Figure 4.6a, left). Similarly to BASELINE, DIAT are the main contributors to isoprene production in the polar oceans and PIC dominate over the tropical regions (Figure 4.6a, right). Finally, the CHLA experiment gives intermediate levels of isoprene production closer to BASELINE than MIN or MAX (Figure 4.6a, left). However, MIX replace DIAT as the global dominant PFT because they contribute the most to isoprene production in latitudes higher than 30°N and in the band of 30-60°S (Figure 4.6a, right). Altogether, the only region where the same PFT dominates isoprene production in the four experiments is the high latitude Southern Ocean (>60°S), where DIAT are always the most important producers. In the tropical regions (30°N–30°S) it is not clear whether PRO or PIC dominate isoprene production.

Finally, we explored whether or not the PFT that dominates isoprene production also dominates the phytoplankton community in terms of its relative contribution to chlorophyll-a levels, according to DARWIN (Figure 4.12). The analysis reveals that, along the climatological year, a coincidence occurs only in 20-30% of the global surface ocean: PRO (mainly placed in the tropical

regions) and DIAT (in the Southern Ocean in summer) are the PFTs who dominate both, isoprene production and chlorophyll-a concentration (Figure 4.12). In 70–80% of the global ocean the PFT that contributes the most to isoprene production is not the same as the PFT that dominates the phytoplankton community. PIC and DIAT are the PFTs that typically dominate isoprene production without being the most abundant phytoplankton. DIAT, PRO and COCC are the PFTs that most often dominate chlorophyll-a concentration but not isoprene production.

Winter



Summer

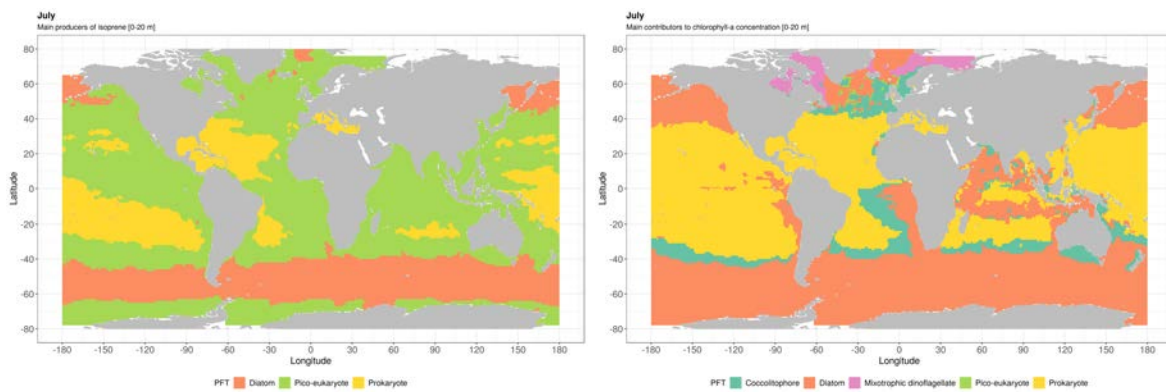


Figure 4.5: Dominance of isoprene production (top) and chlorophyll-a levels (bottom) of each PFT implemented in DARWIN for January and July (BASELINE simulation, Table 4.2).

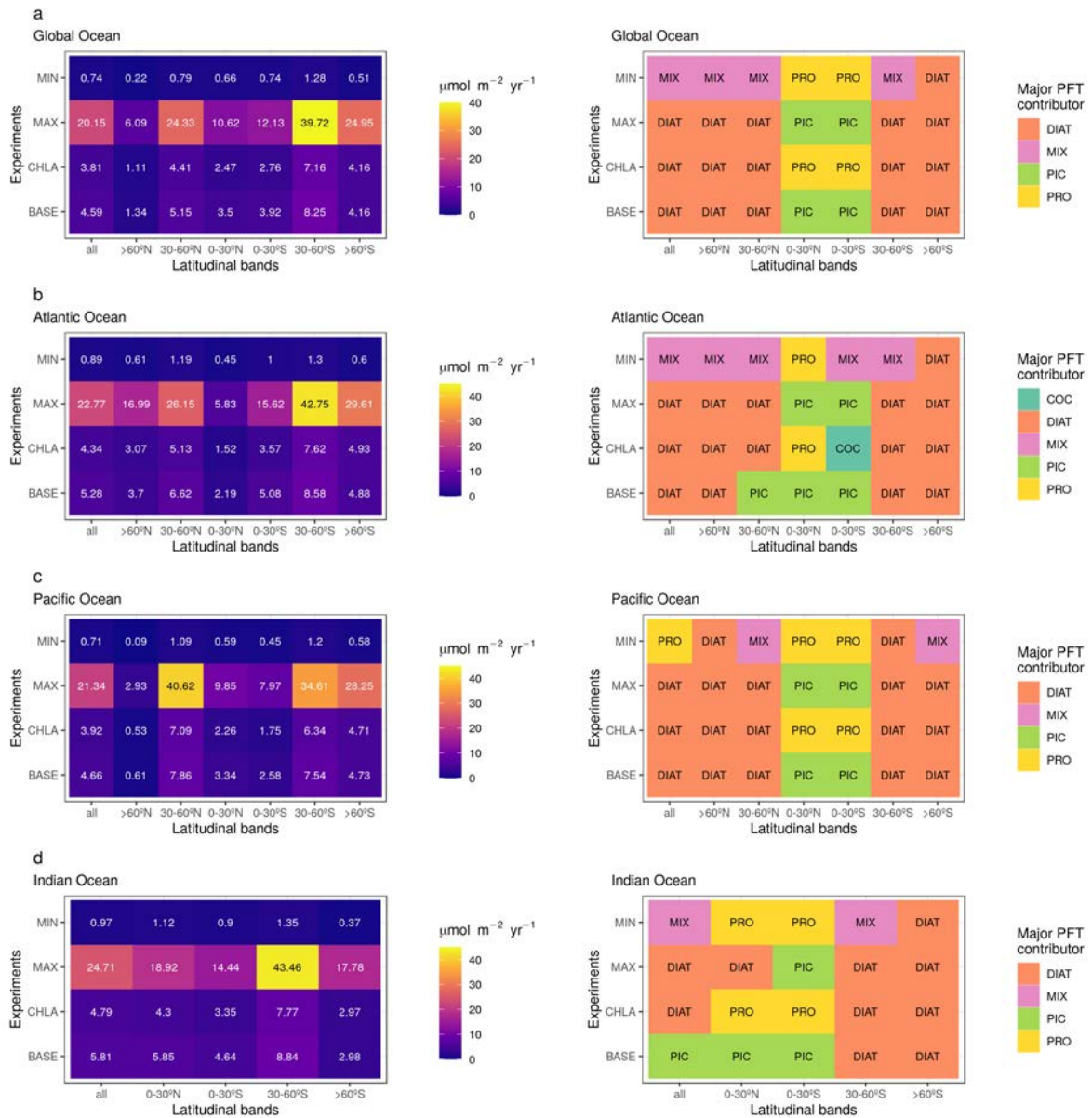


Figure 4.6: Results of the experiments described in Table 4.2. for the global ocean and each of its ocean basins (**A**: Global Ocean, **B**: Atlantic, **C**: Indian, and **D**: Pacific). The right column shows the annual integrated total production of isoprene per latitudinal bands. The left column depicts the DARWIN-predicted dominant PFT in terms of isoprene production in the first 20 meters of the water column during the climatological year.

4.3.4 Sensitivity analysis

Our sensitivity analysis (SA) results show the large differences among the effects that the variation in the values of the PFT-specific isoprene production rates trigger in the total production of isoprene (Figure 4.7). Thus, changes in $\rho_{\text{CHLA}}^{\text{DIAZ}}$ only affect the total production of isoprene by less than 3%. In contrast, $\rho_{\text{CHLA}}^{\text{DIAT}}$ triggers the strongest effects (above 30%). In between, variations in $\rho_{\text{CHLA}}^{\text{COC}}$, $\rho_{\text{CHLA}}^{\text{MIX}}$, $\rho_{\text{CHLA}}^{\text{PIC}}$ and $\rho_{\text{CHLA}}^{\text{PRO}}$ give intermediate values of SI (9.15 to 12.9%).

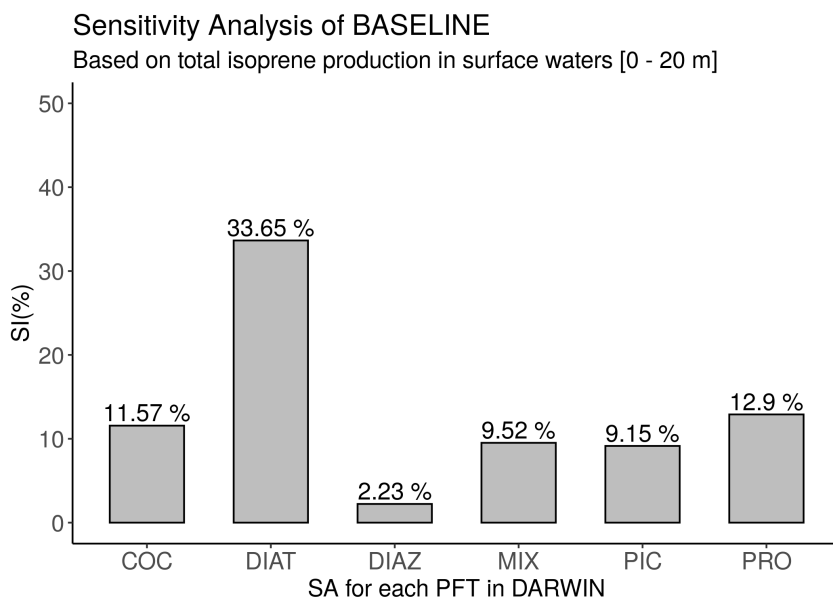


Figure 4.7: Results from the Sensitivity Analysis for our BASELINE simulation. The target variable to measure the effects of varying each parameters by -50% or +50% is the integrated production of isoprene per year in surface waters (0-20 meters).

4.3.5 Isoprene production and concentration in the global ocean

In our data-set of isoprene concentration ($n = 6,000$ raw measurements), there is a clear over-representation of measurements in the Atlantic Ocean, which contrasts with the data scarcity in the Pacific and Indian Oceans (Figure 4.8a). The Southern Ocean has been a region traditionally poorly explored in terms of isoprene concentration measurements (Kameyama et al., 2014; Ooki et al., 2015; Hackenberg et al., 2017). However, in this work, we include our recently published data from TransPEGASO (2014), PEGASO (2015), ACE (2016-2017) (Rodríguez-Ros et al., 2020a,b) and ANDREXII (Wohl et al., 2020) cruises, which have significantly increased the size of the data set in the Southern Ocean. Overall, we observe peaks of isoprene concentration in the Equatorial regions, slightly shifted to northern latitudes (Figure 4.8a and b). High isoprene concentrations are also present in upwelling coastal regions (Mauritanian upwelling, TransPEGASO Cruise) or island blooms in the Southern Ocean (e.g. South Georgia Islands during PEGASO cruise (Nunes et al., 2019a)). To avoid over-representation of locations with repeated measurements, we binned our data by month and gridded them to the cells of 1×1 degrees used in the DARWIN model. After doing so, our sample size fell to $\approx 1,400$ observations. Overall, there is a lack of isoprene measurements all

over the oceans. Trace gas research requires a large number of measurements, both in surface waters and deeper levels of the ocean (Carpenter et al., 2012), not only for the development of simple statistical models, like the ones described in this thesis (Chapters 1 and 2) and previous works (Ooki et al., 2015; Hackenberg et al., 2017); but also to validate the results of global or regional models such as DARWIN or ROMS-BEC (Chapter 3). Consequently, moving towards the development or improvement of any regional or global modelling approach of marine isoprene cycling requires an increase in the current number of measurements of isoprene concentration and ancillary parameters.

We compared the observations of isoprene concentration with isoprene production rates, chlorophyll-a concentration and sea surface temperature from the DARWIN model (Figure 4.9). Although the isoprene concentration is positively correlated with isoprene production rates, sea surface temperature and chlorophyll-a concentration (Figure 4.9a, b and c; respectively), the variance of isoprene concentration explained by any of the three variables is very low (<5%). The fact that modeled isoprene production explains very little of the variance of isoprene concentration indicates that loss processes (ventilation, degradation, mixing) play a big role in regulating isoprene concentration in the surface ocean. Usually, the highest isoprene concentrations are placed in locations where PIC, DIAT and PRO dominate isoprene production. In cold waters where DIAT dominate, isoprene concentrations tend to be lower than in warmer waters where PIC and PRO are the most important isoprene producers (Figure 4.9b).

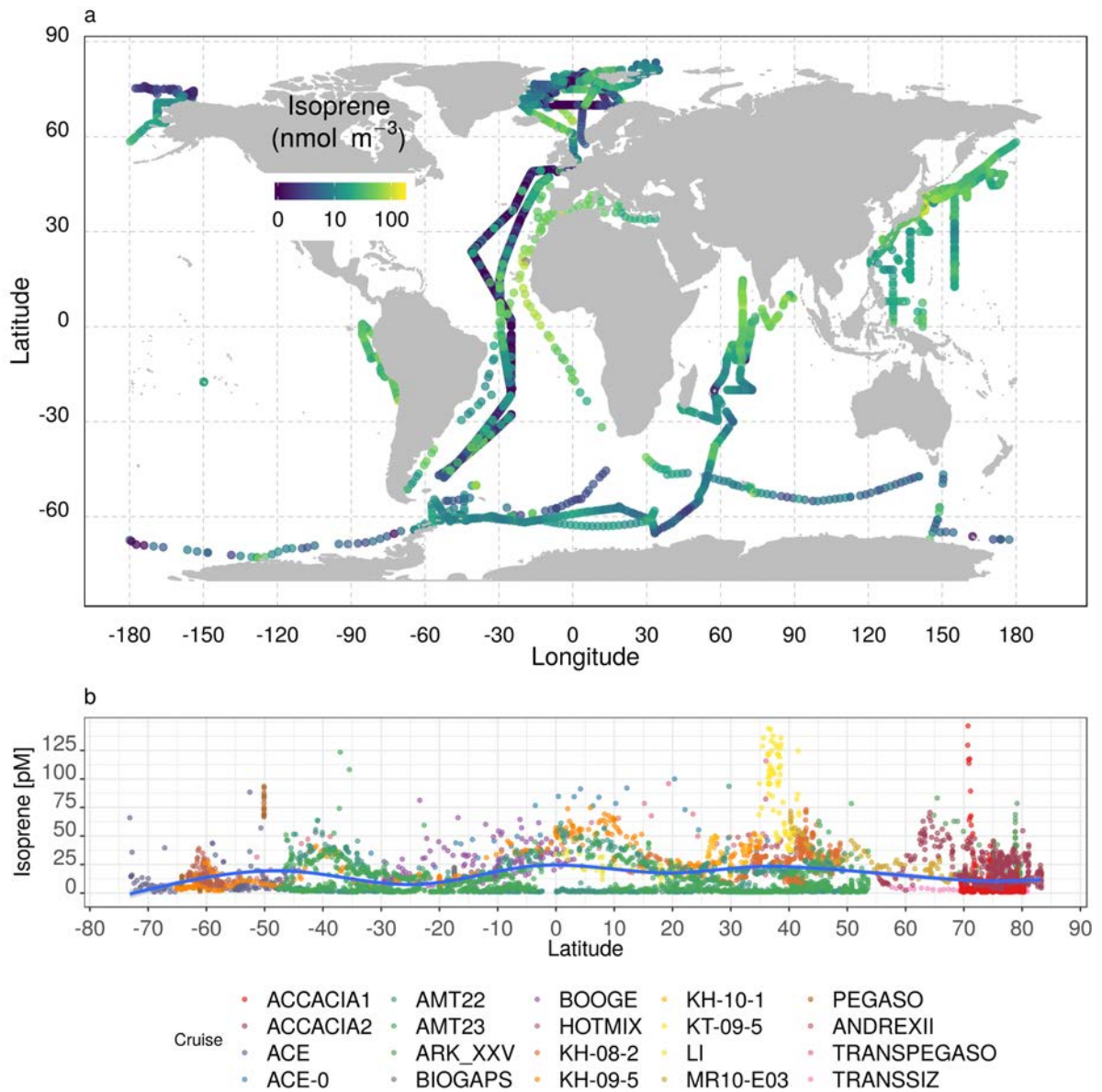


Figure 4.8: Global data-set of isoprene published measurements from cruises compiled in Table 4.3. (a) measurement locations and values. (b) Latitudinal distribution of isoprene concentrations.

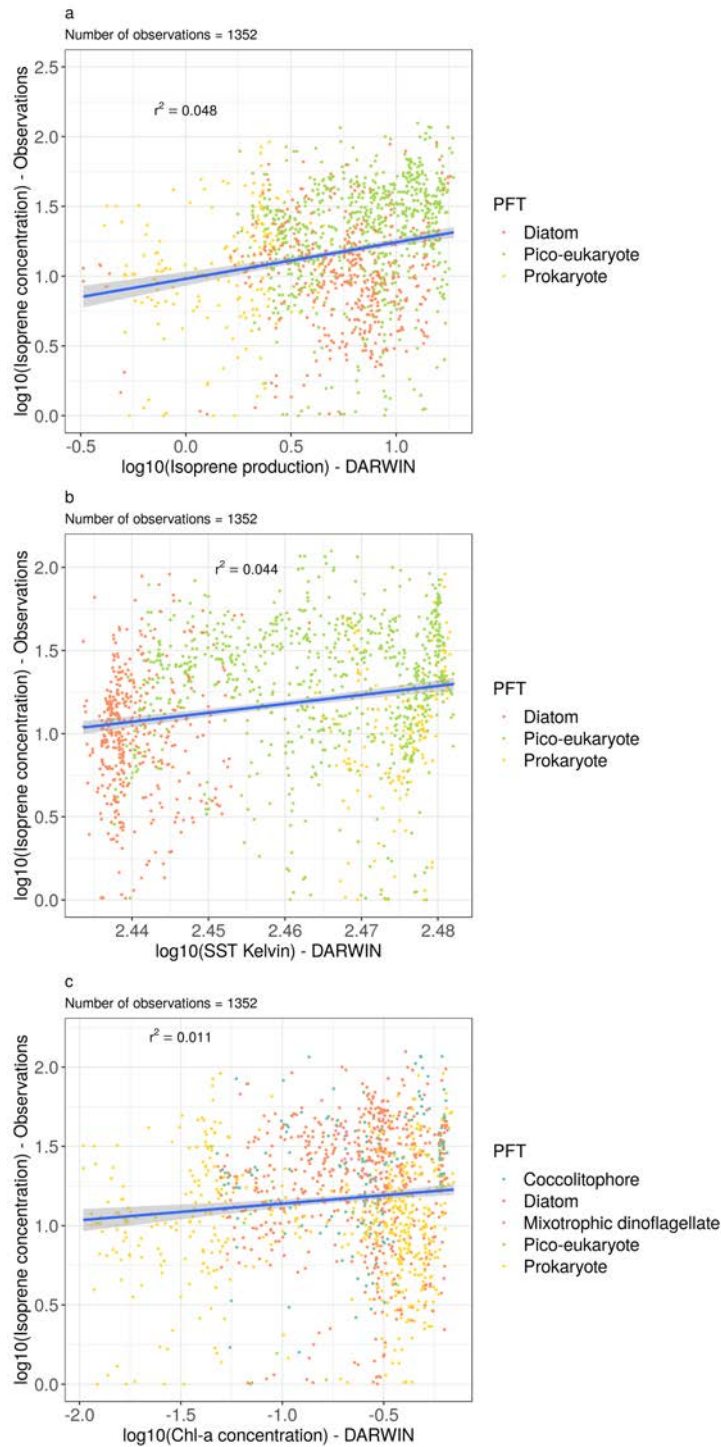


Figure 4.9: (a) Comparison of measurements of isoprene concentration (Table 4.3) with (a) isoprene production rates from the BASELINE simulation of DARWIN, (b) climatological chlorophyll-a concentration from DARWIN, (c) and sea surface temperature.

4.3.6 Uncertainties related to isoprene production

The described patterns of isoprene production in the global ocean isoprene are highly sensitive to changes in the production rates implemented on the DARWIN outputs. In this work we found a clear hot-spot of isoprene production in the eastern tropical Atlantic (Longhurst, 1995) which has not been predicted by Conte et al. (2020), the only prior study that has assessed the production of isoprene in the global ocean using a PFT based ecological model (NEMO-PISCES). Taking into account that the isoprene production in this area is driven by COCC and Conte et al. (2020) only used two PFT's in their configuration of PISCES (Diatoms + others), we suggest that their exclusion of coccolitophores may be the reason why the eastern tropical Atlantic did not show up as an isoprene production hot-spot. Overall, there is a need for better quantification and comprehension of the specific isoprene production rates. Extrapolation of results from a limited number of species to the global ocean is not a realistic approach. For example, (Dani et al., 2017) suggested that diatoms are the largest contributors to isoprene production at the global scale, based on the results from 2 diatom strains cultured in the lab. Although they are possibly right because diatoms are abundant across a large portion of the global ocean, we show that they do not dominate isoprene production in some latitudes and, is the low end of the lab-based specific production rates is considered (MIN experiment), they are even replaced by mixotrophic dinoflagellates at intermediate latitudes (Figure 4.6).

The BASELINE simulation results provide a total production of isoprene in the surface ocean (0-50 m) that amounts $1.43 \text{ Tg C yr}^{-1}$ while the CHLA, RHO.MIN, RHO.MAX experiments gave values of 1.15, 0.24 and $5.88 \text{ Tg C yr}^{-1}$, respectively. This remarkable difference up to one order of magnitude is the consequence of the poorly constrained isoprene production rates from the different PFT's. Looking into the spatial patterns of the total production in our BASELINE simulation, the highest isoprene production rates are placed in the latitudinal band of $30\text{-}60^\circ\text{S}$, while the lowest are found in polar regions, mainly in waters of the Arctic Ocean ($>60^\circ\text{N}$) (respectively, 8.25 and $1.34 \mu\text{mol m}^{-2} \text{ yr}^{-1}$, Figure 4.6a, left). DIAT is the largest contributor to isoprene production at a global scale (Figure 4.6a, right). While DIAT dominate production in latitudes higher than 30°N and 30°S , PIC dominate the tropical regions (from 30°S to 30°N), which represent a larger area than the polar oceans. As expected, the MAX experiment (Table 4.2) shows an increase in isoprene production in all latitudinal bands, peaking in $30\text{-}60^\circ\text{S}$ ($39.72 \mu\text{mol m}^{-2} \text{ yr}^{-1}$, Figure 4.6a, left). In contrast to BASELINE, MAX replaces the dominance of PIC with PRO in tropical waters, except in the bands where DIAT dominate (Figure 4.6a, right). In the MIN experiment, isoprene production decreases one or two orders of magnitude at all latitudes (Figure 4.6a, left). Similarly to BASELINE, DIAT are the main contributors to isoprene production in the polar oceans and PIC dominate over the tropical regions (Figure 4.6a, right). Finally, the CHLA experiment gives intermediate levels of isoprene production closer to BASELINE than MIN or MAX (Figure 4.6a, left). However, MIX replace DIAT as the global dominant PFT because they contribute the most to isoprene production in latitudes higher than 30°N and in the band of $30\text{-}60^\circ\text{S}$ (Figure 4.6a, right). Altogether, the only region where the same PFT dominates isoprene production in the four experiments is the high latitude Southern Ocean ($>60^\circ\text{S}$), where DIAT are always the most important producers. In the tropical regions ($30^\circ\text{N}\text{-}30^\circ\text{S}$) it is not clear whether PRO or PIC dominate isoprene production.

Acknowledgements

This research was supported by the Spanish Ministry of Economy and Competitiveness through the projects PEGASO (CTM2012–37615) and BIOGAPS (CTM2016-81008-R), and the Swiss Polar Institute and Ferring Pharmaceuticals through the project SORPASSO–ACE8 to RS. PRR was supported by a "la Caixa" Foundation PhD Fellowship (2015-2019) and a Fulbright-Spain Fellowship (2019-2020). PRR would like to thank Dr Andrew Barton and his team, for hosting and training him at the Barton Lab (Scripps Institution of Oceanography – UCSD (USA)) from September 2019 to March 2020. The authors are grateful to the British Oceanographic Data Centre (BODC). The authors also want to thank the captain, officers and crew of RV Hespérides and RV Akademik Tryoshnikov, engineers of the Marine Technology Unit (CSIC) and research colleagues for their support and help during the cruises. Model outputs and in situ data are available upon request to the corresponding author.

4.4 Appendix

Isoprene production rates from the literature

Table 4.4: Compilation of isoprene production rates (normalized by chlorophyll-a biomass or number of cells) by different species estimated in laboratory experiments and their culture conditions. References: Milne et al. (1995); Shaw et al. (2003); Bonsang et al. (2010); Colomb et al. (2009); Arnold et al. (2009); Exton et al. (2013). * Rates from Meskhidze et al. (2015) included in this table are the average of Tables 2 and 3 in (Meskhidze et al., 2015).

Taxa	Specie	prod. rate per chia pmol iso mg chia-1 d-1	prod. rate per cell pmol cell-1 d-1	Source	Light intensity (period) $\mu\text{Es} - 1\text{m} - 2$	Nutrients	Temperature Deg. C	Cell volume (source) μm^3
Bacillariophyceae	<i>Chaetoceros affinis</i>	-	$1.09 \cdot 10^{-11}$	Milne et al. (1995)	-(14:10)	-	-	2440 (Harrison et al., 2015)
	<i>Chaetoceros neogracilis</i> (CCMP 1318)	28.48	-	Colomb et al. (2009)	250 (12:12)	F/2	22.5	321 (Harrison et al., 2015)
	<i>Chaetoceros neogracilis</i> (CCMP 1318)	1.26	$1.25 \cdot 10^{-6}$	Bonsang et al. (2010)	100 (12:12)	F/2	20	177.8 (Bonsang et al., 2010)
	<i>Cylindrotheca sp.</i>	2.64	-	Exton et al. (2013)	300 (14:10)	F/2 + Si	16	289 (Harrison et al., 2015)
	Diatoms (elsewhere)	2.48	-	Arnold et al. (2009)	100 (-)	F/2	-	-
	<i>Pelagomonas calceolate</i> (CCMP 1214)	1.6	$5.7 \cdot 10^{-8}$	(Shaw et al., 2003)	45 (14:10)	F/2 + Si	20	-
	<i>Phaeodactylum tricornutum</i> (Falkowski)	2.85	-	Colomb et al. (2009)	250 (12:12)	F/2	23	14 (Shaw et al., 2003)
	<i>Phaeodactylum tricornutum</i> (UTEX 646)	1.12	-	Bonsang et al. (2010)	100 (12:12)	F/2	22.5	-
	<i>Phaeodactylum tricornutum</i>	1.12	$3.2 \cdot 10^{-7}$	Bonsang et al. (2010)	100 (12:12)	F/2	20	-
	<i>Skolotema costatum</i>	1.32	$8.5 \cdot 10^{-7}$	Bonsang et al. (2010)	100 (12:12)	F/2	20	56.23 (Bonsang et al., 2010)
	<i>Skolotema costatum</i>	-	$1.25 \cdot 10^{-6}$	Milne et al. (1995)	-(14:10)	-	20	141.25 (Bonsang et al., 2010)
	<i>Skolotema costatum</i> (CCMP 1332)	1.8	-	Shaw et al. (2003)	90 (14:10)	F/2 + Si	-	215 (Harrison et al., 2015)
	<i>Thalassiosira pseudonana</i> (CCAP 1085/12)	5.76	-	Exton et al. (2013)	300 (14:10)	F/2 + Si	23	385 (Shaw et al., 2003)
	<i>Thalassiosira pseudonana</i> (CCAP 1085/12)	3.89 *	$3.16 \cdot 10^{-8}$ *	Meskhidze et al. (2015)	90 (12:12)	F/2 + Si	22	385 (Shaw et al., 2003)
	<i>Thalassiosira weissflogii</i> (CCMP 1051)	4.56	-	Exton et al. (2013)	300 (14:10)	F/2 + Si	16	54.3 (Harrison et al., 2015)
<i>Thalassiosira weissflogii</i> (CCMP 1051)	3.78 *	$3.69 \cdot 10^{-8}$ *	Meskhidze et al. (2015)	90 (12:12)	F/2 + Si	22	54.3 (Harrison et al., 2015)	
Chlorophyceae	<i>Dunaliella tertiolecta</i>	0.36	$4.9 \cdot 10^{-7}$	Bonsang et al. (2010)	100 (12:12)	F/2	20	12800 (Harrison et al., 2015)
	<i>Dunaliella tertiolecta</i> (CCMP 1320)	1.2	-	Exton et al. (2013)	180 (14:10)	F/2	16	158.49 (Harrison et al., 2015)
	<i>Dunaliella tertiolecta</i> (DUN - Falkowski)	2.85	-	Colomb et al. (2009)	250 (12:12)	F/2	22.5	-
Bacillariophyceae (cold adapted)	<i>Chaetoceros debilis</i>	0.65	$6.07 \cdot 10^{-7}$	Bonsang et al. (2010)	30 (12:12)	F/2	4	199.52 (Bonsang et al., 2010)
	<i>Chaetoceros muelleri</i> (CCAP 1010/3)	9.36	-	Exton et al. (2013)	300 (14:10)	F/2 + Si	16	232 (Harrison et al., 2015)
	Diatoms (Southern Ocean)	1.21	-	Arnold et al. (2009)	30 (12:12)	F/2	4	-
	<i>Flagellariopsis cylindrus</i>	0.96	-	Exton et al. (2015)	160 (14:10)	F/2 + Si	-1	-
	<i>Flagellariopsis kerguelensis</i>	0.56	$1 \cdot 10^{-6}$	Bonsang et al. (2010)	30 (14:10)	F/2	4	5623 (Bonsang et al., 2010)
	<i>Nitzschia sp.</i> (CCMP 1088)	0.96	-	Exton et al. (2013)	160 (14:10)	F/2 + Si	-1	312 (Harrison et al., 2015)
	<i>Synechococcus sp.</i> (CCMP 2745)	0.72	-	Exton et al. (2013)	160 (14:10)	F/2 + Si	-1	-
Cryptophyceae	<i>Rhodomonas lacustris</i> (CCAP 995/3)	9.36	-	Exton et al. (2013)	300 (14:10)	F/2	16	217 (Harrison et al., 2015)
	<i>Rhodomonas salina</i>	2.78 *	$2.08 \cdot 10^{-8}$ *	Meskhidze et al. (2015)	90 (12:12)	F/2	22	217 (Harrison et al., 2015)
Cyanophyceae	<i>Prochlorococcus</i>	9.66	-	Arnold et al. (2009)	100 (12:12)	F/2	20	0.13 (Shaw et al., 2003)
	<i>Prochlorococcus sp.</i> (axenic MED4 - High light)	1.5	$1.4 \cdot 10^{-9}$	Shaw et al. (2003)	110 (14:10)	F/2 + Si	23	0.13 (Shaw et al., 2003)
	<i>Prochlorococcus sp.</i> (MIT 9401)	-	$1.7 \cdot 10^{-9}$	Shaw et al. (2003)	110 (14:10)	F/2 + Si	23	0.13 (Shaw et al., 2003)
	<i>Prochlorococcus sp.</i> (ss120)	-	$1.1 \cdot 10^{-9}$	Shaw et al. (2003)	110 (14:10)	F/2 + Si	23	0.13 (Shaw et al., 2003)
	<i>Synechococcus sp.</i> (CCMP 1334)	11.76	-	Exton et al. (2013)	110 (14:10)	F/2	26	0.4 (Shaw et al., 2003)
	<i>Synechococcus sp.</i> (RCC 40)	4.97	$2.7 \cdot 10^{-8}$	Bonsang et al. (2010)	120 (14:10)	F/2	20	0.4 (Bonsang et al., 2010)
	<i>Synechococcus sp.</i> (WH 8103)	1.4	$4.9 \cdot 10^{-9}$	Shaw et al. (2003)	100 (12:12)	F/2 + Si	23	0.4 (Shaw et al., 2003)
<i>Trichodesmium</i>	3	$1 \cdot 10^{-2}$	Bonsang et al. (2010)	110 (14:10)	F/2	20	-	
Dinophyceae	<i>Amphidinium aperculatum</i> (Aboet)	-	$5.4 \cdot 10^{-6}$	Milne et al. (1995)	-(14:10)	-	-	1440 (Harrison et al., 2015)
	<i>Prorocentrum minimum</i> (Plymouth 18B)	10.08	-	Exton et al. (2013)	300 (14:10)	F/2	16	1120 (Harrison et al., 2015)
	<i>Prorocentrum minimum</i>	3.30 *	$2.41 \cdot 10^{-8}$ *	Meskhidze et al. (2015)	90 (12:12)	F/2	22	1120 (Harrison et al., 2015)
	<i>Karenia brevis</i>	2.05 *	$1.44 \cdot 10^{-8}$ *	Meskhidze et al. (2015)	90 (12:12)	F/2	22	-
	<i>Symbiodinium sp</i> (A1* - CCMP 2464)	4.56	-	Exton et al. (2013)	300 (14:10)	F/2	26	-
	<i>Symbiodinium sp</i> (A13* - CCMP 2469)	17.04	-	Exton et al. (2013)	300 (14:10)	F/2	26	-
	<i>Symbiodinium sp</i> (A20* - D. Pettay)	9.6	-	Exton et al. (2013)	300 (14:10)	F/2	26	-
<i>Symbiodinium sp</i> (B1* - CCMP 2463)	27.6	-	Exton et al. (2013)	300 (14:10)	F/2	26	-	
Prasinophyceae	<i>Micromonas pusilla</i> (CCMP 489)	1.4	$2 \cdot 10^{-8}$	Shaw et al. (2003)	45 (14:10)	F/2 + Si	23	7 (Shaw et al., 2003)
	<i>Prasinococcus capsulatus</i> (CCMP 1614)	32.16	-	Exton et al. (2013)	300 (14:10)	F/2	26	-
	<i>Tetraselmis sp.</i> (CCMP 965)	3.84	-	Exton et al. (2013)	300 (14:10)	F/2	26	-
Prymnesiophyceae	<i>Calcidiscus leptoporus</i> (AC 365)	5.4	-	Colomb et al. (2009)	250 (12:12)	F/2	22.5	-
	<i>Emiliana huxleyi</i> (CCMP 1516)	11.28	-	Exton et al. (2013)	300 (14:10)	F/2	16	113 (Harrison et al., 2015)
	<i>Emiliana huxleyi</i> (CCMP 371)	11.54	-	Colomb et al. (2009)	250 (12:12)	F/2	22.5	39.8 (Bonsang et al., 2010)
	<i>Emiliana huxleyi</i> (CCMP 371)	1	$6.6 \cdot 10^{-8}$	Bonsang et al. (2010)	100 (12:12)	F/2	20	39.8 (Bonsang et al., 2010)
	<i>Emiliana huxleyi</i> (CCMP 373)	1	$3.8 \cdot 10^{-7}$	Shaw et al. (2003)	45 (14:10)	F/2 + Si	23	70 (Shaw et al., 2003)
	<i>Emiliana huxleyi</i> (CCMP 373)	2.88	-	Exton et al. (2013)	300 (14:10)	-	16	113 (Harrison et al., 2015)
	<i>Emiliana huxleyi</i> (MCH)	-	$2.25 \cdot 10^{-6}$	Milne et al. (1995)	-(14:10)	-	-	113 (Harrison et al., 2015)
	<i>Emiliana huxleyi</i> (MCH)	-	$2.3 \cdot 10^{-6}$	Shaw et al. (2003)	45 (14:10)	F/2 + Si	23	113 (Harrison et al., 2015)
	<i>Emiliana huxleyi</i> (WH 1387)	-	$2 \cdot 10^{-7}$	Shaw et al. (2003)	45 (14:10)	F/2 + Si	23	113 (Harrison et al., 2015)
	<i>Gephyrocapsa oceanica</i>	15.36	-	Exton et al. (2013)	300 (14:10)	-	16	-
	<i>Pleurochrysis carterae</i>	2.08 *	$1.35 \cdot 10^{-8}$ *	Meskhidze et al. (2015)	90 (12:12)	-	22	-

Climatology of isoprene production from the DARWIN model

Total production

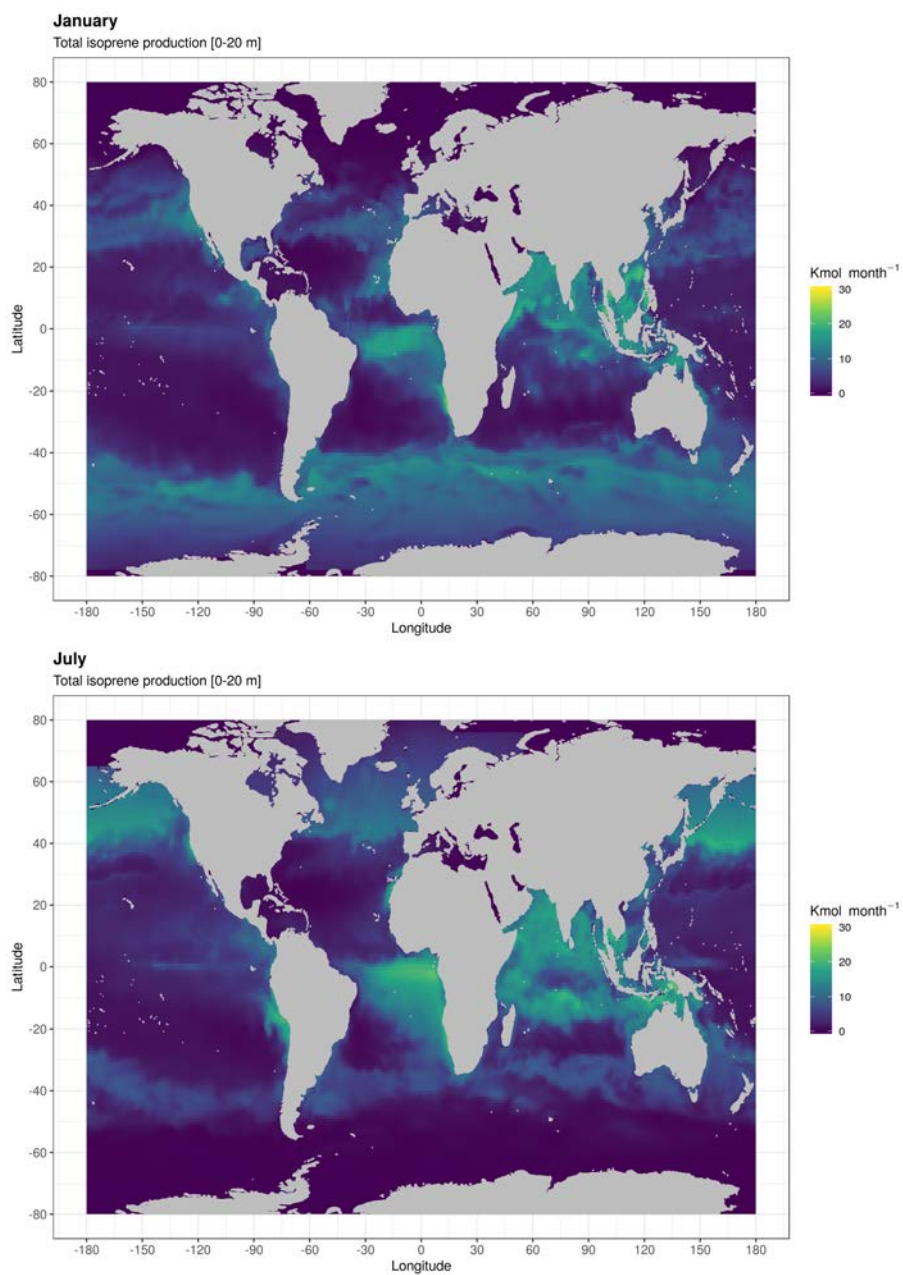


Figure 4.10: Monthly climatology (January and July) of total isoprene production (BASELINE simulation, Table 4.2).

Dominance of minor PFT's in isoprene production

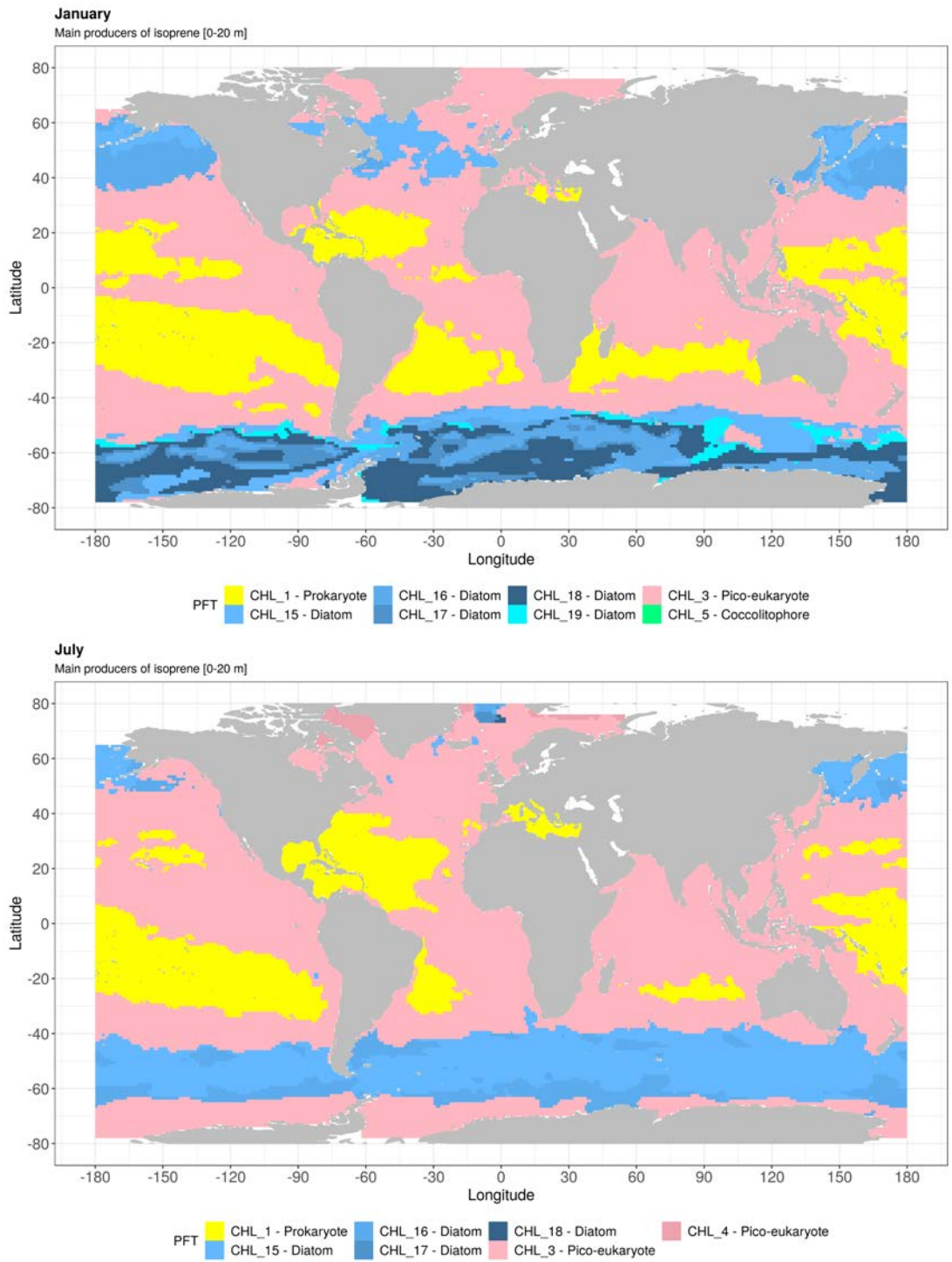


Figure 4.11: Monthly climatology (January and July) of minor PFT's dominating isoprene production in the Global Ocean (BASELINE simulation, Table 4.2).

Dominance in isoprene production levels vs dominance in chlorophyll-a contribution

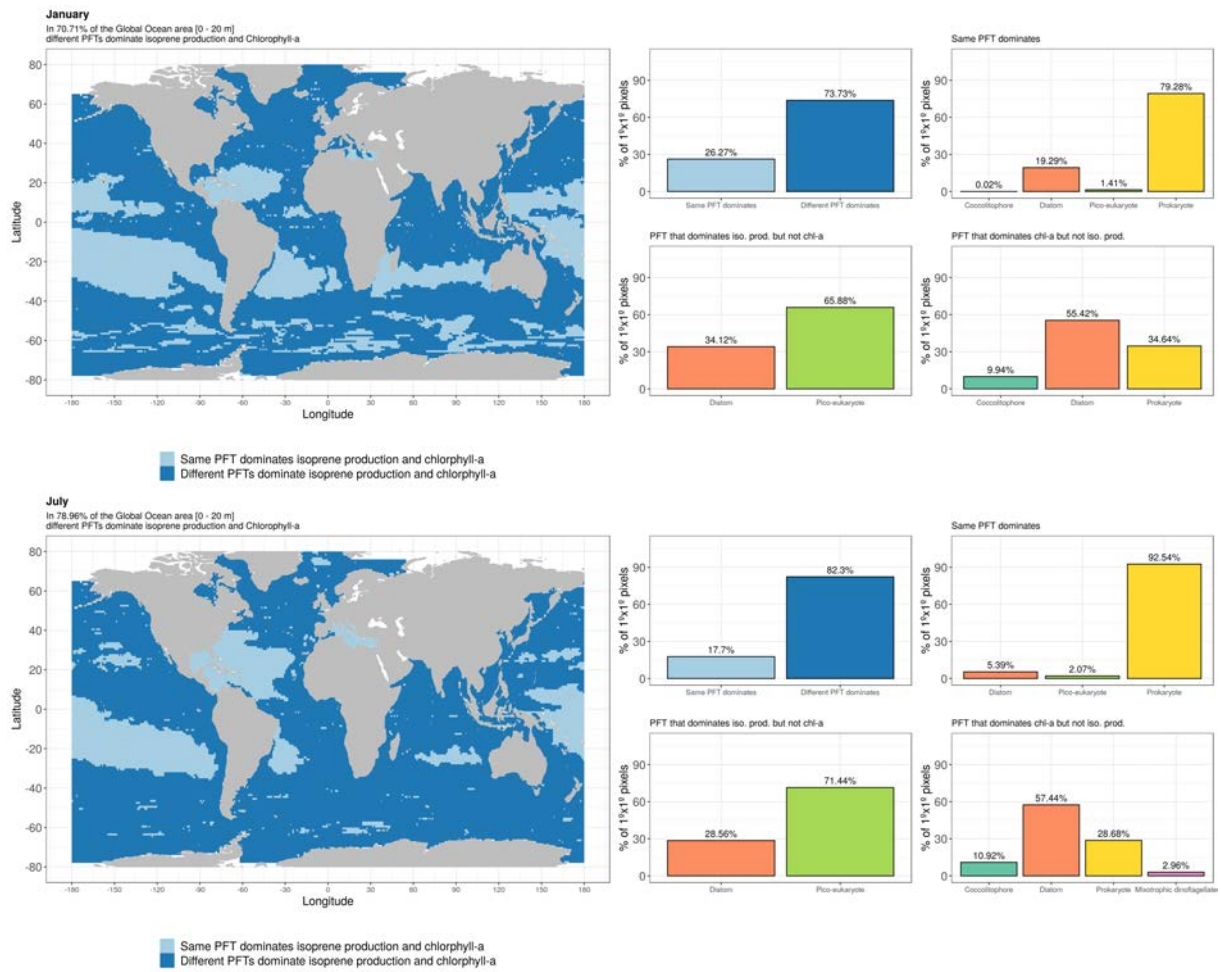


Figure 4.12: Dominance of isoprene production and relative contribution to chlorophyll-a levels of all PFT's in the global surface ocean. This figure shows the results for the climatological months of January and July.

The DARWIN model

In the recent years, the research group at the MIT led by Dr. Mick Follows and Dr. Stephanice Dutkiewicz has developed a global, trait-based model which is an essential tool to study the relationships between marine ecosystem processes and biogeochemical processes in the context of present and future global change scenario (Follows et al., 2007). One of their best achievements was the simulation of several ecotypes of *Prochlorococcus* and *Synechococcus* (Dutkiewicz et al., 2009), marine species of phytoplankton that are numerically dominant in the oligotrophic oceanic regions.

The ecosystem model used in this work is a version of the MIT ecological selection model (Vallina et al., 2014a; Dutkiewicz et al., 2019), it can be forced using one-dimensional (depth-resolved) or three-dimensional physical framework set-ups (see Equations 4.6, 4.7, 4.8, 4.9, 4.10 and 4.11; and Tables 4.5, 4.6 and 4.7). The computer model is written in *Fortran* programming language. The foodweb complexity is modular since we can select any number of species per taxon and trophic level. There are three trophic levels: photo-autotrophic phytoplankton, herbivorous zooplankton and carnivorous zooplankton. For each taxon and trophic level, we can select any number of species; something similar to what is presented in Figure 4.13. The generic herbivore zooplankton feeds upon all phytoplankton species with killing-the-winner (KTW) predation strategy (Vallina et al., 2014b). The generic carnivore zooplankton feeds upon the herbivore zooplankton and upon itself (i.e. closure term). The model mass currencies are nitrogen, phosphorus, iron, and silica and it resolves four types of abiotic compounds: dissolved inorganic nutrients (NO_3 , PO_4 , SiO_2 , Fe), dissolved organic matter (DOM) and particulate organic matter (POM). The model assumes Monod kinetics for the uptake of dissolved inorganic nitrogen ($\text{DIN} = \text{NO}_3 + \text{NH}_4$) and therefore uptake and growth are assumed to be coupled. There is only one nutrient uptake affinity for each species j , which applies to all dissolved nutrients; where μ is the maximum uptake rate and K is the half-saturation. Ammonium is assumed to be taken up preferentially over nitrate (Vallina and Le Quéré, 2008). Also, the model saves you from having to choose to select the specific effects of light on your species, assuming if there is (or not) differential fitness along the solar radiation environmental gradient. Organisms and abiotic compartments are passively mixed in the column water by vertical turbulent diffusion. Only detritus (i.e. POM) is subject to vertical sinking.

In the model, functional diversity refers to phytoplankton species-trait variability along three environmental gradients independently: dissolved nutrient concentration, ocean temperature and photosynthetic active radiation (PAR). Thus, it is possible to have as high a number of functional species as needed. Here, we present an example of 64 functional types of species (Figure 4.14.a), with four optimal levels of nutrients (N_{Opt}), temperature (T_{Opt}) and solar radiation (PAR_{Opt}). Consequently, each of the three environmental gradients define the species niches, which leads to $4 \times 4 \times 4 = 64$ species, each with a particular nutrient-temperature-PAR optimal niche where they are ecologically superior competitors (Figure 4.14.b).

Regarding the uptake strategy, there is a transition from resource gleaners to resource opportunists. This diversity in nutrient uptake strategies results from a gleaner-opportunist trade-off that provides each phytoplankton species with a particular nutrient niche: slow-growing nutrient

gleaners are superior competitors at low nutrient concentration because they have a higher nutrient affinity, while fast-growing nutrient opportunists are superior competitors at high nutrient concentration because they have a higher maximum growth rate (Litchman et al., 2015). This growth-affinity trade-off ($\alpha \cdot \mu_{\max} = \text{constant}$) implies that the species-trait maximum growth (μ_{\max}) alone is enough to define the nutrient uptake curve and thus the optimal nutrient concentration (N_{opt}) of any given uptake strategy. The diversity in temperature and PAR preferences results from different temperature optima (T_{opt}) and PAR optima (PAR_{opt}) with a tolerance range. The phytoplankton community will self-assemble depending on the local environmental conditions (environmental filtering) and the presence of other competitors (resource competition), leading to dynamical simulations of the global biogeography of the modelled phytoplankton species.

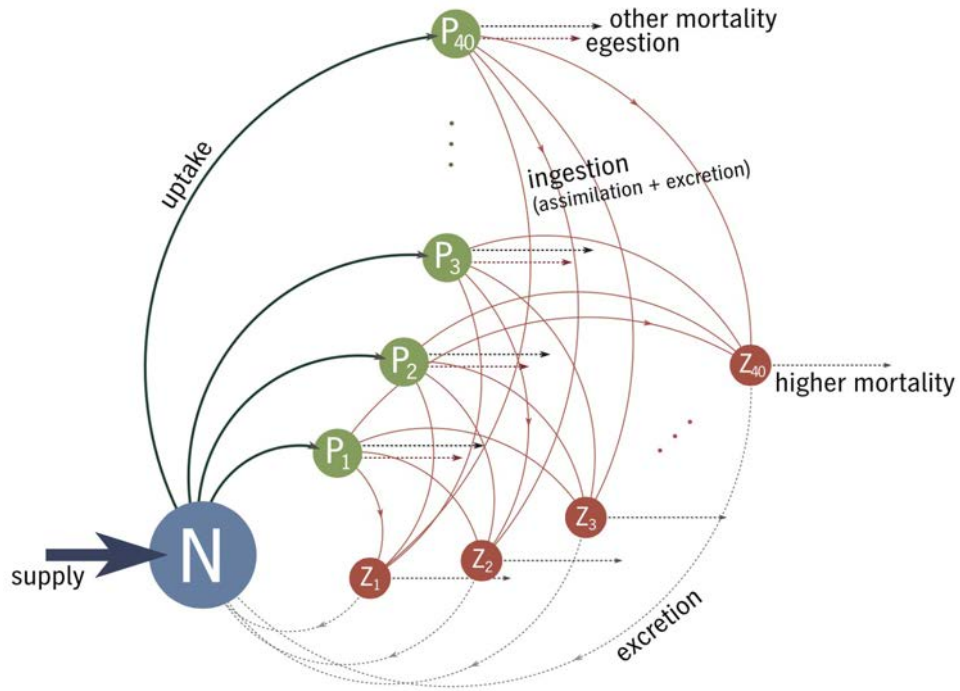


Figure 4.13: Simplification of a marine ecosystem model showing its main parameters. Source: Banas (2011).

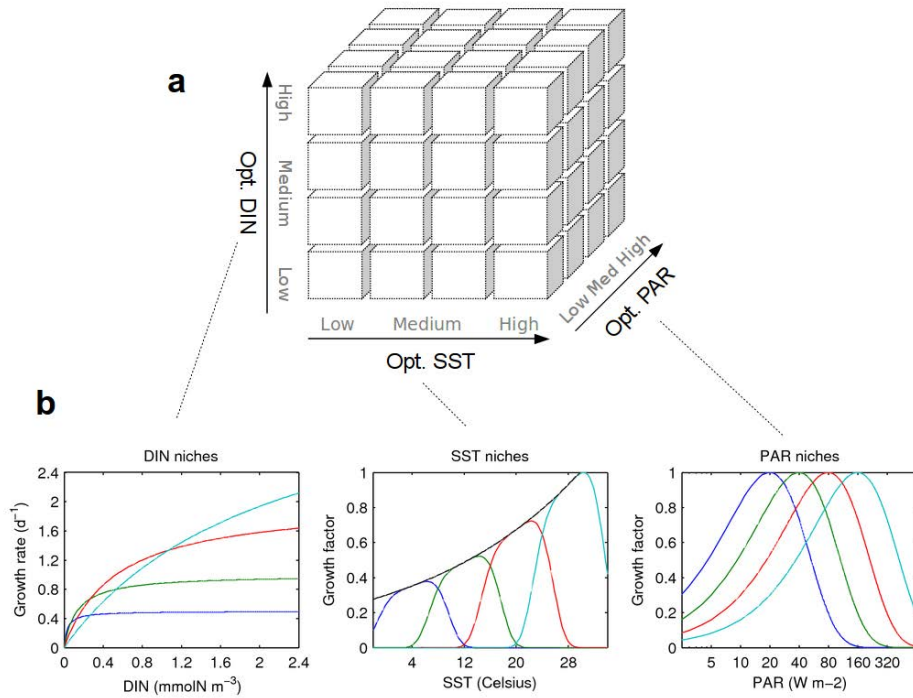


Figure 4.14: Environmental niches along three gradients: temperature (SST), dissolved inorganic nitrogen (DIC) and photosynthetically active radiation (PAR). Source: Pedro Cermeño (Institute of Marine Sciences - CSIC).

1D physical model description

Modified from (Vallina et al., 2008).

General form of the 1D model equations

$$\frac{\partial X_i}{\partial t} = J_i - |\vec{w}| \frac{\partial X_i}{\partial z} + \frac{\partial}{\partial z} (kz \frac{\partial X_i}{\partial z}) \quad (4.3)$$

where X_i = Phytoplankton, Chlorophyll, Volatiles ...; J_i are the biological source/sink terms for each variable i as defined above, $|\vec{w}| \frac{\partial X_i}{\partial z}$ is the vertical sinking (only applies to phytoplankton and detritus), and $\frac{\partial}{\partial z} (kz \frac{\partial X_i}{\partial z})$ is the vertical turbulent diffusion.

Advection (Sinking) and Diffusion Terms

Phytoplankton and Detritus sinking S

$$S(X_i) = |\vec{w}| \frac{\partial X_i}{\partial z} \quad (4.4)$$

for X_i = Phytoplankton, Chlorophyll, Volatiles ...

Turbulent diffusion D

$$D(X_i) = \frac{\partial}{\partial z} (kz \frac{\partial X_i}{\partial z}) \quad (4.5)$$

for X_i = Phytoplankton, Chlorophyll, Volatiles ...

MITesm: Ecosystem equations.**General equations of Predator, Prey and Nutrients. (4.6)**

$$\begin{aligned}
\frac{\partial P_j}{\partial t} &= F_{P_j} - E_{P_j} - G_{P_j} - M_{P_j} + \nabla_z(\kappa \nabla_z P_j) \\
\frac{\partial Z_j}{\partial t} &= F_{Z_j} - E_{Z_j} - G_{Z_j} - M_{Z_j} + \nabla_z(\kappa \nabla_z Z_j) \\
\frac{\partial NO_3}{\partial t} &= -F_P^{NO_3} \\
&\quad + \varepsilon_{(PNO_3)} E_P + \varepsilon_{(ZNO_3)} E_Z \\
&\quad + \Omega_{(PNO_3)} M_P + \Omega_{(ZNO_3)} M_Z \\
&\quad + \delta_{(PONNO_3)} M_{PON} + \delta_{(DONNO_3)} M_{DON} + \delta_{(NH_4NO_3)} M_{NH_4} \\
&\quad + \nabla_z(\kappa \nabla_z NO_3) \\
\frac{\partial NH_4}{\partial t} &= -F_P^{NH_4} - M_{NH_4} \\
&\quad + \varepsilon_{(PNH_4)} E_P + \varepsilon_{(ZNH_4)} E_Z \\
&\quad + \Omega_{(PNH_4)} M_P + \Omega_{(ZNH_4)} M_Z \\
&\quad + \delta_{(PONNH_4)} M_{PON} + \delta_{(DONNH_4)} M_{DON} \\
&\quad + \nabla_z(\kappa \nabla_z NH_4) \\
\frac{\partial DON}{\partial t} &= -M_{DON} \\
&\quad + \varepsilon_{(PDON)} E_P + \varepsilon_{(ZDON)} E_Z \\
&\quad + \Omega_{(PDON)} M_P + \Omega_{(ZDON)} M_Z \\
&\quad + \delta_{(PONDON)} M_{PON} \\
&\quad + \nabla_z(\kappa \nabla_z DON) \\
\frac{\partial PON}{\partial t} &= -M_{PON} \\
&\quad + \varepsilon_{(PPON)} E_P + \varepsilon_{(ZPON)} E_Z \\
&\quad + \Omega_{(PPON)} M_P + \Omega_{(ZPON)} M_Z \\
&\quad + \nabla_z(\kappa \nabla_z PON) + \omega \nabla_z PON
\end{aligned}$$

Matter decomposition. (4.7)

$$\begin{aligned}
M_{NH_4} &= \psi_{NH_4} NH_4 \\
M_{DON} &= \psi_{DON} DON \\
M_{PON} &= \psi_{PON} PON
\end{aligned}$$

Phytoplankton production. (4.8)

$$\begin{aligned}
 F_{P_j} &= F_{P_j}^{NO3} + F_{P_j}^{NH4} \\
 F_{P_j}^{NO3} &= \mu_{P_j}^{max} (Q_{P_j}^{NO3} Q_{P_j}^{SST} Q^{PAR}) P_j \\
 F_{P_j}^{NH4} &= \mu_{P_j}^{max} (Q_{P_j}^{NH4} Q_{P_j}^{SST} Q^{PAR}) P_j \\
 F_P^{NO3} &= \sum_j F_{P_j}^{NO3} \\
 F_P^{NH4} &= \sum_j F_{P_j}^{NH4} \\
 F_P &= \sum_j F_{P_j}
 \end{aligned}$$

$$\begin{aligned}
 Q_{P_j}^{DIN} &= Q_{P_j}^{NO3} + Q_{P_j}^{NH4} \leq 1 \\
 Q_{P_j}^{NH4} &= (NH4 / (K_{P_j}^{DIN} + NH4)) \\
 Q_{P_j}^{NO3} &= (NO3 / (K_{P_j}^{DIN} + NO3)) (1 - Q_{P_j}^{NH4}) \\
 Q_{P_j}^{SST} &= \exp(-(T_{opt}^{P_j} - T)^2 / (2 \sigma_T^2)) \leq 1 \\
 Q^{PAR} &= (I / I_{opt}) \exp(1 - (I / I_{opt})) \leq 1 \\
 I &= I_0 \exp\left(-\int_0^z (k_w + k_p \sum_j P_j) dz\right)
 \end{aligned}$$

Zooplankton production (prey_i, predator_j). (4.9)

$$\begin{aligned}
 Q_{Z_j} &= \sum_i Q_{Z_j}^{P_i} + \sum_i Q_{Z_j}^{Z_i} = Q_{Z_j}^{tot} \leq 1 \\
 Q_{Z_j}^{P_i} &= \frac{\phi_{ij} P_i^\alpha}{(\sum_k \phi_{kj} P_k^\alpha + \sum_k \varphi_{kj} Z_k^\alpha)} Q_{Z_j}^{tot} \\
 Q_{Z_j}^{Z_i} &= \frac{\varphi_{ij} Z_i^\alpha}{(\sum_k \phi_{kj} P_k^\alpha + \sum_k \varphi_{kj} Z_k^\alpha)} Q_{Z_j}^{tot} \\
 Q_{Z_j}^{tot} &= \frac{(\sum_k \phi_{kj} P_k + \sum_k \varphi_{kj} Z_k)^\beta}{K_{Z_j}^\beta + (\sum_k \phi_{kj} P_k + \sum_k \varphi_{kj} Z_k)^\beta} \\
 G_{P_i} &= \sum_j (\mu_{Z_j}^{max} Z_j) Q_{Z_j}^{P_i} \\
 G_{Z_i} &= \sum_j (\mu_{Z_j}^{max} Z_j) Q_{Z_j}^{Z_i} \\
 F_{Z_j} &= (\mu_{Z_j}^{max} Z_j) Q_{Z_j} \\
 F_Z &= \sum_j F_{Z_j}
 \end{aligned}$$

Plankton excretion. (4.10)

$$\begin{aligned}
 E_{P_j} &= (1 - \beta_P) F_{P_j} \\
 E_{Z_j} &= (1 - \beta_Z) F_{Z_j} \\
 E_P &= (1 - \beta_P) F_P \\
 E_Z &= (1 - \beta_Z) F_Z
 \end{aligned}$$

Plankton mortality. (4.11)

$$M_{P_j} = \psi_P P_j$$

$$M_{Z_j} = \psi_Z Z_j$$

$$M_P = \psi_P \sum P_j$$

$$M_Z = \psi_Z \sum Z_j$$

MITesm: Parameters in equations.

Variable	Description	Units
P_j	Phytoplankton species j	mmolN m ⁻³
Z_1	Zooplankton herbivore	mmolN m ⁻³
Z_2	Zooplankton carnivore	mmolN m ⁻³
NO_3	Nitrates	mmolN m ⁻³
NH_4	Ammonium	mmolN m ⁻³
DON	Dissolved Organic Nitrogen	mmolN m ⁻³
PON	Particulate Organic Nitrogen	mmolN m ⁻³

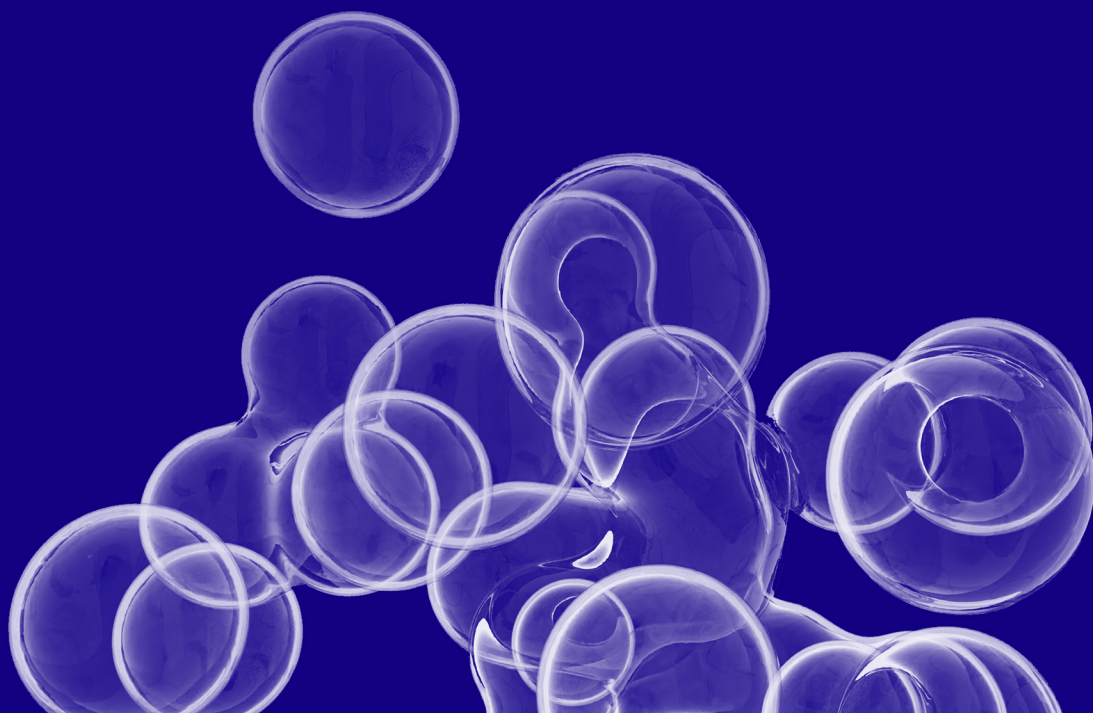
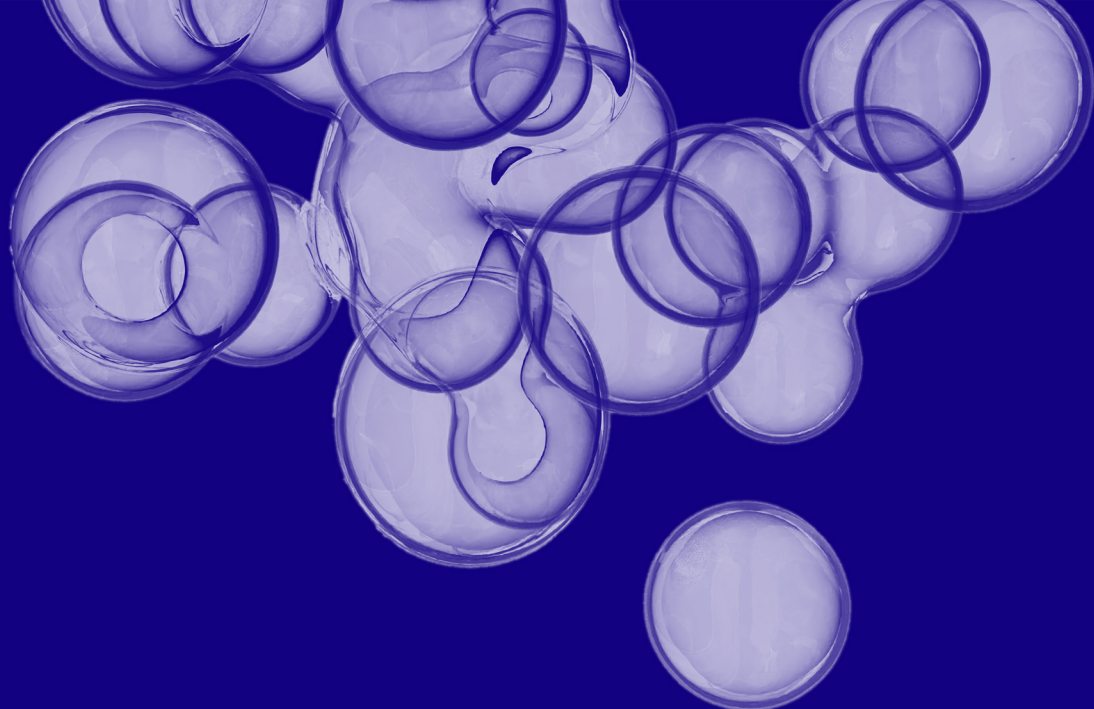
Table 4.5: Ecosystem model state-variables.

Term	Description	Units
F_P	Production of phytoplankton	mmolN m ⁻³ d ⁻¹
$F_P^{NO_3}$	Production of phytoplankton on nitrate	mmolN m ⁻³ d ⁻¹
$F_P^{NH_4}$	Production of phytoplankton on ammonium	mmolN m ⁻³ d ⁻¹
F_Z	Production of zooplankton	mmolN m ⁻³ d ⁻¹
E_P	Excretion of phytoplankton	mmolN m ⁻³ d ⁻¹
E_Z	Excretion of zooplankton	mmolN m ⁻³ d ⁻¹
G_P	Grazing on phytoplankton	mmolN m ⁻³ d ⁻¹
G_Z	Grazing on zooplankton	mmolN m ⁻³ d ⁻¹
M_P	Mortality of phytoplankton	mmolN m ⁻³ d ⁻¹
M_Z	Mortality of zooplankton	mmolN m ⁻³ d ⁻¹
M_{NH_4}	Decomposition of ammonium	mmolN m ⁻³ d ⁻¹
M_{DON}	Decomposition of dissolved organic nitrogen	mmolN m ⁻³ d ⁻¹
M_{PON}	Decomposition of particulate organic nitrogen	mmolN m ⁻³ d ⁻¹

Table 4.6: Ecosystem model terms.

Parameter	Symbol	Units
Phytoplankton maximum specific growth rate	$\mu_{P_j}^{max}$	d^{-1}
Phytoplankton half-saturation for DIN uptake	K_{P_j}	$mmolN\ m^{-3}$
Phytoplankton optimal temperature	$T_{opt}^{P_j}$	$^{\circ}C$
Phytoplankton saturating irradiance	I_{opt}	$W\ m^{-2}$
Phytoplankton temperature tolerance	σ_T	$^{\circ}C$
Phytoplankton assimilation efficiency	β_P	n.d.
Phytoplankton mortality specific rate	ψ_P	d^{-1}
Phytoplankton excretion fraction going to NO3	$\varepsilon_{(PNO3)}$	n.d.
Phytoplankton excretion fraction going to NH4	$\varepsilon_{(PNH4)}$	n.d.
Phytoplankton excretion fraction going to DON	$\varepsilon_{(PDON)}$	n.d.
Phytoplankton excretion fraction going to PON	$\varepsilon_{(PPON)}$	n.d.
Phytoplankton mortality fraction going to NO3	$\Omega_{(PNO3)}$	n.d.
Phytoplankton mortality fraction going to NH4	$\Omega_{(PNH4)}$	n.d.
Phytoplankton mortality fraction going to DON	$\Omega_{(PDON)}$	n.d.
Phytoplankton mortality fraction going to PON	$\Omega_{(PPON)}$	n.d.
Zooplankton herbivore preference on phytoplankton i	ϕ_{i1}	n.d.
Zooplankton carnivore preference on phytoplankton i	ϕ_{i2}	n.d.
Zooplankton herbivore preference on zooplakton i	φ_{i1}	n.d.
Zooplankton carnivore preference on zooplakton i	φ_{i2}	n.d.
Zooplankton maximum specific growth rate	$\mu_{Z_j}^{max}$	d^{-1}
Zooplankton half-saturation for grazing	K_{Z_j}	$mmolN\ m^{-3}$
Zooplankton killing-the-winner parameter	α	n.d.
Zooplankton grazing Hill coefficient	β	n.d.
Zooplankton assimilation efficiency	β_Z	n.d.
Zooplankton mortality specific rate	ψ_Z	d^{-1}
Zooplankton excretion fraction going to NO3	$\varepsilon_{(ZNO3)}$	n.d.
Zooplankton excretion fraction going to NH4	$\varepsilon_{(ZNH4)}$	n.d.
Zooplankton excretion fraction going to DON	$\varepsilon_{(ZDON)}$	n.d.
Zooplankton excretion fraction going to PON	$\varepsilon_{(ZPON)}$	n.d.
Zooplankton mortality fraction going to NO3	$\Omega_{(ZNO3)}$	n.d.
Zooplankton mortality fraction going to NH4	$\Omega_{(ZNH4)}$	n.d.
Zooplankton mortality fraction going to DON	$\Omega_{(ZDON)}$	n.d.
Zooplankton mortality fraction going to PON	$\Omega_{(ZPON)}$	n.d.
NH4 decomposition specific rate	ψ_{NH4}	d^{-1}
NH4 decomposition fraction going to NO3	$\delta_{(NH4NO3)}$	n.d.
DON decomposition specific rate	ψ_{DON}	d^{-1}
DON decomposition fraction going to NO3	$\delta_{(DONNO3)}$	n.d.
DON decomposition fraction going to NH4	$\delta_{(DONNH4)}$	n.d.
PON decomposition specific rate	ψ_{PON}	d^{-1}
PON decomposition fraction going to NO3	$\delta_{(PONNO3)}$	n.d.
PON decomposition fraction going to NH4	$\delta_{(PONNH4)}$	n.d.
PON decomposition fraction going to DON	$\delta_{(PONDON)}$	n.d.
PON sinking rate	ω	$m\ d^{-1}$
PAR irradiance vertical attenuation due to water	k_w	m^{-1}
PAR irradiance vertical attenuation due to self-shading	k_p	$m^2\ mmolN^{-1}$

Table 4.7: Ecosystem model parameters.



Chapter 5

Isoprene turnover in the surface ocean

Chapter 5

Isoprene turnover in the surface ocean

Rafel Simó¹, Pau Cortés¹, Pablo Rodríguez-Ros¹, Marta Masdeu¹

1. Institut de Ciències del Mar. Passeig Marítim de la Barceloneta, 37-49, 08003 Barcelona, Spain

*Retxes de sol atravessen blaus marins,
Ses algues tornen verdes i brillen ses estrelles,
Que ja s'ha fet de nit i es plàncton s'il·lumina
I cantes ses balenes a 30.000 quilòmetres d'aquí.*

Batiscafo Katiuskas - Antònia Font.

Abstract

Isoprene is a chemical ubiquitously produced by the biosphere that accounts for half of the emission of non-methane biogenic volatile organic compounds to the atmosphere. The vast majority of the global isoprene emission is from terrestrial vegetation, but it is the oceanic pervasive source that impacts on the atmospheric oxidative capacity and aerosol numbers and size in the remote marine atmosphere. Of the processes that control isoprene concentration in the ocean, laboratory experiments have addressed production by phytoplankton, but in situ biological and chemical losses have not yet been experimentally quantified. Here we present data from incubation experiments, conducted across contrasting regions of the global ocean, which show that isoprene is consumed in the absence of light and ventilation. Rate constants of isoprene loss are proportional to chlorophyll-*a* concentrations, suggesting they are due to microbial activity, with an intercept that approaches a fixed chemical loss. The proposed equation will allow parameterising the loss term in numerical and remote sensing models for oceanic isoprene emission. Together with estimates of temperature-dependent specific production, our overall results show that marine isoprene is produced and consumed in dynamic cycling by planktonic microbial food webs.

5.1 Introduction

Isoprene (2-methyl-1,3-butadiene) emissions by terrestrial and marine life are of a magnitude similar to the sum of natural and anthropogenic emissions of methane, ca. 500 Tg C year⁻¹ (Guenther et al., 2012; Saunio et al., 2016). Owing to its reactivity and short lifetime in the atmosphere (Seinfeld and Pandis, 2016; Medeiros et al., 2018) (minutes to hours), isoprene impacts on atmospheric chemistry by forming tropospheric ozone, modifying the oxidation behaviour of other organic compounds, and contributing to secondary organic aerosols Claeys et al. (2004); Carlton et al. (2009); Hu et al. (2013). Even though the oceans emit much less isoprene than vegetated land, the potential of biogenic aerosols to influence cloud albedo and lifetimes, hence climate, is large over the vast oceans remote from anthropogenic sources (Andreae and Rosenfeld, 2008; Carslaw et al., 2013).

On land, isoprene is produced and released mainly by trees and shrubs (Pacifico et al., 2009). In the ocean, isoprene is produced primarily by phytoplankton (Bonsang et al., 1992) and also by seaweeds (Broadgate et al., 1997). Whilst in vascular plants isoprene production is related to rapid alleviation of thermal and oxidative stress, and chemical signalling (Loreto and Schnitzler, 2010; McGenity et al., 2018; Murrell et al., 2020), the ecophysiological functions of isoprene biosynthesis in phytoplankton are unknown, yet a similar antioxidant role has been speculated (Dani and Loreto, 2017). In any case, isoprene is ubiquitous in the surface ocean, where it occurs at concentrations mostly within the 1 – 100 nmol m⁻³ range (Ooki et al., 2015; Hackenberg et al., 2017; Rodríguez-Ros et al., 2020b,a; Conte et al., 2020).

Estimations of the global ocean emission of isoprene have been attempted either by “top down” (balancing atmospheric observations with model outputs) or “bottom up” (modelling oceanic isoprene concentration and air-sea flux) approaches, and they diverge by one or two orders of magnitude (maximum range: 0.1 – 12 Tg C year⁻¹) (compilation in Hackenberg et al. (2017)). One of the reasons why the isoprene emission is so badly constrained is our poor knowledge of the magnitude, drivers, distribution and dynamics of its cycling processes. It is thought that not all of the isoprene produced by phytoplankton escapes to the atmosphere because part of it is degraded in seawater, but the actual proportion is unknown. Chemical oxidation is taken for granted because of isoprene’s high reactivity (Huang et al., 2011), but it has never been measured. Likewise, the occurrence of isoprene-degrading bacteria in seawater has been demonstrated (Alvarez et al., 2009; Johnston et al., 2017; Murrell et al., 2020) and a significant microbial sink has been suggested (Palmer and Shaw, 2005; Moore and Wang, 2006; Booge et al., 2018), but it has not been experimentally confirmed, let alone measured, in natural conditions.

With the aim to determine rates of isoprene loss from the surface ocean, we conducted seawater incubations during four oceanographic expeditions. Ten of the eleven experimental sites were located in the open ocean, and one was located offshore on the wide Southwestern Atlantic Shelf. Altogether they covered wide ranges of latitude (40°N – 61°S), sea surface temperature (-0.8 – 28.6°C), daily wind speed (3 – 12 m s⁻¹), fluorometric chlorophyll a (chl_a) concentration (0.1 – 5.8 mg m⁻³), and isoprene concentration (4 – 104 nmol m⁻³) (Figure 5.1, Table 5.1 and 5.2). Water samples from the surface ocean were incubated in glass bottles for 24 hours, at the

in situ temperature and in the dark. First-order loss rate constants were determined from initial and final, and sometimes intermediate, isoprene concentrations (see Methods). Enclosure without headspace prevented any isoprene loss by ventilation, and darkness was assumed to arrest all or most of the biological production (Bonsang et al., 2010) and any photochemical production (Ciuraru et al., 2015b) or degradation. Thus, the measured loss was considered to be the result of microbial degradation and chemical oxidation.

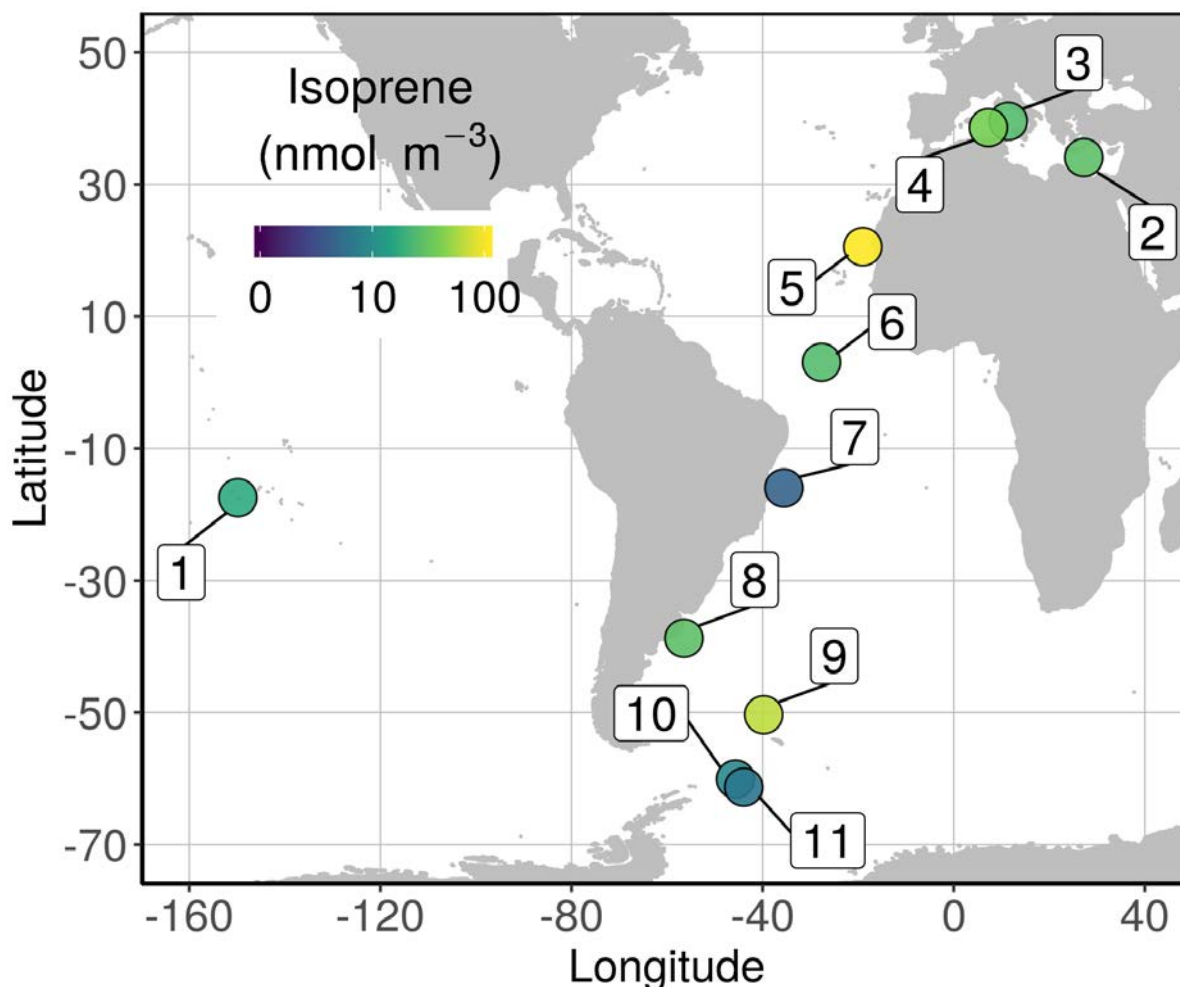


Figure 5.1: Geographical distribution of the experiments. Location of the sampling and incubation sites, coloured for isoprene concentration.

5.2 Methods

5.2.1 Sampling and physical measurements

The HOTMIX cruise (Benavides et al., 2016) traversed the Mediterranean Sea from East to West between 27 April and 29 May 2014 on board the R/V Sarmiento de Gamboa. Seawater was collected with a General Oceanics rosette, equipped with 24 L Niskin bottles. Temperature and salinity were recorded with a SBE911+ CTD system (Sea Bird Sci.). The TransPEGASO cruise (Riemer et al.,

Table 5.1: Sample characteristics and estimates of isoprene process rates. Sample location on map of Figure 5.1, sea surface temperature (SST, which was the temperature of the incubation), chlorophyll-a concentration (chl_a), concentration of heterotrophic prokaryotes (mostly bacteria), isoprene concentration, rate constants for isoprene loss (k_{loss} , biological and chemical) and ventilation (k_{vent}), total turnover time (τ), and specific or chl_a-normalized production rate.

Area sample (# on map)	date (d/m/y)	SST (°C)	chl _a (mg m ⁻³)	bacteria (10 ⁶ cell mL ⁻¹)	isoprene (nmol m ⁻³)	k_{loss} (d ⁻¹)	k_{vent} (d ⁻¹)	total τ (d)	specific prod. rate (nmol (mg chl _a) ⁻¹ d ⁻¹)
Tropical Pacific #1	06/04/2018	28.6	0.31	0.92	17.5	0.06	0.03	11.2	4.8
Mediterranean #2	02/05/2014	18.9	0.15	0.64	27.8	0.09	0.08	6.0	29.9
Mediterranean #3	13/05/2014	19.1	0.19	0.86	25.1	0.07	0.10	6.0	21.3
Mediterranean #4	17/05/2014	16.8	0.15	1.32	39.0	0.03	0.03	15.5	15.8
Atlantic #5	26/10/2014	23.4	0.61	1.46	104.1	0.15	0.08	4.4	37.9
Atlantic #6	30/10/2014	28.1	0.20	1.29	25.0	0.04	0.07	9.3	13.0
Atlantic #7	04/11/2014	25.5	0.11	0.78	4.5	0.08	0.11	5.4	7.3
Atlantic #8	17/11/2014	13.9	1.67	2.64	27.6	0.28	0.16	2.3	7.2
Southern Ocean #9	27/01/2015	5.0	5.77	0.63	64.2	0.64	0.07	1.4	7.9
Southern Ocean #10	15/01/2015	1.0	1.96	0.23	8.8	0.19	0.06	4.0	1.1
Southern Ocean #11	18/01/2015	-0.8	0.29	0.36	6.3	0.06	0.14	4.9	4.2

Table 5.2: Location of the experimental sites, sampling depth, and physical variables. SSS: sea surface salinity; SST: sea surface temperature; Z_{ML} : mixed layer depth; U_{10} 24h: wind speed at 10 m above sea surface, averaged over 24 hours. ^a: Estimated from a monthly climatology (Holte et al., 2017).

Area	date (d/m/y)	latitude	longitude	depth (m)	SSS	SST (°C)	Z_{ML} (m)	U_{10} 24h (m s ⁻¹ -1)
Tropical Pacific	06/04/2018	17.45°S	149.84°W	0.2	36.50	28.6	12 ^a	2.8
Mediterranean	02/05/2014	34.07°N	27.22°E	4	36.68	18.9	20	6.4
Mediterranean	13/05/2014	39.57°N	11.40°E	4	37.80	19.1	15	6.2
Mediterranean	17/05/2014	38.60°N	7.25°E	4	37.68	16.8	20	4.4
Atlantic	26/10/2014	20.55°N	19.03°W	5	36.05	23.4	23 ^a	6.6
Atlantic	30/10/2014	3.05°N	27.67°W	5	35.99	28.1	37 ^a	7.5
Atlantic	04/11/2014	15.99°S	35.54°W	5	37.45	25.5	34 ^a	9.2
Atlantic	17/11/2014	38.75°S	56.46°W	5	33.48	13.9	18 ^a	9.3
Southern Ocean	27/01/2015	50.33°S	39.78°W	4	33.70	5.0	58	11.8
Southern Ocean	15/01/2015	60.07°S	45.67°W	4	33.70	1.0	21	7.2
Southern Ocean	18/01/2015	61.30°S	43.95°W	4	33.19	-0.8	12	8.4

2000) crossed the Atlantic Ocean from North to South on the R/V Hesperides, between 20 October and 21 November 2014. Surface seawater was sampled using the ship's underway pumping system, which had the water intake located 4-5 m below sea level. All the parts of the centrifugal pump (BKMKC-10.11, Tecnum) that were in contact with the fluid were made of polypropylene and glass. Seawater temperature and salinity were recorded continuously via the flow-through thermosalinograph SBE21 SeaCAT (Sea Bird Sci.). The PEGASO cruise (Zamanillo et al., 2019a) was conducted on board de R/V Hesperides in the regions of Antarctic Peninsula, South Orkney and South Georgia Islands from 2 January to 11 February 2015. Seawater samples were collected from

either the underway pumping system intake (same as above) or the uppermost (4 m) bottle of the rosette on SBE911+ CTD casts, which recorded temperature and salinity. The BIOGAPS-Moorea expedition took place between 2 and 27 April 2018 at the northern coast of the island of Mo'orea, French Polynesia. Surface (0.2 m) seawater was hand-collected from a boat 3.5 km offshore over a water column depth of 1100 m. Seawater temperature was recorded with a SBE56 sensor (Sea Bird Sci.) continuously flushed with pumped-in surface seawater. The sample was taken to the Gump Research Station (University California Berkeley) on the island for processing.

5.2.2 Incubations

In all cases, duplicate all-glass bottles (0.5 L) were completely filled, leaving no headspace. One of the bottles was analysed in duplicate for isoprene within 1-2 hours after collection, to set the initial concentration. The other bottle was dark-incubated for 24 hours in a tank with constant flushing of pumped-in surface ocean water, to keep incubation temperature the same as in situ. At the conclusion of the incubation time isoprene concentration was analysed in duplicate. In some cases (samples HOTMIX H04, H15 and H19, PEGASO B3, BIOGAPS-Moorea OO), an intermediate point was sampled and analysed after 9-11h. The loss rate constant of isoprene k_{loss} (d^{-1}) was calculated as the slope of $\text{Ln}(\text{concentration})$ vs. time, under two assumptions: (a) consumption follows first order kinetics, as in the case of other trace gases such as dimethyl sulphide (Toole et al., 2006) and methyl halides (Tokarczyk et al., 2003); (b) isoprene production by phytoplankton, which is linked to photosynthesis (Bonsang et al., 2010), is arrested over the 24 h of incubation in the dark; if biosynthesis resumed for a while, this would have reduced apparent loss and would have caused underestimation of k_{loss} .

5.2.3 Isoprene concentration

Isoprene was measured along with other volatile compounds on a gas chromatography-mass spectrometry system (5975-T LTM GC/MS, Agilent Technologies). Aliquots of 25 mL were drawn from the glass bottle with a glass syringe with a teflon tube, and filtered through a 25 mm glass fibre filter while introduced into a purge and trap system (Stratum, Tekmar Teledyne). Volatiles were stripped by bubbling with 40 mL min^{-1} of ultrapure He for 12 minutes, trapped on solid adsorbent at room temperature and thermally desorbed (250°C) into the GC. Isoprene, monitored as m/z 67 in selected ion monitoring mode, had a retention time of 2.4 min in the LTM DB-VRX chromatographic column held at 35°C . The detection limit was 1 pmol L^{-1} , and the median analytical precision was 5%. In HOTMIX, TransPEGASO and PEGASO, calibration was performed by injections of a gaseous mixture of isoprene in N_2 . In BIOGAPS-Moorea, a liquid standard solution prepared in cold methanol and subsequently diluted in MilliQ water was used instead.

5.2.4 Isoprene ventilation rate constant

The isoprene ventilation or air-sea exchange fluxes (F_{vent} , in $\text{nmol m}^{-2} \text{d}^{-1}$) were calculated as:

$$F_{\text{vent}} = k_{\text{AS}} \cdot ([\text{iso}_w] - [\text{iso}_a]/K_H) \approx k_{\text{AS}} \cdot [\text{iso}_w] \quad (5.1)$$

where $[\text{iso}_w]$ is the isoprene concentration in surface sea water, $[\text{iso}_a]$ is the isoprene concentration in the air, K_H is the Henry's Law constant for isoprene, and k_{AS} is the gas exchange velocity (cm hd^{-1}). Air-side isoprene can be considered near zero and neglected for flux calculations because isoprene is highly reactive in the atmosphere and it is largely supersaturated in the surface ocean. k_{AS} was estimated from Wanninkhof (2014):

$$k_{\text{AS}} = 0.251 \cdot U_{10}^2 \cdot (Sc/660)^{-0.5} \quad (5.2)$$

where U_{10} is the wind speed at 10 m (m s^{-1}), and Sc is the Schmidt number (non-dimensional). On cruises, wind speed was measured by the ships' meteorological stations and averaged over a period of 24 hours, which was the duration of the incubations. In offshore Mo'orea, we recorded wind speed on the boat with a portable Skywatch BL500 micrometeorological station. This instantaneous wind speed was converted to the daily average by applying the factor between instantaneous and daily average wind speeds measured at the Gump Station on shore. Sc was computed as Palmer and Shaw (2005):

$$Sc = 3913.15 + 162.13 \cdot SST + 2.67 \cdot SST^2 + 0.012 \cdot SST^3 \quad (5.3)$$

where SST is in degrees Celsius ($^{\circ}\text{C}$). To convert the ventilation flux F_{vent} ($\text{nmol m}^{-2} \text{d}^{-1}$) into the rate constant k_{vent} (d^{-1}), the flux was divided by the mixed layer depth (Z_{ML} , m) and by the isoprene concentration (nmol m^{-3}), assuming that the surface concentration was the mixed-layer concentration (Booge et al., 2016). During HOTMIX and PEGASO, Z_{ML} was determined from CTD profiles as the depth at which density was 0.125 kg m^{-3} higher than that at 5 m. In the case of the TransPEGASO cruise and the Mo'orea expedition, where no CTD casts were conducted, we used the geo-localized monthly values from a global climatology (Holte et al., 2017).

5.2.5 Isoprene vertical mixing rate constant

In the case of the three PEGASO samples, k_{mix} was estimated from measured vertical profiles of isoprene concentration and the turbulent diffusion across the pycnocline (K_z). Thus, the vertical mixing flux at the bottom of the ML (F_{mix} , $\text{nmol m}^{-2} \text{d}^{-1}$) was calculated as:

$$F_{\text{mix}} = K_z \cdot (\Delta[\text{iso}]/\Delta z) \quad (5.4)$$

where a $K_z = 2.6 \text{ m}^2 \text{d}^{-1}$ (or $0.3 \text{ cm}^2 \text{s}^{-1}$) was considered appropriate yet conservative for the Southern Ocean (Yang et al., 2013), $\Delta[\text{iso}]$ (nmol m^{-3}) was the isoprene concentration gradient across the upper pycnocline, and Δz (m) was the distance covered by this gradient. Depending on the location of the concentration maximum, F_{mix} was positive (loss term, export from the ML) or negative (gain term, import into the ML). k_{mix} (d^{-1}) was calculated by dividing F_{mix} by the surface isoprene concentration and Z_{ML} (determined from the CTD profiles as above). For HOTMIX, TransPEGASO and BIOGAPS-Moorea, k_{mix} could not be estimated from in situ data and a fixed value of -0.005 d^{-1} was taken from the global integral suggested by the model of Conte et al. (2020).

5.2.6 Chlorophyll *a* concentration

Seawater 250-mL samples were filtered on glass fibre filters, which were extracted with 90% acetone at 4°C in the dark for 24 hours. Fluorescence of extracts was measured with a calibrated Turner Designs fluorometer. No phaeopigment corrections were applied.

5.2.7 Bacterial abundance

Aliquots of 2 mL of the initial sample were fixed with 1% paraformaldehyde plus 0.05% glutaraldehyde and stored frozen at -80°C. Numbers of heterotrophic bacteria (actually prokaryotic heterotrophs, including archaea) were determined by flow cytometry after staining with SYBR-Gree (Gasol and Del Giorgio, 2000). The population of cells with higher fluorescence content in the green fluorescence vs. side scatter plot was considered high nucleic acid containing (HNA) bacteria.

5.3 Results and Discussion

5.3.1 Isoprene loss rate: variability and drivers

Loss rate constants ($k_{\text{loss}} = k_{\text{bio}} + k_{\text{chem}}$) varied over an order of magnitude, ranging 0.03 – 0.64 d⁻¹ with a median of 0.08 d⁻¹ (Table 5.1). They showed proportionality to the chl*a* concentration (Figure 5.2a) that was best described by this linear regression equation:

$$k_{\text{loss}} = 0.10 \cdot [\text{chl}a] + 0.05 \quad (5.5)$$

The fact that the variability of k_{loss} is largely driven by [chl*a*] strongly suggests that the variable term ($0.10 \cdot [\text{chl}a]$) corresponds to microbial consumption (k_{bio}), which in our experiments gave values between 0 and 0.59 d⁻¹, with a median of 0.03 d⁻¹. With a lack of experimental measurements, a pioneering modelling study (Palmer and Shaw, 2005) proposed the use of a fixed k_{bio} at 0.06 d⁻¹; recently (Booge et al., 2018), though, the need for a variable k_{bio} spanning at least between 0.01 and 0.1 d⁻¹ was invoked to balance observed concentrations with predictions of the production term from phytoplankton culture data, once the ventilation and chemical losses were accounted for. Our experimental results indicate that such variable k_{bio} indeed exists and spans even a broader range. We attribute this k_{bio} to degradation or utilisation by heterotrophic bacteria. There is sparse but solid evidence (Alvarez et al., 2009; Johnston et al., 2017) for the presence in marine waters of isoprene-degrading bacteria belonging mainly to the phylum Actinobacteria. The same study (Alvarez et al., 2009) demonstrated the potential for bacterial consumption after isoprene additions at concentrations at least four orders of magnitude higher than natural concentrations. Our k_{loss} did not show any significant correlation with the total bacterial abundance (Table 5.1), not even with the abundance of high nucleic acid-containing bacteria (Table 5.3), which are considered to be the more active members of the bacterial community (Lebaron et al., 2001). It must be noted, though, that bacterial abundance does not necessarily parallel bacterial activity, less so the activity

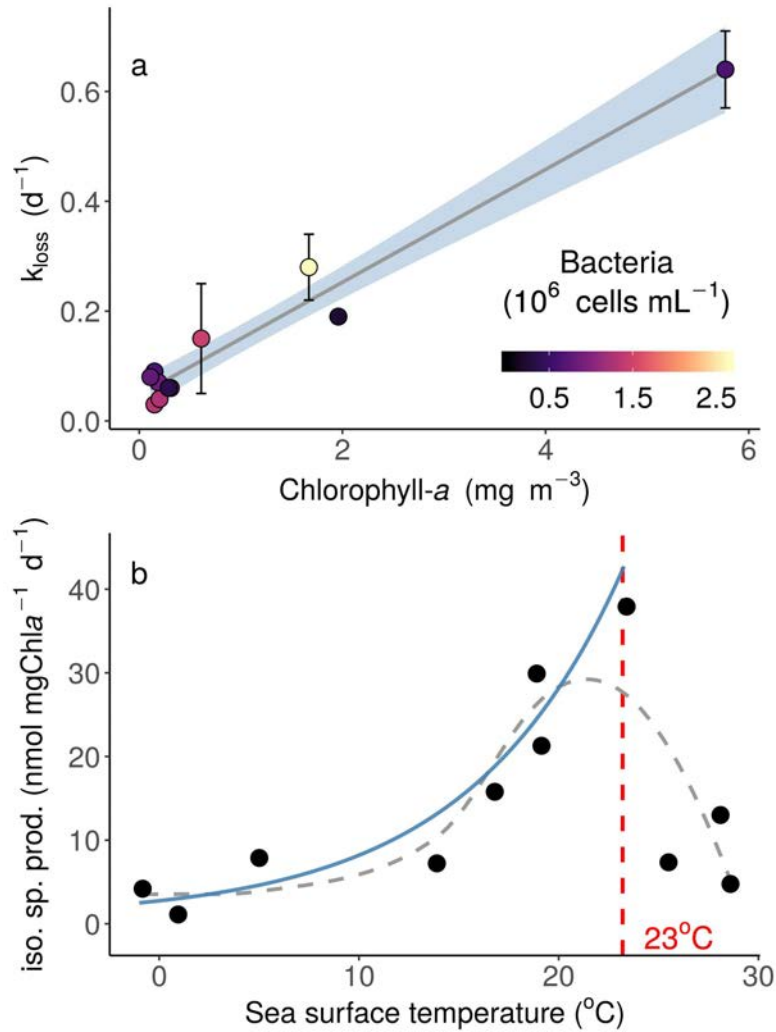


Figure 5.2: Isoprene processes and their main drivers. a. Rate constant of isoprene loss in dark incubations (k_{loss} , considered to be microbial and chemical consumption) vs. chlorophyll-a concentration. The linear regression equation is $k_{\text{loss}} = 0.10 \cdot [\text{chl}a] + 0.05$ ($R^2=0.96$, $p=10^{-7}$, $n=11$). Error bars represent the experimentally-determined standard error of k_{loss} . The colour scale of the circles indicates bacterial abundances. b. Specific (chl-a-normalised) rate of isoprene production vs sea-water temperature (SST) across the sample series. The dashed line is the general smoothed trend. The blue line is the exponential adjustment at $\text{SST} < 23^{\circ}\text{C}$: $\text{isoprene sp.prod.} = 2.04 \cdot e^{(0.13 \cdot \text{SST})} + 0.71$ ($R^2=0.85$, $p=10^{-3}$, $n=8$).

of specific phyla, whereas a general trend of higher bacterial activity with higher chl-a concentration is commonly observed (Gasol and Duarte, 2000). Circumstantial evidence in one study (Sinha et al., 2007) suggested that the cosmopolitan cyanobacterium *Synechococcus* might consume isoprene; if confirmed, this could have contributed to the correlation between k_{loss} and $[\text{chl}a]$. However, the three highest k_{loss} were measured in waters colder than 14°C where *Synechococcus* occurred at very low biomass (Zamanillo et al., 2019a,b). We therefore believe that the k_{bio} term of k_{loss} corresponded mainly to degradation by specialized heterotrophic bacteria.

The intercept of Equation 5.5 could be attributable to a less variable loss by chemical

Table 5.3: Measured biological variables and isoprene process rate constants. chl_a: chlorophyll a concentration; BA: bacterial (prokaryotic heterotroph) abundance; HNA-BA: high nucleic acid containing bacterial abundance; k_{loss} : rate constant of isoprene loss in incubations (microbial degradation + chemical oxidation); k_{vent} : rate constant of isoprene ventilation to the atmosphere; k_{mix} : rate constant of isoprene vertical mixing by turbulent diffusion at the bottom of the mixed layer (negative means import into the surface mixed layer); k_{prod} : rate constant of isoprene production, assuming 24-h steady state for the isoprene concentration. ^a: Taken from the global integral suggested by the model of Conte et al. (2020).

Area	date (d/m/y)	chl _a (mg m ⁻³)	BA (10 ⁵ cells mL ⁻¹)	HNA-BA	isoprene (nmol m ⁻³)	k_{loss} (d ⁻¹)	k_{vent} (d ⁻¹)	k_{mix} (d ⁻¹)	k_{prod} (d ⁻¹)
Tropical Pacific	06/04/2018	0.31	9.23	4.22	17.5	0.06	0.03	-0.005 ^a	0.09
Mediterranean	02/05/2014	0.15	6.38	1.94	27.8	0.09	0.08	-0.005 ^a	0.17
Mediterranean	13/05/2014	0.19	8.61	3.66	25.1	0.07	0.10	-0.005 ^a	0.17
Mediterranean	17/05/2014	0.15	13.16	6.12	39.0	0.03	0.03	-0.005 ^a	0.06
Atlantic	26/10/2014	0.61	14.56	12.01	104.1	0.15	0.08	-0.005 ^a	0.23
Atlantic	30/10/2014	0.20	12.90	1.05	25.0	0.04	0.07	-0.005 ^a	0.11
Atlantic	04/11/2014	0.11	7.83	3.50	4.5	0.08	0.11	-0.005 ^a	0.19
Atlantic	17/11/2014	1.67	26.37	10.64	27.6	0.28	0.16	-0.005 ^a	0.44
Southern Ocean	27/01/2015	5.77	6.33	3.79	64.2	0.64	0.07	0.001	0.71
Southern Ocean	15/01/2015	1.96	2.32	1.21	8.8	0.19	0.06	-0.005	0.25
Southern Ocean	18/01/2015	0.29	3.59	1.63	6.3	0.06	0.14	-0.010	0.20

oxidation (Huang et al., 2011; Riemer et al., 2000). In remarkable support to this, the value of the intercept, 0.05 d^{-1} , is identical to the k_{chem} commonly used hitherto (Conte et al., 2020; Palmer and Shaw, 2005; Booge et al., 2016), which was calculated from reaction rate constants and estimated concentrations of reactive oxygen species in the surface ocean.

In spite of the limited number of experiments, the fact that they cover a wide range of contrasting oceanic regions and conditions confers to Equation 5.5 the potential to be used in numerical models of marine isoprene cycling, replacing the fixed term for microbial consumption (Palmer and Shaw, 2005; Booge et al., 2016). The k_{loss} vs. [chl_a] relationship can also be used to predict k_{loss} from remote sensing chl_a measurements (Galí et al., 2015, 2018):

$$[\text{chl}_{\text{a,sat}}] = 0.79 \cdot [\text{chl}_{\text{a}}]^{0.78} \quad (R^2 = 0.66, n > 1,000) \quad (5.6)$$

Substitution in Equation 5.5 results in:

$$k_{\text{loss}} = 0.14 \cdot [\text{chl}_{\text{a,sat}}]^{1.28} + 0.05 \quad (5.7)$$

which is our recommended equation for k_{loss} prediction from satellite chl_a. Note that only the variable k_{bio} term changes from Equation 5.5, while the k_{chem} (intercept) is maintained at 0.05 d^{-1} .

5.3.2 Comparison of isoprene sinks

The change of isoprene concentration ($[iso]$) in the surface mixed layer over time can be described as the budget of sources and sinks:

$$\Delta[iso]/\Delta t = [iso] \cdot (k_{prod} - k_{loss} - k_{vent} - k_{mix}) \quad (5.8)$$

where k_{prod} , k_{vent} and k_{mix} are the rate constants of isoprene production, ventilation to the atmosphere and vertical mixing by turbulent diffusion, respectively. We calculated k_{vent} from our sampling sites over a period of 24 hours (Table 1). Ventilation has been considered to be the main isoprene sink from the upper mixed layer of the ocean (Palmer and Shaw, 2005). In our sampling sites, k_{loss} was 0.4 to 10 times the k_{vent} (median 1.2). That is, loss through microbial + chemical consumption was of the same order as ventilation, sometimes considerably faster. k_{mix} was estimated to be one order of magnitude lower than the other process rates (Table 5.3), and in all cases but one it was calculated or assumed not to be a loss term but an import term into the mixed layer, because vertical profiles generally show maximum isoprene concentrations below the mixed layer (Hackenberg et al., 2017; Milne et al., 1995). Altogether, the microbial, chemical and ventilation losses resulted in total turnover times of isoprene between 1.4 and 16 days, median 5 days.

5.3.3 Isoprene production

Assuming steady state for isoprene concentrations over 24 hours, i.e., $\Delta[iso]/\Delta t = 0$ in Equation 5.8, the sum of the rate constants of all sinks ($k_{loss} + k_{vent}$) equals the rate constant of isoprene production (k_{prod}), with k_{mix} adding to either side depending on whether it is an import to or an export from the mixed layer (Table 5.3). The product of k_{prod} by the isoprene concentration gives the isoprene production rate, which can be normalised to the chl_a concentration. This specific isoprene production rate varied between 1 and 38 nmol (mg chl_a)⁻¹ d⁻¹ (Table 1), median 8 nmol (mg chl_a)⁻¹ d⁻¹. These values are within the broad range reported across phytoplankton taxa from laboratory studies with monocultures (0.3 – 32, median 3 nmol (mg chl_a)⁻¹ d⁻¹, $n = 124$; see compilations in Booge et al. (2016); Meskhidze et al. (2015)).

Five of the eleven sites gave values > 13 nmol (mg chl_a)⁻¹ d⁻¹, i.e., in the higher end of the laboratory data range. This is not unexpected, since measurements in monoculture experiments are typically conducted before reaching nutrient limitation, below light saturation, and in the absence of UV radiation, to mention three stressors commonly occurring in the surface open ocean. If isoprene biosynthesis and release is enhanced by these stressors, as is the case in vascular plants (Pacífico et al., 2009; Loreto and Schnitzler, 2010), then monoculture-derived results will easily render underestimates of isoprene production in the open ocean. Production by heterotrophic bacteria (Fall and Copley, 2000) could have also contributed to increase apparent specific isoprene production rates, but the occurrence and significance of this process in the marine environment is unknown. While expanding the lab-derived database of specific isoprene production rates across phytoplankton taxa is always desirable, we argue there is a need for in situ measurements if we are to reliably predict isoprene production in the ocean.

Close inspection of the phytoplankton taxonomic composition of all samples (data not shown) revealed no clear relationship to the isoprene specific production rates. Instead, a pattern was apparent with the sea surface temperature (SST), which was also the temperature of the incubations. Specific production rates increased exponentially with SST across the eight sampling sites between -0.8°C and 23.4°C , and dropped drastically at higher SST (Figure 5.2b). Several studies with phytoplankton monocultures have reported positive dependence of isoprene specific production rates on temperature (Meskhidze et al., 2015; Fall and Copley, 2000; Shaw et al., 2003; Gantt et al., 2009; Exton et al., 2013). Among these, Meskhidze et al. (2015) described that the increase with temperature reaches an optimum for production that varies among phytoplankton strains and with light intensity, but falls around $23\text{--}26^{\circ}\text{C}$. The most detailed study (Shaw et al., 2003) was conducted with a *Prochlorococcus* strain; remarkably, the specific production rate vs. temperature curve for this cyanobacterium strain was almost identical to that of Figure 5.2b, with an exponential increase until 23°C and a drop thereafter. This is the canonical curve type of enzymatic activities, but the thermal behaviour of the enzymes for isoprene synthesis in marine unicellular algae has not yet been characterized¹⁵. In spite of the lack of a mechanistic explanation, we conclude that temperature does more than phytoplankton taxonomy to govern chl_a-normalised isoprene production across regions of the open ocean.

5.3.4 Revising the magnitude and players of the marine isoprene cycle

Our results allow redrawing the isoprene cycle in the surface ocean (Figure 5.3). Until now, the focus had entirely been on the production term, considering specific production rates by phytoplankton as though they were constitutive and shaped by phylogeny (Booge et al., 2016), with occasional emphasis on acclimation (Meskhidze et al., 2015; Shaw et al., 2003, 2010). Even though teasing apart phylogeny and acclimation at the cross-basin and seasonal scales is not an easy task because environmental stressors are interlinked with species and community succession, our results call for a deeper exploration of the ecophysiological drivers of isoprene biosynthesis by phytoplankton. As a matter of fact, whilst absolute isoprene production is *grosso modo* related to phytoplankton biomass and primary production (Figure 5.3), the isoprene concentration does not necessarily follow indicators of phytoplankton biomass such as chl_a but it is further tuned by environmental factors such as SST (Ooki et al., 2015; Dani and Loreto, 2017; Hackenberg et al., 2017; Rodríguez-Ros et al., 2020a,b).

We also show that the loss terms in the cycle are more complex and variable than believed, with a microbial sink that is tightly coupled to production and can dominate over ventilation in chl_a-rich waters (Figure 5.3). The resulting total turnover times of isoprene in the surface mixed layer are in the order of one or two weeks in the oligotrophic ocean but can be as short as one to four days in productive waters. The metabolic mechanisms and microorganisms involved in isoprene consumption warrant further investigation because this important sink will be regulated by triggers of microbial speciation and activity, potential co-metabolisms, and microbial mortality by predators and viruses. All in all, isoprene concentration and emission to the atmosphere can no longer be regarded as controlled only by phytoplankton biomass and functional types, but intimately connected to the structure of the pelagic microbial food web.

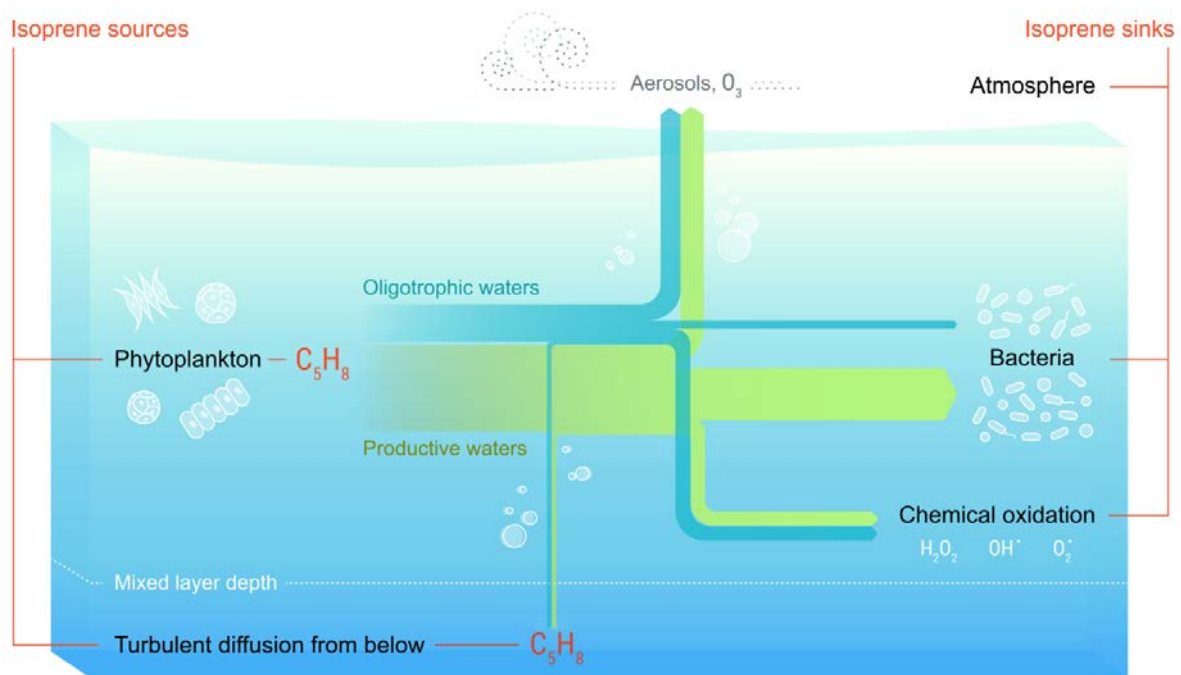


Figure 5.3: Steady state cycling processes of isoprene in the surface ocean, according to oceanic productivity. Process rates averaged from the seven oligotrophic sites with $[chl a] < 0.5 \text{ mg m}^{-3}$ (blue arrows) and from the four productive sites with $[chl a] > 0.5 \text{ mg m}^{-3}$ (green arrows). The width of the arrows is proportional to the magnitude of the process rate. Note the change in the relative magnitude of the sinks.

Aknowledgements

This research was supported by the Spanish state funding plan for science through projects PEGASO (CTM2012-37615) and BIOGAPS (CTM2016-81008-R) to RS. We are thankful to J.M. Gasol and J. Arístegui for providing the chlorophyll and bacterial data from HOTMIX, S. Nunes, M. Estrada and M.M. Sala for the chlorophyll and bacterial data from PEGASO and TransPEGASO, and C. Marrasé and M. Cabrera for the chlorophyll and bacterial data from Mo'orea. We are grateful to the crews and technicians on board the R/Vs Sarmiento de Gamboa and Hesperides, and to the managers and staff of the Gump Station in Mo'orea (administered by UC Berkeley). PC and MMN were supported by FPI PhD fellowships from the Spanish state funding plan for science, while PRR was supported by a "La Caixa" Foundation PhD fellowship. RS is holder of a European Research Council Advanced Grant (2019-2024).



Discussion

Discussion

No nos hagamos, pues, ilusiones: si la vida de un hombre basta para saber algo de todas las disciplinas humanas, apenas es suficiente para dominar hasta el detalle una o dos de ellas.

Reglas y consejos sobre investigación científica

Dr. Santiago Ramón y Cajal (Nobel Prize in Physiology or Medicine 1906)

Drivers and modelling of isoprene distribution in the Southern Ocean

During the last decades, the trace gas DMS, which acts as Secondary Aerosol (SA) and Cloud Condensation Nuclei (CCN) precursor, has been studied in SO waters (Vallina et al., 2006) to assess the validity of the CLAW hypothesis (Charlson et al., 1987) in this remote region. In contrast, other relevant trace gases for SA and CCN formation over the ocean have received less attention. This is the case of isoprene, although the Southern Ocean has been suggested to be a relevant area in terms of isoprene emission (Meskhidze and Nenes, 2006; Luo and Yu, 2010; Booge et al., 2016). In this PhD thesis on isoprene, we have focused on this region in Chapters 1, 2 and 3. Up to date, only three studies have been conducted in the waters of the Southern Ocean (SO) to study which were the main drivers of isoprene concentration: Kameyama et al. (2010), Ooki et al. (2015), and Hackenberg et al. (2017). In these, chlorophyll-a and sea surface temperature have demonstrated some degree of predictive capacity for isoprene concentrations. However, these three studies showed limitations, in temporal and spatial resolution as well as their experimental design, to understand the distribution of isoprene in the SO. In **Chapters 1 and 2** of this thesis, we took advantage of three new cruises which took place in waters of the SO (TransPEGASO, PEGASO and ACE) to explore the drivers of marine isoprene distribution, and proposed statistical models based on in situ and remotely-sensed predictor variables.

In **Chapter 1** (Rodríguez-Ros et al., 2020a), we explored the question of which are the spatial distribution and main drivers and of isoprene concentration in the SO. We found that isoprene concentrations ranged from 1 to ≈ 100 pM in all the cruise measurements compiled for this study. We found that higher values of isoprene concentrations occurred in waters with high chlorophyll-a and higher temperature. Overall, the higher concentrations were found in productive and warmer waters, while low concentrations occurred in cold high latitude waters of the open ocean. We observed the peak of isoprene concentrations around ≈ 40 °S and water temperatures of 15 °C previously reported by Ooki et al. (2015), which highlights the important of the sub-polar front as a hotspot of isoprene distribution. Regarding the studied cruises, PEGASO showed the highest isoprene concentrations because it targeted preferentially blooming areas. Overall, peaks of isoprene concentration occurred in shelf, coastal waters, and island-associated blooms where phytoplankton communities were not iron-limited Morris and Sanders (2011); Moore et al. (2013a); Hoppe et al. (2017). The rest of isoprene measurements rarely exceeded 50 pM. As to the variables that drive isoprene distribution in the SO, we found that the most relevant were the ones related to phytoplankton abundance and primary production. Thus, isoprene was significantly correlated with chlorophyll-a and other pigments, and showed no correlation with physical variables (solar radiation, sea surface temperature, mixing layer depth) or nutrients. Isoprene concentrations were correlated with all phytoplankton groups, specially with diatoms. Since in land vegetation isoprene production and emission is suggested to be a photoprotective mechanism (Sharkey and Yeh, 2001), we explored the relationship between the concentrations of isoprene and photo-protective pigments, already proposed by Hackenberg et al. (2017). Isoprene positively correlated with photo-protective pigments, as much as it did with light-harvesting pigments. Our results, therefore, did not arise any new evidence for isoprene being involved in photoprotection.

Based on the information obtained regarding the drivers of isoprene in SO waters, we proposed statistical models to predict isoprene concentrations using the measurements taken during the TransPEGASO, PEGASO and ACE cruises. Similarly to the proposed algorithms of Ooki et al. (2015) and Hackenberg et al. (2017) for polar waters, we developed our models based upon the relationship of isoprene concentration to chlorophyll-a (from fluorometric and HPLC techniques) and sea surface temperature. We found a shifting regime based on a sea surface temperature threshold: above or below 3.4 °C. In each regime the correlation of isoprene with chlorophyll-a were different, being higher for the waters above 3.4 °C. A very similar threshold (3.3 °C) was also found by (Ooki et al., 2015), although they also included measurements from the Arctic Ocean. The cross-validation of our model with those of Ooki et al. (2015) and Hackenberg et al. (2017) revealed that our model performs better predicting isoprene concentrations, which can be due to the wider ranges of chlorophyll-a and sea surface temperature incorporated from the PEGASO and ACE cruises. At this point, we must highlight that one of the main challenges when combining data sets from different studies are the potential methodological biases in the measurements of isoprene concentrations and ancillary variables. A clear example of this is the KH-5-10 cruise (Kameyama et al. (2010)), whose isoprene concentrations were much higher than any cruise ever performed in SO waters, and were removed from this study after a personal communication with the authors. However, these methodological biases can be more subtle and the potential errors in isoprene concentrations depending on the instrument or sampling and analytical techniques have not been assessed in any published inter-calibration or meta-analysis. In Chapter 1, where we used measurements from three cruises in which we used the same instrumental setup and methodology, some of these biases are avoided or, at least, reduced; making our findings more robust.

In **Chapter 2** (Rodríguez-Ros et al., 2020b), we provided a new statistical model based on remotely-sensed variables to detect isoprene concentrations in the Southern Ocean: ISOREMS (*Isoprene Southern Ocean Remote Sensing*). To develop it, we matched in situ measurements of isoprene concentration from six different cruises (PEGASO, ACE, ANDREXII, KH-09-5 (Ooki et al., 2015), and AMT22 & 23 (Hackenberg et al., 2017)) with remote sensed variables, following the method described in Galí et al. (2018). Specifically, we tested the potential predictive capacity of the following variables obtained from MODIS-Aqua satellite (accessed in February 2019, 2019): chlorophyll-a, sea surface temperature, particulate inorganic carbon, particulate organic carbon, depth of the euphotic layer, and photosynthetically active radiation. Among them, we found that the best predictors were chlorophyll-a and sea surface temperature. The resulting climatology (2002-2018) of isoprene concentrations and fluxes estimated with ISOREMS were coincident with the patterns of isoprene distribution described in **Chapter 1**. Thus, the highest concentrations and emissions were found in biologically productive waters such as the Antarctic and South Atlantic Shelves, and next to Sub-antarctic islands. Moreover, we also detected the band of higher isoprene concentrations and emissions approximately between 40 – 50°S, and a seasonal peak in summer; being January the month with highest values for both, concentrations and emission fluxes. Although the distribution patterns of concentrations and emissions derived from ISOREMS were similar, emissions showed a more spread distribution with weaker gradients towards continental shelves and islands. Regarding the total climatological emission of isoprene, we estimated a value of 0.063 Tg C yr⁻¹, which supports the order of magnitude suggested by the several bottom-up approaches

performed up to date (Bonsang et al., 1992; Milne et al., 1995; Broadgate et al., 1997; Palmer and Shaw, 2005; Arnold et al., 2009; Gantt et al., 2009; Booge et al., 2016; Brüggemann et al., 2018). Altogether, ISOREMS constitutes a useful tool to study the role of oceanic emissions in climate and the oxidative capacity of the atmosphere over the SO by providing realistic inputs for atmospheric and climatic models.

In summary, the results from **Chapters 1 and 2** supported the idea that the complexity of the Southern Ocean (Ardyna et al., 2017) constitutes a challenge for the model development of trace gases (Neukermans et al., 2018). Meso and sub-meso scales processes, such as eddies driving blooms, create areas with a strong heterogeneity that may include hot-spots of isoprene concentration and emissions. Thus, we strongly recommend performing processes-oriented research cruises, like PEGASO, that will help to increase our understanding of marine isoprene cycling in bloom and upwelling spots Ardyna et al. (2019); specially in the latitudinal band of 40-50 °S. Nevertheless, these studies must be complemented with cruises like ACE, which describe the isoprene distribution over large low-productivity areas, across biological and physical boundaries Ardyna et al. (2017). All the aforementioned would be necessary to develop and validate future model like ISOREMS, not only for the Southern Ocean but also for other regions and the global scale. On this line, we have contributed to the expansion of the existing data-set of isoprene measurements in the ocean, with a significant contribution to measurements in SO waters (Figure 5.4). Before this PhD thesis, the scarcity of measurements in this area made the validation of modelling approaches in the area quite challenging (Conte et al., 2020). We believe that the new data presented here will contribute to solve this issue.

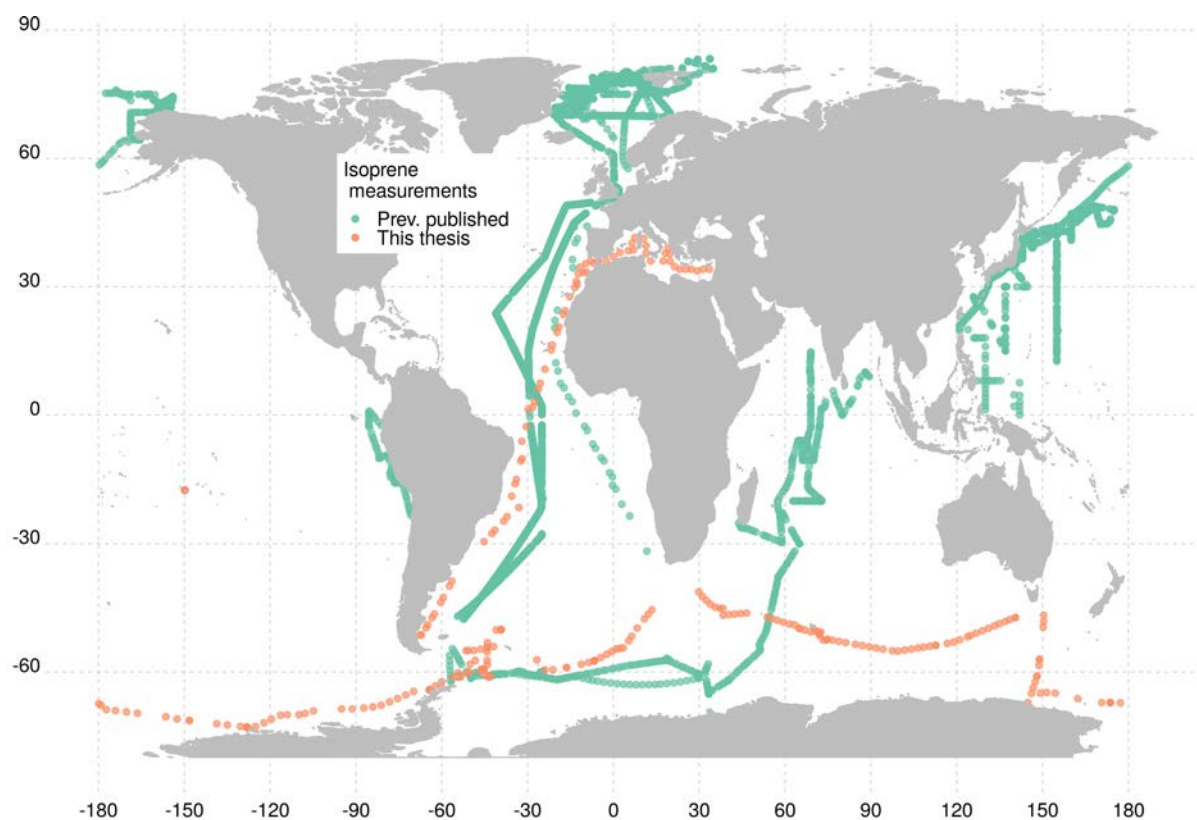


Figure 5.4: Contribution of our cruises to the global dataset of isoprene concentrations.

Combining laboratory and Lagrangian studies in the Southern Ocean

Isoprene production rates normalized by chlorophyll-a ($\rho_{\text{CHLA}}^{\text{PFT}}$) have been determined in laboratory conditions during the exponential growth phase of phytoplankton monocultures (Shaw et al., 2003; Bonsang et al., 2010; Exton et al., 2013; Meskhidze et al., 2015). Among all the species for which values of $\rho_{\text{CHLA}}^{\text{PFT}}$ have ever been estimated (Booge et al., 2016), only 21 are present in natural conditions in the Southern Ocean. Furthermore, values of $\rho_{\text{CHLA}}^{\text{PFT}}$ had not been estimated specifically for the Southern Ocean from field measurements and experiments. In **Chapter 3**, for the first time we estimated $\rho_{\text{CHLA}}^{\text{PFT}}$ from field data, using the Lagrangian studies performed during PEGASO. We found that the values estimated for diatoms and coccolitophores in natural conditions were higher than the mean of the published rates from laboratory experiments (Booge et al., 2016). On the same cruise, we determined for the first time the rates of chemical and biological losses for the Southern Ocean (Chapter 5). This has long been an issue (Shaw et al., 2003; Alvarez et al., 2009; Booge et al., 2018) that has prevented the correct implementation of the full cycling of isoprene in models. Altogether, our field-determined production and loss rates suggest that isoprene cycling in the Southern Ocean is faster than previously thought. We suggest that the methodology followed to estimate isoprene production and degradation rates during PEGASO should be repeated in other regions and opens the door to understand the cycling of isoprene in the ocean. The implementation of these new production and loss rates in the ROMS-BEC model (Nissen et al., 2018) revealed that isoprene concentration is mostly constrained to surface waters (0-20 m). Among the PFT's implemented in ROMS-BEC (Diatoms, Coccolitophores and *Small mixed phytoplankton*), diatoms dominate total isoprene production. However, our field-determined values of $\rho_{\text{CHLA}}^{\text{PFT}}$ for diatoms and coccolitophores were very similar, which revealed that the dominant role of diatoms in isoprene production is due to their higher abundance. We also showed that isoprene production by coccolitophores peaks in the area known as the "Great Calcite Belt" (Balch et al., 2011, 2016). In conclusion, our experimental results suggest that PFT-specific production rates of isoprene may be significantly higher than those estimated from monoculture experiments in the lab. Nevertheless, we must highlight that these results have some limitations since (1) we were not able to determine the value of $\rho_{\text{CHLA}}^{\text{PFT}}$ for *Phaeocystis*, a common bloom former in the Southern Ocean (DiTullio et al., 2000); and (2) ROMS-BEC has a positive chlorophyll bias at high SO latitudes, resulting partly from model-derived higher temperatures, shallower mixed layer depths (ZML) and missing ecosystem complexity. In consequence, the comparison of our modelled concentrations with in situ measurements showed opposite latitudinal patterns.

Shedding light on isoprene production

Isoprene production rates normalized by chlorophyll-a have been determined in a series of lab-focused works (Shaw et al., 2003; Bonsang et al., 2010; Exton et al., 2013; Meskhidze et al., 2015) and used in different modelling approaches to estimate isoprene distribution and/or cycling in the oceans (Arnold et al., 2009; Booge et al., 2016; Conte et al., 2020). However, the behaviour of isoprene production in contrasting environmental conditions, such as light or temper-

ature, has only been assessed in Meskhidze et al. (2015). In this thesis we took advantage of these published rates and implemented them in two different biogeochemical-ecological modelling approaches in **Chapters 3 and 4**, using the ROMS-BEC and DARWIN models, respectively. This type of biogeochemical-ecological models have been repeatedly proposed as the next step towards modeling the cycling of marine isoprene and solving the quantitative gap between bottom-up and top-down estimates of isoprene emission (Booge et al., 2016; Hackenberg et al., 2017; Brüggemann et al., 2018). Biogeochemical-ecological models are able to fully represent marine isoprene cycling both in time and space. Up to date, only Conte et al. (2020) has attempted to implement isoprene production rates normalized per chlorophyll-a ($\rho_{\text{CHLA}}^{\text{PFT}}$) in a model of this kind: PISCES. However, in their model configuration they only used 2 PFTs and laboratory estimates of $\rho_{\text{CHLA}}^{\text{PFT}}$. As discussed in **Chapters 3 and 4**, there are strong discrepancies among the experimental isoprene production rates ($\rho_{\text{CHLA}}^{\text{PFT}}$) even for strains of the same species. In Table 5.4 we have gathered all the $\rho_{\text{CHLA}}^{\text{PFT}}$ estimates used in **Chapters 3 and 4**. Remarkably, the values of $\rho_{\text{CHLA}}^{\text{PFT}}$ for diatoms and coccolithophores obtained from solving the cycling of isoprene in PEGASO blooms (Chapter 3, BASELINE simulation) are higher than estimates from laboratory experiments or retrieved using the light factors from Gantt et al. (2009) and Booge et al. (2018). Overall, we demonstrated that it is possible to estimate values of $\rho_{\text{CHLA}}^{\text{PFT}}$ from Lagrangian experiments. Therefore, this methodology can be used to determine the production rates for other PFT's than the ones from Chapter 3, if future Lagrangian experiments are conducted.

There is a remaining question regarding the production of isoprene by phytoplankton, which is essential to solve when attempting its modelling: Is isoprene constitutive of all phytoplankton groups, of each specific phytoplankton group, or its production is mainly driven by environmental factors? Isoprene production has been detected in all phytoplankton species tested up to date, so the role of isoprene as a by-product of the photosynthetic process is clear, although there are differences among the tested species Booge et al. (2016). However, several works have assumed that isoprene production is independent of the PFT, or there is no need to use many different PFT's and their respective isoprene production rates. On this line, Conte et al. (2020) only used 2 PFT's to study the global cycling of isoprene (diatoms and *others*) and Dani et al. (2017) suggested that only the production by diatoms is enough to estimate the total production of marine isoprene. In terrestrial plants, despite isoprene production and emission vary among species (Pacífico et al., 2009), environmental factors are believed to be the main drivers at the regional and global scales (Zhao et al., 2017). Something similar was observed by Shaw et al. (2003) and Meskhidze et al. (2015) with marine species of phytoplankton, after testing the effects of light and temperature on the isoprene production by cultured strains. However, only two species of phytoplankton have ever been tested for the synergistic effects of light and temperature on isoprene production: *Thalassiosira weissflogii* and *Thalassiosira pseudonana* (Meskhidze et al., 2015). All in all, an important role of environmental factors in isoprene production can not be ignored, as it can be even more important than the taxonomic composition of phytoplankton communities. Consequently, we suggest that values of $\rho_{\text{CHLA}}^{\text{PFT}}$ must be corrected with environmental descriptors, such as light or temperature, as recently proposed by Conte et al. (2020). By doing so, a better implementation of the isoprene production process will be possible in ecological-biogeochemical models.

Finally, as shown in **Chapter 4**, there is a promising relationship between isoprene produc-

tion rates per number of cells ($\rho_{\text{Cells}}^{\text{PFT}}$) and cell size of the organisms. Unfortunately, only Bonsang et al. (2010) made the effort to estimate the cell volume of their experimental strains. We were able to include a few new values of cell volume using the data set of Harrison et al. (2015), which resulted in a decrease in the explained variance from $r^2 = 0.97$ to $r^2 = 0.77$. Consequently, although more data of $\rho_{\text{Cells}}^{\text{PFT}}$ and cell sizes are necessary to see if this relationship is universal or it changes depending on the PFT, this opens the door to the implementation of $\rho_{\text{Cells}}^{\text{PFT}}$ in ecological models which use size-class PFT's.

Table 5.4: Summary of isoprene production rates ($\rho_{\text{CHLA}}^{\text{PFT}}$) estimates per PFTs in this thesis: Chapter 3 (DARWIN-MITgsm) and Chapter 4 (ROMS-BEC). ^a: Estimated in Lagrangian experiments during PEGASO. ^b: Estimated using Booge et al. (2016). ^c: Estimated in Lagrangian experiments during PEGASO using the light factors from Booge et al. (2018) or Gantt et al. (2009). ^d: Estimated using Booge et al. (2016) and Meskhidze et al. (2015).

Chapter	Run name	$\rho_{\text{CHLA}}^{\text{DIAT}}$	$\rho_{\text{CHLA}}^{\text{PRO}}$	$\rho_{\text{CHLA}}^{\text{COCC}}$	$\rho_{\text{CHLA}}^{\text{DIAZ}}$	$\rho_{\text{CHLA}}^{\text{PIC}}$	$\rho_{\text{CHLA}}^{\text{MIX}}$	$\rho_{\text{CHLA}}^{\text{SP}}$	
		mmol mgChl ⁻¹ d ⁻¹							
Chapter 3	BASELINE ^a	12.14	-	10.98	-	-	-	0.69	
ROMS-BEC:	LAB ^b	2.06	-	5.54	-	-	-	5.73	
Southern Ocean	EF. BOOGE ^c	1.2	-	2.5	-	-	-	3.5	
	EF. GANTT ^c	7.8	-	4.9	-	-	-	6.5	
Chapter 4	BASELINE ^d	3.79	5.38	5.16	3	12.46	6.94	-	
DARWIN:	CHLA ^d	All $\rho_{\text{CHLA}}^{\text{PFT}} = 4.53$							-
Global Ocean	RHO. MAX ^d	28.48	11.76	15.36	4.7	32.16	27.6	-	
	RHO. MIN ^d	1.12	1.4	1	1.6	1.4	4.56	-	

New insights on the turnover of isoprene in the surface global ocean

The marine cycle of isoprene in the ocean is still far from being conceptually described and experimentally assessed. Uncertainties related to isoprene production have been largely described in Chapters 3 and 4 of this thesis, and in the previous section. Degradation of isoprene is probably the most unknown part of the marine isoprene cycle and has been pointed out to be the main responsible for the gap between bottom-up and top-down emissions (Booge et al., 2018). This gap in our understanding of isoprene degradation challenges the modelling of marine isoprene cycling (Booge et al., 2016). Isoprene degradation has been proposed to be driven by bacteria and chemical reaction with radicals O₂ and OH (Palmer and Shaw, 2005). However, no isoprene degradation rate by bacteria or chemical radicals has been ever measured and published for the ocean (Booge et al., 2018; McGenity et al., 2018).

In **Chapter 5** of this thesis, we presented data from incubation experiments performed during HOTMIX, TransPEGASO, PEGASO and BIOGAPS. In those, we demonstrated for the first time that isoprene is consumed in the absence of light and ventilation. Moreover, we found that rates of isoprene degradation are directly related to chlorophyll-a levels, and the intercept of that

relationship is coincident with the previously suggested value (0.05 d^{-1}) for chemical degradation (Palmer and Shaw, 2005). The full cycling is synthesized in Figure XX. Furthermore, we showed that chlorophyll-normalized isoprene production increases with sea surface temperature and drops drastically beyond 23°C ; this is in agreement with laboratory results reported by Shaw et al. (2003) and Meskhidze et al. (2015). Although this represents a typical curve of enzymatic activity, the thermal behaviour of the enzymes in charge of isoprene synthesis have not yet been characterized (Dani and Loreto, 2017). Our results suggest that the specific isoprene production is more controlled by temperature than by phytoplankton taxonomy. Furthermore, although ventilation has been considered as the main sink of isoprene in the surface ocean (Booge et al., 2016, 2018), our values of isoprene ventilation to the atmosphere were from 2.5 times higher to 10 times lower than bacterial and chemical degradation (taken together as k_{conc}). In a similar way, vertical mixing was estimated to be one order of magnitude lower than the rest of the loss rates. Overall, the results of Chapter 5 show that marine isoprene is produced and consumed in dynamic cycling by planktonic microbial food webs with a total turnover times between 1.4 and 16 days, and a median of 5 days. This is significantly faster than previously suggested in previous works (e.g. from 16 to 100 days in Hackenberg et al. (2017)). These results solved for the first time the question of the relative magnitudes of the production and consumption rates of isoprene in the open ocean and, consequently, pave the road towards the correct parametrization of the full cycling of marine isoprene in future remote sensing and ecological modelling studies.

Emission of isoprene: bottom-up or top-down estimates?

As discussed in this PhD thesis, there is a current debate about the different estimates of total emission of marine isoprene between bottom-up ($\approx 1 \text{ Tg C yr}^{-1}$) and top-down (up to 12 Tg C yr^{-1}) approaches (see compilation in Brüggemann et al. (2018)). In **Chapters 2 and 3**, we quantified the emissions of isoprene from Southern Ocean waters using two different approaches, respectively: remote sensing retrieval and biogeochemical-ecological modelling. When analyzing monthly climatological fields from both chapters, we observed that they agreed in many aspects regarding the seasonality of isoprene concentrations and emissions, peaking in summer and in coastal areas and island blooms. However, ROMS-BEC results disagree with ISOREMS in the latitudinal distribution of the maximum isoprene concentration and emission levels. Thus, while isoprene peaks in the latitudinal band of 50°S in ROMS-BEC (Chapter 3), with ISOREMS (Chapter 2) the maximum isoprene emission is shifted northwards, to around 40°S . This discrepancy may be due to the aforementioned biases in ROMS-BEC prediction of chlorophyll-a. As to the total emission of isoprene in the SO, IROREMS **Chapter 2** rendered a value of $0.063 \text{ Tg C year}^{-1}$, and ROMS-BEC **Chapter 3** gave $0.071 \text{ Tg C year}^{-1}$, representing the 5-74% and 6 – 84%, respectively, of previous global estimates (see compilation in Brüggemann et al. (2018)). All in all, both estimates are quite similar and support the order of magnitude of the bottom-up estimates (Figure 5.5) and their upper limits exceed the percentage of the global ocean represented by the SO waters, which is $\approx 27\%$ when taking 40°S as the northern limit. Altogether, these emission estimates from **Chapters 2 and 3** do not reject the relevance of the SO, a region particularly sensitive to aerosols of marine origin, for the SOA budget.

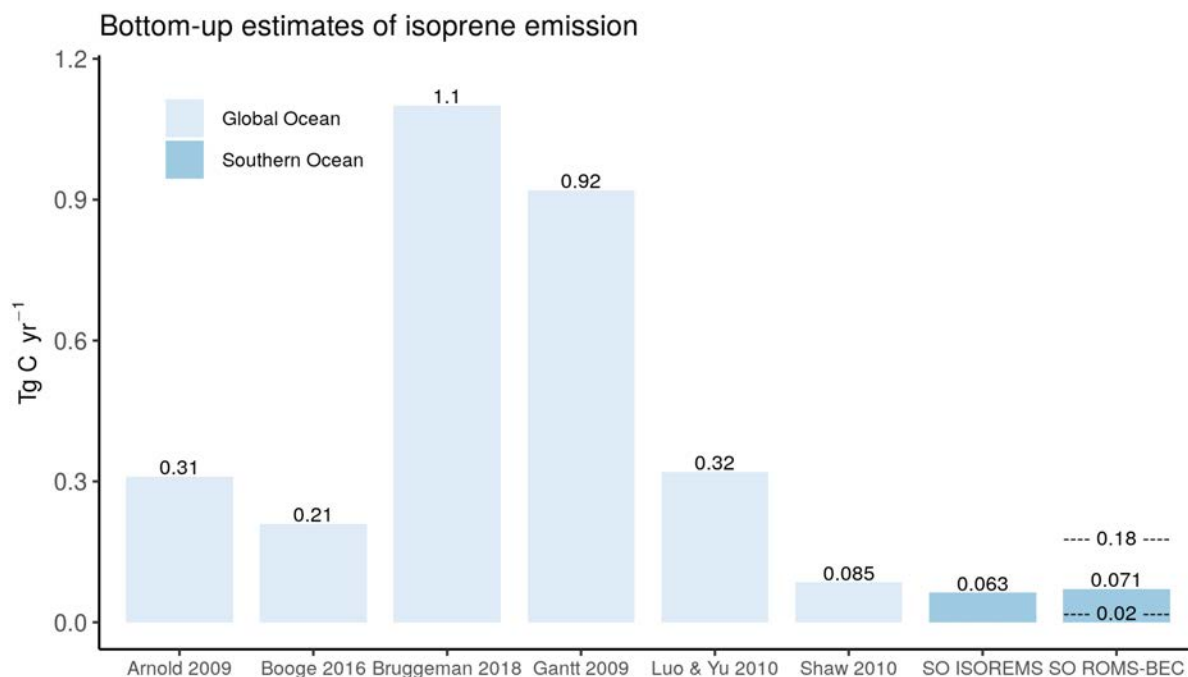


Figure 5.5: Estimates of isoprene emission from the Southern Ocean, calculated in Chapters 2 and 3 of this thesis, in comparison with global bottom-up estimates from previous works (Brüggemann et al., 2018).

Moreover, the results from DARWIN-MITgsm model also contributed to the debate about global emission values estimated from bottom-up and top-down approaches. The global phytoplankton production of isoprene in our DARWIN-MITgsm setup (BASELINE simulation, Chapter 4) amounts 1.82 Tg C yr⁻¹, which is similar to the production estimate by Conte et al. (2020): 1.52 Tg C yr⁻¹. In their work, they estimated a total emission to the atmosphere of 0.66 Tg C yr⁻¹, representing 43.4% of the total production. However, this emission value is the result of adding the photochemical production of isoprene from the surface microlayer; without the photochemical production the emission amounted 0.27 Tg C yr⁻¹. Since we did not model the full cycle of isoprene in Chapter 4, we are not able to estimate the global emission of isoprene. However, our total phytoplankton production of isoprene (1.82 Tg C yr⁻¹) supports the range of emissions provided by bottom-up studies (≈ 1 Tg C yr⁻¹) rather than top-down (up to 12 Tg C yr⁻¹), since the emission of isoprene can not be higher than its total production. Moreover, our estimate of the total production of isoprene in the Southern Ocean ($>40^{\circ}\text{S}$) is 0.39 Tg C yr⁻¹. This represents 22% of the global production estimated by DARWIN, while the global oceanic area belonging in the SO is $\approx 27\%$). On the other hand, the total isoprene production by phytoplankton in the SO estimated with ROMS-BEC (BASELINE simulation) is 0.43 Tg C yr⁻¹. The fact that this value is 10% higher than the estimate from DARWIN-MITgsm can be due to two reasons: (1) ROMS-BEC overestimates chlorophyll-a levels at certain locations of the Southern Ocean, (2) the values of specific production rates implemented in ROMS-BEC were significantly higher. All in all, the isoprene emission to the atmosphere derived from ROMS-BEC accounted for 16.5% of the production by phytoplankton, which is a very similar proportion to that in the model of Conte et al. (2020) (17%), excluding the photochemical production. In conclusion, our results from the ISOREMS, ROMS-BEC and DARWIN-MITgsm models (**Chapters 2, 3 and 4**,

respectively) support the range of global emissions from bottom-up studies (Figure 5.5).

Concluding considerations about modelling of marine isoprene

In this PhD thesis, we have provided new findings that altogether represent an stimulating contribution to the existing debate about the suitability of simple models or ecological-biogeochemical models to study the distribution and cycling of marine isoprene. In this last section, we focus on the pros and cons of both approaches, and highlight the main findings.

In **Chapter 1**, we provided a model to calculate isoprene concentration based on its relationship with chlorophyll-a with the biggest dataset up to date, and validated the results with data from previous field studies. However, these type of models have many limitations, one of them being that relationships based on in situ measured chlorophyll-a can not be directly applied to remotely-sensed chlorophyll-a (Moutier et al., 2019). Moreover, the data of chlorophyll-a came from different cruises that used different analytical procedures, making these measurements a non-harmonized dataset. This hampers implementing them in atmospheric models or remote sensing models of any kind. We solve this issue in **Chapter 2**, proposing ISOREMS as the first statistical model to predict isoprene concentrations based on remote sensing data (chlorophyll-a and sea surface temperature). With the limitation in the fact that the Southern Ocean is a cloudy region (Neukermans et al., 2018), challenging for remote sensing techniques, ISOREMS allows a synoptic assessment of isoprene distribution over the entire SO and offers a promising alternative to studies based purely on field measurements. We should note, though, that the models provided in Chapter 1 and Chapter 2 explain, respectively, 43 – 69%, and 45% of the variance. Overall, **simple statistical models**, mainly those developed from remotely-sensed variables, allow the synoptic study and assessment of isoprene concentrations in the surface ocean at the global scale. Thanks to that, they hold potential to provide realistic inputs to atmospheric and climate models in order to estimate the emission of isoprene and its eventual role as a SOA precursor (Gantt et al., 2009; Shaw et al., 2010). Nevertheless, the current data scarcity of isoprene measurements makes the development of a global simple model based on remotely-sensed variables still a challenge. Furthermore, the correlation of isoprene concentration with in situ measured ancillary variables has been demonstrated, in this PhD thesis and in previous works (Ooki et al., 2015; Hackenberg et al., 2017), to vary depending on the oceanic region. Consequently, we could expect a similar differential behavior when attempting to develop a unique model for the global ocean based on remotely-sensed variables. This issue was pointed out for DMS in Galí et al. (2018), where their proposed model showed different performance depending on the oceanic province, being the Southern Ocean one of the most challenging areas, if not the most. We suggest that when more data of isoprene measurement will be incorporated to the existing global database, it will be possible to detect and characterize regional biases prior attempting its modelling. Altogether, we suggest that regional models similar to ISOREMS must be developed for the rest of oceanic areas in order to estimate the patterns of isoprene concentration, and its eventual emission to the atmosphere, avoiding the extrapolation to the global scale from very sparse datasets. A mosaic of regional models would contribute to close the current existing gap between bottom-up and top-down approaches of global isoprene emission, shedding light on the

relevance of isoprene as one of the main SOA precursors in the remote marine boundary layer.

The use of more complex **models of the ecological-biogeochemical type**, such as ROMS-BEC or DARWIN-MITgsm (respectively, Chapters 3 and 4), to study the marine isoprene cycle partially solves some of the caveats found in the use of simple statistical models, although its pros come along with some cons. On the pros side, ecological-biogeochemical models allow the modelling of the full cycle of marine isoprene through the parametrization of all its production and loss processes. Thus, it is possible to reconstruct not only the surface levels of isoprene concentrations at the global scale but also its vertical distribution and transport. Moreover, these models can be projected into future conditions and assess how the changing environment due to climate warming may influence the cycling of isoprene. On the cons side, however, a model of this type relies on the correct conceptual description and implementation of its terms, which depends on whether experimental works have addressed them, and how accurate their results are. As we have shown along this PhD thesis, this is a current issue for marine isoprene studies for several reasons. Thus, isoprene production and degradation rates are far from being constrained, and the relevance of potential processes are still under discussion, which is the case for isoprene photoproduction in the surface microlayer (Ciuraru et al., 2015b; Brüggemann et al., 2018). Another advantage of this type of models is that sensitivity analyses and model experiments help to detect the main uncertainties and parameters to be constrained in future experimental work, and even which model processes may need to be conceptually revisited. The findings of this thesis will contribute to the improvement of future approaches using ecological-biogeochemical modelling. Specifically, we provide a new methodology to estimate isoprene production rates in Lagrangian occupations and propose new values for the Southern Ocean (Chapter 3). We also assess all published values of specific isoprene production rates and identify which phytoplankton species and taxa must be better constrained (Chapter 4). Finally, we suggest a new parameterization for isoprene degradation rates based on their relationship with chlorophyll-a (Chapter 5).

Future perspectives

- The current data scarcity of isoprene measurements in the oceans makes the development and validation of models a challenging task that must be overtaken in the coming years. Specifically, more studies need to be conducted in contrasting oceanic regions to address the differential behaviour of isoprene. On this line, large open ocean areas like most of the Pacific Ocean are poorly sampled. Data scarcity also occurs in productive regions like the eastern tropical Atlantic, which have emerged in this thesis as a relevant hot-spot for isoprene production. Moreover, present and future measurements must be compiled, and dynamically updated, in a global database in a similar way than it has been done for other trace gases such as DMS (Lana et al., 2011).
- Up to date, there is not any time series of isoprene concentration in the open or oligotrophic ocean. We motivate future researchers to create a set of time series of isoprene concentration and ancillary variables in contrasting regions of the ocean. Moreover, isoprene measurements should be incorporated to existing time series in coastal stations (e.g. Blanes Bay (NW Mediterranean), Scripps Pier (Pacific Ocean), Rothera (W Antarctic Peninsula), etc) or in the few existing time series in the open ocean (e.g. the Bermuda Atlantic Time-series Study (BATS) or the Hawaii Ocean Time-series (HOT)). Doing so, it will be possible to understand, and eventually model, the daily and seasonal cycle of marine isoprene. To achieve this goal, the development of a 1-D model for the cycling of isoprene can be a useful tool, in a similar way than it was done for DMS in the Sargasso sea (Vallina et al., 2008).
- Following the method provided in Chapter 2, the creation of a global model for remote sensing retrieval of isoprene concentrations in the Global Ocean will be a useful tool to be used in atmospheric and climate models. However, we suggest to develop a suite of remote-sensing based models for different regions of the ocean and avoid the extrapolation of the findings in a region to a global scale.
- Isoprene production rates by the different PFT's have been proved to be far from being precisely constrained. Thus, more experiments are needed to quantify the specific production rates of isoprene by the different phytoplankton species as well as its dependence on environmental variables such as light and sea surface temperature (Meskhidze et al., 2015). Moreover, the combination of experiments performed in laboratory conditions and in the field, following the methodology proposed in the Chapter 3 of this thesis, will contribute to clarify the strong current discrepancies in the published isoprene production rates. In the same way, incubation experiments in dark conditions in the field have been proven to be instrumental to resolve isoprene degradation rates in productive (chla-rich) waters. We believe that more experiments of this type are needed to better constrain isoprene degradation at the regional and global scales.
- Degradation of isoprene must be further investigated using molecular tools. In a similar way to that employed by (McGenity et al., 2018; Murrell et al., 2020) to identify the genes that regulate the degradation of isoprene in terrestrial bacteria, the gene of marine bacteria can be

identified. By knowing which genes codify for isoprene degradation we will be able to determine if bacteria are the only consumers or other organisms may be involved in the biological degradation pathway of isoprene. The known genes that codify for isoprene degradation in terrestrial microbes (McGenity et al., 2018) could be a starting point to search in marine microbial metagenomics (Woyke et al., 2009). Enrichments and isolations of marine bacteria capable of degrading isoprene would be an alternative approach, by sequencing the genomes of isolates or sequencing Single Amplified Genomes (SAGs) from enriched assemblages (Yoon et al., 2011). The finding of isoprene degradation genes does not imply that those genes are being expressed. Therefore, metatranscriptomic techniques (Ottesen et al., 2011) will be necessary to determine whether the genes of degradation of isoprene are active.

- The study of isoprene concentration and emission patterns using a global ecological-biogeochemical model, such as DARWIN, is the next step. Although Conte et al. (2020) have recently used a similar model (PISCES) to study isoprene cycling in the global ocean, they only implemented two PFT's in their model configuration: diatoms and *others*. There is room for improvement by the inclusion of more realistic phytoplankton communities. Nevertheless, as stated previously, the validation of these future modelling works will not be possible without enlarging the global database of isoprene measurements.
- Despite on land ecosystems the multiple roles of isoprene are rather well-known (Sharkey and Yeh, 2001), for example as a release product in response to plant stress (Laothawornkitkul et al., 2008b) or playing a key role in plant-herbivore interactions (Laothawornkitkul et al., 2008a), it is still a mystery how this biogenic compound participates in ecological or biochemical processes in marine ecosystems. We could not shed further light on the potential photoprotective role of isoprene (Chapter 1). The ecophysiological roles of isoprene in marine organisms still remain unsolved.

Conclusions

Chapter 1. We assessed the drivers of isoprene in the Southern Ocean. Hot-spots of isoprene concentration in the Southern Ocean occurred in biologically enriched areas non limited by iron such as islands, and coasts of Antarctica. Furthermore, we detected a band of higher isoprene concentrations around 40°S and water temperatures of 15°C. Overall, isoprene concentration is driven by phytoplankton abundance, specially diatoms, and primary productivity over physical or environmental variables. We provided an empirical relationship of isoprene concentration with chlorophyll-a which showed a differential behaviour when sea surface temperature is below or above 3.4°C. Finally, we were not able to demonstrate any photo-protective role of isoprene for phytoplankton, so this question still remains open.

Chapter 2. ISOREMS is the first satellite-only based algorithm for the retrieval of isoprene concentration in the Southern Ocean. Sea surface concentrations from six cruises were matched with remotely-sensed variables from MODIS Aqua, and isoprene was best predicted by multiple linear regression with chlorophyll-a and sea surface temperature. Climatological (2002-2018) isoprene distributions computed with ISOREMS revealed high concentrations in coastal and near-island waters, and within the 40°-50 °S latitudinal band. Isoprene seasonality paralleled phytoplankton productivity, with annual maxima in summer. The annual Southern Ocean emission of isoprene was estimated at 0.063 Tg C yr⁻¹. The algorithm can provide spatially and temporally realistic inputs to atmospheric and climate models.

Chapter 3. We resolved isoprene cycling at three sampling sites in the Southern Ocean (SO) and estimated in situ isoprene production rates by diatoms, coccolithophores and a group of *small mixed phytoplankton*, as well as isoprene loss rate constants. For diatoms and coccolithophores, these field-derived specific production rates are at the high end of existing laboratory-based rates measured with algal monocultures. Experimentally determined isoprene loss rate constants vary largely among the sampling sites, but are also higher than the ones prescribed hitherto. We implemented these experimental data with an isoprene cycling module in an ecosystem model of the SO (ROMS-BEC). According to ROMS-BEC model, diatoms were the most abundant phytoplankton in the SO (> 40°S) and the SO (> 40°S) contributes 0.071 Tg C year⁻¹ to the global oceanic emissions of isoprene. Ecological modelling of trace gases is a complementary approach to statistical and remote sensing models to synoptically assess marine isoprene production, degradation and emission patterns in SO waters. The model developed here is a useful tool to point out the biggest uncertainties to be experimentally solved by future laboratory and fieldwork.

Chapter 4. Global production of marine isoprene ranges from 0.4 to 9.8 Gmol yr⁻¹. Isoprene production is constrained to surface levels and peaks in summer around the bands of 40°S and 40°N. Nevertheless, other regions, such as the eastern tropical Atlantic, are also hot-spots of isoprene production. The PFT dominance of phytoplankton production is really heterogeneous all over the oceans, and usually (70–80% of global ocean surface area) the PFT that dominates isoprene production is not the one that contributes the most to community biomass. Diatoms dominate the production of isoprene in the polar regions over the year but not in the tropical and subtropical re-

gions, where pico-eukaryotes and prokaryotes play a predominant role. However, we must stress that these results are biased by the use of isoprene production rates calculated in laboratory experiments, which showed strong discrepancies even among strains of the same species.

Chapter 5. Isoprene is dynamically produced and consumed by planktonic microbial food webs in the open ocean, often being the biological+chemical degradation more important than ventilation to the atmosphere, and much faster than vertical mixing. Chlorophyll-a normalized (specific) isoprene production increases with sea surface temperature and drops dramatically beyond 23°C, which suggest that phytoplankton taxonomy is less important than previously thought. Isoprene degradation by bacteria and chemical radicals is directly related to chlorophyll-a levels, which allows its parameterization in future modelling works. Altogether, we suggested a median turnover times of isoprene of 5 days, which is faster than previously stated by most studies.

Bibliography

- accessed in February 2019, M.-A. O. C. L. (2019). Nasa goddard space flight center, ocean ecology laboratory, ocean biology processing group.
- Airs, R. L. and Archer, S. D. (2010). Analysis of glycine betaine and choline in seawater particulates by liquid chromatography/electrospray ionization/mass spectrometry. *Limnology and Oceanography: Methods*, 8(10):499–506.
- Alvarez, L. A., Exton, D. A., Timmis, K. N., Suggett, D. J., and McGenity, T. J. (2009). Characterization of marine isoprene-degrading communities. *Environmental microbiology*, 11(12):3280–3291.
- Andreae, M. and Rosenfeld, D. (2008). Aerosol–cloud–precipitation interactions. part 1. the nature and sources of cloud-active aerosols. *Earth-Science Reviews*, 89(1):13–41.
- Antoine, D., Thomalla, S., Berliner, D., Little, H., Moutier, W., Olivier-Morgan, A., Robinson, C, R.-K. T., and Schuback, N. (2019). Phytoplankton pigment concentrations of seawater sampled during the antarctic circumnavigation expedition (ace) during the austral summer of 2016/2017. (version 1.0) [data set]. *Zenodo*.
- Archer, S. D., Goldson, L. E., Liddicoat, M. I., Cummings, D. G., and Nightingale, P. D. (2007). Marked seasonality in the concentrations and sea-to-air flux of volatile iodocarbon compounds in the western english channel. *Journal of Geophysical Research: Oceans*, 112(C8).
- Ardyna, M., Claustre, H., Sallée, J.-B., D'Ovidio, F., Gentili, B., Van Dijken, G., D'Ortenzio, F., and Arrigo, K. R. (2017). Delineating environmental control of phytoplankton biomass and phenology in the southern ocean. *Geophysical Research Letters*, 44(10):5016–5024.
- Ardyna, M., Lacour, L., Sergi, S., d'Ovidio, F., Sallée, J.-B., Rembauville, M., Blain, S., Tagliabue, A., Schlitzer, R., Jeandel, C., et al. (2019). Hydrothermal vents trigger massive phytoplankton blooms in the southern ocean. *Nature communications*, 10(1):2451.
- Arneth, A., Monson, R., Schurgers, G., Niinemets, Ü., and Palmer, P. (2008). Why are estimates of global terrestrial isoprene emissions so similar (and why is this not so for monoterpenes). *Atmos. Chem. Phys.*, 8(16):4605–4620.
- Arnold, S., Spracklen, D., Williams, J., Yassaa, N., Sciare, J., Bonsang, B., Gros, V., Peeken, I., Lewis, A., Alvain, S., et al. (2009). Evaluation of the global oceanic isoprene source and its impacts on marine organic carbon aerosol. *Atmospheric Chemistry and Physics*, 9(4):1253–1262.
- Baker, A., Turner, S., Broadgate, W., Thompson, A., McFiggans, G., Vesperini, O., Nightingale, P., Liss, P., and Jickells, T. (2000). Distribution and sea-air fluxes of biogenic trace gases in the eastern atlantic ocean. *Global Biogeochemical Cycles*, 14(3):871–886.
- Balch, W., Drapeau, D., Bowler, B., Lyczkowski, E., Booth, E., and Alley, D. (2011). The contribution of coccolithophores to the optical and inorganic carbon budgets during the southern ocean gas exchange experiment: New evidence in support of the “great calcite belt” hypothesis. *Journal of Geophysical Research: Oceans*, 116(C4).

- Balch, W. M., Bates, N. R., Lam, P. J., Twining, B. S., Rosengard, S. Z., Bowler, B. C., Drapeau, D. T., Garley, R., Lubelczyk, L. C., Mitchell, C., et al. (2016). Factors regulating the great calcite belt in the southern ocean and its biogeochemical significance. *Global Biogeochemical Cycles*, 30(8):1124–1144.
- Banas, N. S. (2011). Adding complex trophic interactions to a size-spectral plankton model: Emergent diversity patterns and limits on predictability. *Ecological modelling*, 222(15):2663–2675.
- Behrenfeld, M. J. and Boss, E. (2006). Beam attenuation and chlorophyll concentration as alternative optical indices of phytoplankton biomass. *Journal of Marine Research*, 64(3):431–451.
- Benavides, M., Bonnet, S., Hernández, N., Martínez-Pérez, A. M., Nieto-Cid, M., Álvarez-Salgado, X. A., Baños, I., Montero, M. F., Mazuecos, I. P., Gasol, J. M., et al. (2016). Basin-wide n₂ fixation in the deep waters of the mediterranean sea. *Global Biogeochemical Cycles*, 30(6):952–961.
- Bintanja, R., Severijns, C., Haarsma, R., and Hazeleger, W. (2014). The future of antarctica's surface winds simulated by a high-resolution global climate model: 1. model description and validation. *Journal of Geophysical Research: Atmospheres*, 119(12):7136–7159.
- Bonsang, B., Gros, V., Peeken, I., Yassaa, N., Bluhm, K., Zöllner, E., Sarda-Esteve, R., and Williams, J. (2010). Isoprene emission from phytoplankton monocultures: the relationship with chlorophyll-a, cell volume and carbon content. *Environmental Chemistry*, 7(6):554–563.
- Bonsang, B., Polle, C., and Lambert, G. (1992). Evidence for marine production of isoprene. *Geophysical Research Letters*, 19(11):1129–1132.
- Booge, D., Marandino, C. A., Schlundt, C., Palmer, P. I., Schlundt, M., Atlas, E. L., Bracher, A., Saltzman, E. S., and Wallace, D. W. (2016). Can simple models predict large-scale surface ocean isoprene concentrations? *Atmospheric Chemistry and Physics*, 16(18):11807–11821.
- Booge, D., Schlundt, C., Bracher, A., Endres, S., Zäncker, B., and Marandino, C. A. (2018). Marine isoprene production and consumption in the mixed layer of the surface ocean—a field study over two oceanic regions. *Biogeosciences (BG)*, 15:649–667.
- Boyce, D. G., Lewis, M. R., and Worm, B. (2010). Global phytoplankton decline over the past century. *Nature*, 466(7306):591.
- Broadgate, Liss, and Penkett (1997). Seasonal emissions of isoprene and other reactive hydrocarbon gases from the ocean. *Geophysical Research Letters*, 24(21):2675–2678.
- Broadgate, Malin, Küpper, Thompson, and Liss (2004). Isoprene and other non-methane hydrocarbons from seaweeds: a source of reactive hydrocarbons to the atmosphere. *Marine Chemistry*, 88(1):61–73.
- Brüggemann, M., Hayeck, N., and George, C. (2018). Interfacial photochemistry at the ocean surface is a global source of organic vapors and aerosols. *Nature communications*, 9(1):2101.
- Carlton, A., Wiedinmyer, C., and Kroll, J. (2009). A review of secondary organic aerosol (soa) formation from isoprene.
- Carpenter, L. J., Archer, S. D., and Beale, R. (2012). Ocean-atmosphere trace gas exchange. *Chemical Society Reviews*, 41(19):6473–6506.
- Carpenter, L. J., MacDonald, S. M., Shaw, M. D., Kumar, R., Saunders, R. W., Parthipan, R., Wilson, J., and Plane, J. M. (2013). Atmospheric iodine levels influenced by sea surface emissions of inorganic iodine. *Nature Geoscience*, 6(2):108–111.
- Carshaw, K., Boucher, O., Spracklen, D., Mann, G., Rae, J., Woodward, S., and Kulmala, M. (2010). A review of natural aerosol interactions and feedbacks within the earth system. *Atmospheric Chemistry & Physics*, 10(4).
- Carshaw, K., Lee, L., Reddington, C., Pringle, K., Rap, A., Forster, P., Mann, G., Spracklen, D., Woodhouse, M., Regayre, L., et al. (2013). Large contribution of natural aerosols to uncertainty in indirect forcing. *Nature*, 503(7474):67–71.

- Cassar, N., Wright, S. W., Thomson, P. G., Trull, T. W., Westwood, K. J., de Salas, M., Davidson, A., Pearce, I., Davies, D. M., and Matear, R. J. (2015). The relation of mixed-layer net community production to phytoplankton community composition in the southern ocean. *Global Biogeochemical Cycles*, 29(4):446–462.
- Charlson, R. J., Lovelock, J. E., Andreae, M. O., and Warren, S. G. (1987). Oceanic phytoplankton, atmospheric sulphur, cloud albedo and climate. *nature*, 326(6114):655.
- Ciuraru, R., Fine, L., Pinxteren, M. v., D'Anna, B., Herrmann, H., and George, C. (2015a). Unravelling new processes at interfaces: photochemical isoprene production at the sea surface. *Environmental science & technology*, 49(22):13199–13205.
- Ciuraru, R., Fine, L., van Pinxteren, M., D'Anna, B., Herrmann, H., and George, C. (2015b). Photosensitized production of functionalized and unsaturated organic compounds at the air-sea interface. *Scientific reports*, 5.
- Claeys, M., Graham, B., Vas, G., Wang, W., Vermeylen, R., Pashynska, V., Cafmeyer, J., Guyon, P., Andreae, M. O., Artaxo, P., et al. (2004). Formation of secondary organic aerosols through photooxidation of isoprene. *Science*, 303(5661):1173–1176.
- Cleveland, C. C. and Yavitt, J. (1998). Microbial consumption of atmospheric isoprene in a temperate forest soil. *Appl. Environ. Microbiol.*, 64(1):172–177.
- Colomb, A., Gros, V., Alvain, S., Sarda-Estève, R., Bonsang, B., Moulin, C., Klüpfel, T., and Williams, J. (2009). Variation of atmospheric volatile organic compounds over the southern indian ocean (30–49 s). *Environmental Chemistry*, 6(1):70–82.
- Conte, L., Szopa, S., Aumont, O., Gros, V., and Bopp, L. (2020). Sources and sinks of isoprene in the global open ocean: simulated patterns and emissions to the atmosphere. *Journal of Geophysical Research: Oceans*.
- Cook, S. S., Whittock, L., Wright, S. W., and Hallegraeff, G. M. (2011). Photosynthetic pigment and genetic differences between two southern ocean morphotypes of *emiliania huxleyi* (haptophyta) 1. *Journal of phycology*, 47(3):615–626.
- Cui, T., Green, H. S., Selleck, P. W., Zhang, Z., O'Brien, R. E., Gold, A., Keywood, M., Kroll, J. H., and Surratt, J. D. (2019). Chemical characterization of isoprene- and monoterpene-derived secondary organic aerosol tracers in remote marine aerosols over a quarter century. *ACS Earth and Space Chemistry*.
- Dall'Osto, M., Ovadnevaite, J., Paglione, M., Beddows, D. C., Ceburnis, D., Cree, C., Cortés, P., Zamanillo, M., Nunes, S. O., Pérez, G. L., et al. (2017). Antarctic sea ice region as a source of biogenic organic nitrogen in aerosols. *Scientific reports*, 7(1):6047.
- Dani, K. S., Benavides, A. M. S., Michelozzi, M., Peluso, G., Torzillo, G., and Loreto, F. (2017). Relationship between isoprene emission and photosynthesis in diatoms, and its implications for global marine isoprene estimates. *Marine Chemistry*, 189:17–24.
- Dani, K. S. and Loreto, F. (2017). Trade-off between dimethyl sulfide and isoprene emissions from marine phytoplankton. *Trends in plant science*, 22(5):361–372.
- DiTullio, G., Grebmeier, J., Arrigo, K., Lizotte, M., Robinson, D., Leventer, A., Barry, J., VanWoert, M., and Dunbar, R. (2000). Rapid and early export of *phaeocystis antarctica* blooms in the ross sea, antarctica. *Nature*, 404(6778):595.
- Dutkiewicz, S., Cermenon, P., Jahn, O., Follows, M. J., Hickman, A. E., Taniguchi, D. A., and Ward, B. A. (2019). Dimensions of marine phytoplankton diversity. *Biogeosciences Discussions*, pages 1–46.
- Dutkiewicz, S., Follows, M. J., and Bragg, J. G. (2009). Modeling the coupling of ocean ecology and biogeochemistry. *Global Biogeochemical Cycles*, 23(4).
- Egan, L. (2008). Determination of nitrate and/or nitrite in brackish or seawater by flow injection analysis. quickchem method 31-107-04-1-c.

- El Khawand, M., Crombie, A. T., Johnston, A., Vavlline, D. V., McAuliffe, J. C., Latone, J. A., Primak, Y. A., Lee, S.-K., Whited, G. M., McGenity, T. J., et al. (2016). Isolation of isoprene degrading bacteria from soils, development of isoa gene probes and identification of the active isoprene-degrading soil community using dna-stable isotope probing. *Environmental microbiology*, 18(8):2743–2753.
- Exton, D., Suggestt, D. J., McGenity, T. J., and Steinke, M. (2013). Chlorophyll-normalized isoprene production in laboratory cultures of marine microalgae and implications for global models. *Limnology and Oceanography*, 58(4):1301–1311.
- Exton, D. A., McGenity, T. J., Steinke, M., Smith, D. J., and Suggestt, D. J. (2015). Uncovering the volatile nature of tropical coastal marine ecosystems in a changing world. *Global change biology*, 21(4):1383–1394.
- Fall, R. and Copley, S. D. (2000). Bacterial sources and sinks of isoprene, a reactive atmospheric hydrocarbon. *Environmental microbiology*, 2(2):123–130.
- Fay, A. and McKinley, G. (2014). Global open-ocean biomes: mean and temporal variability. *Earth System Science Data*, 6(2):273–284.
- Follows, M. J., Dutkiewicz, S., Grant, S., and Chisholm, S. W. (2007). Emergent biogeography of microbial communities in a model ocean. *science*, 315(5820):1843–1846.
- Fu, H., Ciuraru, R., Dupart, Y., Passananti, M., Tinel, L., Rossignol, S., Perrier, S., Donaldson, D. J., Chen, J., and George, C. (2015). Photosensitized production of atmospherically reactive organic compounds at the air/aqueous interface. *Journal of the American Chemical Society*, 137(26):8348–8351.
- Galí, M., Devred, E., Babin, M., and Levasseur, M. (2019). Decadal increase in arctic dimethylsulfide emission. *Proceedings of the National Academy of Sciences*, 116(39):19311–19317.
- Galí, M., Devred, E., Levasseur, M., Royer, S.-J., and Babin, M. (2015). A remote sensing algorithm for planktonic dimethylsulfoniopropionate (dmSP) and an analysis of global patterns. *Remote Sensing of Environment*, 171:171–184.
- Galí, M., Levasseur, M., Devred, E., Simó, R., and Babin, M. (2018). Sea-surface dimethylsulfide (dms) concentration from satellite data at global and regional scales. *Biogeosciences*, 15(11):3497–3519.
- Gantt, B., Meskhidze, N., and Kamykowski, D. (2009). A new physically-based quantification of isoprene and primary organic aerosol emissions from the world's oceans. *Atmos. Chem. Phys. Discuss*, 9:2933–2965.
- Gasol, J. M. and Del Giorgio, P. A. (2000). Using flow cytometry for counting natural planktonic bacteria and understanding the structure of planktonic bacterial communities. *Scientia Marina*, 64(2):197–224.
- Gasol, J. M. and Duarte, C. M. (2000). Comparative analyses in aquatic microbial ecology: how far do they go? *FEMS Microbiology Ecology*, 31(2):99–106.
- Gervais, F., Riebesell, U., and Gorbunov, M. Y. (2002). Changes in primary productivity and chlorophyll a in response to iron fertilization in the southern polar frontal zone. *Limnology and Oceanography*, 47(5):1324–1335.
- Gibb, S. W., Mantoura, R. F. C., and Liss, P. S. (1999). Ocean-atmosphere exchange and atmospheric speciation of ammonia and methylamines in the region of the nw arabian sea. *Global Biogeochemical Cycles*, 13(1):161–178.
- Grasshoff, K., Kremling, K., and Ehrhardt, M. (2009). *Methods of seawater analysis*. John Wiley & Sons.
- Gray, C. M., Helmig, D., and Fierer, N. (2015). Bacteria and fungi associated with isoprene consumption in soil. *Elem Sci Anth*, 3.
- Guenther, A., Hewitt, C. N., Erickson, D., Fall, R., Geron, C., Graedel, T., Harley, P., Klinger, L., Lerdau, M., McKay, W., et al. (1995). A global model of natural volatile organic compound emissions. *Journal of Geophysical Research: Atmospheres*, 100(D5):8873–8892.
- Guenther, A., Jiang, X., Heald, C., Sakulyanontvittaya, T., Duhl, T., Emmons, L., and Wang, X. (2012). The model of emissions of gases and aerosols from nature version 2.1 (megan2. 1): an extended and updated framework for modeling biogenic emissions.

- Guenther, A., Karl, T., Harley, P., Wiedinmyer, C., Palmer, P., and Geron, C. (2006). Estimates of global terrestrial isoprene emissions using megan (model of emissions of gases and aerosols from nature). *Atmospheric Chemistry and Physics*, 6(11):3181–3210.
- Hackenberg, S., Andrews, S., Airs, R., Arnold, S., Bouman, H., Brewin, R., Chance, R., Cummings, D., Dall'Olmo, G., Lewis, A., et al. (2017). Potential controls of isoprene in the surface ocean. *Global Biogeochemical Cycles*, 31(4):644–662.
- Hansen, H. and Grasshoff, K. (1983). Automated chemical analysis. In *Methods of seawater analysis*, pages 347–379. Verlag Chemie Weinheim.
- Harrison, P. J., Zingone, A., Mickelson, M. J., Lehtinen, S., Ramaiah, N., Kraberg, A. C., Sun, J., McQuatters-Gollop, A., and Jakobsen, H. H. (2015). Cell volumes of marine phytoplankton from globally distributed coastal data sets. *Estuarine, Coastal and Shelf Science*, 162:130–142.
- Haumann, F. A. (2016). *Southern Ocean response to recent changes in surface freshwater fluxes*. Ph.d thesis, ETH Zürich.
- Heal, M. R., Kumar, P., and Harrison, R. M. (2012). Particles, air quality, policy and health. *Chemical Society Reviews*, 41(19):6606–6630.
- Henry, T., Robinson, C., Haumann, F., Thomas, J., Hitchings, J., Schuback, N., Tsukernik, M., and Leonard, K. (2020). Physical and biogeochemical oceanography data from conductivity, temperature, depth (ctd) rosette deployments during the antarctic circumnavigation expedition (ace). *ACE Expedition data-sets*.
- Henze, D. K. and Seinfeld, J. H. (2006). Global secondary organic aerosol from isoprene oxidation. *Geophysical Research Letters*, 33(9).
- Higgins, H. W., Wright, S. W., and Schluter, L. (2011). Quantitative interpretation of chemotaxonomic pigment data. *Cambridge University Press*.
- Hirata, T., Hardman-Mountford, N., Brewin, R., Aiken, J., Barlow, R., Suzuki, K., Isada, T., Howell, E., Hashioka, T., Noguchi-Aita, M., et al. (2011). Synoptic relationships between surface chlorophyll-a and diagnostic pigments specific to phytoplankton functional types. *Biogeosciences*, 8(2):311–327.
- Hoegh-Guldberg, O. and Bruno, J. F. (2010). The impact of climate change on the world's marine ecosystems. *Science*, 328(5985):1523–1528.
- Holeton, C. L., Nedelec, F., Sanders, R., Brown, L., Moore, C. M., Stevens, D. P., Heywood, K. J., Statham, P. J., and Lucas, C. H. (2005). Physiological state of phytoplankton communities in the southwest atlantic sector of the southern ocean, as measured by fast repetition rate fluorometry. *Polar Biology*, 29(1):44–52.
- Holte, J., Talley, L. D., Gilson, J., and Roemmich, D. (2017). An argo mixed layer climatology and database. *Geophysical Research Letters*.
- Hoppe, C., Klaas, C., Ossebaar, S., Soppa, M. A., Cheah, W., Laglera, L., Santos-Echeandia, J., Rost, B., Wolf-Gladrow, D., Bracher, A., et al. (2017). Controls of primary production in two phytoplankton blooms in the antarctic circumpolar current. *Deep Sea Research Part II: Topical Studies in Oceanography*, 138:63–73.
- Hu, Q.-H., Xie, Z.-Q., Wang, X.-M., Kang, H., He, Q.-F., and Zhang, P. (2013). Secondary organic aerosols over oceans via oxidation of isoprene and monoterpenes from arctic to antarctic. *Scientific reports*, 3.
- Huang, D., Zhang, X., Chen, Z., Zhao, Y., and Shen, X. (2011). The kinetics and mechanism of an aqueous phase isoprene reaction with hydroxyl radical. *Atmospheric Chemistry and Physics*, 11(15):7399.
- Johnston, A., Crombie, A. T., El Khawand, M., Sims, L., Whited, G. M., McGenity, T. J., and Colin Murrell, J. (2017). Identification and characterisation of isoprene-degrading bacteria in an estuarine environment. *Environmental microbiology*, 19(9):3526–3537.

- Kameyama, S., Tanimoto, H., Inomata, S., Tsunogai, U., Ooki, A., Takeda, S., Obata, H., Tsuda, A., and Uematsu, M. (2010). High-resolution measurement of multiple volatile organic compounds dissolved in seawater using equilibrator inlet–proton transfer reaction-mass spectrometry (ei–ptr-ms). *Marine Chemistry*, 122(1):59–73.
- Kameyama, S., Yoshida, S., Tanimoto, H., Inomata, S., Suzuki, K., and Yoshikawa-Inoue, H. (2014). High-resolution observations of dissolved isoprene in surface seawater in the southern ocean during austral summer 2010–2011. *Journal of Oceanography*, 70(3):225–239.
- Kim, M. J., Novak, G. A., Zoerb, M. C., Yang, M., Blomquist, B. W., Huebert, B. J., Cappa, C. D., and Bertram, T. H. (2017). Air-sea exchange of biogenic volatile organic compounds and the impact on aerosol particle size distributions. *Geophysical Research Letters*, 44(8):3887–3896.
- Kolber, Z. S., Prášil, O., and Falkowski, P. G. (1998). Measurements of variable chlorophyll fluorescence using fast repetition rate techniques: defining methodology and experimental protocols. *Biochimica et Biophysica Acta (BBA)-Bioenergetics*, 1367(1):88–106.
- Kroll, J. H., Ng, N. L., Murphy, S. M., Flagan, R. C., and Seinfeld, J. H. (2006). Secondary organic aerosol formation from isoprene photooxidation. *Environmental science & technology*, 40(6):1869–1877.
- Kuhn, A., Dutkiewicz, S., Jahn, O., Clayton, S., Rynearson, T., Mazloff, M., and Barton, A. (2019). Temporal and spatial scales of correlation in marine phytoplankton communities. *Journal of Geophysical Research: Oceans*.
- Kurihara, M., Iseda, M., Ioriya, T., Horimoto, N., Kanda, J., Ishimaru, T., Yamaguchi, Y., and Hashimoto, S. (2012). Brominated methane compounds and isoprene in surface seawater of sagami bay: Concentrations, fluxes, and relationships with phytoplankton assemblages. *Marine Chemistry*, 134:71–79.
- Kurihara, M., Kimura, M., Iwamoto, Y., Narita, Y., Ooki, A., Eum, Y.-J., Tsuda, A., Suzuki, K., Tani, Y., Yokouchi, Y., et al. (2010). Distributions of short-lived iodocarbons and biogenic trace gases in the open ocean and atmosphere in the western north pacific. *Marine Chemistry*, 118(3):156–170.
- Lamb, B., Guenther, A., Gay, D., and Westberg, H. (1987). A national inventory of biogenic hydrocarbon emissions. *Atmospheric Environment (1967)*, 21(8):1695–1705.
- Lana, A., Bell, T., Simó, R., Vallina, S., Ballabrera-Poy, J., Kettle, A., Dachs, J., Bopp, L., Saltzman, E., Stefels, J., et al. (2011). An updated climatology of surface dimethylsulfide concentrations and emission fluxes in the global ocean. *Global Biogeochemical Cycles*, 25(1).
- Laothawornkitkul, J., Paul, N. D., Vickers, C. E., Possell, M., Mullineaux, P. M., Hewitt, C. N., and Taylor, J. E. (2008a). The role of isoprene in insect herbivory. *Plant signaling & behavior*, 3(12):1141–1142.
- Laothawornkitkul, J., Paul, N. D., Vickers, C. E., Possell, M., Taylor, J. E., Mullineaux, P. M., and Hewitt, C. N. (2008b). Isoprene emissions influence herbivore feeding decisions. *Plant, cell & environment*, 31(10):1410–1415.
- Le Clainche, Y. L., Levasseur, M., Vézina, A., Dacey, J. W., and Saucier, F. J. (2004). Behaviour of the ocean dms (p) pools in the sargasso sea viewed in a coupled physical-biogeochemical ocean model. *Canadian Journal of Fisheries and Aquatic Sciences*, 61(5):788–803.
- Lebaron, P., Servais, P., Agogué, H., Courties, C., and Joux, F. (2001). Does the high nucleic acid content of individual bacterial cells allow us to discriminate between active cells and inactive cells in aquatic systems? *Appl. Environ. Microbiol.*, 67(4):1775–1782.
- Legendre, P. and Legendre, L. F. (2012). *Numerical ecology*. Elsevier.
- Lewis, A., Hopkins, J., Read, K., Carpenter, L., Pilling, M., and Stanton, J. (2005). Sources and sinks of acetaldehyde, acetone and methanol in north atlantic marine boundary layer air. *Atmos. Chem. Phys*, 5:1963–1974.
- Li, J.-L., Zhai, X., Ma, Z., Zhang, H.-H., and Yang, G.-P. (2019). Spatial distributions and sea-to-air fluxes of non-methane hydrocarbons in the atmosphere and seawater of the western pacific ocean. *Science of The Total Environment*.

- Liakakou, E., Vrekoussis, M., Bonsang, B., Donousis, C., Kanakidou, M., and Mihalopoulos, N. (2007). Isoprene above the eastern mediterranean: Seasonal variation and contribution to the oxidation capacity of the atmosphere. *Atmospheric Environment*, 41(5):1002–1010.
- Liao, H., Henze, D. K., Seinfeld, J. H., Wu, S., and Mickley, L. J. (2007). Biogenic secondary organic aerosol over the united states: Comparison of climatological simulations with observations. *Journal of Geophysical Research: Atmospheres*, 112(D6).
- Litchman, E., Edwards, K. F., and Klausmeier, C. A. (2015). Microbial resource utilization traits and trade-offs: implications for community structure, functioning, and biogeochemical impacts at present and in the future. *Frontiers in microbiology*, 6:254.
- Longhurst, A. (1995). Seasonal cycles of pelagic production and consumption. *Progress in oceanography*, 36(2):77–167.
- Loreto, F. and Schnitzler, J.-P. (2010). Abiotic stresses and induced bvocs. *Trends in plant science*, 15(3):154–166.
- Lovelock, J. (1979). A new look at life on earth. *New York*.
- Lovelock, J. (2003). Gaia: the living earth. *Nature*, 426(6968):769–770.
- Lovelock, J. E. and Margulis, L. (1974). Atmospheric homeostasis by and for the biosphere: the gaia hypothesis. *Tellus*, 26(1-2):2–10.
- Luo, G. and Yu, F. (2010). A numerical evaluation of global oceanic emissions of α -pinene and isoprene. *Atmospheric Chemistry and Physics*, 10(4):2007–2015.
- Matsunaga, S., Mochida, M., Saito, T., and Kawamura, K. (2002). In situ measurement of isoprene in the marine air and surface seawater from the western north pacific. *Atmospheric Environment*, 36(39):6051–6057.
- Matsunaga, S., Wiedinmyer, C., Guenther, A., Orlando, J., Karl, T., Toohey, D., Greenberg, J., and Kajii, Y. (2005). Isoprene oxidation products are a significant atmospheric aerosol component. *Atmospheric Chemistry and Physics Discussions*, 5(6):11143–11156.
- McGenity, T. J., Crombie, A. T., and Murrell, J. C. (2018). Microbial cycling of isoprene, the most abundantly produced biological volatile organic compound on earth. *The ISME journal*, page 1.
- McKay, W., Turner, M., Jones, B., and Halliwell, C. (1996). Emissions of hydrocarbons from marine phytoplankton—some results from controlled laboratory experiments. *Atmospheric Environment*, 30(14):2583–2593.
- Medeiros, D., Blitz, M., James, L., Speak, T., and Seakins, P. (2018). Kinetics of the reaction of oh with isoprene over a wide range of temperature and pressure including direct observation of equilibrium with the oh adducts. *The Journal of Physical Chemistry A*, 122(37):7239–7255.
- Meier, W., Fetterer, F., Savoie, M., Mallory, S., Duerr, R., and Stroeve, J. (2017). Noaa/nsidc climate data record of passive microwave sea ice concentration, version 3, national snow and ice data center.
- Meskhidze, N. and Nenes, A. (2006). Phytoplankton and cloudiness in the southern ocean. *Science*, 314(5804):1419–1423.
- Meskhidze, N., Sabolis, A., Reed, R., and Kamykowski, D. (2015). Quantifying environmental stress-induced emissions of algal isoprene and monoterpenes using laboratory measurements. *Biogeosciences*, 12(3):637–651.
- Milne, P. J., Riemer, D. D., Zika, R. G., and Brand, L. E. (1995). Measurement of vertical distribution of isoprene in surface seawater, its chemical fate, and its emission from several phytoplankton monocultures. *Marine Chemistry*, 48(3):237–244.
- Montes-Hugo, M., Doney, S. C., Ducklow, H. W., Fraser, W., Martinson, D., Stammerjohn, S. E., and Schofield, O. (2009). Recent changes in phytoplankton communities associated with rapid regional climate change along the western antarctic peninsula. *Science*, 323(5920):1470–1473.

- Moore, C., Mills, M., Arrigo, K., Berman-Frank, I., Bopp, L., Boyd, P., Galbraith, E., Geider, R., Guieu, C., Jaccard, S., et al. (2013a). Processes and patterns of oceanic nutrient limitation. *Nature geoscience*, 6(9):701–710.
- Moore, C. J., Moore, S. L., Weisberg, S. B., Lattin, G. L., and Zellers, A. F. (2002). A comparison of neustonic plastic and zooplankton abundance in southern california's coastal waters. *Marine Pollution Bulletin*, 44(10):1035–1038.
- Moore, J. K., Lindsay, K., Doney, S. C., Long, M. C., and Misumi, K. (2013b). Marine Ecosystem Dynamics and Biogeochemical Cycling in the Community Earth System Model [CESM1(BGC)]: Comparison of the 1990s with the 2090s under the RCP4.5 and RCP8.5 Scenarios. *Journal of Climate*, 26(23):9291–9312.
- Moore, R., Oram, D., and Penkett, S. (1994). Production of isoprene by marine phytoplankton cultures. *Geophysical Research Letters*, 21(23):2507–2510.
- Moore, R. and Wang, L. (2006). The influence of iron fertilization on the fluxes of methyl halides and isoprene from ocean to atmosphere in the series experiment. *Deep Sea Research Part II: Topical Studies in Oceanography*, 53(20-22):2398–2409.
- Moore, R. M. (2006). Methyl halide production and loss rates in sea water from field incubation experiments. *Marine chemistry*, 101(3):213–219.
- Morris, P. J. and Sanders, R. (2011). A carbon budget for a naturally iron fertilized bloom in the southern ocean. *Global Biogeochemical Cycles*, 25(3).
- Moutier, W., Thomalla, S. J., Bernard, S., Wind, G., Ryan-Keogh, T. J., and Smith, M. E. (2019). Evaluation of chlorophyll-a and poc modis aqua products in the southern ocean. *Remote Sensing*, 11(15):1793.
- Müller, J.-F., Stavrakou, T., Wallens, S., Smedt, I. D., Roozendaal, M. V., Potosnak, M., Rinne, J., Munger, B., Goldstein, A., and Guenther, A. (2008). Global isoprene emissions estimated using megan, ecmwf analyses and a detailed canopy environment model. *Atmospheric Chemistry and Physics*, 8(5):1329–1341.
- Mungall, E. L., Abbatt, J. P., Wentzell, J. J., Lee, A. K., Thomas, J. L., Blais, M., Gosselin, M., Miller, L. A., Papakyriakou, T., Willis, M. D., et al. (2017). Microlayer source of oxygenated volatile organic compounds in the summertime marine arctic boundary layer. *Proceedings of the National Academy of Sciences*, 114(24):6203–6208.
- Murrell, J. C., McGenity, T. J., and Crombie, A. T. (2020). Microbial metabolism of isoprene: a much-neglected climate-active gas. *Microbiology*, page micro000931.
- Neukermans, G., Harmel, T., Galí, M., Rudorff, N., Chowdhary, J., Dubovik, O., Hostetler, C., Hu, Y., Jamet, C., Knobelspiesse, K., et al. (2018). Harnessing remote sensing to address critical science questions on ocean-atmosphere interactions. *Elem Sci Anth*, 6(1).
- Nissen, C., Vogt, M., Münnich, M., Gruber, N., and Haumann, F. A. (2018). Factors controlling coccolithophore biogeography in the southern ocean. *Biogeosciences*, 15(22):6997–7024.
- Nunes, S., Latasa, M., Delgado, M., Emelianov, M., Simó, R., and Estrada, M. (2019a). Phytoplankton community structure in contrasting ecosystems of the southern ocean: South georgia, south orkneys and western antarctic peninsula. *Deep Sea Research Part I: Oceanographic Research Papers*.
- Nunes, S., Perez, G. L., Latasa, M., Zamanillo, M., Delgado, M., Ortega-Retuerta, E., Marrasé, C., Simó, R., and Estrada, M. (2019b). Size fractionation, chemotaxonomic groups and bio-optical properties of phytoplankton along a transect from the mediterranean sea to the sw atlantic ocean. *Scientia Marina*.
- O'Dowd, C. D., Aalto, P., Hmeri, K., Kulmala, M., and Hoffmann, T. (2002a). Aerosol formation: Atmospheric particles from organic vapours. *Nature*, 416(6880):497–498.
- O'Dowd, C. D., Facchini, M. C., Cavalli, F., Ceburnis, D., Mircea, M., Decesari, S., Fuzzi, S., Yoon, Y. J., and Putaud, J.-P. (2004). Biogenically driven organic contribution to marine aerosol. *Nature*, 431(7009):676–680.

- O'Dowd, C. D., Jimenez, J. L., Bahreini, R., Flagan, R. C., Seinfeld, J. H., Hämeri, K., Pirjola, L., Kulmala, M., Jennings, S. G., and Hoffmann, T. (2002b). Marine aerosol formation from biogenic iodine emissions. *Nature*, 417(6889):632–636.
- Ooki, A., Nomura, D., Nishino, S., Kikuchi, T., and Yokouchi, Y. (2015). A global-scale map of isoprene and volatile organic iodine in surface seawater of the arctic, northwest pacific, indian, and southern oceans. *Journal of Geophysical Research: Oceans*, 120(6):4108–4128.
- Ottesen, E. A., Marin III, R., Preston, C. M., Young, C. R., Ryan, J. P., Scholin, C. A., and DeLong, E. F. (2011). Metatranscriptomic analysis of autonomously collected and preserved marine bacterioplankton. *The ISME journal*, 5(12):1881.
- Pacifico, F., Harrison, S., Jones, C., and Sitch, S. (2009). Isoprene emissions and climate. *Atmospheric Environment*, 43(39):6121–6135.
- Palmer, P. I. and Shaw, S. L. (2005). Quantifying global marine isoprene fluxes using modis chlorophyll observations. *Geophysical Research Letters*, 32(9).
- Peng, G., Meier, W., Scott, D., and Savoie, M. (2013). A long-term and reproducible passive microwave sea ice concentration data record for climate studies and monitoring. *Earth Syst. Sci. Data*, 5:311–318.
- Pinkernell, S. and Beszteri, B. (2014). Potential effects of climate change on the distribution range of the main silicate sinker of the southern ocean. *Ecology and evolution*, 4(16):3147–3161.
- Pöhlker, C., Wiedemann, K. T., Sinha, B., Shiraiwa, M., Gunthe, S. S., Smith, M., Su, H., Artaxo, P., Chen, Q., Cheng, Y., et al. (2012). Biogenic potassium salt particles as seeds for secondary organic aerosol in the amazon. *Science*, 337(6098):1075–1078.
- Richter, U. and Wallace, D. W. (2004). Production of methyl iodide in the tropical atlantic ocean. *Geophysical Research Letters*, 31(23).
- Riemer, D. D., Milne, P. J., Zika, R. G., and Pos, W. H. (2000). Photoproduction of nonmethane hydrocarbons (nmhcs) in seawater. *Marine Chemistry*, 71(3):177–198.
- Rodriguez, F., Varela, M., and Zapata, M. (2002). Phytoplankton assemblages in the gerlache and bransfield straits (antarctic peninsula) determined by light microscopy and chemtax analysis of hplc pigment data. *Deep Sea Research Part II: Topical Studies in Oceanography*, 49(4-5):723–747.
- Rodríguez-Ros, P., Cortés, P., Robinson, C. M., Hassler, C., Royer, S.-J., Estrada, M., Sala, M. M., and Simó, R. (2020a). Distribution and drivers of marine isoprene concentration across the southern ocean. *Atmosphere*.
- Rodríguez-Ros, P., Galí, M., Cortés, P., Robinson, C. M., Antoine, D., Wohl, C., Yang, M., and Simó, R. (2020b). Remote sensing retrieval of isoprene concentrations in the southern ocean. *Geophysical Research Letters*.
- Rosenfeld, D., Zhu, Y., Wang, M., Zheng, Y., Goren, T., and Yu, S. (2019). Aerosol-driven droplet concentrations dominate coverage and water of oceanic low-level clouds. *Science*, 363(6427):eaav0566.
- Royer, S.-J., Mahajan, A., Galí, M., Saltzman, E., and Simó, R. (2015). Small-scale variability patterns of dms and phytoplankton in surface waters of the tropical and subtropical atlantic, indian, and pacific oceans. *Geophysical Research Letters*, 42(2):475–483.
- RStudio Team (2015). *RStudio: Integrated Development Environment for R*. RStudio, Inc., Boston, MA.
- Ryan-Keogh, T. and Robinson, C. (2020). Phytoplankton photophysiology utilities: A python toolbox for the standardisation of processing active chlorophyll fluorescence data. *Submitted to Frontiers in Marine Science Aquatic Physiology*.
- Ryan-Keogh, T. J., Macey, A. I., Nielsdóttir, M. C., Lucas, M. I., Steigenberger, S. S., Stinchcombe, M. C., Achterberg, E. P., Bibby, T. S., and Moore, C. M. (2013). Spatial and temporal development of phytoplankton iron stress in relation to bloom dynamics in the high-latitude north atlantic ocean. *Limnology and oceanography*, 58(2):533–545.

- Saavedra-Pellitero, M., Baumann, K.-H., Flores, J.-A., and Gersonde, R. (2014). Biogeographic distribution of living coccolithophores in the Pacific sector of the Southern Ocean. *Marine Micropaleontology*, 109:1–20.
- Sailley, S. F., Vogt, M., Doney, S. C., Aita, M., Bopp, L., Buitenhuis, E. T., Hashioka, T., Lima, I., Le Quere, C., and Yamanaka, Y. (2013). Comparing food web structures and dynamics across a suite of global marine ecosystem models. *Ecological Modelling*, 261:43–57.
- Saiz-Lopez, A. and von Glasow, R. (2012). Reactive halogen chemistry in the troposphere. *Chemical Society Reviews*, 41(19):6448–6472.
- Saunoy, M., Bousquet, P., Poulter, B., Peregon, A., Ciais, P., Canadell, J. G., Dlugokencky, E. J., Etiope, G., Bastviken, D., Houweling, S., et al. (2016). The global methane budget 2000–2012. *Earth System Science Data*, 8(2):697–751.
- Schlitzer, R., Anderson, R. F., Dodas, E. M., Lohan, M., Geibert, W., Tagliabue, A., Bowie, A., Jeandel, C., Maldonado, M. T., Landing, W. M., et al. (2018). The geotraces intermediate data product 2017. *Chemical Geology*, 493:210–223.
- Seinfeld, J. H. and Pandis, S. N. (2016). *Atmospheric chemistry and physics: from air pollution to climate change*. John Wiley & Sons.
- Sharkey, T. D., Wiberley, A. E., and Donohue, A. R. (2008). Isoprene emission from plants: why and how. *Annals of Botany*, 101(1):5–18.
- Sharkey, T. D. and Yeh, S. (2001). Isoprene emission from plants. *Annual review of plant biology*, 52(1):407–436.
- Shaw, S. L., Chisholm, S. W., and Prinn, R. G. (2003). Isoprene production by prochlorococcus, a marine cyanobacterium, and other phytoplankton. *Marine Chemistry*, 80(4):227–245.
- Shaw, S. L., Gantt, B., and Meskhidze, N. (2010). Production and emissions of marine isoprene and monoterpenes: a review. *Advances in Meteorology*.
- Shchepetkin, A. F. and McWilliams, J. C. (2005). The regional oceanic modeling system (roms): a split-explicit, free-surface, topography-following-coordinate oceanic model. *Ocean Modelling*, 9(4):347–404.
- Sinha, V., Williams, J., Meyerhöfer, M., Riebesell, U., Paulino, A., and Larsen, A. (2007). Air-sea fluxes of methanol, acetone, acetaldehyde, isoprene and dms from a norwegian fjord following a phytoplankton bloom in a mesocosm experiment. *Atmospheric Chemistry and Physics*, 7(3):739–755.
- Srivastva, N., Vishwakarma, P., Bhardwaj, Y., Singh, A., Manjunath, K., and Dubey, S. K. (2017). Kinetic and molecular analyses reveal isoprene degradation potential of methyllobacterium sp. *Bioresource technology*, 242:87–91.
- Stocker, T., Qin, D., Plattner, G., Tignor, M., Allen, S., Boschung, J., Nauels, A., Xia, Y., Bex, B., and Midgley, B. (2013). *ipcc, 2013: climate change 2013: the physical science basis. contribution of working group i to the fifth assessment report of the intergovernmental panel on climate change*.
- Suggett, D. J., Moore, C. M., Hickman, A. E., and Geider, R. J. (2009). Interpretation of fast repetition rate (frr) fluorescence: signatures of phytoplankton community structure versus physiological state. *Marine Ecology Progress Series*, 376:1–19.
- Tokarczyk, R., Goodwin, K. D., and Saltzman, E. S. (2003). Methyl chloride and methyl bromide degradation in the southern ocean. *Geophysical research letters*, 30(15).
- Toole, D., Slezak, D., Kiene, R., Kieber, D., and Siegel, D. (2006). Effects of solar radiation on dimethylsulfide cycling in the western atlantic ocean. *Deep Sea Research Part I: Oceanographic Research Papers*, 53(1):136–153.
- Tortell, P. D., Payne, C. D., Li, Y., Trimborn, S., Rost, B., Smith, W. O., Riesselman, C., Dunbar, R. B., Sedwick, P., and DiTullio, G. R. (2008). Co2 sensitivity of southern ocean phytoplankton. *Geophysical Research Letters*, 35(4).
- Tran, S., Bonsang, B., Gros, V., Peeken, I., Sarda-Estève, R., Bernhardt, A., and Belviso, S. (2013). A survey of carbon monoxide and non-methane hydrocarbons in the arctic ocean during summer 2010. *Biogeosciences*, 10(3):1909–1935.

- Vallina, S. and Le Quéré, C. (2008). Preferential uptake of nh_4^+ over no_3^- in marine ecosystem models: A simple and more consistent parameterization. *ecological modelling*, 218(3):393–397.
- Vallina, S. M., Follows, M., Dutkiewicz, S., Montoya, J. M., Cermeno, P., and Loreau, M. (2014a). Global relationship between phytoplankton diversity and productivity in the ocean. *Nature communications*, 5.
- Vallina, S. M., Simó, R., Anderson, T. R., Gabric, A., Cropp, R., and Pacheco, J. M. (2008). A dynamic model of oceanic sulfur (dmos) applied to the sargasso sea: Simulating the dimethylsulfide (dms) summer paradox. *Journal of Geophysical Research: Biogeosciences*, 113(G1).
- Vallina, S. M., Simó, R., and Gassó, S. (2006). What controls ccn seasonality in the southern ocean? a statistical analysis based on satellite-derived chlorophyll and ccn and model-estimated oh radical and rainfall. *Global Biogeochemical Cycles*, 20(1).
- Vallina, S. M., Simó, R., Gassó, S., de Boyer-Montégut, C., Del Río, E., Jurado, E., and Dachs, J. (2007). Analysis of a potential “solar radiation dose–dimethylsulfide–cloud condensation nuclei” link from globally mapped seasonal correlations. *Global Biogeochemical Cycles*, 21(2):0886–6236.
- Vallina, S. M., Ward, B., Dutkiewicz, S., and Follows, M. (2014b). Maximal feeding with active prey-switching: A kill-the-winner functional response and its effect on global diversity and biogeography. *Progress in Oceanography*, 120:93–109.
- Van Neste, A., Duce, R. A., and Lee, C. (1987). Methylamines in the marine atmosphere. *Geophysical Research Letters*, 14(7):711–714.
- Wanninkhof, R. (1992). Relationship between wind speed and gas exchange over the ocean. *Journal of Geophysical Research: Oceans*, 97(C5):7373–7382.
- Wanninkhof, R. (2014). Relationship between wind speed and gas exchange over the ocean revisited. *Limnology and Oceanography: Methods*, 12(6):351–362.
- Wingenter, O. W., Haase, K. B., Strutton, P., Friederich, G., Meinardi, S., Blake, D. R., and Rowland, F. S. (2004). Changing concentrations of co , ch_4 , c_5h_8 , ch_3br , ch_3i , and dimethyl sulfide during the southern ocean iron enrichment experiments. *Proceedings of the National Academy of Sciences of the United States of America*, 101(23):8537–8541.
- Wohl, C., Brown, I., Kitidis, V., Jones, A., Sturges, W., Nightingale, P., and Yang, M. (2020). Underway seawater and atmospheric measurements of volatile organic compounds in the southern ocean. *Biogeosciences*, 17(9):2593–2619.
- Wohl, C., Capelle, D., Jones, A., Sturges, W. T., Nightingale, P. D., Else, B. G., and Yang, M. (2019). Segmented flow coil equilibrators coupled to a proton transfer reaction mass spectrometer for measurements of a broad range of volatile organic compounds in seawater. *Ocean Science*.
- Wolters, M. (2002). Determination of silicate in brackish or seawater by flow injection analysis. quickchem method 31-114-27-1-d, 12 p. *Methods manual. Lachat Instruments*.
- Woyke, T., Xie, G., Copeland, A., Gonzalez, J. M., Han, C., Kiss, H., Saw, J. H., Senin, P., Yang, C., Chatterji, S., et al. (2009). Assembling the marine metagenome, one cell at a time. *PLoS one*, 4(4):e5299.
- Yang, M., Archer, S., Blomquist, B., Ho, D., Lance, V., and Torres, R. (2013). Lagrangian evolution of dms during the southern ocean gas exchange experiment: The effects of vertical mixing and biological community shift. *Journal of Geophysical Research: Oceans*, 118(12):6774–6790.
- Yentsch, C. S. and Menzel, D. W. (1963). A method for the determination of phytoplankton chlorophyll and phaeophytin by fluorescence. In *Deep Sea Research and Oceanographic Abstracts*, volume 10, pages 221–231. Elsevier.
- Yoon, H. S., Price, D. C., Stepanauskas, R., Rajah, V. D., Sieracki, M. E., Wilson, W. H., Yang, E. C., Duffy, S., and Bhattacharya, D. (2011). Single-cell genomics reveals organismal interactions in uncultivated marine protists. *Science*, 332(6030):714–717.

- Yvon-Lewis, S. A., Butler, J. H., Saltzman, E. S., Matrai, P. A., King, D. B., Tokarczyk, R., Moore, R. M., and Zhang, J.-Z. (2002). Methyl bromide cycling in a warm-core eddy of the north atlantic ocean. *Global biogeochemical cycles*, 16(4).
- Zamanillo, M., Ortega-Retuerta, E., Nunes, S., Estrada, M., Sala, M. M., Royer, S.-J., López-Sandoval, D. C., Emelianov, M., Vaqué, D., Marrasé, C., et al. (2019a). Distribution of transparent exopolymer particles (tep) in distinct regions of the southern ocean. *Science of The Total Environment*, 691:736–748.
- Zamanillo, M., Ortega-Retuerta, E., Nunes, S., Rodríguez-Ros, P., Dall'Osto, M., Estrada, M., Montserrat Sala, M., and Simó, R. (2019b). Main drivers of transparent exopolymer particle distribution across the surface atlantic ocean. *Biogeosciences*, 16(3):733–749.
- Zapata, M., Rodríguez, F., and Garrido, J. L. (2000). Separation of chlorophylls and carotenoids from marine phytoplankton: a new hplc method using a reversed phase c8 column and pyridine-containing mobile phases. *Marine Ecology Progress Series*, 195:29–45.
- Zeinali, N., Altarawneh, M., Li, D., Al-Nu'airat, J., and Dlugogorski, B. Z. (2016). New mechanistic insights: Why do plants produce isoprene? *ACS omega*, 1(2):220–225.
- Zhao, D., Buchholz, A., Tillmann, R., Kleist, E., Wu, C., Rubach, F., Kiendler-Scharr, A., Rudich, Y., Wildt, J., and Mentel, T. F. (2017). Environmental conditions regulate the impact of plants on cloud formation. *Nature communications*, 8(1):1–8.
- Zimmerman, P., Greenberg, J., and Westberg, C. (1988). Measurements of atmospheric hydrocarbons and biogenic emission fluxes in the amazon boundary layer. *Journal of Geophysical Research: Atmospheres*, 93(D2):1407–1416.
- Zindler, C., Marandino, C. A., Bange, H. W., Schütte, F., and Saltzman, E. S. (2014). Nutrient availability determines dimethyl sulfide and isoprene distribution in the eastern atlantic ocean. *Geophysical Research Letters*, 41(9):3181–3188.
- Zinser, E. R. (2018). The microbial contribution to reactive oxygen species dynamics in marine ecosystems. *Environmental microbiology reports*, 10(4):412–427.
- Ziska, F., Quack, B., Abrahamsson, K., Archer, S., Atlas, E., Bell, T., Butler, J., Carpenter, L., Jones, C., Harris, N., et al. (2013). Global sea-to-air flux climatology for bromoform, dibromomethane and methyl iodide. *Atmospheric Chemistry and Physics*, 13(17):8915–8934.

Acknowledgements

We are groot.
The Guardians of the Galaxy

No one is an island.
IDLES

Sorprende ver cómo 4 años y un holgado "y pico", pandemia mediante, quedan recogidos en estas 249 páginas en algo que no pesa ni un kilo. Dicen que "el saber no ocupa lugar" pero sí que ocupa mucho tiempo. Y dicho tiempo suele trascurrir sentado delante de un ordenador, acumulando grasa. Así que el saber sí que ocupa lugar pero no dónde la mayoría de gente cree.

En primer lugar, debo agradecer a mis directores de tesis, Rafel Simó (ICM-CSIC) y Sergio Vallina (IEO-Gijón) por permitirme aprender de su mano. Cuando empecé el doctorado, Sergio, que también fue estudiante de doctorado de Rafel me dijo: "lo bueno de trabajar con Rafel es que nunca tienes miedo a equivocarte". Y *puedo prometer y prometo* que eso sigue siendo así. Una tesis doctoral consiste en equivocarse la mayor parte del tiempo y, a veces, obtener resultados interesantes. Y ya si son publicables, fetén. La ciencia no debería ser posible sin empatía, pedagogía y trabajo en equipo. Afortunadamente, yo he podido realizar mi doctorado en un ambiente que cumplía estos requisitos y más. Sirva mi dedicatoria también para todos aquellos y, más aún, aquellas, que no han gozado de dicho privilegio que no debería ser tal, sino condición necesaria e irrenunciable. Por ello, doy gracias por la oportunidad de formarme bajo ese paraguas que evita empaparse de muchas de las frustraciones de esta etapa.

També vull donar les gràcies a en Martí Galí per haver sigut "codirector a l'ombra". Vaig començar la meva tesi amb una estada al Quèbec i, entre fred i tempestes de neu, vaig aprendre com mirar els oceans polars amb els ulls d'un satèl·lit. El problema eren i són els núvols, que no ens deixen veure molt; tot i que també refreden el planeta, que és el que nosaltres estudiem. Quina paradoxa! Semblaria que els núvols no volen revelar que passa sota la pell de l'oceà. Però, tot i així, els hi hem pogut destapar uns quants secrets.

Mis compañeras de doctorado Pau Cortés, Marina Zamanillo, Sarah-Jane Roger y Marta Masdeu tienen también su lugar destacado en esta tesis, por haber compartido tantos momentos, océanos y continentes. Tampoco puedo olvidarme de los integrantes de ICM Young Researchers,

por haber sido unos compañeros inigualables. No daré nombres porque no quiero que se me olvide nadie. Solo os diré que esta etapa se acaba, aunque parezca que no. Por último, gracias a todos los investigadores e investigadoras y personal de administración y servicios del ICM-CSIC, por haberme enseñado tanto estos años.

Merci également à tout le groupe Océan Québec et Takuvik de l'Université Laval du Québec: Maurice Levasseur, Martine Lizotte et Marcel Babin. Un hiver au Québec est magnifique, c'était amusant, mais un seul. Trop froid pour quelqu'un du sud de l'Espagne. Avec vous, j'ai appris à regarder l'océan depuis l'espace. Vous n'avez pas besoin d'être astronaute pour le faire!

Danke schön Cara Nissen, Meike Vogt and Nicolas Gruber and the rest of the Environmental Physics (UP, ETH Zürich) group for training me in ecological modelling. Also thank you for your patience and treating me since the very beginning as an independent scientist. Special thanks to Cara, the most promising young scientist I have met during these years, for teaching me many things, not only science relate. I already miss Zurich and I think still preserve some of the "swissness" (impatience when the bus is 1 minute delayed, etc.).

Gracias a la Dra. Susana Flecha y la Dra. Iris Hendriks por permitirme trabajar en el Instituto Mediterráneo de Estudios Avanzados - IMEDEA (CSIC-UIB). Nada mejor que escribir la tesis en la Serra de Tramuntana. Os debo un seminario, no se me olvida. Ahora que vivo en Marllorca ya no puedo escaparme.

Special thanks to Andrew Barton, who supported me since the very beginning in pursuing my "American dream" at the Scripps Institution of Oceanography (University of California, San Diego). Thanks to the rest of Barton Lab, specially to Benjamin Post for being my office mate during the last months of my PhD (not an easy task!).

Gracias a mis compañeros de *Ecomandanga* (que, como la vida, se abre camino), La Facultad Invisible (donde "hay más premios que ganas de trabajar, pero se hacen cosas") y APECS Spain (ojalá se convierta en la entidad que merece ser).

Gracias al Departament d'Enginyeria Hidràulica, Marítima i Ambiental (EHMA) de la Universitat Politècnica de Catalunya (UPC), especialmente a Genoveva Comas, Carmen García Codony, Agustín Sánchez Arcilla y Daniel Sánchez Marco. Habéis hecho de mi doctorado un camino mucho más fácil. Gracias especialmente a Agustín por permitirme compartir docencia con él en la UPC y la Universitat de Barcelona (UB).

Gracias también a los equipos humanos de OverLeaf, Dropbox y R-Studio. Así como a toda esa gente que echa unas horas respondiendo dudas en StackOverflow, la auténtica Torre de Babel de nuestros tiempos. Y a SciHub, por no dejarnos caer a muchos investigadores durante la pandemia de COVID-19.

Mucha gente llega al doctorado habiendo pasado por pocos o ningún otro grupo de investigación en su carrera. Por suerte o por desgracia, ese no ha sido mi caso. Como la carrera investigadora es un continuo (desgraciadamente con mucho *interruptus* contractual), no puedo olvidarme de aquellos que me han enseñado ciencia desde que empecé en este mundo con 19 años

hasta antes de comenzar el doctorado. Gracias al Departamento de Ecología e Hidrología de la Universidad de Murcia (Ángel Pérez Ruzafa y Concepción Marcos), al Instituto de Ciencias del Mar de Andalucía del CSIC (Emma Huertas y Susana Flecha), al Departamento de Física de la Universidad de Murcia (Pedro Jiménez y Juan Pedro Montávez), al OceanLab de la University of Aberdeen (Evina Gontikaki y Ursula Witte) y al IMEDEA CSIC-UIB (Susana Agustí, María Isabel Cerezo y Carlos Duarte).

Finalmente, gracias a mis padres y padrinos por ser la brisa en mi espalda en tantas travesías en el mar y también en tierra. A mis tías y tíos, abuelas y abuelos, primas y primos y a mis hermanos por el apoyo durante todos estos años, a pesar de todas las horas que esta tesis nos ha quitado. También a mis amigos José Manuel Pereñíguez y Borja López por ser, además de los mejores maestros de ceremonia posibles, conocedores de los mejores y peores momentos de esta tesis y, en general, de mi vida, por acompañarme siempre tan lejos y siempre tan cerca. Y, por supuesto, al resto de mis amigos y amigas y familia de Cartagena, Murcia, Mallorca, Barcelona, Madrid y tantos otros allende los mares; por haberme escuchado hablar de esta tesis durante tantos años. Sobre todo, teniendo en cuenta que seguramente no entenderais algunas cosas o, incluso, os diesen igual. No voy a dar más nombres por si algún día nos convertimos en delincuentes o, pero aún, famosos y nos relacionan. En contra de lo que suele decirse, yo creo que uno tiene que mantener a su lado a quienes están cerca en los momentos buenos, ya que en los momentos malos o tristes suele aparecer demasiada gente. Sigamos juntos que esto no ha hecho más que empezar.

En conclusión, durante la tesis uno se da cuenta (insistentemente) de sus propias limitaciones, así como de las limitaciones de aquello que estudia. Finalmente, acaba entendiendo que existen cosas aún muy lejos de ser comprendidas en su totalidad y otras que seguramente no tengan respuesta o la misma sea poliédrica como, por ejemplo, saber *hacia dónde va el management*. Y esta, como tantas otras tantas cuestiones, también busca su respuesta y en ello estamos.

Por último, añadir que no dejéis de leer. Hay cosas más entretenidas que 249 páginas de isopreno marino, aunque dudo que estén escritas con tanto cariño.

En los libros podemos refugiar nuestros sueños para que no se mueran de frío.

Fernando Fernán Gómez como *Don Gregorio* en "La Lengua de las mariposas"

Curriculum vitae

Pablo Rodríguez-Ros

Cartagena (1990), Región de Murcia, Spain

Contact: rodriguezrospablo@gmail.com

Website: <https://rodriguezrospablo.com>

Education

PhD in Marine Sciences (UPC-UB) – 2020

MSc in Social Communication of Scientific Research (VIU) – 2019

MSc in Global Change (UIMP-CSIC) – 2014

BSc in Environmental Sciences (UMU) – 2013

Research stays

- Scripps Institution of Oceanography - UCSD (6 months), 2019-2020
- IMEDEA-CSIC (5 months), 2019
- ETH Zurich x2: 1 month (2018) and 4 months (2017).
- Takuvik-U. Laval (3 months), 2016

Teaching

- MSc in Science Communication - Valencia International University. 2019-2020.
- MSc in Oceanography - University of Barcelona. 2016 - 2019. Biological Oceanography & Natural disasters & Risks.
- BSc in Marine Sciences - University of Barcelona. 2017 - 2019. Ocean Physics.

Fieldwork

- Mo'orea Island, French Polynesia, BIOGAPS project, 4 weeks, 2018
- Antarctic Circumnavigation Expedition, 8 weeks, 2016-2017
- Antarctic Ocean, PEGASO cruise, 6 weeks, 2015
- Atlantic Ocean, TransPEGASO cruise, 4 weeks, 2014

Courses and training

- IV LINCGlobal Iberoamerican School. (Morillo de Tou, Huesca, Spain). October, 2018.
- 7th SOLAS Summer School 2018. July – August, 2018. Surface Ocean – Lower Atmosphere Study (SOLAS) Project. Corsica, France.
- GODAE Ocean View International School 2017. October, 2017. New Frontiers in Operational

Oceanography. Mediterranean Institute for Advanced Studies-IMEDEA (CSIC-UIB). Mallorca, Spain.

- EuroMarine Working Group PlankBioS Workhop. June, 2017. Present and future plankton biogeography and the link between community structure, marine ecosystem functioning and ecosystem service provision. AZTI. San Sebastian, Basque Country, Spain.
- 2016 PALEOGENiE summer school. July, 2016. A Practical Introduction to Ecological Modelling. University of Bristol. Bristol, Reino Unido.

Grants and prizes

- Fulbright Grant (2019-2020) | PhD Research. 1 year contract in order to finish the PhD at Scripps – University of California San Diego (UCSD). Grant: 33,000 Euros.
- PhD Fellowship from “la Caixa” Foundation (2015-2019). Grant: 113,500 Euros.
- International Research Stays for Scientists. 2017 and 2018 editions. Polytechnic University of Catalonia (UPC) – “la Caixa” Foundation. Grant: 2 x 2,000 Euros. Zurich, Switzerland.
- Excellence MSc Grant. 2014. Menéndez Pelayo International University (UIMP). Mallorca, Spain. Prize: 1,000 Euros.
- “Outstanding Graduation Award in Environmental Sciences”. 2013. An special prize for the student with the highest mark of his BSc class. University of Murcia. Murcia, Spain. Prize: 200 Euros.
- ERASMUS Study Program. 2013. 9 months (January - September, 2013) at the University of Aberdeen, Scotland, United kingdom. University of Murcia. Murcia, Spain. Grant: 1,200 Euros.

Selected Publications

- Rodríguez-Ros, P., Cortés, P., Robinson, C. M., Nunes, S., Hassler, C., Royer, S. J., ... Simó, R. (2020). Distribution and Drivers of Marine Isoprene Concentration across the Southern Ocean. *Atmosphere*, 11(6), 556.
- Rodríguez-Ros, P., Galí, M., Cortés, P., Robinson, C. M., Antoine, D., Wohl, C., ... Simó, R. (2020). Remote sensing retrieval of isoprene concentrations in the Southern Ocean. *Geophysical Research Letters*, e2020GL087888.
- Simó, R., Cortés, Pau., Rodríguez-Ros, P., Masdeu, Marta. Isoprene turnover in the surface ocean. Submitted.
- Zamanillo, M., Ortega-Retuerta, E., Nunes, S., Rodríguez-Ros, P., Dall’Osto, M., Estrada, M., ... Simó, R. (2019). Main drivers of transparent exopolymer particle distribution across the surface Atlantic Ocean. *Biogeosciences*, 16(3).

Selected Conferences

- Ocean Sciences Meeting. San Diego, California, 2020. “Remote sensing retrieval of isoprene concentrations in the Southern Ocean”. Pablo Rodríguez-Ros, Martí Gali, Pau Cortés, Charel Wohl, Mingxi Yang, Charlotte M Robinson, David Antoine and Rafel Simó.
- SOLAS Open Science Conference 2019 – Hokkaido. April 2019, Hokkaido, Japan. “Ecological modelling of the biogenic emission of isoprene in the Southern Ocean”. Pablo Rodríguez-Ros, Cara Nissen, Pau Cortés, Nicolas Gruber, Sergio Vallina, Rafel Simó, Meike Vogt.
- SIBECOL 2019 – Ecological Iberian Society. February 2019, Barcelona. “Ecological modelling of the biogenic emission of isoprene in the Southern Ocean”. Pablo Rodríguez-Ros, Cara Nissen, Pau Cortés, Nicolas Gruber, Sergio Vallina, Rafel Simó, Meike Vogt.

